(2)

CONTRACTOR'S MEETING IN PROPULSION

Sponsored by

AIR FORCE OFFICE OF SCIENTIFIC RESEARCH

and

UNIVERSITY OF COLORADO AT BOULDER

10-14 JUNE 1991

Center for Combustion Research
Department of Mechanical Engineering
Boulder, Colorado 80309-0427

University of Colorado at Boulder

REPORT DOCUMENTATION PAGE

Form Approved
OMB No. 0704-0188

1. AGENCY USE ONLY (Leave blank)	2. REPORT DATE	3. REPORT TYPE AND DATES COVERED
	2 August 1991	Technical

4. TITLE AND SUBTITLE
(U) AFOSR Contractors Meeting in Propulsion

5. FUNDING NUMBERS
PE - 61102F
PR - 2308

6. AUTHOR(S)
M A Birkan and J M Tishkoff

7. PERFORMING ORGANIZATION NAME(S) AND ADDRESS(ES)
Air Force Office of Scientific Research
Building 410
Bolling AFB DC 20332-6448

8. PERFORMING ORGANIZATION REPORT NUMBER
AFOSR-TR- 91 0713

9. SPONSORING/MONITORING AGENCY NAME(S) AND ADDRESS(ES)
AFOSR/NA
Building 410
Bolling AFB DC 20332-6448

10. SPONSORING/MONITORING AGENCY REPORT NUMBER

11. SUPPLEMENTARY NOTES

12a. DISTRIBUTION/AVAILABILITY STATEMENT
Approved for public release; distribution is unlimited

12b. DISTRIBUTION CODE

13. ABSTRACT (Maximum 200 words)

Abstracts are given for research in airbreathing combustion, rocket propulsion, and diagnostics in reacting media supported by the Air Force Office of Scientific Research.

14. SUBJECT TERMS
Instability, Flames, Propulsion, Gas Turbines, Combustion, Shear Layer, Supersonic, Soot, Sprays, Lasers, Fluorescence, Spectroscopy, Rocket, Plasma, Scramjets

15. NUMBER OF PAGES
282

16. PRICE CODE

17. SECURITY CLASSIFICATION OF REPORT	18. SECURITY CLASSIFICATION OF THIS PAGE	19. SECURITY CLASSIFICATION OF ABSTRACT	20. LIMITATION OF ABSTRACT
Unclassified	Unclassified	Unclassified	UL

CONTRACTORS MEETING IN PROPULSION

Sponsored By

AIR FORCE OFFICE OF SCIENTIFIC RESEARCH

and

THE UNIVERSITY OF COLORADO AT BOULDER

Holiday Inn
Boulder, Colorado
10-14 June 1991

TABLE OF CONTENTS

AGENDA

AFOSR CONTRACTORS MEETING ON PROPULSION

10-14 JUNE 1991

MONDAY, 10 June 1991

Reacting Flow Experiments/Predictions, Chair: D.M. Mann, ARO

1:15 - 1:30	Welcome and Administrative Announcements
1:30 - 2:00	High Resolution Measurements of Strained Diffusion Layer Structure and Extinction in Turbulent Flows, W.J.A. Dahm, University of Michigan
2:00 - 2:30	Nonlinear Spectroscopy of Multicomponent Droplets and 2-3 Dimensional Measurements in Flames, M.B. Long, Yale University
2:30 - 3:00	Flame-Turbulence Interactions, D.A. Santavicca, Penn State University
3:00 - 3:30	Combustion Research, W.M. Roquemore, Wright Laboratory
3:30 - 4:00	Break
4:00 - 4:30	Mapping Closures for Turbulent Combustion, S.B. Pope, Cornell University
4:30 - 5:00	Vortex Simulation of Turbulent Flows, A.F. Ghoniem, MIT
5:00 - 5:30	Chemical Kinetics and Aerodynamic Structures of Flames C.K. Law, Princeton University
5:30 - 7:30	Break
7:30 - 9:30	Workshops: Reacting Flows, M.B. Long, Yale University Future Fuel Requirements, J.T. Edwards, Wright Laboratory

TUESDAY, 11 June 1991

Supersonic Combustion, Chair; G.S. Roy, ONR

8:30 - 9:15	Research on Supersonic Turbulent Reacting Flows C.T. Bowman, Stanford University
9:15 - 10:00	Shock Enhancement and Control of Hypersonic Combustion E.E. Zukoski and F.E. Marble, California Institute of Technology
10:00 - 10:30	Break
10:30 - 11:15	Chemical Reactions in Turbulent Mixing Flows P.E. Dimotakis, California Institute of Technology
11:15 - 12:00	Theories of Turbulent Combustion in High Speed Flows, F.A. Williams and P.A. Libby, Univ. of California-San Diego, KNC Bray, Cambridge University
12:00 - 1:30	Break

Oblique Detonations, Chair: C. John Marek, NASA Lewis

1:30 - 2:00	Controlling Combustion and Maximizing Heat Release in a Reacting Compressible Free Shear Layer, D. Nixon, Nielsen Engineering & Research, Inc.
2:00 - 2:30	Ramjet Research, A.S. Nejad, Wright Laboratory
2:30 - 3:00	Initiation and Modification of Reaction by Energy Additions; Kinetic and Transport Phenomena, F.E. Fendell and M.S. Chou, TRW, Inc.
3:00 - 3:30	Numerical Studies of the Ram Accelerator E.S. Oran, J.P. Boris, K. Kailasanath and C. Li, Naval Research Laboratory
3:30 - 4:00	Break
4:00 - 5:00	Business Meeting, Investigators in Dr. Tishkoff's program only
5:00 - 7:30	Break
7:30 - 9:30	Workshops: Compressible Turbulence/Supersonic Combustion, M.G. Mungal, Stanford Univ. Fuel Sprays, R.D. Reitz, University of Wisconsin

WEDNESDAY, 12 June 1991

Plenary Session

9:00 - 9:30	Prof. Susan Avery Assoc. Dean of Engineering and Applied Science University of Colorado at Boulder
9:30 - 10:00	Col. Arthur L. Pavel AFOSR Commander/Deputy Director
10:00 - 10:30	Break
10:30 - 11:00	Dr. C.I. Chang Director Directorate of Aerospace Sciences
11:00 - 11:20	Dr. Julian Tishkoff Program Manager
11:20 - 11:40	Dr. Mitat A. Birkan Program Manager
11:40 - 2:00	Break

Advanced Propulsion I, Chair: M.A. Birkan, AFOSR

2:00 - 2:45	Advanced Propulsion Concepts P.G. Carrick, Propulsion Directorate, Phillips Laboratory
2:45 - 3:15	Arcing Phenomena on High Voltage Power Systems, D.E. Hastings, MIT
3:15 - 3:45	Break
3:45 - 4:15	Biefield-Brown Effect, R.L. Talley, Viritay Technology, Inc.
4:15 - 4:45	ICRF Plasma Heating in the Tandem Mirror Rocket, T.F. Yang, MIT
4:45 - 5:15	Electron-Cyclotron-Resonance Plasma Acceleration F.E. C. Culick, California Institute of Technology

THURSDAY, 13 June 1991

Chemical Propulsion I, Chair: K.O. Farner, Phillips Laboratory

8:30 - 9:15	Overview: Liquid-Fuelled Propulsion Systems D. Penn, K.O. Farner, Propulsion Directorate, Phillips Laboratory
9:15 - 10:00	Fundamentals of Acoustic Instability in Liquid-Fuelled Rockets F.A. Williams, University of California-San Diego
10:00 - 10:30	Break
10:30 - 11:00	Role of Unsteady Atomization on Liquid Rocket Instability J.W. Daily, University of Colorado at Boulder
11:00 - 11:30	Acoustic Waves in Complicated Geometries, V. Yang, Penn State
11:30 - 12:00	Combustion Instability Phenomena, R.J. Santoro, Penn State
12: - 2:00	Break

Chemical Propulsion II, Chair: D. Weaver, Phillips Laboratory

2:00 - 2:45	Overview: Solid-Fuelled Propulsion Systems D. Weaver, Propulsion Directorate, Phillips Laboratory
2:45 - 3:15	Flow Turning Phenomena, L.M. Matta, Georgia Inst. of Technology (substituting for B.T. Zinn, Georgia Tech)
3:15 - 3:45	Solid Rocket Combustion, D.R. Kassoy, University of Colorado at Boulder
3:45 - 4:15	Break
4:15 - 4:45	Chemical Phenomena at Burning Surfaces, T.B. Brill, University of Delaware
4:45 - 5:15	Kinetic Studies of Metal Combustion, A. Fontijn, RPI
5:15 - 5:45	Gas Phase Kinetics of Nitramine Propellant Combustion M. Branch, University of Colorado at Boulder

FRIDAY, 14 June 1991

Advanced Propulsion II, Chair: R.A. Spores, Phillips Laboratory

8:30 - 9:15	Overview: Plasma Propulsion R.A. Spores, Propulsion Directorate, Phillips Laboratory
9:15 - 10:00	Performance Characteristics of Plasma Thrusters M. Martin-Sanchez, MIT
10:00 - 10:30	Break
10:30 - 11:00	Laser Sustained Plasmas in Non-Local Thermal Equilibrium Conditions H. Krier, University of Illinois at Urbana
11:00 - 11:30	Plasma Instabilities and Transport in the MPD Thruster A.J. Kelly, Princeton University
11:30 - 12:00	Picosecond Laser Breakdown Thresholds in Gases, D. Keefer, UTSI
12:00 - 12:30	Basic Processes of Plasma Propulsion, H.O. Schrade, University of Stuttgart
12:30	ADJOURN

HIGH RESOLUTION MEASUREMENTS of STRAINED DIFFUSION LAYER STRUCTURE and EXTINCTION in TURBULENT FLOWS

AFOSR Grant No. 89-0541

Werner J.A. Dahm

Gas Dynamics Laboratories
Department of Aerospace Engineering
The University of Michigan
Ann Arbor, MI 48109-2140

Summary/Overview

The objective of this research program is to conduct a detailed experimental study the fine scale structure of the molecular mixing process in turbulent shear flows. Such measurements have in the past been difficult to obtain due in part to *(i)* the necessity of resolving the finest molecular diffusion scales in the flow, and *(ii)* the need for simultaneously determining all three components of the instantaneous scalar gradient vector field. In the present program we are experimentally obtaining fully resolved three- and four-dimensional, spatio-temporal, laser induced fluorescence imaging measurements of the conserved scalar field $\zeta(\mathbf{x},t)$ from which the corresponding molecular mixing rate field $(ReSc)^{-1}\nabla\zeta\cdot\nabla\zeta(\mathbf{x},t)$ can be determined. The resulting data volumes are numerically analyzed to directly determine details of the underlying fine scale structure associated with the molecular mixing process in turbulent flows. This structure is used to develop an improved understanding of the chemical reaction and local extinction processes in turbulent reacting flows. The combined results are yielding a clearer physical picture for the fine structure of the molecular mixing and chemical reaction processes in turbulent reacting flows.

Technical Discussion

A physically correct understanding of the processes by which molecular mixing and chemical reactions occur in turbulent shear flows is central to the development of techniques for enhancing the rates of mixing and combustion in advanced airbreathing propulsion systems, and to the development of new theoretical and computational methods for assessing the complex phenomena at work in turbulent reacting flows. When the molecular mixing process is formulated in terms of a conserved scalar field $\zeta(\mathbf{x},t)$, the associated scalar energy dissipation rate per unit mass $(ReSc)^{-1}\nabla\zeta\cdot\nabla\zeta(\mathbf{x},t)$ gives the local instantaneous rate of molecular mixing throughout the flow. The equilibrium structure of chemical reactions occurring within the flow can then be extracted from such fully-resolved simultaneous scalar and scalar dissipation rate measurements in turbulent flows.

The present study involves four-dimensional scalar field measurements from which the true scalar gradient field and its temporal evolution can be directly determined to yield previously unobtainable details of the fine structure of mixing. During the previous year the diagnostic technique for experimentally obtaining such measurements based on direct imaging of laser induced fluorescence in turbulent shear flows was developed and a first set of measurements made. Recent work has focused on detailed analysis of results obtained. Each such four-dimensional spatio-temporal data space consists of a temporal succession of individual three-dimensional spatial data volumes, each comprised of up to 256 individual two-dimensional spatial data planes, each of which consists of 256 × 256 individual data points. The spatial separations between adjacent points are smaller than the local strain-limited molecular diffusion scale λ_D

in the scalar field. Similarly, the temporal separation between successive spatial data planes and between successive spatial data volumes are smaller than the local strain-limited diffusion scale passage time λ_D/u. These resolution requirements place an upper limit on the Reynolds number (typically around 6,000) at which such fully-resolved four-dimensional measurements can currently be obtained. The resulting conserved scalar data are then simultaneously differentiable in all three spatial dimensions and in time, allowing detailed investigation of the molecular mixing process in the turbulent flow.

The technique is based on fully-resolved high-speed acquisition of 8-bit successive planar imaging measurements of the laser induced fluorescence from a conserved scalar in the turbulent flow. A collimated laser beam is swept by a pair of very low inertia galvanometric mirror scanners, whose timing is slaved to the imaging array, in a raster pattern through the scalar field. The fluorescence from each sweep of the laser beam is imaged onto a photodiode array, driven by an externally generated clock producing variable pixel data rates up to 11 MHz, corresponding to continuous acquisition of up to 142 such spatial data planes per second. The fluorescence data from the array is then serially acquired through a programmable digital port interface, digitized to 8-bits digital resolution, and then ported into a 16 MB high-speed dual-ported data buffer from which it is continuously written to a 3.1 GB high-speed parallel transfer disk rank. The system achieves a sustained data throughput rate to the disks of up to 9.3 MB/sec.

In order to meet these resolution requirements the present measurements are obtained in the fully-developed self-similar far field ($x/d^* = 230$) of an axisymmetric turbulent jet at local outer scale Reynolds numbers $Re_\delta \equiv (u\delta/\nu)$ ranging from 3,000 – 6,000. However, the size of the image volume in the flow is much smaller than the local outer scale δ and is comparable to the local inner scale λ_ν of the flow. As a result, when the data are normalized with the local inner flow scales $l^* \equiv \lambda_\nu$ and $u^* \equiv (\nu/\lambda_\nu)$, where $\lambda_\nu \sim \delta \cdot Re_\delta^{-3/4}$ is the local strain-limited vorticity diffusion lengthscale, then provided the separation between the local inner and outer flow scales is sufficiently wide (i.e. Re_δ is high enough) the molecular mixing process captured within this four-dimensional data space should be largely independent of the outer scale Reynolds number and, moreover, of the outer scale variables and therefore also of the particular shear flow. In this sense, the fine scale structure seen here is believed to be largely generic to $Sc \gg 1$ molecular mixing in all turbulent shear flows and not merely specific to the particular measurement conditions.

Figure 1 shows the measured 8-bit conserved scalar field in three parallel spatially adjacent 256 × 256 data planes from the same data volume in a four-dimensional data space $\zeta(x,t)$. The color levels denote the local conserved scalar value $\zeta(x,t)$ at each point. Each data plane shown spans approximately $^1/_{17}$ of the local outer scale $\delta(x)$, and approximately 1.6 times the local inner scale $\lambda_\nu(x)$, in each direction. The upper left frame in Figure 2 shows the true scalar energy dissipation rate field $log_e \nabla\zeta\cdot\nabla\zeta(x,t)$ obtained by direct differentiation of the data in the three adjacent scalar planes in Figure 4. Linear central difference approximations have been used to evaluate the three components of the scalar gradient vector field $\nabla\zeta(x,t)$, with no explicit smoothing or filtering of the results. The 256 different color levels denote increasing values of the mixing rate. The remaining frames in Figure 2 show same spatial data plane but from four temporally successive three-dimensional data volumes.

Fine structure maps of the instantaneous scalar and scalar dissipation fields such as those in Figures 1 and 2 clearly show that essentially all of the molecular mixing occurs in thin laminar sheet-like layers. Both isolated and interacting layers can be seen. The internal structure of the molecular mixing within these layers can also be examined from our measurements, and confirms that strain-limited solutions of the Burgers and Townsend form give a remarkably accurate description of the true scalar energy dissipation profiles within these layers. This has significant implications for the understanding of the mixing and chemical reaction processes in turbulent reacting flows, as well as for their theoretical description and numerical modeling.

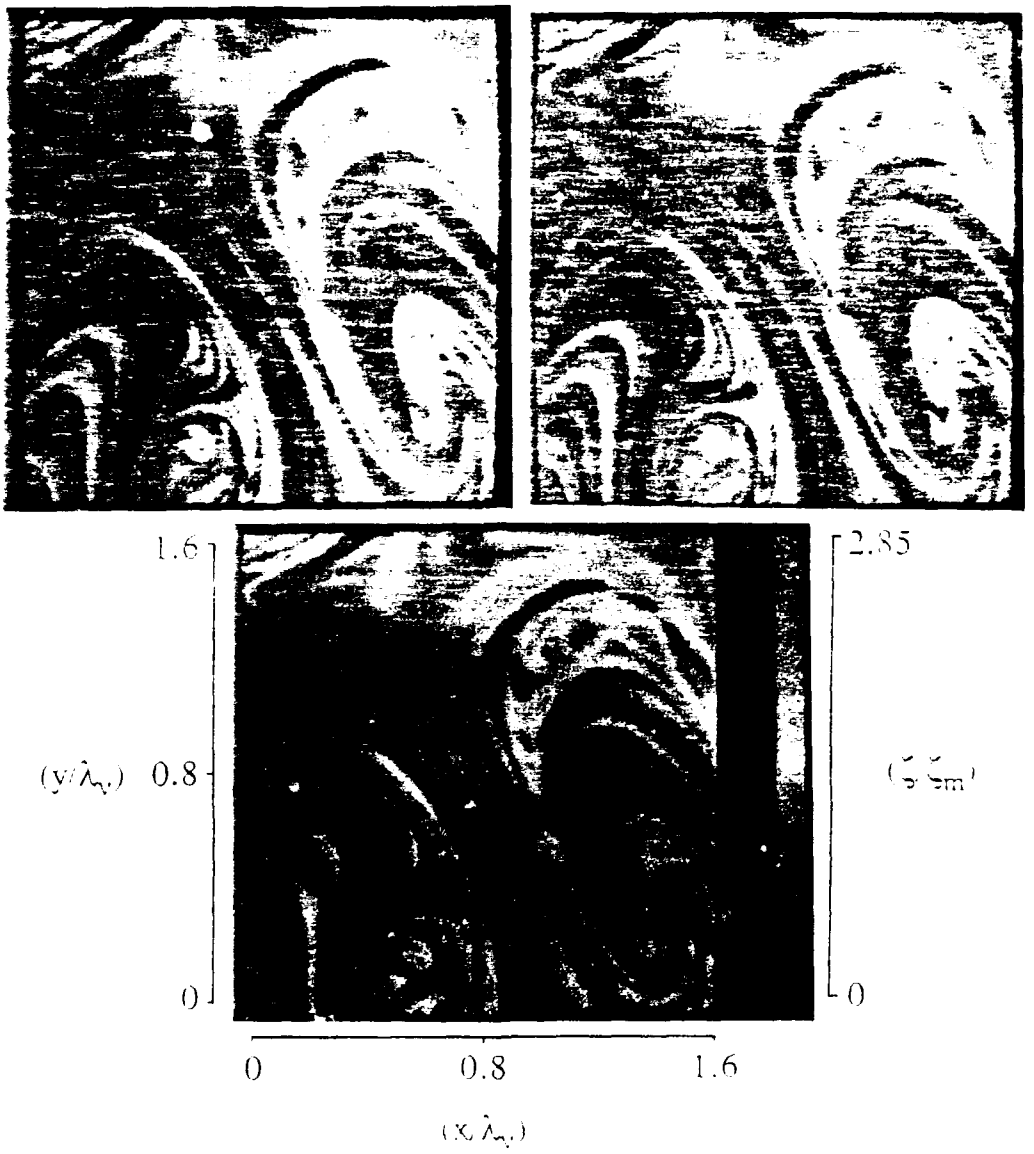

Fig. 1. The measured conserved scalar field $\zeta(x,t)$ in three typical successive 256 × 256 spatial data planes from a measured four-dimensional data space. The 256 different colors denote the local conserved scalar value at each data point. The three planes are shown in order of increasing z in the clockwise direction, beginning at the upper left. Each data plane spans approximately $^1/_{17}$ of the local outer scale δ, or approximately 1.6 times the local inner scale λ_v, in both directions. The time evolution of the true scalar energy dissipation rate field $\nabla\zeta \cdot \nabla\zeta(x,t)$, obtained by differentiation of these data in all three spatial directions, is shown in Fig. 2.

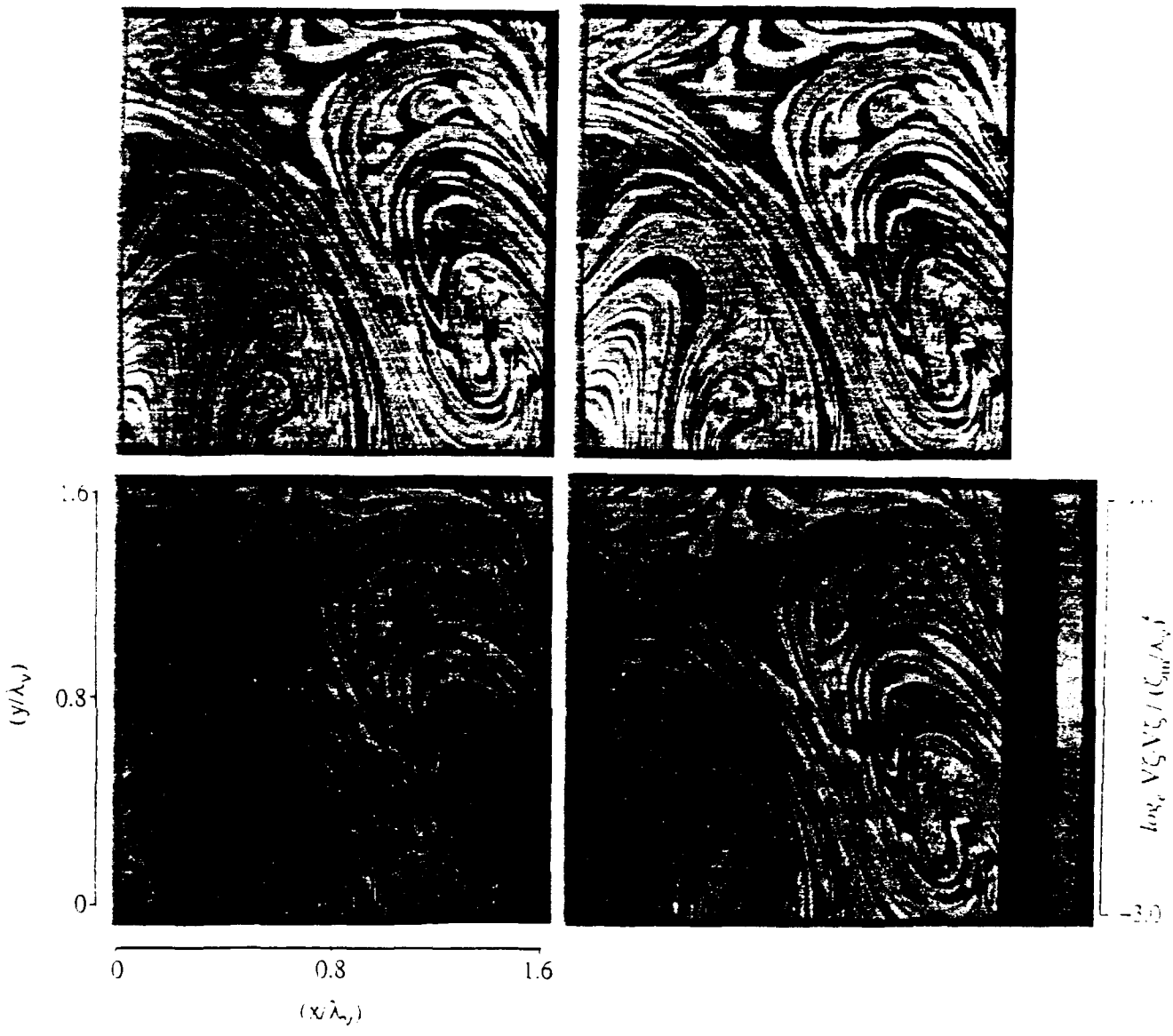

Fig. 2. The time evolution of the logarithm of the scalar energy dissipation rate field $log_e \nabla\zeta \cdot \nabla\zeta(\mathbf{x},t)$ in a typical spatial data plane. The upper left frame is obtained by direct differentiation of the conserved scalar data in the three adjacent data planes shown in Fig. 1 using linear central differences. The 256 different colors give the logarithm of the local instantaneous mixing rate in the flow. The additional frames show the same data plane from four temporally successive three-dimensional spatial data volumes. Time increases in the clockwise direction beginning at the upper left. Note the fine structure of the molecular mixing process as a collection of sheet-like strained laminar diffusion layers.

TWO- AND THREE-DIMENSIONAL MEASUREMENTS IN FLAMES

AFOSR Grant No. 91-0150

Marshall B. Long (Co-Principal Investigator)

Yale University
Department of Mechanical Engineering and Center for Laser Diagnostics
New Haven, Connecticut 06520-2157

SUMMARY/OVERVIEW

Our work concentrates on the development and application of laser diagnostic techniques for studying turbulent reacting flows. Because of the importance of spatial information in understanding the interaction between turbulence and chemistry, measurement techniques capable of mapping scalars in two and three dimensions have been developed. In the current phase of our work, we are seeking to augment the information provided by these multidimensional scalar measurements by adding simultaneous velocity imaging.

TECHNICAL DISCUSSION

During the initial period of this research grant, specific areas of progress include the following:

1. Digital Particle Image Velocimetry

Over the past several years, particle image velocimetry (PIV) has been established as a viable means for making quantitative measurements of two velocity components within a plane intersecting a flow.[1] The technique is based on recording images of a seeded flow illuminated by a multiple-pulsed laser sheet. Two components of the velocity are determined from the separation of the particle images and the known time between laser pulses. In most work done to date, photographic film is used to record the images because of its high spatial resolution. In the last few years, however, electronic imaging devices with higher spatial resolution have become available. We have investigated the use of a cooled 2048 x 2048 pixel CCD detector for recording PIV data.

There are several advantages to the use of electronic imaging for PIV. Probably the most significant is the elimination of the need for photographic processing of the film. Since the images are available in nearly real time, optimization of the focusing, temporal separation of the laser pulses, and illumination sheet intensity is possible. Additional advantages of using cooled CCD arrays relate to their linearity and large dynamic range. This capability may permit the determination of the third velocity component or the resolution of the directional ambiguity in PIV.

Experimentally, the use of a cooled CCD array for digital PIV is quite straightforward. The second or third harmonic of a double-pulsed Nd-YAG laser is formed into an illumination sheet that intersects the flow. The laser pulse separation can be varied between 40 and 200 μsec, and is selected according to the mean flow velocity. The scattered light is imaged onto the CCD detector with the optical axis of the collection lenses oriented normal to the illumination sheet. Figure 1 shows the particle image pairs recorded by the CCD with the processed velocity vectors superposed on the raw data. A paper describing the use of cooled CCD detectors for digital PIV will be submitted for publication.[2]

2. Simultaneous velocity and scalar imaging

Another advantage of the digital PIV described above is its compatibility with previously developed scalar imaging techniques. In an initial set of experiments, laser-induced biacetyl fluorescence has been combined with digital PIV to allow simultaneous measurement of the nozzle gas concentration and the velocity field in a turbulent nonreacting jet. Figure 2 shows the nozzle gas concentration field with the processed velocity field superposed on it. The nozzle gas was seeded with biacetyl as a marker, and both the nozzle gas and the coflow were seeded with submicron-sized aerosols for the PIV measurements. The third harmonic of a Nd:YAG laser (355nm) excited biacetyl fluorescence at 470 nm, which was imaged onto a 384 x 576 pixel CCD detector through an interference filter. The Lorenz-Mie scattering from the aerosols was imaged onto the 2048 x 2048 element CCD for the velocity measurement.

Preliminary experiments are now being done to extend the velocity and scalar imaging work to reacting flows. In our initial experiments, biacetyl fluorescence and digital PIV will be used to map the unburned gas concentration and the velocity in a turbulent premixed jet flame. Simultaneous concentration and velocity data in flames will show the position of the flame front as well as the velocity of the gasses through the flame front. These data should be useful for studying extinction and for understanding the coupling between the turbulence and the chemical reactions.

REFERENCES

1. D.L. Reuss, R.J. Adrian, C.C. Landreth, D.T. French, and T.D. Fansler, "Instantaneous Planar Measurements of Velocity and Large-Scale Vorticity and Strain Rate in an Engine Using Particle-Image Velocimetry," SAE Paper 890616, 1989.

2. K.M. Lyons and M.B. Long, "Digital Particle Image Velocimetry by Direct CCD Imaging," to be submitted to Exp. Fluids.

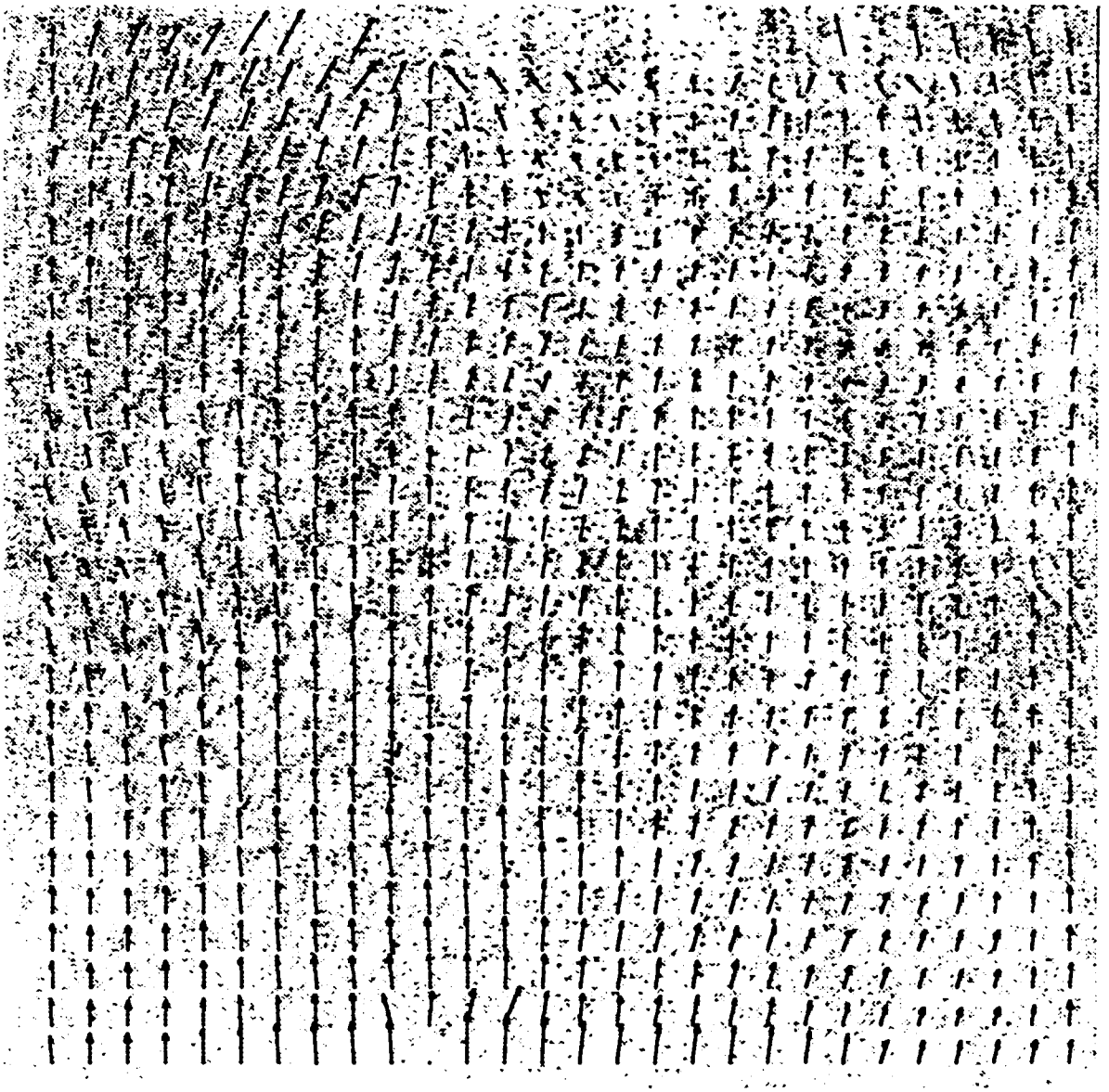

Fig. 1 Data obtained in a PIV experiment with the resultant velocity vectors shown as an overlay. The images of particles illuminated by a double-pulsed Nd-YAG laser are recorded on a 2048 x 2048 pixel cooled CCD camera. For each 128 x 128 pixel region, the average particle displacement during the time between the laser pulses is found by applying successive Fourier transforms to the data. By knowing the time duration between the laser pulses, the velocities can be found. The imaged region was 1.6 x 1.6 nozzle diameters and was centered 5 nozzle dimeters downstream from the 6 mm nozzle exit. The jet was a gas phase flow seeded with sub-micron particles. The jet exit velocity was 3 m/s.

Fig. 2 A measurement of the nozzle gas concentration overlayed with the velocity field from Fig. 1. The concentration measurement was made simultaneously with the PIV measurement by using the third harmonic of an Nd-YAG laser. Lorenz-Mie scattering from the particles at 355 nm was recorded by the high resolution detector for the velocity measurement while the biacetyl fluorescence at 470 nm was recorded by a 384 x 576 pixel CCD camera. The concentration field is 2.5 x 3.8 nozzle diameters centered 5.1 nozzle diameters downstream.

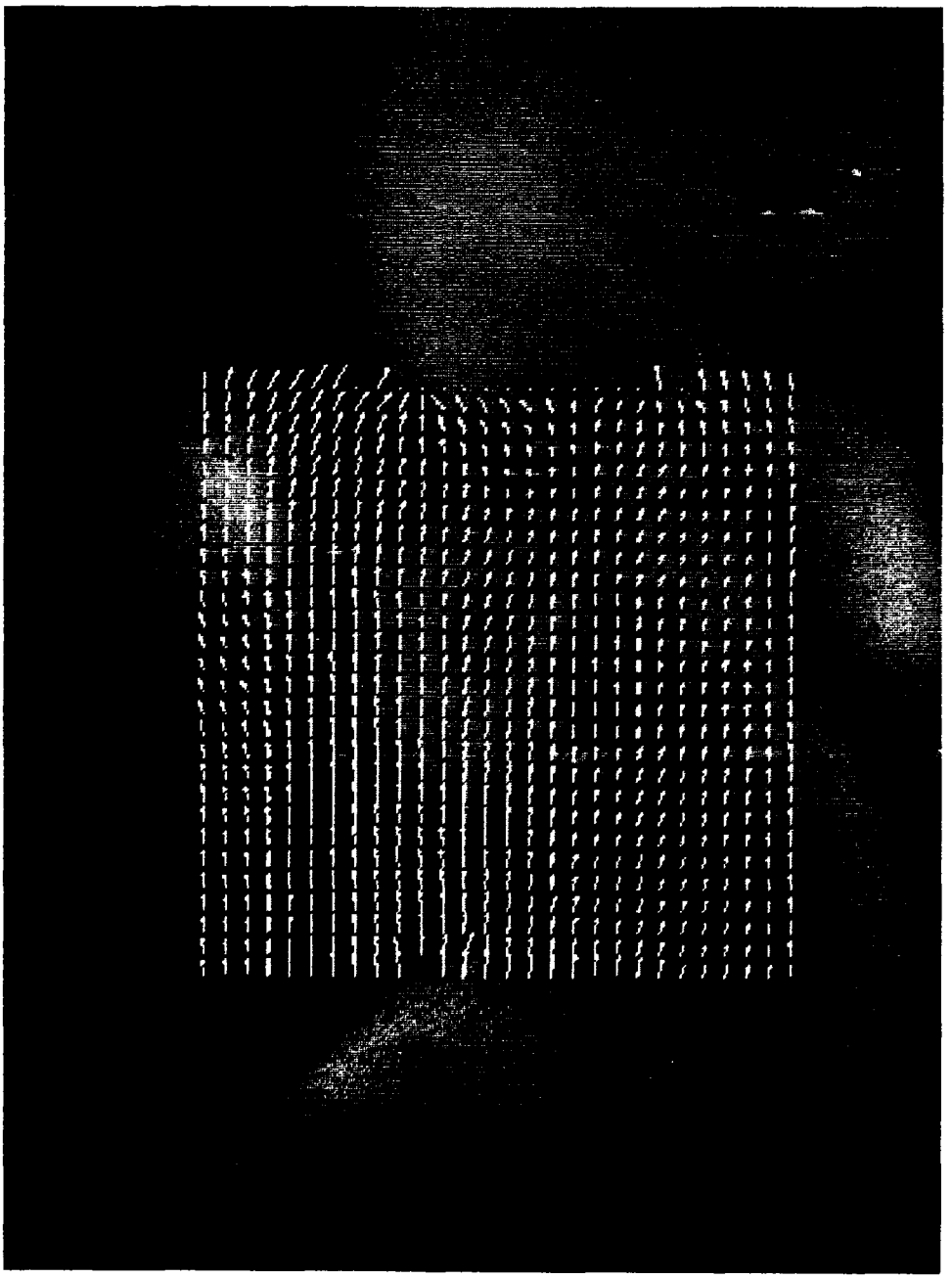

FLAME-TURBULENCE INTERACTIONS

(AFOSR Grant No. AFOSR-90-0025)

Principal Investigator: Domenic A. Santavicca

Department of Mechanical Engineering
Propulsion Engineering Research Center
Penn State University
University Park, PA 16802

SUMMARY/OVERVIEW

The objective of this research is to obtain an improved understanding of flame-turbulence interactions in premixed turbulent flames. Experiments are conducted in a one-dimensional, freely propagating turbulent flame configuration and a single vortex-laminar flame configuration. LDV and PIV are used to characterize the velocity field and two-dimensional laser induced fluorescence is used to characterize the flame structure. Of specific interest is the fractal nature of the flame structure, the effect of strain and preferential diffusion on flame propagation and extinction, and the mechanisms of flame generated turbulence. Such information is of critical importance to the formulation and validation of improved turbulent combustion models and will lead to a better understanding of the factors which determine the mass burning rate and flame-out limits of real combustors.

TECHNICAL DISCUSSION

Flame Generated Turbulence: Using a one-dimensional, freely propagating flame configuration measurements of the turbulence properties across premixed turbulent flames have been made at turbulence Reynolds numbers as large as 650. The observed changes in the turbulence field across the flame front are quite pronounced. The turbulence intensity is enhanced significantly, with most of the increase occurring in the velocity component normal to the mean flame front. This results in a large degree of anisotropy behind the flame. Distinct shifts are observed in the spectral distribution, again with the normal and parallel components behaving differently. With the possible exception of the turbulence time scale, all of the changes are sensitive to the upstream turbulence levels. The magnitude of turbulence production also depends on heat release. Interpretation of these results with respect to the various mechanisms of turbulence generation clearly indicates the importance of baroclinic effects as a source of turbulence production.

Flame Curvature and Orientation: The one-dimensional, freely propagating flame configuration is also used to study the effect of turbulence on turbulent flame structure. Measurements of flamelet curvature and orientation have been obtained from OH planar laser-induced fluorescence images of the flame boundary by applying a curve-tracing difference formula with interval length

of the order of the inner cutoff scale. Use of this particular interval length is essential for accurate tracing of the flame boundary with implicit filtering of extraneous noise that can introduce significant errors in the curvature measurements. The distributions of flamelet curvature are found to be symmetric with respect to the zero mean (Figure 1), while the variance increases with increasing u'/S_L. These distributions can be approximated by Gaussian distribution functions. The positive and negative mean curvatures show a nearly square-root dependence on u'/S_L, whereas the mean flamelet radius of curvature is approximately a factor of two larger than the Taylor scale of turbulence in the approach flow. The effect of Lewis number on flamelet curvature is evidenced by a 20% increase in mean curvature which is attributed to unstable flame fronts at Lewis number less than unity. The evolution of flamelet orientation with increasing u'/S_L shows a trend toward isotropy, which is estimated to prevail when u' becomes an order of magnitude larger than S_L. For unstable flame fronts (Le<1), flamelets are more randomly oriented and thus isotropy may be achieved for somewhat smaller ratio of u'/S_L.

Inner Cutoff: Our previous work regarding the fractal nature of premixed turbulent flames has primarily dealt with the fractal dimension of the flame surface and its variation with the turbulence and flame properties. Characterization of the flame area, however, also requires knowledge of the so-called inner and outer cutoffs. Experiments have shown the outer cutoff to be of the order of the integral scale of turbulence, but there is little consensus regarding an appropriate value for the inner cutoff or smallest scale of flame wrinkling. In this study flame structure measurements were made using planar laser induced OH fluorescence in order to achieve sufficient spatial resolution to allow determination of the inner cutoff. Inner cutoff measurements have been made at values of u'/S_L from 1.0 to 6.0 for both diffusionally stable and unstable conditions. These measurements have been compared to the various inner cutoff estimates which have been proposed, including a modified Gibson scale that we have proposed which accounts for intermittency effects (Figure 2).

Flame-Vortex Interaction: The experimental apparatus which is being used to study flame-vortex interactions is illustrated schematically in Figure 3. The laminar test section is operated with premixed propane and air at 1 atmosphere and 300 K. The optically accessible test section is 10 cm x 10 cm in cross-section and 350 cm in length. The upper rod is used to stabilize a laminar V-flame and the lower rod produces individual vortices, in the form of a vortex street, which interact with the laminar flame front. By varying the approach flow velocity and equivalence ratio and the diameter and location of the vortex generating rod, it is possible to change the relevant parameters, i.e. the laminar flame speed, the laminar flame thickness, the vortex diameter and the vortex strength.

The measurement techniques which are being employed to characterize the flame-vortex interaction are all two-dimensional techniques which take advantage of the inherit two-dimensionality of this experimental configuration. These techniques include particle imaging velocimetry (PIV) and planar laser induced fluorescence (PLIF).

The PIV technique provides a measurement of two velocity components over a plane at a given instant of time and therefore measures not only the local velocity but also provides characterization of the structure of the velocity field. The PLIF technique is being used to obtain two-dimensional measurements of the gas temperature and composition using OH and CH fluorescence. OH PLIF is used to measure either the gas temperature or the OH concentration profile. The OH concentration is used to define the flame boundary, while the OH gas temperature and the CH concentration measurements are used to define the local reaction zone thickness. To date, OH PLIF measurements have been made using a temperature intensitive excitation scheme to obtain images of the flame boundary. Typical results are shown in Figure 4, where the OH fluorescence signal strength is shown (white corresponds to maximum OH concentration). Figure 4 shows results for three different gas velocities and three different size vortex rods. The case with no vortex rod is also shown for comparison. As expected, larger vortices, i.e. generated by a larger rod, produce larger "wrinkles" in the flame front. It is also apparent that the degree of flame front wrinkling increases with increasing vortex strength, i.e. greater gas velocity in this case. A systematic study of the relationship between the scale and curvature of the flame front "wrinkle" and the strength and size of the vortices is in progress. In addition, the experimental procedures for the PLIF OH thermometry and CH measurements are under development.

PUBLICATIONS

1. Santavicca, D. A., Liou, D. and North, G. L., "A Fractal Model of Turbulent Flame Kernel Growth," SAE Paper No. 900024 (1990).

2. Videto, B. D. and Santavicca, D. A., "Flame-Turbulence Interactions in a Freely Propagating Premixed Flame," Comb. Sci. and Tech., Vol. 70, pp. 47-73 (1990).

3. North, G. L. and Santavicca, D. A., "The Fractal Nature of Premixed Turbulent Flames," Comb. Sci and Tech., Vol. 72, pp. 215-232 (1990).

4. Lee, T.-W., North, G. L. and Santavicca, D. A., "Visualization of Turbulent Premixed Flame Fronts: Comparison Between Mie Scattering and OH Fluorescence Imaging," ESSCI Fall Meeting (1990).

5. Videto, B. D. and Santavicca, D. A., "Turbulence Measurements in a Propagating , Premixed Flame," ESSCI Fall Meeting (1990).

6. Lee, T.-W., North, G. L. and Santavicca, D. A., "Curvature and Orientation Statistics of Turbulent Premixed Flame Fronts," WSSCI Spring Meeting (1991).

7. Videto, B. D. and Santavicca, D. A., "A Turbulent Flow System for Studying Turbulent Combustion Processes," Comb. Sci. and Tech., Vol. 76, p. 159 (1991).

8. North, G. L., Lee, T.-W. and Santavicca, D. A., "Fractal Analysis of Small-Scale Structures in Premixed Turbulent Flames," submitted to Comb. Sci. and Tech. (1991).

9. Videto, B. D. and Santavicca, D. A., "Flame Generated Turbulence in Highly Turbulent Premixed Flames," submitted to Comb. Sci. and Tech. (1991).

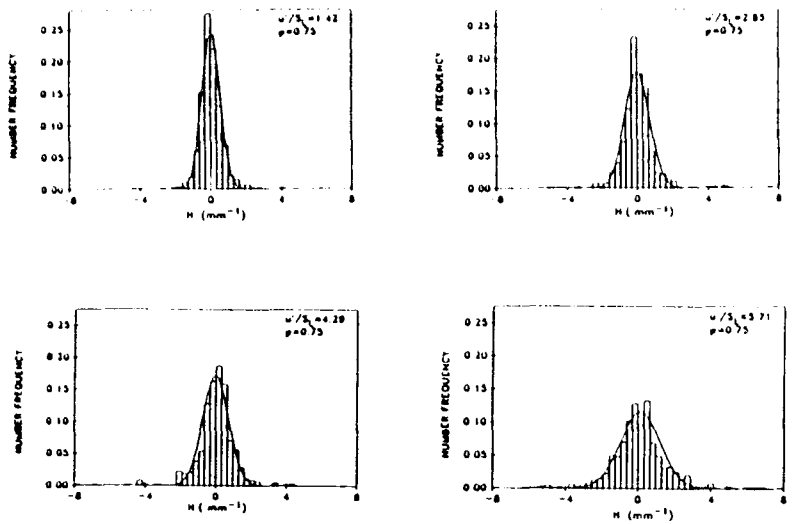

Figure 1. Flamelet curvature probability density functions.

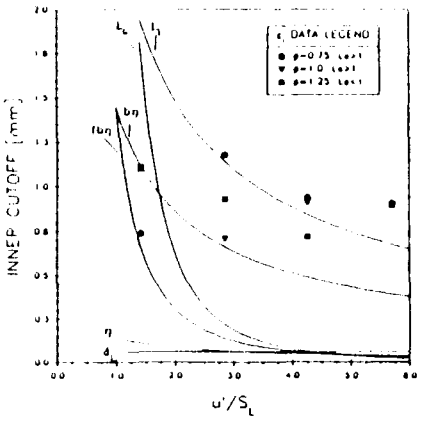

Figure 2. Comparison between inner cutoff predictions and measurements.

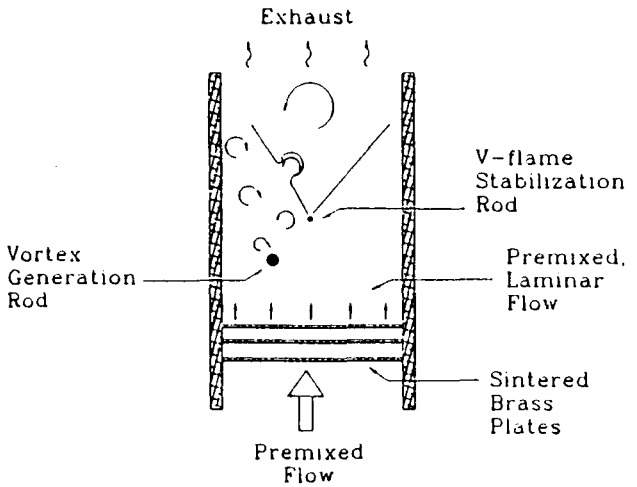

Figure 3. Flame-vortex experiment

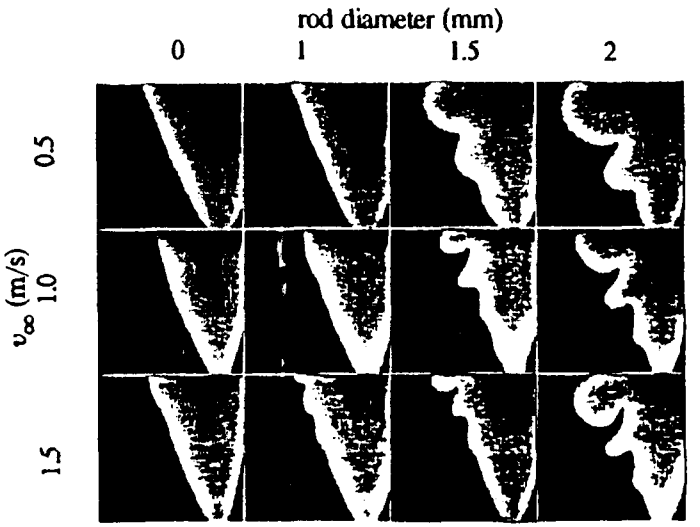

Figure 4. PLIF OH measurements of flame-vortex interaction

MAPPING CLOSURES FOR TURBULENCE COMBUSTION

AFOSR Grant No. 91-0184

Principal Investigator: Stephen B. Pope

Sibley School of Mechanical and Aerospace Engineering
Cornell University
Ithaca, New York 14853-7501

SUMMARY/OVERVIEW:

An important ingredient of the turbulent-combustion problem is the coupling between reaction and molecular diffusion, dominantly on the smallest scales. Perhaps the simplest statistical description that can represent the basic phenomena is the joint pdf of a scalar and its gradient. In the evolution equation for this joint pdf, the principal modelling challenge is associated with molecular diffusion. In this project a mapping closure is being developed for this joint pdf equation, using a combined theoretical and computational approach.

TECHNICAL DISCUSSION

Introduction

A simple way to understand the theoretical problem of turbulent combustion is to consider how (at a given point) the fluid composition changes with time. There are three processes that cause this change: convection, reaction, and molecular diffusion. In pdf methods the first two of these processes are treated exactly, while the third—molecular diffusion—has to be modelled. Many other theoretical and experimental studies lead to the same conclusion: the major current issue in turbulent combustion is to understand and model the effects of molecular diffusion.

The focus of this work is the joint pdf of composition and its gradient. The addition of the composition gradient—compared to pdf methods currently in use—provides valuable information on the microstructure of the composition field that is responsible for molecular diffusion. One virtue of this approach is that it can reconcile flamelet and nonflamelet notions in both premixed and diffusion flames (Pope 1990). For the joint pdf of composition and its gradient contains the same information as the joint pdf of mixture fraction and its dissipation rate, that is the cornerstone of flamelet models of diffusion flames (Peters 1984). Similarly, this joint pdf contains full information on the surface-to-volume ratio, which is used in flamelet models for premixed combustion.

A most promising recent advance is the development of *mapping closures* (Chen et al. 1989, Kraichnan 1990, Pope 1991, Gao 1991). This is a completely new formalism that yields "constant-free" pdf closures. In its initial application to the marginal pdf of a scalar (Pope 1991) the accuracy of the mapping closure has been remarkable. In this work, a mapping closure will be developed for the joint pdf of a scalar and its gradient.

Approach

Mapping closure is a *formalism* rather than a *model*. Thus, if the formalism is successfully applied to one problem, then it can readily be extended to all problems of the same type. The principal closure problem is connected with the molecular diffusion term. If the formalism can be developed for a simple diffusion problem, then it can be extended to others. The simplest diffusion problem is the unsteady heat conduction equation with no velocity field and no source term.

To a large extent, mapping closures developed for two-dimensional problems can be extended to the three-dimensional case of practical interest. Thus the initial objective of the research is to develop a mapping closure for the 2D heat conduction equation with random initial conditions.

Mapping

Mapping closures can be understood in terms of three different fields. The first is the *turbulent field* $\phi(\mathbf{x},t)$, which is the scalar evolving according to the 2D heat conduction equation

$$\frac{\partial \phi}{\partial t} = \Gamma \nabla^2 \phi. \tag{1}$$

In the statistical closure, $\phi(\mathbf{x},t)$ is not known in detail: all that is known is $f(\psi, \gamma;t)$—the joint pdf of ϕ and $|\nabla\phi|$.

The second field is the specified *Gaussian field* $\theta(\mathbf{z})$. Without loss of generality we take $\langle\theta\rangle=0$, $\langle\theta^2\rangle=1$. Then all statistics of the field are determined by the spectrum of θ, which is to be specified.

The third field is the *surrogate field* $\phi^S(\mathbf{x},t)$. This is obtained as a mapping of the Gaussian field:

$$\phi^S(\mathbf{x},t) = X(\theta(\mathbf{z},t),t), \tag{2}$$

with

$$\mathbf{z} = \mathbf{J}(\mathbf{x},t). \tag{3}$$

The amplitude mapping X, and the deformation **J** are to be chosen so that ϕ^S has the same joint pdf as ϕ.

The fundamental closure assumption is that (for each infinitesimal time increment) the joint pdf of the turbulent field evolves identically to the joint pdf of the surrogate field. This is a closure, since the surrogate field is known statistically in terms of the specified Gaussian field and the known mappings X and J.

Current Status

There are several plausible ways to construct the mappings X and **J**. At present we are performing a computational implementation of one mapping to explore its properties (including existence!). The deformation **J** is specified to be volume preserving, so that it does not affect the marginal pdf of amplitude. Thus the mapping X is the established amplitude mapping (Chen et al 1989).

The deformation is performed as an incompressible flow

$$\mathbf{J}(\mathbf{x},t) = \int_{-\infty}^{t} \mathbf{u}\,(\mathbf{x},s)ds. \tag{4}$$

The velocity field $\mathbf{u}(x,s)$ is specified by requiring that the associated strain-rate field change the gradients $|\nabla\phi^{s}|$ to match the conditional pdf of $|\nabla\phi|$.

This work is in progress, and the success of the method has yet to be established.

Outlook

The computational implementation of the mapping will be completed. Then, the closure itself will be investigated computationally, by comparing the results to those obtained by DNS. The closure will then be developed analytically.

References

Chen, H., Chen S., and Kraichnan, R.H. (1989) Phys. Rev. Lett., **63**, 2657.

Gao, F. (1991) Phys. Fluids A, **3**, 511.

Kraichnan, R.H. (1990) Phys. Rev. Lett., **65**, 575.

Peters, N. (1984) Prog. Energy Combust. Sci., **10**, 319.

Pope, S.B. (1990) Twenty-third Symp. (Int'l.) on Combust., The Combustion Institute (in press).

Pope, S.B. (1991) "Mapping closures for turbulent mixing and reaction" Theoretical and Computational Fluid Dynamics (to be published).

VORTEX SIMULATION OF TURBULENT COMBUSTION

(AFOSR Grant No. 89-0491)

Principal Investigator: Ahmed F. Ghoniem

Department of Mechanical Engineering
Massachusetts Institute of Technology
Cambridge, MA 02139

SUMMARY/OVERVIEW

The objectives of this work are the development of accurate and efficient numerical methods for the simulation of the flowfield, mixing and burning rate in high Reynolds number shear flows and the application of these methods to study flow-combustion interactions To avoid numerical diffusion and ensure adaptivity, Lagrangian, grid-free methods are used to transport the vorticity and scalar gradients along particle trajectories. At moderate Damkohler numbers, the chemical reaction is integrated within the transport elements. At high Damkohler numbers, flame sheet models are utilized to facilitate the incorporation of complex kinetics. During this year, we focused on the effect of variable density on the shear layer growth under unforced and forced conditions, and analyzed ignition, burning enhancement and extinction of a strained flame in the flamelet limit using an efficient model.

TECHNICAL REPORT

Spatial density gradients, even at the low Mach number limit, can influence the dynamics of shear flow through the baroicinic torque resulting from the interaction between the density and pressure gradients. At high Reynolds number, the pressure gradient reaches large values due to the growth of the instability and the curvature of the streamlines. Depending on the sign of the baroclinic term, it may enhance or diminish the vorticity leading to the continuous redistribution of the vorticity field within the large structures, resulting in the formation of asymmetric structures which impacts the entrainment levels and their proportions from both streams. The problem is compounded by the coupling between the vorticity and the pressure gradients. We have performed simulations of a spatially developing variable density shear layer under unforced and forced conditions, using the transport element method, to validate our schemes and develop some insight into this problem [1]. The essential conclusions were checked by conducting some three-dimensional simulations of a temporally growing layer with variable density [2].

For a shear layer with a velocity ratio of two, and with forcing provided only by the asymmetric boundary conditions (a splitter plate on one side and an exit boundary on the other side, i.e. a free shear layer) we have performed simulations for density ratios ranging from 1/3 and 3 (slow stream to fast stream density). The growth rate of the layer, defined by the slopes of the lines at which the mean density deviates from the density difference between the two streams by 1%, increases with the density ratio. The growth rate is 30% higher when the density ratio is changed from 1/3 to 3. The volumetric entrainment into the shear layer exhibited a strong dependence on the density ratio as well. Relative to the case of a uniform-density layer, a non-uniform density layer entrains (by volume) more from the low density fluid, with the time-average ratio of low density to high density fluid within the shear layer changing from 0.65 to 2.0 as the density ratio is flipped from 1/3 to 3. Both effects are consistent with the observation that the large eddies move with respect to the mean velocity of the two streams, in the direction of the heavier stream. Arguments based on vorticity generation are found to explain the physical origin of these observations. The large eddies, while resembling a vortex monopole in the uniform density case, acquire a vortex dipole form, pointing in the direction of the lighter stream in the variable density case. The interactions between the dipoles and the mean flow and among themselves constitute the origin of the physics exhibited by the results. All results were in quantitative agreement with experimental results. A sample of these results are shown in figure 1.

In the case of a forced shear layer, some unexpected results were encountered. The trends observed in the unforced case regarding the volumetric entrainment and eddy convection were

confirmed, and the early growth of the layer agreed with the results of linear stability theory. However, the trends of the growth rate vs. density ratio was drastically different form those seen in the unforced case. In the forced layer, we found that for a momentum ratio less than one, the growth rate decreases as the density ratio increases reaching a minimum around unity momentum ratio. The opposite is true for momentum ratio larger than one. In both cases, the growth rate can be substantially higher than in the unforced case for the same density ratio. Inspection of the vortex structures revealed that while in the early stages, and until the fundamental instability mode saturates, the layer dynamics resembles that of the unforced layer, the later stages, when eddy pairing is expected to be the dominant mechanism of growth, are different. Equal or nearly equal momenta in the two streams suppresses the tendency of neighboring eddies to pair by equilibrating their cross stream motion. On the other hand, substantially different momenta amplify the cross stream interaction between neighboring eddies and accelerates pairing. Clearly, the momentum ratio is a critical parameter in determining the outcome of forcing a variable density shear layer. Results of this study are summarized in figure 2.

Application of the transport element method to a reacting shear layer, documented in Ref [2,3] shows that the structure of the reaction zone, when accurately resolved using several layers, changes from a zone distributed over an area of a scale comparable to the vorticity scale to smaller and thinner zones of a much smaller thickness. These simulations were conducted for Damkohler number in the range of 0.1 - 10. Increasing the Damkohler number beyond 10 required an excessively large number of transport elements to accurately resolve both the vorticity field and the reaction zone. This prompted exploring an approach based, in principle, on an-inner-expansion-outer-expansion formulation of the problem in which within each time step, computations of different phenomena are conducted in different computational domains and then coupled using the appropriate boundary conditions. In its simplest form, in which the coupling is weak, this approach resembles a flame sheet formulation of the turbulent combustion problem. The coupling proceeds in the same way as that described in the transport element method. The approach requires an accurate and efficient solution of the flame structure with finite diffusion and chemical kinetics. Such method has been formulated using a series of coordinate transformations to produce a locally adaptive grid for resolving the flame structure employing the smallest number of points possible. The method has been applied to study strained flames, and some of the results are discussed next.

Figure 3 shows the effect of a constant strain rate on the ignition delay time and the steady burning of a diffusion flame. Close to extinction, where the strain is ~ 6×10^{-4} s^{-1}, the ignition delay is a strong function of the strain rate. The ignition time increases with strain due to the heat loss enhancement by the strain rate which maintains the temperature within the reaction zone low. Close to extinction, the peak reaction rate before the steady state, and the steady reaction rate are also independent of strain, while the ignition delay increases. Thus, if a strained flame is extinguished, it may be unlikely to re-ignite if the strain rate remains higher longer than the ignition delay at this particular strain. The peak steady-state temperature and the steady burning rate are shown as functions of the strain rate in figure 4. Parametric studies show that while the shapes of these curves are almost independent of the activation energy (almost a square root shape), the critical strain of extinction decreases as the activation energy increases.

REFERENCES

1. Soteriou, M., Knio, O.M. and Ghoniem, A.F., "Manipulation of the growth rate of a variable density, spatially developing mixing layer via external modulation," AIAA-91-0081.

2. Krishnan, A., Knio, O.M.,and Ghoniem, A. F., "Lagrangian simulation of the early stages of a reacting jet," the 23rd Symposium (Int.) on Combustion, Proceedings in press.

3. Knio, O.M.,and Ghoniem, A.F., "Three-dimensional simulation of a reacting shear layer in the limit of an isothermal reaction," to appear in the AIAA Journal, 1991.

4. Soteriou, M. and Ghoniem, A.F., "Ignition delay, burning enhancement and extinction in a strained diffusion flame," to be submitted for publication.

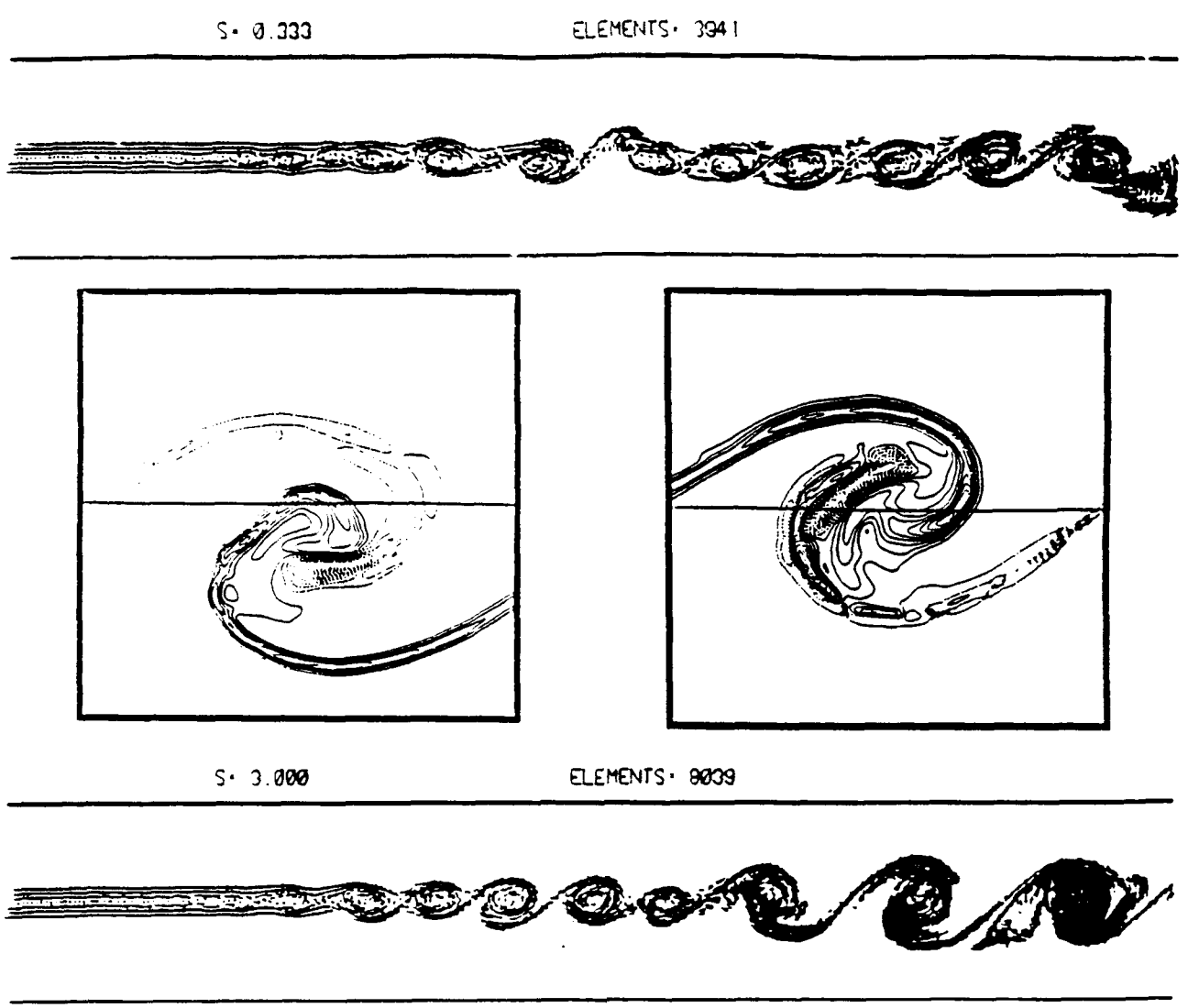

Figure 1. The top and bottom plots show the instantaneous location and relative-to-the-mean-velocity of all vortex elements in the case of an unforced shear layer with velocity ratio of one-half (bottom stream to top stream) for density ratio of one-third (top plot) and three (bottom plot). The two plots in the middle show the vorticity contours of a particular eddy (marked) in both cases where broken lines indicate positive vorticity.

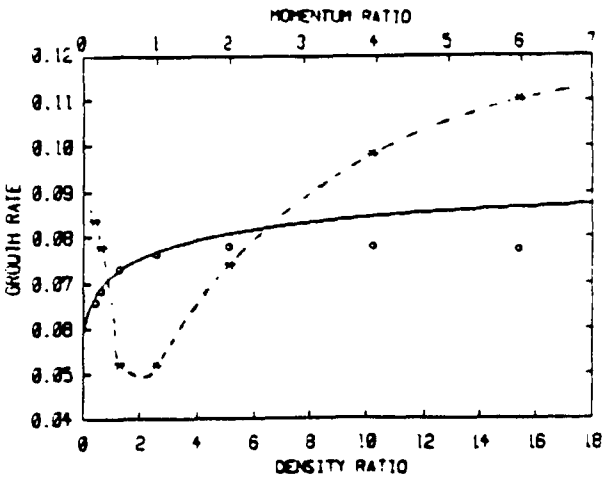

Figure 2. The effect of the density ratio and momentum ratio (low velocity to high velocity streams) on the growth rate of a forced shear layer (both fundamental and subharmonic), shown as a broken line. The solid line shows the results for an unforced layer with the open circles indicating the same results corrected for the change in the free-stream velocities due to confinement.

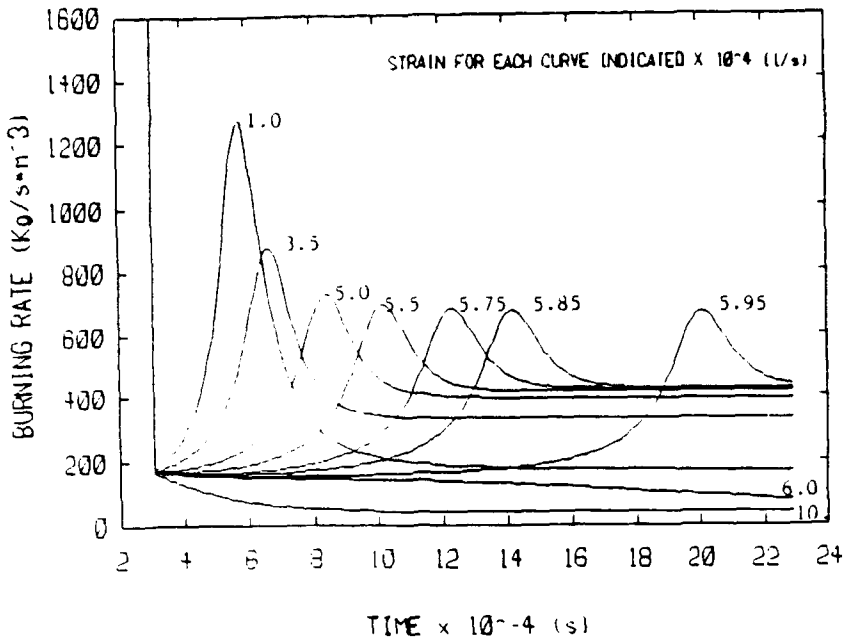

Figure 3. Effect of strain rate on burning history of a diffusion flame. The normalized activation energy is 10, the pre-exponential factor is 4×10^7, the normalized adiabatic flame temperature is 6, and the mass equivalence ratio is one. The flame is ignited by a spark that lasts for one time step.

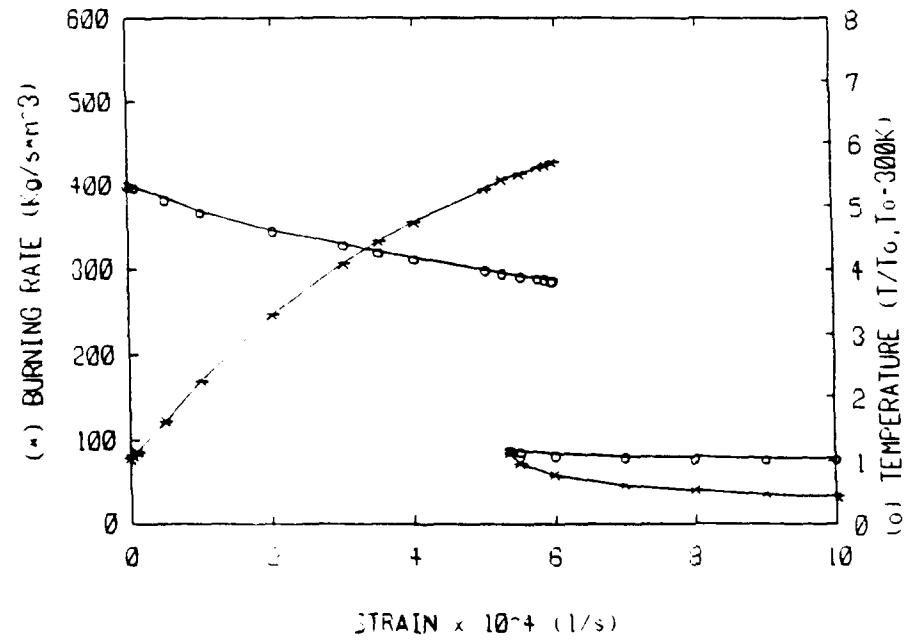

Figure 4. Steady state burning rate and maximum temperature within reaction zone for the flame shown in figure 3. Note the sudden extinction and the "cool" burning branch of the curve.

CHEMICAL KINETIC AND AERODYNAMIC STRUCTURES OF FLAMES

(AFOSR Grant No. 89-0293)

Principal Investigator: Chung K. Law

Princeton University
Princeton, NJ 08544

SUMMARY/OVERVIEW:

The objective of the present program is to study the structure of laminar premixed and diffusion flames through (a) non-intrusive experimental determination in reduced and elevated pressure environments, (b) computational simulation using detailed flame and kinetic codes, and (c) asymptotic analysis for the reduced mechanisms. During the reporting period (1) a theory has been proposed and experimentally substantiated for the phenomenon of flammability limits, (2) the laminar flame speeds of methane and the C_2-hydrocarbons mixtures with O_2 and N_2 have been experimentally determined up to 8 atmospheres, and (3) the laminar flame speeds of methanol/air mixtures have been determined over extensive concentration ranges and its kinetics studied using data obtained from flames, flow and static reactors, and shock tubes.

TECHNICAL DISCUSSIONS:

1. A Kinetic Criterion of Flammability Limits

While "flammability limit" has a long and prominent history in the description of combustion phenomena, a clear and unique fundamental definition, which would also allow for its unambiguous theoretical and experimental determination, has yet to be identified. As a consequence, the term "flammability limit" has been widely and loosely applied to diverse situations of unsustainable combustion, many of which represent only limits of flame extinction or failures of flame stabilization or spreading under very specific burning situations. Clearly, if flammability limit is indeed a useful fundamental concept, then a combustible fuel/oxidizer system can have only a lean limit and a rich limit, which occur at two distinct concentrations. As such, these two flammability limits should be unique physico-chemical properties of a combustible system, independent of such external influences as conductive and convective heat losses, aerodynamic straining, gravity-related phenomena, and etc. The extinction limits of this system, however, can span the entire concentration spectrum bounded by the lean and rich flammability limits, and are dependent on the nature and intensity of the external extinction mechanism(s) in operation for given burning situations.

In view of the above specifications, the configuration based on which flammability limit can be usefully defined is the state at which steady propagation of the one-dimensional, planar premixed flame in the doubly-infinite domain fails to be possible, as originally adopted by Spalding in his attempt to define such a limit. The failure of propagation can be caused by several factors. The most crucial and omnipresent process is the chain branching and termination mechanism. Thus, as the flammability limit is approached, the continuous reduction of the flame temperature weakens the temperature-sensitive branching reaction(s) relative to the termination reaction(s) which are in general less temperature sensitive, and causes a slowdown in the overall reaction. While it is not clear whether failure of flame propagation can be induced by this kinetic slowdown alone or additional loss mechanisms are needed, it is reasonable to require that if they are indeed needed, then their influences must be in such a way that the flammability limit can still be defined in terms of a mixture concentration alone at a given ambient temperature and pressure, and is therefore insensitive to the actual nature and magnitude of these loss mechanisms as long as they are present. It is conjectured that the chain mechanism(s) will have weakened the reaction to such an extent at the flammability limit

that the flame extinguishes when being perturbed by the various unavoidable loss mechanisms in the system.

In the present study we have first experimentally determined the "flammability limits" of a variety of mixtures, conforming as closely as possible to our definition of such a limit. We then propose a criterion, which is based on the kinetic consideration of the sensitivity of the termination reaction to the branching reaction, from which flammability limits can be determined from first principles. These are briefly described in the following. In the present study we have also restricted to fuel/oxidizer systems consisting only of the reactive elements of carbon, hydrogen, and oxygen.

The experimental methodology basically involves the establishment of two symmetrical, planar, almost-adiabatic flames in a nozzle-generated configuration, and the determination of the velocity profile along the centerline of the flow using LDV. The velocity gradient ahead of the the local minimum point of the velocity profile is identified as a reference imposed strain rate $K(\phi)$ experienced by the stretched flame, for the given fuel to air equivalence ratio ϕ of the mixture. By continuously increasing the stretch rate, the flames will approach each other and extinction of the flame ensemble will eventually occur at a distinct stretch rate $K_{ex}(\phi)$. Thus by plotting K_{ex} versus ϕ, for sufficiently small values of K_{ex}, a limiting concentration ϕ^* is obtained through linear extrapolation to $K_{ex}=0$; ϕ^* is then the flammability limit according to our definition. Figure 1 shows such a determination.

In order to arrive at a rational criterion of flammability limits, we first computationally solve the structure of an adiabatic one-dimensional planar flame with detailed reaction mechanism for a given mixture concentration. From such a calculation the dominant branching and termination reactions can be identified through sensitivity analysis. If we represent the net rate of the dominant branching reaction by its maximum value w_B, and the net rate of the corresponding termination reaction at the location of the maximum branching reaction rate by w_T (see Fig. 2), then the response of w_B to w_T as the reactant concentration varies can be expressed as

$$w_T \sim w_B^{\alpha(\phi)}$$

It is clear that for $\alpha<1$, w_T responds to w_B in either a gradual or decelerative manner. However, for $\alpha>1$ the response is accelerative. It is therefore reasonable to expect that at ϕ^* defined by

$$\alpha(\phi^*) = 1,$$

the chain mechanism could become sufficiently sensitive to loss perturbations that the flame extinguishes readily. We therefore propose that the mixture concentration ϕ^* at which the above equality is satisfied can be identified as the flammability limit of the mixture. Figure 3 shows a plot of α, termed the flammability exponent, as a function of the equivalence ratio for the 1 atm CH_4/air system.

Extensive experimental and theoretical determinations of the flammability limits have been performed for the C-H-O system. The results are summarized in Table 1. The close agreements between the experimental and calculated results are quite obvious, and are demonstrated in Fig. 4 in which the experimental concentration limits (percent of fuel in the mixture, Ω) are plotted against the calculated concentration limits. Furthermore, the following insights on the properties of flammability limits have been gained.

(a) The computed flame speeds assume finite values at the limits, implying that the limit phenomenon is an abrupt one.

(b) $H+O_2 \rightarrow OH+O$ is the dominant branching reaction for all the lean and rich flammability limits studied.

(c) $H+O_2+M \rightarrow HO_2+M$ is the dominant termination reaction for all lean limits and the rich limits of H_2/air mixtures.

(d) $CH_4+H \rightarrow CH_3+H_2$ is the termination reaction for rich limits of CH_4/air mixtures.

(e) The location of the maximum of the dominant termination reaction merges with the maximum of the dominant branching reaction at the state of the flammability limit, indicating radical scavenging attains its maximum efficiency at the limit.

2. Determination of Laminar Flame Speeds

Extensive efforts have been expended at determining the laminar flame speeds of various combustible mixtures using the counterflow technique developed under prior support by AFOSR. The availability of accurate values of the laminar flame speed not only is essential for the modeling of more complex combustion phenomena such as those related to turbulent flames, but they can also be used in the development of chemical kinetic schemes in that a necessary condition for the validity of a scheme is that its predicted flame speed should agree with the experimental value. During the reporting period we have determined the laminar flame speeds of methane and the C_2-hydrocarbons mixtures with O_2 and N_2 up to 8 atmospheres. The laminar flame speeds of methanol/air mixtures have also been determined for alternate fuels applications and for studies of the HO_2 kinetics. We are currently analyzing these data.

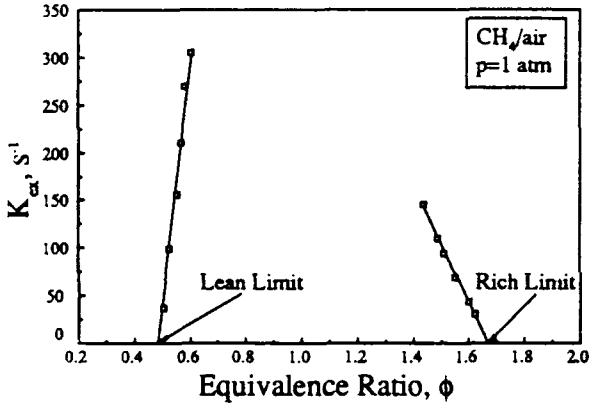

Figure 1

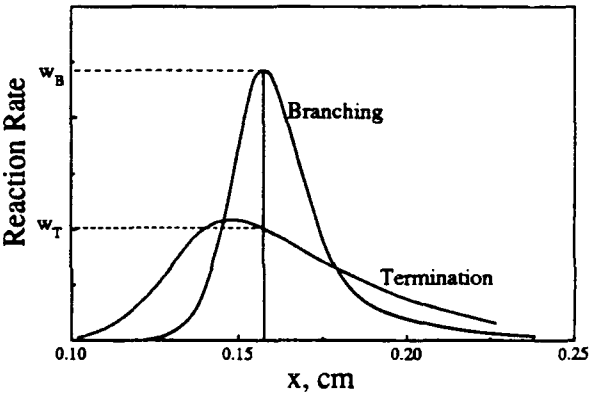

Figure 2

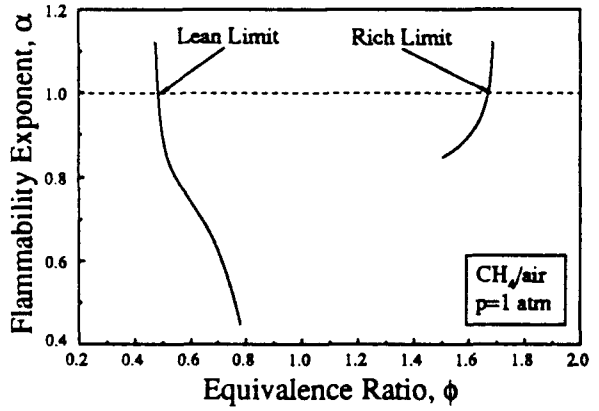

Figure 3

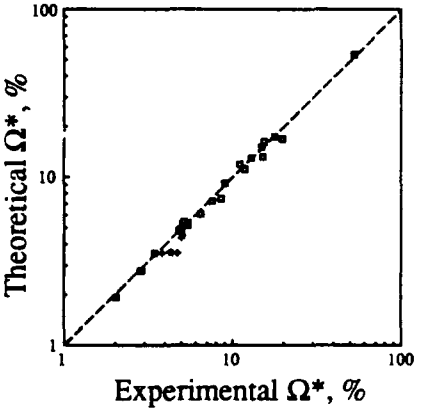

Figure 4

Table 1

(L/R)	Mixture	p, atm	Experimental Ω^* (ϕ^*)	T_{ad}, K	S_u^o, cm/s	Theoretical Ω^* (ϕ^*)
(L)	CH_4/air	3.00	5.18 (0.52)	1520	----	5.46 (0.55)
(L)	CH_4/air	2.00	5.08 (0.51)	1500	----	5.18 (0.52)
(R)	CH_4/air	2.00	15.5 (1.75)	1727	4.0	16.1 (1.82)
(L)	CH_4/air	1.00	4.80 (0.48)	1442	4.3	4.80 (0.48)
(R)	CH_4/air	1.00	14.9 (1.67)	1782	5.3	15.1 (1.69)
(L)	CH_4/air	0.75	4.90 (0.49)	1461	5.0	4.90 (0.49)
(L)	CH_4/air	0.50	4.80 (0.48)	1481	6.0	4.80 (0.48)
(L)	CH_4/air	0.375	5.08 (0.51)	1480	9.0	4.51 (0.45)
(L)	CH_4/air	0.25	4.99 (0.50)	1470	11.1	4.32 (0.43)
(L)	CH_4/"Ar-air"	1.0	3.45 (0.34)	1412	3.9	3.55 (0.35)
(R)	CH_4/"Ar-air"	1.0	17.9 (2.07)	1771	7.5	17.4 (2.00)
(L)	CH_4/[0.5925Ar+0.1975He+0.21O_2][a]	1.0	3.84 (0.38)	1525	10.4	3.55 (0.35)
(L)	CH_4/[0.395Ar+0.395He+0.21O_2][a]	1.0	4.23 (0.42)	1634	20.5	3.60 (0.36)
(L)	CH_4/[0.1975Ar+0.5925He+0.21O_2][a]	1.0	4.42 (0.44)	1687	31.5	3.55 (0.35)
(L)	CH_4/"He-air"	1.0	4.70 (0.47)	1765	43.8	3.55 (0.35)
(L)	CH_4/[0.18O_2+0.82N_2][a]	1.0	4.96 (0.58)	1477	4.7	4.88 (0.57)
(L)	CH_4/[0.151O_2+0.849N_2][a]	1.0	4.95 (0.69)	1475	5.0	4.81 (0.67)
(R)	CH_4/[0.151O_2+0.849N_2][a]	1.0	9.06 (1.32)	1682	4.6	9.25 (1.35)
(L)	[0.94CH_4+0.06CH_3Br]/air[a]	1.0	5.42 (0.57)	1597	----	5.15 (0.54)
(L)	H_2/air	1.5	6.52 (0.17)	828	----	---- (----)
(L)	H_2/air	1.0	6.30 (0.16)	811	----	---- (----)
(L)	H_2/air	0.5	5.74 (0.14)	767	----	---- (----)
(R)	$H_2/O_2/N_2$ (ϕ=1.6)[b]	1.0	15.2 (----)	1067	7.0	13.1 (----)
(R)	$H_2/O_2/N_2$ (ϕ=1.6)[b]	0.75	11.9 (----)	903	1.0	11.1 (----)
(R)	$H_2/O_2/N_2$ (ϕ=1.6)[b]	0.5	8.49 (----)	736	0.5	7.43 (----)
(R)	$H_2/O_2/N_2$ (ϕ=2.0)[b]	1.0	19.8 (----)	1101	12.0	16.9 (----)
(L)	[0.25CH_4+0.75H_2]/air[a]	1.0	5.66 (0.25)	998	----	---- (----)
(L)	[0.50CH_4+0.50H_2]/air[a]	1.0	5.10 (0.32)	1136	----	---- (----)
(L)	[0.75CH_4+0.25H_2]/air[a]	1.0	5.03 (0.41)	1313	----	5.27 (0.43)
(L)	C_2H_6/air	1.0	2.91 (0.50)	1506	7.2	2.80 (0.48)
(R)	C_2H_6/[0.16O_2+0.84N_2][a]	1.0	7.59 (1.80)	1512	3.0	7.20 (1.70)
(L)	C_2H_4/air	1.0	2.92 (0.43)	1516	5.8	2.79 (0.41)
(R)	C_2H_4/[0.12O_2+0.88N_2][a]	1.0	6.44 (1.72)	1484	3.2	6.09 (1.62)
(L)	C_2H_2/air	1.0	2.86 (0.35)	1400	9.0	2.78 (0.34)
(L)	C_3H_8/air	1.0	2.06 (0.50)	1511	7.6	1.94 (0.47)
(L)	[0.92CO+0.08H_2]/air	1.0	11.2 (0.30)	1277	1.8	11.9 (0.32)
(L)	[0.92CO+0.08H_2]/[0.113O_2+0.887N_2][a]	1.0	13.0 (0.66)	1408	4.1	13.0 (0.66)
(R)	[0.92CO+0.08H_2]/[0.113O_2+0.887N_2][a]	1.0	52.5 (4.90)	1245	8.5	54.0 (5.20)

[a] Species coefficients represent mole fractions in fuel and/or oxidizer mixtures.
[b] Flammability limit obtained by varying the nitrogen dilution for fixed ϕ.

RESEARCH ON SUPERSONIC TURBULENT REACTING FLOWS

(AFOSR Contract No. 90-0151)

Principal Investigators: C. T. Bowman, R. K. Hanson, M. G. Mungal, and W. C. Reynolds

Department of Mechanical Engineering
Stanford University
Stanford, CA 94305-3032

SUMMARY/OVERVIEW:

An experimental and computational investigation of supersonic combustion flows is being conducted to gain a more fundamental understanding of mixing and chemical reaction in supersonic flows. The research effort comprises three interrelated elements: (1) an experimental study of mixing and combustion in a supersonic mixing layer; (2) development of laser-induced fluorescence techniques for time-resolved, two-dimensional imaging of species concentration, temperature and velocity; and (3) numerical simulations of compressible reacting flows.

TECHNICAL DISCUSSION:

Experiments on Mixing and Reaction in Supersonic Flow

Experimental investigation of supersonic mixing continued during the past year. Planar laser-induced fluorescence (PLIF) has been used to investigate the scalar mixing field for low and moderate compressibility. In these experiments, NO is seeded at about 1500-3500 ppm into the low-speed stream and acts as a passive scalar. The A-X(0,0) $Q_1(10.5)$ transition of NO is pumped at 226.160 nm with broadband collection of the resulting fluorescence. Due to the quenching conditions and the chosen pump line, the resulting fluorescence is proportional to the NO mole fraction.

Figure 1 shows a perspective view of the scalar mixing field in a small region of the flow extending from 28 to 33 cm downstream of the splitter tip. The high levels (background) represent pure low-speed fluid, the low levels (foreground) represents pure high-speed fluid, while intermediate levels represent mixed fluid, to within the resolution of the measurement volume. The low compressibility case shows NO mole fractions which tend to be uniform in the cross-stream direction and ramped in the streamwise direction. The moderate compressibility case also shows streamwise ramps, but two levels of NO mole fraction are often observed in the cross-stream direction. We also find considerable structure to structure variations. Further results are found in Ref. 1.

We have also found a possible mixing enhancement, Ref. 2, which is reported next. Figure 2(a) shows the experimental arrangement whereby a disturbance that emanates from the sidewall is allowed to interact with the layer at the splitter tip. This perturbation results in significant distortion of the layer leading to increased mixing volume, as can be seen in a time-averaged view of the layer shown in Fig. 2(b). Since a wave system is used to produce the layer perturbations, we conclude that there is no analog in subsonic flow to the response seen here.

We recently have configured the supersonic flow facility for combustion tests. Specifically, the vitiation air heater has been operated over a broad range of temperatures. Stagnation temperatures up 1800 K, needed to produce ignition in the mixing layer, have been achieved. A splitter tip has been designed and fabricated for the combustion tests to provide convective Mach numbers which overlap those used in the non-reacting flow experiments. A make-up oxygen flow system has been designed for the high-speed vitiated air stream, and a hydrogen flow system for the low-speed stream has been installed. Initial combustion tests will be conducted to establish the ignition envelope for the facility.

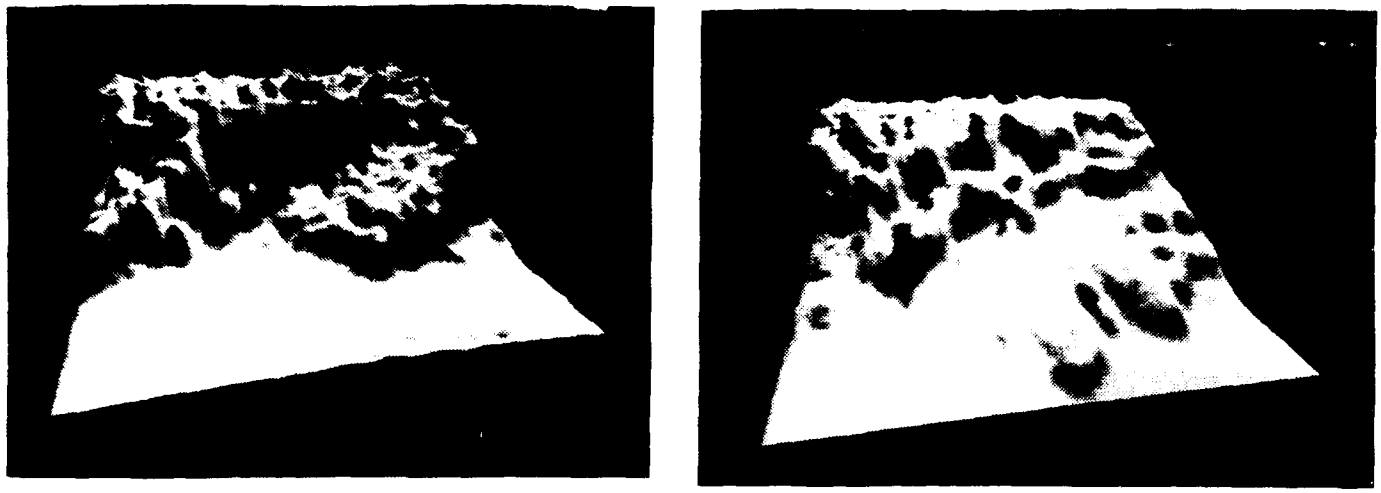

(a) (b)

Fig. 1. PLIF images of NO mole fraction in the mixing layer. (a) $M_c = 0.28$; (b) $M_c = 0.62$.

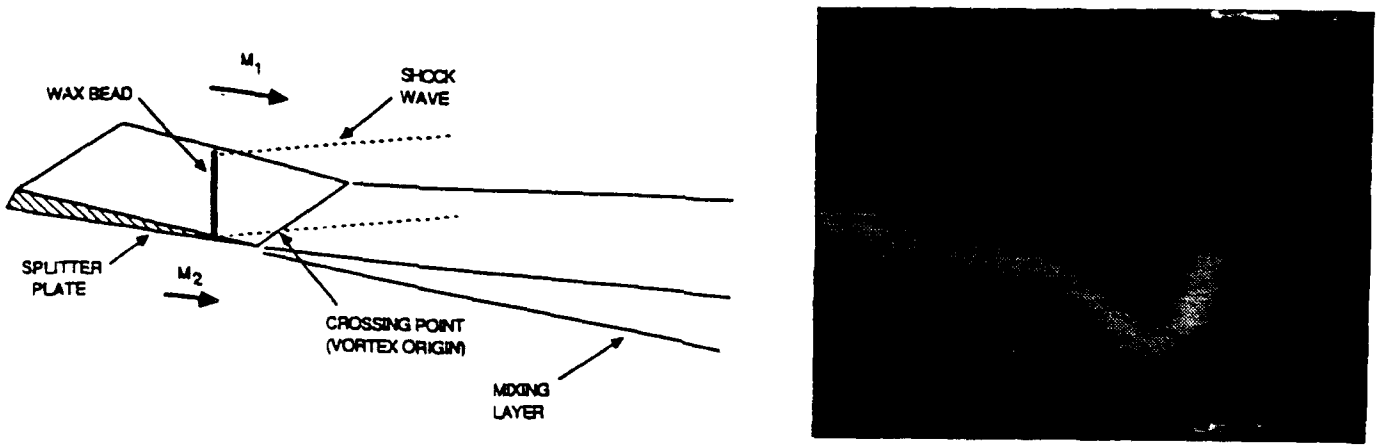

(a) (b)

Fig. 2. Effects of a single side-wall disturbance generator on the mixing layer. (a) schematic diagram; (b) resulting flowfield perturbation when viewed upstream at x = 25 cm. $M_c = 0.28$.

Development of Supersonic Flow Diagnostics

This research is aimed at establishing Planar Laser-Induced Fluorescence (PLIF) techniques for imaging in supersonic flows, particularly including various shock tube and tunnel flowfields and the supersonic mixing layer facility at Stanford. Work during the past year has been in four areas: (1) flow facility development; (2) flowfield code development; (3) PLIF imaging of shock-induced ignition; and (4) PLIF imaging of supersonic jet mixing and combustion.

Recent facility development has been associated with our shock tube, Ref. 3. Primary projects have included design and fabrication of a shock tunnel extension to the shock tube and a pulsed valve assembly which enables study of transverse jets in supersonic cross-flow behind incident shock waves. Both projects have been completed satisfactorily, although further refinements will be made to improve performance during this next year.

Work to assemble a computer code describing supersonic underexpanded free jets with vibrational nonequilibrium has been completed, Ref. 4. This code, based on the method of characteristics, is needed to design and interpret PLIF imaging experiments in high-speed, vibrationally relaxing flows. This particular flowfield is attractive experimentally in that it is relatively easy to generate and it provides a stringent test of diagnostic strategies owing to the large range of flowfield parameters found in the region between the jet exit plane and the Mach disc.

Experiments aimed at developing PLIF imaging concepts for studies of H_2–O_2 ignition were completed and reported at the 23rd Combustion Symposium, Ref. 5. The approach taken was to monitor OH production in the region adjacent to a shock tube end wall which had been modified to include a shallow groove. The local nonuniformities in reflected shock properties caused by this disturbance provide a trigger mechanism for ignition useful over a wide range from weak to strong ignition events. These experiments revealed significant flow structure which would not have been observable with conventional flow visualization schemes. Details of the work are available in Ref. 5.

Finally, our most recent work has been concerned with developing variants of PLIF suitable for study of mixing and combustion of transverse jets in supersonic cross-flow, Ref. 6. Experiments were done in a shock tube, using a pulsed valve assembly to introduce transverse jets of either NO (a non-reactive tracer for mixing studies) or H_2 (reactive case) into the hot, supersonic flow behind an incident shock wave. Example results for single-shot images acquired with two laser-sheet orientations, in both the non-reacting and reacting cases, are shown in Fig. 3. The left-hand images reveal the presence of unsteady large-scale structures in the mixing/combustion region downstream of a stable barrel shock and Mach disc region. The right-hand images are for transverse illumination of the flow at an axial location of x/D = 15. These images reveal significant three-dimensionality in the flow as well as enhanced combustion in the boundary layer adjacent to the lower wall. Details are available in Ref. 6.

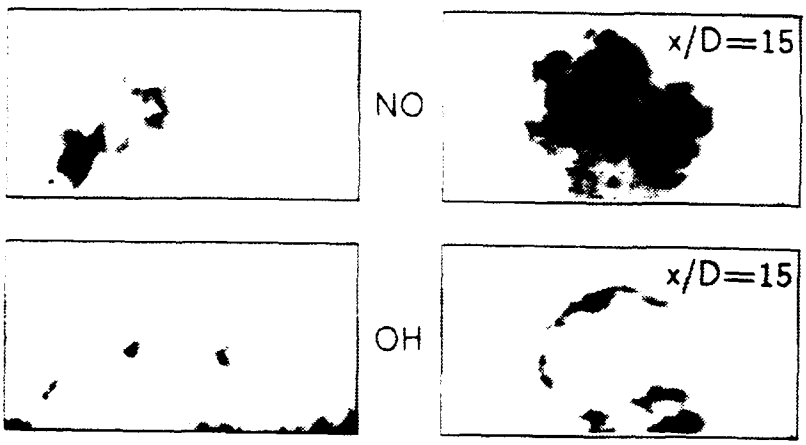

Fig. 3. Single-shot PLIF images of nonreacting (NO) and reacting (OH) transverse jets in supersonic crossflow: (a) side-view images; (b) end-view images. Region imaged is 11×22 mm; free stream conditions: M = 1.4, P = 0.4 atm, T = 2100 K; jet parameters: P_0 = 3.4 atm, T_0 = 300 K, D = 2 mm.

Stability and Numerical Simulation

This phase of the program, under the direction of Prof. W. C. Reynolds, has two objectives: (1) to provide guidance to the setup and interpretation of the experiments through a combination of stability analysis and numerical simulations; (2) to provide guidance to turbulence modeling through direct numerical simulations of turbulent flows. The numerical simulations are carried out at NASA/Ames Research Center under the auspices of the Stanford/Ames Center for Turbulence Research.

The first work, reported by Sandham and Reynolds 1989, Ref. 7, involved stability analysis and extensive numerical simulations of the time-developing compressible mixing layer. This work provided the first hint that the non-reacting compressible mixing layer at convective Mach numbers M_c above about 0.6 would show increasing three-dimensionality with increasing M_c. This prompted a modification of the experimental facility to allow visualization of the three-dimensionality, which was indeed observed in the experiments of Clemens and Mungal, Ref. 8. More recent stability analysis by Planche and Reynolds 1991, Ref. 9, showed that heat addition (chemical reaction) would tend to

restore the dominance of two-dimensional modes. Their simulations and stability analysis suggest that the large-eddy structure in a reacting mixing layer will consist of vortices associated with two sets of relatively independent parallel mixing layers, each arising from one of the two maxima of the vorticity-density product that occurs on either side of the layer.

Planche and Reynolds, Ref. 9, introduce the concept of *flame-convective Mach number* M_f to account for differences in stagnation temperature of the two streams. Their stability analysis suggest that the growth rate of a reacting layer at a given M_f will be the same of that of a non-reacting layer at $M_c = M_f$, i.e. that M_f is the proper data correlation parameter for reacting mixing layers.

In a study just completed, Blaisdell, Mansour, and Reynolds, Ref. 10, conducted extensive numerical simulations of homogeneous compressible turbulent shear flow. They found that this flow develops a turbulence state that is independent of the initial field, with an rms Mach number of approximately 0.7. Isolated three-dimensional eddy shocklets observed between the legs of hairpin vortical structures were found to account for much of the increase in dissipation due to dilitation. Recent models for the dilitation dissipation were well supported by these simulations, and new ideas for modeling were suggested.

The reacting mixing layer simulations are very computer-intensive, and consequently these have been moved from the Cray Y-MP to a hypercube parallel processor computer, where excellent performance has been obtained. The future work on this project will focus on completion and analysis of representative three-dimensional direct simulations of the time-developing reacting mixing layer, from which we expect to learn a great deal about the detailed structure of such flows that will aid in planning and interpreting the experiments.

References

1. N. T. Clemens, P. H. Paul, M. G. Mungal, and R. K. Hanson (1991), "Scalar Mixing in the Supersonic Shear Layer", AIAA-91-1720, to be presented at the AIAA 22nd Fluid Dynamics, Plasma Dynamics and Lasers Conference, Honolulu, Hawaii.
2. N. T. Clemens and M. G. Mungal (1991), "Effects of Side-Wall Disturbances on the Supersonic Mixing Layer", to appear J. Prop. Power.
3. B. K. McMillin, P. H. Paul and R. K. Hanson (1990), "Planar Laser-Induced Fluorescence Imaging of Nitric Oxide in Shock Tube Flows with Vibrational Nonequilibrium," AIAA J., in press; also paper AIAA-90-1519 at AIAA 21st Fluid Dynamics, Plasmadynamics and Lasers Conf., Seattle WA.
4. J. L. Palmer, B. K. McMillin and R. K. Hanson (1991), "Planar Laser-Induced Fluorescence Imaging of Underexpanded Free Jet Flow in a Shock Tunnel Facility," to be presented at AIAA 22nd Fluid Dynamics, Plasma Dynamics and Lasers Conference, Honolulu, Hawaii.
5. B. K. McMillin, M. P. Lee, P. H. Paul and R. K. Hanson (1990), "Planar Laser-Induced Fluorescence Imaging of Shock-Induced Ignition," Twenty-Third Symposium (International) on Combustion, The Combustion Institute, in press; presented at Twenty-Third Symposium (International) on Combustion, Orleans, France.
6. M. P. Lee, B. K. McMillin, J. L. Palmer and R. K. Hanson (1991), "Two-Dimensional Imaging of Mixing and Combustion of Transverse Jets in Shock Tube Flows," submitted to J. Prop. and Power.
7. N. D. Sandham and W. C. Reynolds (1989), "A Numerical Investigation of the Compressible Mixing Layer," Report TF-45, Department of Mechanical Engineering Stanford University.
8. N. T. Clemens and M. G. Mungal (1990), "Two- and Three-Dimensional Effects in the Supersonic Mixing Layer," AIAA-90-1978, AIAA/SAE/ASME/ASEE 26th Joint Propulsion Conference; also to appear AIAA J.
9. O. Planche and W. C. Reynolds (1991), "Compressibility Effect on the Supersonic Reacting Mixing Layer," AIAA-91-0739, 29th Aerospace Sciences Meeting, Reno, NV.
10. G. A. Blaisdell, Mansour and W. C. Reynolds (1991), "Numerical Simulations of Compressible Homogeneous Turbulence," Report TF-50, Department of Mechanical Engineering, Stanford University.

SHOCK-INDUCED MIXING AND COMBUSTION IN A VORTEX

AFOSR Grant Nos. 89-0413 and 90-0188

Principal Investigator:

E. E. Zukoski
California Institute of Technology
Pasadena, California 91125

SUMMARY/OVERVIEW:

An experimental and computational study is being made of a novel technique to enhance the mixing and combustion in a supersonic flow between a jet of hydrogen and a coflowing stream of air. Impinging oblique shocks are used to produce streamwise vorticity at the interface between the hydrogen jet and air. The vorticity produced in this interaction causes rapid distortion of the interface and rapid mixing of the hydrogen and air. This process is being studied experimentally in shock-tube and wind-tunnel facilities. Combustion in this type of vortex is being studied in a burner where combustion is initiated in the mixing layer between a premixed flow of fuel and air, and the hot products of combustion contained in a recirculation zone produced by a rearward-facing step.

TECHNICAL DISCUSSION

1. SHOCK-INDUCED MIXING INVESTIGATION

During the past year we have been studying shock-induced mixing of helium jet with air in supersonic flows, and combustion in a vortex produced at the interface between premixed fuel-air mixture and burned products of that mixture. Under the support of another grant we are also studying the application of the shock-induced mixing ideas to a fuel injector for a hypersonic combustion system. The injector has been studied in tests carried out in the high Reynolds number, Mach 6 wind tunnel at Langley Field, NASA.

Shock-Tube Experiments: Studies are being carried out in the shock tube because we have shown that a two- dimensional transient flow gives an excellent picture of many of the features of the three-dimensional steady interaction between a standing shock and the steady flow of a hydrogen jet imbedded in air.

Experimental work in the shock tube has concentrated on understanding the mixing produced by the passage of a shock over a cylinder of helium whose axis is parallel to the shock front. In the experiments discussed here the "cylinder" was a vertically directed laminar jet of helium which was injected into the test section of a 43-cm shock tube. Shocks with Mach numbers of 1.10 to 2.0 have been studied in the shock tube and the concentration field by shock impingement on the jet is being observed by use of a Rayleigh scattering technique. In each experiment, the distortion of the helium cylinder was recorded by an enhanced video camera with an exposure time of about 0.7 microseconds. In the past similar measurements were made with an picture of the observed made by measuring the fluorescence radiation produced by the excitation of biacetyl dye by a pulse of laser light.

The dye was mixed with the helium prior to its injection. We have abandoned this technique in favor of the Rayleigh scattering technique because of problems in interpretation of the data due to the large differences between the diffusion coefficients of the dye and helium gas.

This study is carried out by John Budzinski and the experimental parameters of interest are the Mach number of the incident shock, the density ratio between the injected flow and the surrounding air, the initial density gradient in the jet, the geometry of the jet, and time after the interaction starts. We measure the geometry of the distorted jet, its motion relative the ambient fluid, and the degree of mixing of the helium with the air.

We have shown that an accurate picture of the whole process can be assembled by taking photographs of nominally identical experiments at different times after the start of the interaction. The apparatus allows study of the flow for several milliseconds after shock impingement and our primary aim is to develop an understanding of the scaling of the interaction with initial size of the cylinder and the incident Mach number.

The Rayleigh scattering technique, applied by Budzinski, gives us a more detailed understanding of the structure of the mixing between the helium and the air than did the biacetyl technique.

Given the success of this technique, we have abandoned the experiments in which the helium was originally contained within a thin plastic cylinder and are now collecting data concerning the effect on the mixing rate of changing the shock Mach number from 1.1 to 2.0, and the density ratio of the gases inside and outside the cylinder from 0.07 to 0.5. The effects of a reflected shock on the mixing process will also be studied.

Wind Tunnel Experiments: Studies are being carried out in a Mach 2.6 flow to investigate the mixing produced by shear forces when a hydrogen jet imbedded in an air stream passes through a shock wave. This process is not modeled in the shock-tube experiments and may be important in real systems when substantial differences between the velocities of hydrogen and air exist.

Dr. L. Hill and R. Moore are in the process of building a Mach 2.6, continuous-flow wind tunnel, with a cross-section of 6.25 by 6 cm and a total pressure of one atmosphere, which will allow the influence of shear to be examined experimentally. In the experiments, parallel flows of air and a hydrogen jet will pass through an oblique shock and the resulting mixing processes will be measured with the Mie scattering technique. Scattering of a laser light sheet by ice particles formed by condensation in the wind-tunnel nozzle will be the primary experimental technique. The wind tunnel is substantially completed and we expect to start our experimental investigation during the summer of 1991.

A fuel injection concept for hypersonic combustion systems, whose design was based on this AFOSR Program, has been carried out in the high Reynolds number, Mach 6 wind tunnel at Langley Field, NASA by Dr. Ian Waitz. The results of this program and comparison with the work described here are described in the thesis by Waitz. We hope to be able test this injection concept with the combustion of hydrogen injectant in the new T5 Facility at Caltech. This facility, which was completed during the past year under the direction of

Dr. Hans Hornung, will allow testing with combustion of hydrogen for several milliseconds at a static pressure of 1/3 atmosphere, a total temperature of 10,000 K, and a Mach number of 5.3.

Computational Program: The computations of shock-induced mixing have been carried out with the a code supplied to us in two versions by J. Boris at NRL, Silver Springs Maryland. The aim of these calculations is to give guidance for the selection of parameters to be used in the experimental work, to allow us to determine approximately values of parameters such as vorticity (which we can not measure in the experiments), and to help in the development of scaling laws for the mixing process.

The computational program, carried out on the San Diego Cray XMP using time made available by the NSF, has been completed and the results are available in the thesis by Dr. Joe Yang. Calculations which have been completed include studies of the effect on mixing of the initial gradients and distortions of the edge of the helium cylinder, the ratio of cylinder diameter to duct height, the Mach number of the shock for the range 1.1 – 2.0, the density ratio between the cylinder fluid and ambient gas, the geometry of the cylinder, and the use of multiple cylinders arranged in several configurations.

Analysis of these computations has led to the development of scaling procedures for prediction of the circulation, rate of distortion, and velocity of the light gas relative to the ambient gas, which are produced by the impinging shock as a function of the density ratio and incident shock Mach number. Comparison with other computational results is good and a comparison with experimental results is being carried out now.

A qualitative measure of mixing has been obtained by comparing the length of contours of a fixed helium mass fraction.

2. COMBUSTION IN A VORTEX

In a practical application, the enhanced mixing technique described above involves the generation of longitudinal vortices in the mixing layer between coflowing hydrogen jets and the ambient air stream. Combustion will occur at the interface between the hydrogen jets and air as the vortices roll up and hence we have been interested in studying combustion in a vortex. The flow being studied now is that produced by vortices shed from a rearward-facing step which forms the lower wall of a two-dimensional combustion chamber and which acts as a flame holder for a premixed flow of fuel and air which passes over the step. Combustion occurs in the mixing layer formed downstream of the step between the unburnt fuel-air flow, which separates from the lip of the step, and products of combustion which recirculate behind the step. For certain sets of values for the gas speed and fuel-air ratio, a combustion instability develops which produces a regular shedding of vortices from the lip of the step at frequencies which range between 180 to 530 Hz.

T. Zsak studying the combustion within these vortices with a variety of experimental techniques which include pressure measurements throughout the combustion system, hot-wire velocity measurements in the cold gas at the flame holder lip, ionization probes inserted into the hot gas downstream of the flame holder lip, shadowgraph photographs obtained with a high-speed movie camera, photographs of the intensity of chemiluminescence ob-

tained with an enhanced video camera, and spark shadowgraph photographs of the density field.

All of these signals can be obtained continuously and simultaneously except the last two which can only be obtained at a rate of 30/second; in addition the shadowgraph and photographs of the chemiluminescence must be separated by at least a 10-microsecond time delay. We have been using a phase-locking technique with the shadowgraph and video camera photographs to obtain data from many vortices and build up a composite picture of the development of the combustion process.

In addition, we have been using a two-beam LDV to measure the velocity field of the flow as a function of position and time. The phase-locking technique must be used here again so that data taken at different positions and times can be correlated.

Using these techniques and continuous record of pressure, hot-wire measurements of the cold gas speed at the flame holder lip, and ionization probe measurements at several positions within the hot gas, we are now mapping the heat release pattern, as indicated by the chemiluminescence, the density field from the shadowgraph photographs, and velocity field in the vortex.

Results obtained with these techniques are being analyzed now to find the downstream motion and rate of growth of the vortex, the delay time between vortex shedding and the ignition of the upstream mixing layer, and the body of the vortex as a function of the initial velocity and pressure perturbations, the mean flow speed, and the fuel-air ratios.

Our initial impressions that the ignition of the vortex is delayed several milliseconds after the shedding process begins and that the rate of energy release grows rapidly after about three milliseconds for a stoichiometric mixture have been confirmed. The data also suggest that stretching of the interface between the hot products and the combustible mixture by the rapid growth of the vortex may inhibit combustion at the interface.

PAPERS:

Marble, F. E., Zukoski, E. E., Hendricks, G. J. and Jacobs, J., "Shock Enhancement of Supersonic Combustion Processes," accepted for presentation at the 26th Joint Propulsion Conference sponsored by the AIAA/SAE/ASME/ASEE.

Yang, J., "An Analytical and Computational Investigation of Shock-Induced Vortical Flows with Applications to Supersonic Combustion," PhD Thesis, California Institute of Technology, June 1991.

Waitz, I., "An Investigation of Contoured Wall Injectors for Hypervelocity Mixing Augmentation," PhD Thesis, California Institute of Technology, June 1991.

Waitz, I., Marble, F. E., and Zukoski, E. E., "An Investigation of Contoured Wall Injectors for Hypervelocity Mixing Augmentation," accepted for presentation at the 27th Joint Propulsion Conference sponsored by the AIAA/SAE/ASME/ASEE.

CHEMICAL REACTIONS in TURBULENT MIXING FLOWS

AFOSR Grant 90-0304

P. E. Dimotakis, J. E. Broadwell and A. Leonard

Graduate Aeronautical Laboratories
California Institute of Technology
Pasadena, California 91125

Summary/Overview

The purpose of this research is to conduct fundamental investigations of turbulent mixing, chemical reaction and combustion processes in turbulent, subsonic and supersonic free shear flows. Our program is comprised of an experimental effort, an analytical and modeling effort, a computational effort, and a diagnostics development and data-acquisition effort, the latter as dictated by specific needs of our experiments. Our approach is to carry out a series of detailed theoretical and experimental studies primarily in two, well-defined, fundamentally important flow fields: free shear layers and axisymmetric jets. The investigations of turbulent jet mixing are co-sponsored by the Gas Research Institute. To elucidate molecular transport effects, experiments and theory concern themselves with both liquids and gases. The computational studies are, at present, focused at fundamental issues pertaining to the computational simulation of both compressible and incompressible flows.

Technical discussion

Experimental investigations performed in the GALCIT Supersonic Shear Layer Facility during the last year included:

1. Non-reacting flows from low to moderately high compressibility ($0.09 < M_{c1}^{(i)} < 0.96$). These were designed to search for large scale structures and shock waves, and to measure shear layer growth rates that could be compared to previous results (Papamoschou & Roshko 1988, Chinzei *et al.* 1986, Clemens & Mungal 1990).

2. Reacting flows at medium to moderately high compressibility ($M_{c1}^{(i)} = 0.51, 0.96$), which utilized $H_2/F_2/NO$ chemistry, patterned after the incompressible experiments of Mungal & Dimotakis (1984) and Hermanson & Dimotakis (1989). These experiments were designed to make measurements of the molecular mixing rate in supersonic shear layers.

3. Laser Rayleigh-scattering imaging experiments of non-reacting flows spanning the range from low to moderately high compressibility ($0.14 < M_{c1}^{(i)} < 0.96$). These experiments were designed to overcome the limitation of spanwise signal integration of the Schlieren imaging system which was used in the first two phases of the program. These Rayleigh-scattering experiments imaged a thin slice of the shear layer at the centerline location of the test section.

The Laser Rayleigh-scattering experiments are in the process of being analyzed at this time. The key results from the first two phases will be summarized below.

Figure 1 is a Schlieren photograph of a non-reacting He/Ar flow. This flow represents the highest compressibility investigated thus far ($M_{c1}^{(i)} = 0.96$). The shear layer is seen to grow linearly and does not appear to be dominated by the large-scale, two-dimensional structures found in incompressible shear layers. This absence of structure, in our experiments, is generally found even in the lower compressibility flows, a result that is somewhat at variance with the results of Clemens & Mungal (1990). Also visible in Fig. 1 is a pattern of shock and expansion waves in the low-speed fluid, created by shear layer structures travelling at supersonic velocities with respect to the low-speed stream. The inferred convection velocity of these structures is considerably higher than that predicted from the standard isentropic model, but it is in accord with the convection velocity measurements of Papamoschou (1989) and seems to be accounted for by a new theory for this behavior (Dimotakis 1991).

Figure 2 is a plot of normalized growth rate data in which the current results are compared to those of previous investigators. The agreement is seen to be good except for a few cases at low compressibility. Our results suggest the existence of two branches at $M_{c1}^{(i)} \simeq 0.1$, depending on whether the high-speed free stream is supersonic, or subsonic. The reasons for this difference are not understood at the present time, but they do suggest that the convective Mach number parameter $M_{c1}^{(i)}$ does not scale all of the compressibility effects in the planar shear layer.

In the reacting flow experiments, fast kinetics was achieved even in the highest compressibility flow ($M_{c1}^{(i)} = 0.96$) through the use of moderate concentrations (4%) of H_2 and F_2. The fast chemistry regime enables us to conduct 'flip' experiments (*cf.* Mungal & Dimotakis 1984, Koochesfahani & Dimotakis 1986) which yield estimates for the amount of molecular mixing in the shear layer. Figure 3 shows three temperature profiles across the shear layer for the $M_{c1}^{(i)} = 0.51$ flip experiments. The profile shifts toward the lean reactant in a manner similar to the incompressible experiments performed by Mungal & Dimotakis (1984), *etc.* Analysis of these data yields the following estimates for the volume fraction of molecularly mixed fluid within the shear layer:

$$\frac{\delta_m}{\delta} \simeq 0.40 \ , \quad \text{at} \quad M_{c1}^{(i)} = 0.51 \ , \qquad \text{and} \qquad \frac{\delta_m}{\delta} \simeq 0.31 \ , \quad \text{at} \quad M_{c1}^{(i)} = 0.96 \ .$$

These can be compared to the estimate $\delta_m/\delta \simeq 0.49$ for incompressible shear layers (Dimotakis 1989). While some of the difference may be attributable to the higher Reynolds numbers in these experiments, the inference to be drawn here is that compressibility *decreases* the molecular mixing in the shear layer.

These results are documented in a recently completed thesis (Hall 1991), which is available upon request. In the next set of experiments, presently in progress, we have increased the high speed stream Mach number to $M_1 = 2.5$.

A new high pressure combustion facility was built to investigate mixing and chemical reactions in an axisymmetric, turbulent jet. F_2 and NO, both diluted with N_2, were used in the first experiments as reactants. The line-integrated temperature rise was measured

by a set of long, thin, resistance wire thermometers stretched across the jet centerline at 16 downstream locations from $x/d_0 = 30$ to 240. Runs at several stoichiometric mixture ratios ϕ for Reynolds numbers in the range $10^4 \leq Re \leq 1.5 \times 10^5$ were performed to determine the dependence of flame length on Reynolds number. The Reynolds number was varied through density, *i.e.*, pressure, while the jet exit velocity and exit diameter were held constant. The time-averaged line integral of temperature, measured along the transverse axis of the jet by the wires, displays a logarithmic dependence on x/d^* within the flame zone, as had been conjectured. The line integral asymptotes to a constant value beyond the flame tip, as predicted from scaling and similarity arguments for a momentum-dominated jet.

The main result of the work is that the flame length, as estimated from the temperature measurements, varies with Reynolds number. Specifically, the normalized flame length L_f/d^* displays a linear dependence on ϕ with a slope that decreases up to $Re \simeq 2 \times 10^4$, and is then constant to the highest Reynolds numbers investigated. Additionally, the measurements revealed a "mixing virtual origin", defined as the far-field flame length extrapolated to $\phi = 0$, that increases up to $Re \simeq 2 \times 10^4$, and then decreases to the highest Reynolds numbers investigated. These results suggest that the mixing process is not Reynolds number independent up to $Re \simeq 1.5 \times 10^5$. A separate set of experiments indicated that the experiments above were momentum-dominated to the farthest measuring station and that the kinetics of the chemical reactions were fast compared to the characteristic mixing time. The transition from the momentum-dominated to the buoyancy-dominated regime was identified in another set of experiments. Significantly, using a jet velocity in excess of 60 m/s, the adiabatic flame temperature rise had to be less than 7 K for buoyancy not to influence entrainment to the farthest station ($x/d = 240$) investigated. A separate set of experiments investigated the dependence on Damköhler number and established the transition to the fast kinetics regime. A documentation of this work will be available as a thesis in the near future (Gilbrech 1991).

In recent experiments in liquid phase jets, we reaffirmed that scalar fluctuation spectra on the centerline of turbulent jets do not exhibit the k^{-1} regime that had been predicted by Batchelor (1959) at high wavenumbers, *i.e.*, at small spatial scales. This is in agreement with a recently appreciated argument, namely that such a spectrum power-law regime does not possess the correct asymptotic behavior in the limit of high Schmidt numbers (Dimotakis & Miller 1990). These experimental and theoretical findings have important consequences in the context of turbulent mixing and combustion. They suggest that the classical models for the strain rate field, at high Reynolds numbers and the smallest scales where non-premixed combustion at fast kinetics is taking place, need to be reexamined. The strain rate field, in turn, is responsible for such behavior as local extinction phenomena and finite kinetic rate effects in general. It has to be mastered to the point where it can be correctly described if reliable models of mixing and combustion are to be formulated.

In other experiments in liquid phase jets, we are examining the Reynolds number dependence of the behavior of scalar fluctuations and, by comparison with recently completed work in non-reacting, gas phase turbulent jet mixing (Dowling 1988, Dowling & Dimotakis 1990), also Schmidt number effects. Again, in the context of the interests of the AFOSR, the emphasis here is not so much on liquid phase mixing as on the behavior of the strain rate field at small scales. A first presentation of this work was made at a recent *IUTAM*

Symposium (Miller & Dimotakis 1990) and will appear in a special supplement to the May 1991 issue of the *Physics of Fluids A*. A more complete documentation of this part of the work will be available soon in the form of a Ph.D. thesis (Miller 1991).

Finally, we have made progress in our efforts to model non-premixed diffusion flames in turbulent jets. The model, dubbed the Two-Stage Lagrangian Model, is based on ideas proposed by Broadwell, Breidenthal, and Mungal in recent years (Broadwell & Breidenthal 1982; Broadwell 1987; Broadwell & Mungal 1988, 1990) and represents a joint development between Caltech; SANDIA, Livermore; and R. Dibble, presently at Berkeley. G. Mungal, at Stanford, has also participated in discussions that have contributed to this effort in the last few years. A recent progress report (Lutz *et al.* 1991) was made at the *AIAA Aerospace Sciences Meeting* (Reno, Nevada). Among other things, progress was made this last year in identifying the importance of buoyancy in the description and modeling of hydrocarbon diffusion flames, as was also recognized in the experimental gas phase, chemically reacting jet work described above.

References

BATCHELOR, G. K. [1959] "Small-scale variation of convected quantities like temperature in turbulent fluid. Part 1. General discussion and the case of small conductivity", *J. Fluid Mech.* **5**, 113–133.

BROADWELL, J. E. [1987] "A Model for Reactions in Turbulent Jets: Effects of Reynolds, Schmidt, and Damköhler Numbers", US-France Workshop on Turbulent Reactive Flows (Rouen, France), 7–10 July 1987. Published: *Turbulent Reactive Flows*, (eds. R. Borghi and S. N. B. Murthy, *Lecture Notes in Engineering* **40**, Springer-Verlag New York Inc., 1989), 257–277.

BROADWELL, J. E. and BREIDENTHAL, R. E. [1982] "A Simple Model of Mixing and Chemical Reaction in a Turbulent Shear Layer", *J. Fluid Mech.* **125**, 397–410.

BROADWELL, J. E. and MUNGAL, M. G. [1988] "Molecular Mixing and Chemical Reactions in Turbulent Shear Layers", Proceedings, 22nd *Symposium (International) on Combustion* (The Combustion Institute), 579–587.

BROADWELL, J. E. and MUNGAL, M. G. [1990] "Large-scale Structures and Molecular Mixing", *IUTAM Symposium on Fluid Mechanics of Stirring and Mixing* (La Jolla, California), 20–24 August 1990. To appear in *Phys. Fluids A* .

CHINZEI, N., MASUA, G., KOMURO, T. MURAKAMI, A. and KUDOU, K. [1986] "Spreading of two-stream supersonic turbulent mixing layers", *Phys. Fluids* **29**(5), 1345-1347.

CLEMENS, N. T. and MUNGAL, M. G. [1990] "Two- and Three-Dimensional Effects in the Supersonic Mixing Layer", 26th *AIAA/SAE/ASME/ASEE Joint Propulsion Conference* (Orlando, FL), 10–12 July 1990, AIAA-90–1978.

DIMOTAKIS, P. E. [1989] "Turbulent Free Shear Layer Mixing and Combustion", Pro-

ceedings, 9th *ISABE* (Athens, Greece), 3-9 September 1989, 58-79.

DIMOTAKIS, P. E. [1991] "On the convection velocity of turbulent structures in supersonic shear layers", *AIAA 22nd Fluid Dynamics, Plasma Dynamics and Lasers Conference* (Honolulu, 24-26 June 1990), AIAA-91-1724.

DIMOTAKIS, P. E. and MILLER, P. L. [1990] "Some consequences of the boundedness of scalar fluctuations", *Phys. Fluids A* **2**(11), 1919-1920.

DOWLING, D. R. [1988] *Mixing in gas phase turbulent jets*, Ph.D. thesis, California Institute of Technology.

DOWLING, D. R. and DIMOTAKIS, P. E. [1990] "Similarity of the concentration field of gas-phase turbulent jets", *J. Fluid Mech.* **218**, 109.

GILBRECH, R. J. [1991] *An Experimental Investigation of Chemically-Reacting, Gas-Phase Turbulent Jets*, Ph.D. thesis, California Institute of Technology.

HALL, J. L. [1991] *An Experimental Investigation of Structure, Mixing and Combustion in Compressible Turbulent Shear Layers*, Ph.D. thesis, California Institute of Technology.

HERMANSON, J. C. and DIMOTAKIS, P. E. [1989] "Effects of heat release in a turbulent reacting shear layer", *J. Fluid Mech.* **199**, 333-375.

KOOCHESFAHANI, M. M. and DIMOTAKIS, P. E. [1986] "Mixing and chemical reactions in a turbulent liquid mixing layer", *J. Fluid Mech.* **170**, 83-112.

LUTZ, A. E., KEE, R. J., DIBBLE, R. W. and BROADWELL, J. E. [1991] "A Model for Detailed Chemical Kinetics in Turbulent Nonpremixed Jet Flames", *AIAA 29th Aerospace Sciences Meeting*, 7-10 January 1991 (Reno, Nevada), AIAA 91-0478.

MILLER, PAUL, L. [1991] *Mixing in High Schmidt Number Turbulent Jets*, Ph.D. thesis, California Institute of Technology.

MILLER, P. L. and DIMOTAKIS, P. E. [1990] "Reynolds Number Dependence of Scalar Fluctuations in a Turbulent Jet", *IUTAM Symposium on Fluid Mechanics of Stirring and Mixing* (La Jolla, California), 20-24 August 1990, Paper PB.4. To appear, *Phys. Fluids A* (May 1991).

MUNGAL, M. G. and DIMOTAKIS, P. E. [1984] "Mixing and combustion with low heat release in a turbulent mixing layer", *J. Fluid Mech.* **148**, 349-382.

PAPAMOSCHOU, D. [1989] "Structure of the compressible turbulent shear layer", *AIAA 27th Aerospace Sciences Meeting*, 9-12 January 1989 (Reno, Nevada), AIAA Paper 89-0126.

PAPAMOSCHOU, D. and ROSHKO, A. [1988] "The Compressible Turbulent Shear Layer: An Experimental Study", *J. Fluid Mech.* **197**, 453-477.

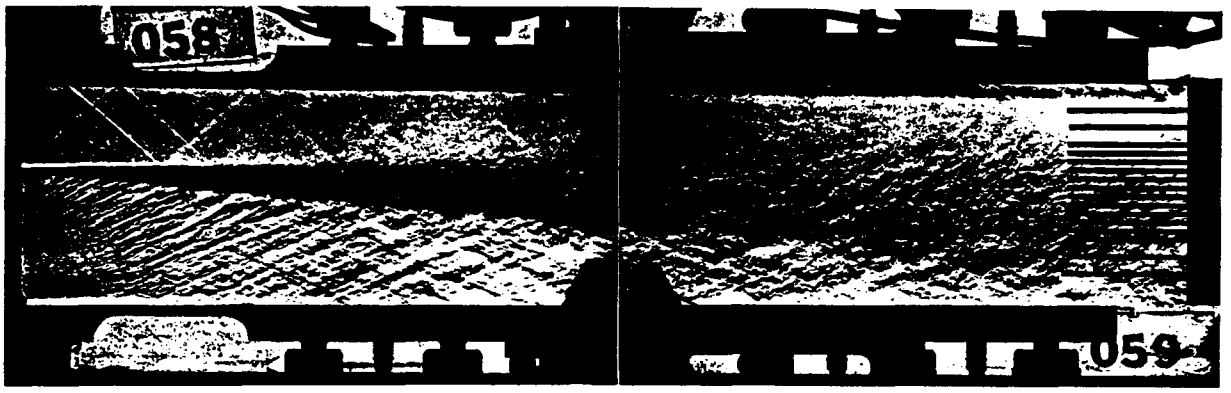

Fig. 1: Composite Schlieren Photograph For Case 1 (He/Ar) Flow.

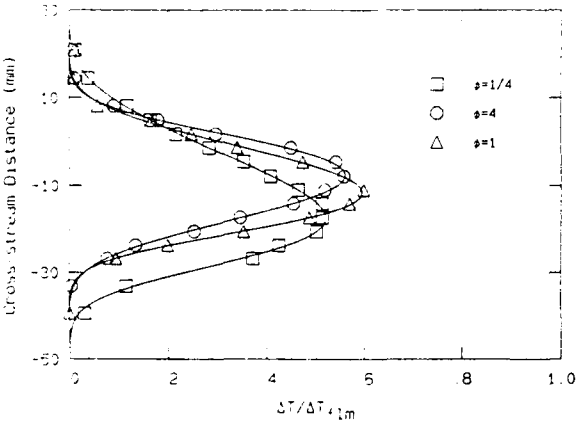

Fig. 3 Normalized Temperature Profiles For The Case 3 Flip Experiment

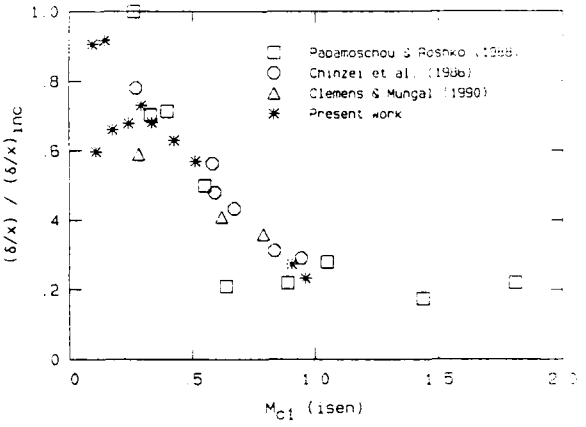

Fig. 2 Normalized Growth Rate of All Cases Plotted with Other Available Data

THEORIES OF TURBULENT COMBUSTION IN HIGH SPEED FLOWS

(AFOSR Grant No. 89-0310)

Principal Investigators: P.A. Libby and F.A. Williams
Department of Applied Mechanics and Engineering Sciences
University of California, San Diego, La Jolla, CA 92093-0310

SUMMARY/OVERVIEW

The objective of this research is to improve understanding of the chemical kinetics and fluid dynamics of turbulent combustion in high-speed flows. Supersonic combustion in hydrogen-air mixtures is being addressed by theoretical approaches that distinguish between reaction-sheet and distributed-reaction regimes. The work seeks to identify effects of compressibility in turbulent combustion, methods for including compressibility in theoretical analyses, and reduced chemical-kinetic mechanisms appropriate for supersonic combustion. The results may help to enhance capabilities of reasonable computations of high-speed turbulent reacting flows.

TECHNICAL DISCUSSION

Research from a previous AFOSR grant, the publication of which is being supported by the present grant, is listed as the initial references [1-3].

In new work, attention has been focused first on nonpremixed hydrogen-air combustion [4], for flight between altitudes of 20 and 70 km and at Mach numbers from 1 to 25, with combustor Mach numbers about 1/3 flight Mach numbers. The relevant Damköhler and Reynolds numbers were estimated for this range of conditions and found to lie in the reaction-sheet regime. Therefore, attention was focused on determining structures of hydrogen-air diffusion flamelets that may be elements of the turbulent diffusion flames under these conditions, for counterflow flames at pressures from 0.5 to 10 atmospheres and initial temperatures from 300 K to 1200 K. Numerical integrations were performed for air-side strain rates from 60 s^{-1} to extinction. The numerical results were compared with predictions of an asymptotic analysis that involved reduction to one-step chemistry through introduction of steady-state and partial-equilibrium approximations. Reasonable agreement was found for concentrations in the main reaction zone at low strain rates but not otherwise, thereby motivating the further reduced-mechanism studies discussed below.

The computations began with a 21-step mechanism but found 8 of the steps to be relatively unimportant, so that a 13-step mechanism (among 8 species, H_2, O_2, H, O, OH, HO_2, H_2O_2 and H_2O) was obtained. For counterflow hydrogen-air diffusion flames at normal atmospheric pressure with feed streams at room temperature these computations gave an extinction strain rate of 8140 s^{-1}, nearly twice the best experimental value available at the time. However, the experiments involved jets that had not closely approximated the potential-flow boundary conditions of theoretical computations. Subsequently, Pellett et al at NASA Langley (AIAA Preprint 91-0370) improved the experiment to match the boundary conditions of the theory better and obtained the results shown by the open circles in Fig. 1, giving an extinction strain rate of 8250 s^{-1} for the pure fuel, in excellent agreement with our prediction. We recently extended our calculations to diluted fuels, obtaining the squares marked "theory" in Fig. 1. The agreement with experiment is seen to remain excellent over the entire dilution range. For comparison, earlier computational results by Dixon-Lewis (triangles) and recent computations by Isaac and Ho (diamonds) also are shown in Fig. 1. The latter are in reasonable agreement with our results; differences are attributable mainly to selection of different rate parameters for elementary steps.

Experimental results for counterflow axial velocity v_z as a function of axial coordinate z will depend appreciably on flow configuration, as may be inferred from Fig. 2, which applies to a methane-air diffusion flame with plug-flow boundary conditions. These and other aspects of flamelet models of turbulent flames have been discussed in a review [5] that soon will appear. New theoretical analyses [6] have applied asymptotic methods for large Reynolds and Zel'dovich numbers to predict displacement effects resulting from heat release in different counterflow configurations. Figure 2 shows an illustrative result that indicates how a two-term outer expansion improves agreement with experiment for the velocity profiles in the outer zones as well as for the location z_s of the stagnation plane. In this example the air-side strain rate of 540 s^{-1} for the one-term expansion is increased to 710 s^{-1} for the two-term expansion, demonstrating the importance of the displacement correction.

Since peak combustor temperatures on the order of 3000 K are anticipated for some operating conditions with hydrogen-air flames, questions arose concerning possible influences of nitrogen chemistry on flame structure and extinction. We therefore augmented our chemical-kinetic scheme to include nitrogen chemistry. Representative results shown in Fig. 3 demonstrate negligible influences of nitrogen chemistry on flame structure and extinction. The largest effect was a decrease in peak flame temperature by about 30 K when 10^{-3} ppm of NO was added to the air stream. For these developed flames nitrogen chemistry is unimportant; influences on ignition have not yet been investigated.

Simpler kinetics are desirable to enable computations to be performed in more complex configurations. For this reason, the effect of deleting H_2O_2 from the system was investigated. Figure 4 demonstrates the negligible effect of H_2O_2 on temperatures and extinction for operating conditions of interest. Further simplification is provided by employing reduced chemical-kinetic mechanisms. A four-step mechanism is obtained by imposing steady states for HO_2 and H_2O_2, and a three-step mechanism results from further introducing an O-atom steady state. Some flame-structure computations have now been completed with each of these reduced mechanisms. Figures 5-8 show results from the four-step mechanism for the dependence of peak temperature and of hydrogen and oxygen mole fractions on the mixture fraction based on specific enthalpy. The agreement with results of the full mechanism is seen to be good and to improve with increasing strain rate, over the range of these figures. This suggests utility of reduced mechanisms. Of greatest interest will be a two-step mechanism, obtained by postulating an OH steady state as well. Work is proceeding towards flame-structure calculations with this two-step mechanism.

Further research towards ascertaining influences of kinetic energy, compressibility and high Mach numbers in high-speed combustion has identified an integral equation that can be used to analyze compressible counterflows between parallel porous plates [7]. It was observed that this same general type of formulation can describe rotational compressible flow in solid-propellant rocket-motor ports, and therefore the corresponding analysis was developed [8], with applications to choking in nozzleless rocket motors. These studies indicate general characteristics of compressibility effects relevant to supersonic combustion. Future work is intended to address influences of large pressure and temperature fluctuations on the combustion in high-speed flows.

REFERENCES

1. S.C. Li, "Optical Measurement of Size Histories of Boron Particles in Ignition and Combustion Stages in a Flat-Flame Burner," Combustion Science and Technology, to appear, 1991.

2. S.C. Li and F.A. Williams, "Ignition and Combustion of Boron in Wet and Dry Atmospheres," Twenty-Third Symposium (International) on Combustion, The Combustion Institute, Pittsburgh, to appear, 1991.

3. S.C. Li and F.A. Williams, "Ignition and Combustion of Boron Particles," Second International Symposium on Special Topics in Chemical Propulsion: Combustion of Boron-Based Solid Propellants and Solid Fuels, Lampoldshausen, West Germany, 1991.

4. E. Gutheil and F.A. Williams, "A Numerical and Asymptotic Investigation of Structures of Hydrogen-Air Diffusion Flames at Pressures and Temperatures of High-Speed Combustion," Twenty-Third Symposium (International) on Combustion, The Combustion Institute, Pittsburgh, to appear, 1991.

5. P.A. Libby, "Comments on the Interaction of Turbulence and Chemical Kinetics," Proceedings of the ICASE/NASA Combustion Workshop, to appear, October 1989.

6. J.S. Kim, P.A. Libby and F.A. Williams, "On the Displacement Effects of Laminar Flames," Western States Section, The Combustion Institute Boulder, CO, March 19, 1991.

7. G. Balakrishnan, A. Liñán and F.A. Williams, "Compressibility Effects in Thin Channels with Injection," AIAA Journal, to appear, July, 1991.

8. G. Balakrishnan, A. Liñán and F.A. Williams, "Inviscid Flow in Laterally Burning Solid-Propellant Rocket Motors," Western States Section, The Combustion Institute, San Diego, CA, October 14-16, 1990.

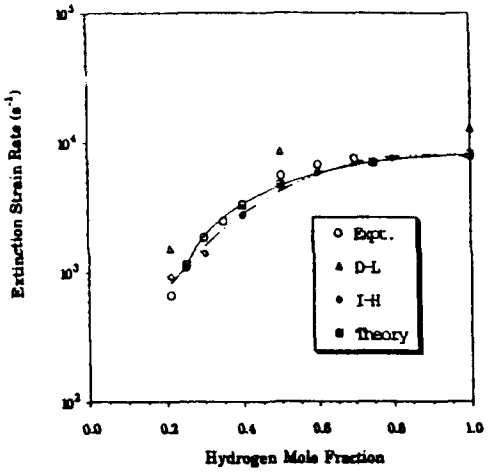

Fig. 1 The dependence of the air-side extinction strain rate on the hydrogen mole fraction in the fuel stream for counterflow mixing of hydrogen-nitrogen mixtures with air at 1 atm and 300 K feed-stream temperatures with potential-flow boundary conditions.

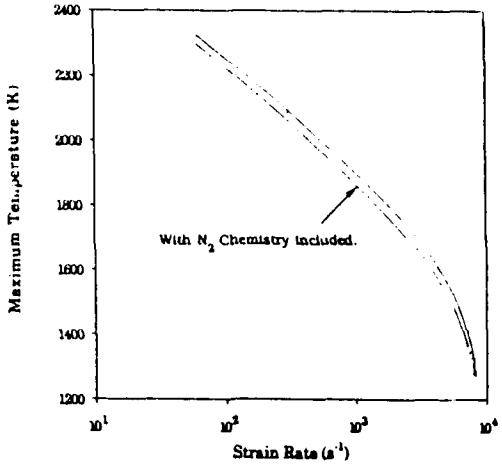

Fig. 3 The maximum temperature as a function of strain rate with and without nitrogen chemistry included for hydrogen-air diffusion flames at 1 atm and 300 K feed-stream temperatures.

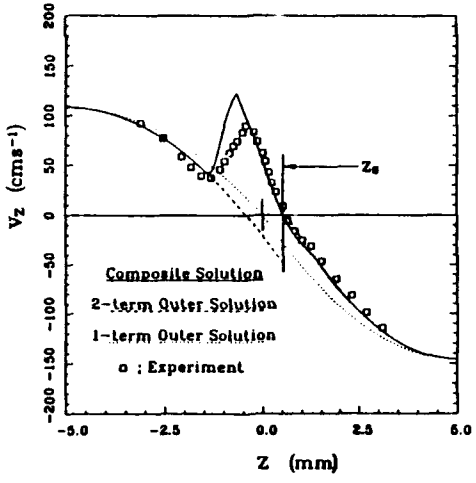

Fig. 2 The axial velocity as a function of the axial distance, for a methane-air diffusion flame at 1 atm with room-temperature feed streams, comparing LDV experimental results of Law et al (points) with one-term and two-term asymptotic expansions for the outer solutions as well as the composite expansion.

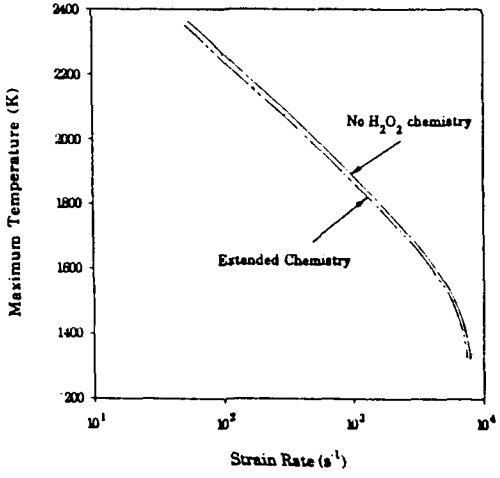

Fig. 4 The maximum temperature as a function of strain rate with and without H_2O_2 chemistry included for hydrogen-air diffusion flames at 1 atm and 300 K feed-stream temperatures.

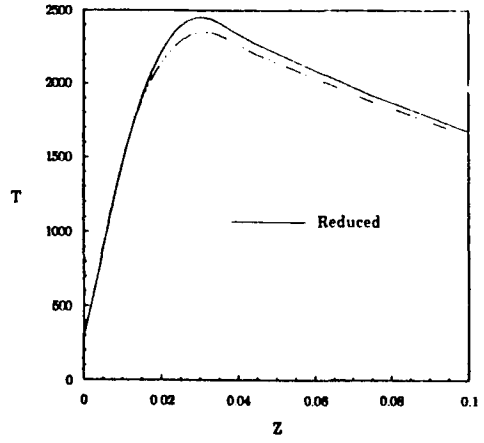

Fig. 5 The dependence of the temperature on the mixture fraction based on the specific enthalpy for hydrogen-air diffusion flames at 1 atm and 300 K feed-stream temperatures, for full and four-step (reduced) mechanisms, at an air-side strain rate of 60 s^{-1}.

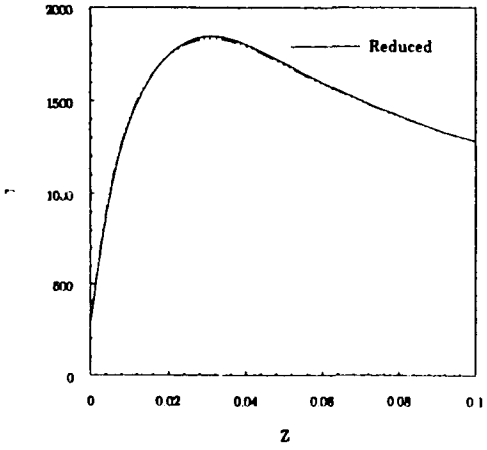

Fig. 6 The dependence of the temperature on the mixture fraction based on the specific enthalpy for hydrogen-air diffusion flames at 1 atm and 300 K feed-stream temperatures, for full and four-step (reduced) mechanisms, at an air-side strain rate of 1500 s^{-1}.

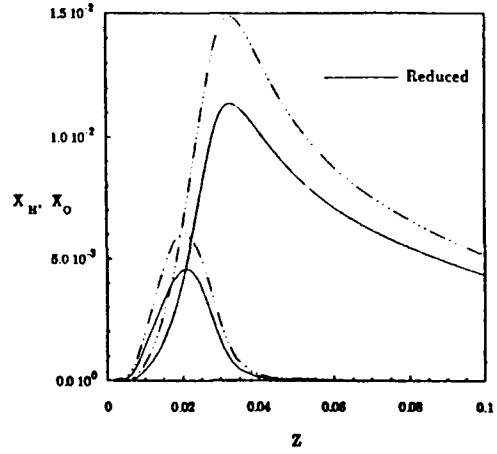

Fig. 7 The dependence of the hydrogen and oxygen mole fractions on the mixture fraction based on the specific enthalpy for hydrogen-air diffusion flames at 1 atm and 300 K feed-stream temperatures, for full and four-step (reduced) mechanisms, at an air-side strain rate of 60 s^{-1}.

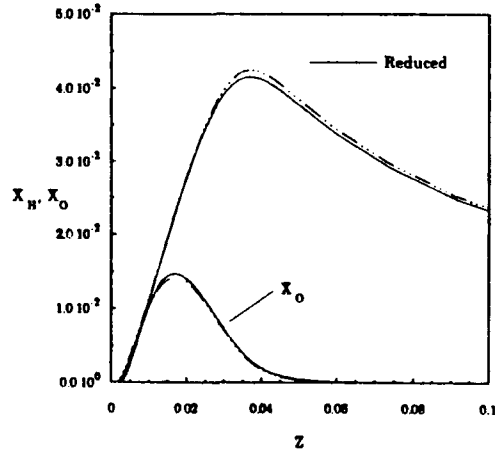

Fig. 8 The dependence of the hydrogen and oxygen mole fractions on the mixture fraction based on the specific enthalpy for hydrogen-air diffusion flames at 1 atm and 300 K feed-stream temperatures, for full and four-step (reduced) mechanisms, at an air-side strain rate of 1500 s^{-1}.

THE EFFECTS OF COMPRESSIBILITY ON A SUPERSONIC MIXING LAYER

AFOSR Contract No. F49620-88-C-0003

Principal Investigator: David Nixon

Nielsen Engineering & Research, Inc.
510 Clyde Avenue
Mountain View, CA 94043-2287

OVERVIEW

The objective of the work is to identify the flow mechanisms that cause the decrease in spreading rate of supersonic mixing layers as the convective Mach number increases and to suggest means of enhancing the mixing. Two approaches have been taken, one numerical and one analytic. A computer code, TMRC,[1] has been used to simulate both time and space developing two-dimensional mixing layers to get some indication of the flow physics. In addition, three-dimensional spatially developing mixing layers have been simulated. The numerical studies indicate that some accuracy problems may exist in existing algorithms. To complement the numerical study a simple analysis[2] has been developed which explains the variation of mixing rate with convective Mach number. The analysis seems to indicate that little can be done to enhance mixing as such, although the real problem of simultaneous mixing and combustion may be more amenable to control. The analysis[3] has been extended to include heat release as a first step in this direction. The following discussion is concerned with the numerical simulations; the initial analysis has been presented in earlier meetings.

TECHNICAL DISCUSSION

Numerical simulations of both time and space evolving mixing layers have been performed. The code used is TMRC which is a fourth-order accurate code developed at Nielsen Engineering & Research (NEAR) for impinging jet flows. These calculations were performed to get some insight into two-dimensional mixing layers; a typical example of such a calculation is shown in Figure 1. At present the numerical results are similar to those obtained by other investigators.

Two- and three-dimensional numerical simulations of a compressible shear layer at a convective Mach number of M_c were calculated to investigate the hypothesis that three-dimensionality was essential to maintaining mixing at high values of M_c. This was believed to be true because the explicit effects of compressibility, found so important in NEAR's theory of reduced mixing, would be relieved through allowance for spanwise flow. The results of the simulation displayed in Figures 2 and 3 lend support to NEAR's belief in the importance of three-dimensional flow. In Figure 2 spanwise vorticity contours, ω_z, are plotted for two-(top) and three-(bottom) dimensional flow; in Figure 3, the layer growth rates of the two simulations is plotted. As is apparent in both figures, the three-dimensional layer grows most quickly. By examining planar Mach numbers in both simulations, the

three-dimensional flow is found to be less prone to shock formation because of relief through the spanwise direction. Just as shock formation over swept wings is dependent upon the Mach number normal to the leading edge, and not that parallel to the chord, so also in these three-dimensional mixing layers, it is the Mach number of the flow projected on xy planes (the plane of the two-dimensional calculation), rather than the total Mach number, that expresses the effect of compressibility. In the two-dimensional flow, Mach numbers vary between -.59 and .69 when referenced to the frame moving at M = 1.5, the nominal speed of the large eddies. To compare the three-dimensional flow on this basis, its total Mach numbers were projected onto planes $z = constant$. In 20 of the 23 z coordinate planes (i.e., 80% of the flow volume), the projected Mach numbers in the moving reference frame were less than within the two-dimensional flow. Reduction of both positive and negative Mach numbers in this reference frame ranged from 19% to 8%, with an average of 13% in both cases. Even if the three planes (in which some of the planar Mach numbers were greater than within the two-dimensional flow) were added, the average Mach number variation in the entire flow runs between -.51 and .63, a 13% and 9% reduction compared to the two-dimensional case.

It is apparent from these considerations that the shear layer does find a relief from the effects of compressibility through flow in the spanwise direction. This is true even when the convective Mach number is relatively low. There does not seem to be a reason why similar relief should not be obtained at higher convective Mach numbers. As M_c increases, three-dimensional velocities will allow the flow to avoid shocks longer and make them weaker when they inevitably appear.

An attempt was made to calculate a case where shocks occur in the two-dimensional flow, and then add longitudinal vortices to see if shock formation could be delayed or weakened with an accompanying increase in mixing. At $M_c = 1$. a two-dimensional flow with shocks was obtained, but attempts to establish a strongly three-dimensional flow at this condition failed due to numerical problems. The inability of artificial dissipation mechanisms to handle the more rapid growth of small scales due to vortex stretching in three dimensions resulted in nonphysical results for the density. It was judged more prudent to accept failure at this condition than attempt extraordinary measures that might reduce the connection between simulation results and flow physics. It is believed that this is a general problem in time dependent simulations at these kinds of flow conditions, and deserves further study.

In the hopes of increasing the efficiency and accuracy of projected numerical simulations of two- and three-dimensional shear layers, new classes of finite difference and related finite volume techniques were investigated. These techniques (so called Padé, or compact schemes) were described in a recent paper by Lele.[4] At the cost of some small extra numerical work, such schemes theoretically provide greater accuracy and superior ability to capture steeper gradients than standard central difference or finite volume techniques on the same grid. Interest at NEAR centered on the finite volume formulation. In the course of thoroughly investigating it, NEAR discovered that the finite volume formulation actually produced neither the accuracy nor the gradient capturing ability predicted.

In essence the finite volume technique requires two steps: an interpolation and then a difference. Even though the interpolation step is optimized for accuracy and gradient capturing, the result after differencing two such interpolants has neither of these properties, and it is the differenced result which is the final approximation to the partial differential

equation. Thus the difference between two fourth-order interpolants produces a second-order approximation to the *pde* with gradient capturing ability little improved over standard finite volume techniques. The technical details behind the degradation of these techniques' desirable properties are described in Ref. 2, along with a modification to the formulation, developed at NEAR, that recovers both its accuracy and gradient capturing abilities. The phenomena described there and their solution have general applicability to all finite volume techniques, not just these Padé schemes. The fix is counterintuitive, for one obtains a higher order approximation to a *pde* by lowering, not raising, the accuracy of the interpolation process which is one of the two constituents of the technique. The effectiveness of NEAR's modifications for recovering accuracy can be seen in Figure 4, where the final error terms actually resulting from interpolation and then differencing using the schemes originally proposed by Lele, and those developed by NEAR, are plotted. The original technique (triangles)has final approximation errors proportional to h^2 (h = grid spacing), though the interpolation was accurate to h^4. NEAR's modified scheme (circles) has final errors proportional to h^4, though the interpolants are only accurate to h^2. Lastly is shown (inverted triangles) a NEAR-developed scheme that obtains an h^{10} final approximation from an h^2 interpolation, though at the cost of reduced gradient capturing ability.

After reformulating the finite volume technique to recover its desirable properties, the technique was implemented in NEAR's numerical code. There it proved to work fine at low Mach numbers, but was unusable in situations where shocks were expected. Apparently because of its ability to capture steeper gradients, standard artificial dissipation techniques needed to smooth pre- and post-shock oscillations were ineffective. The method had to be scrapped as a result, and all numerical simulations were run with fairly standard finite volume techniques. Complementary artificial dissipation methods for Padé finite volume techniques must be invented if these schemes are to be useful in compressible flows.

REFERENCES

1. Childs, R. E.: Jet Noise Predictions from Unsteady Navier-Stokes Simulations. AIAA Paper 91-0493, 1991.
2. Nixon, D., Keefe, L. R., and Kuhn, G. D.: The Effects of Compressibility on a Supersonic Mixing Layer. AIAA Paper 90-0706, 1990.
3. Nixon, D., Keefe, L. R., and Kuhn, G. D.: Effects of Compressibility on a Supersonic Mixing Layer. NEAR TR 421, 1991.
4. Lele, S.: Direct Numerical Simulation of Compressible Free Shear Flows. AIAA Paper 89-0374, 1989.

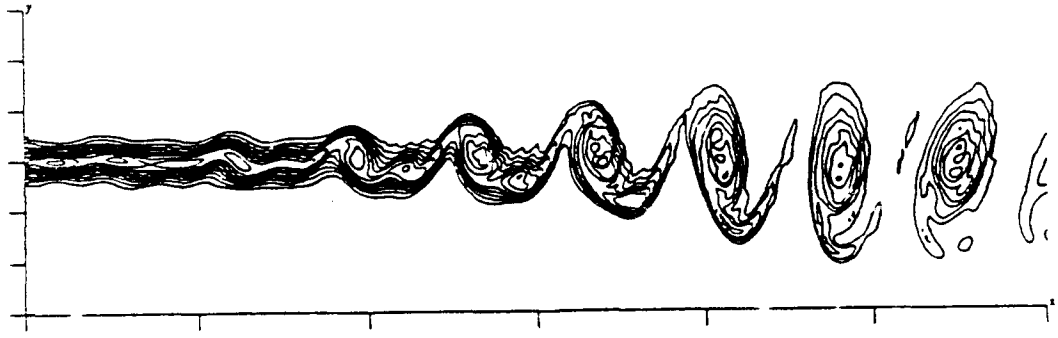

FIGURE 1. Vorticity contours in a two-dimensional mixing layer. $M_1 = 2.0$, $M_2 = 1.2$, $M_c = .4$.

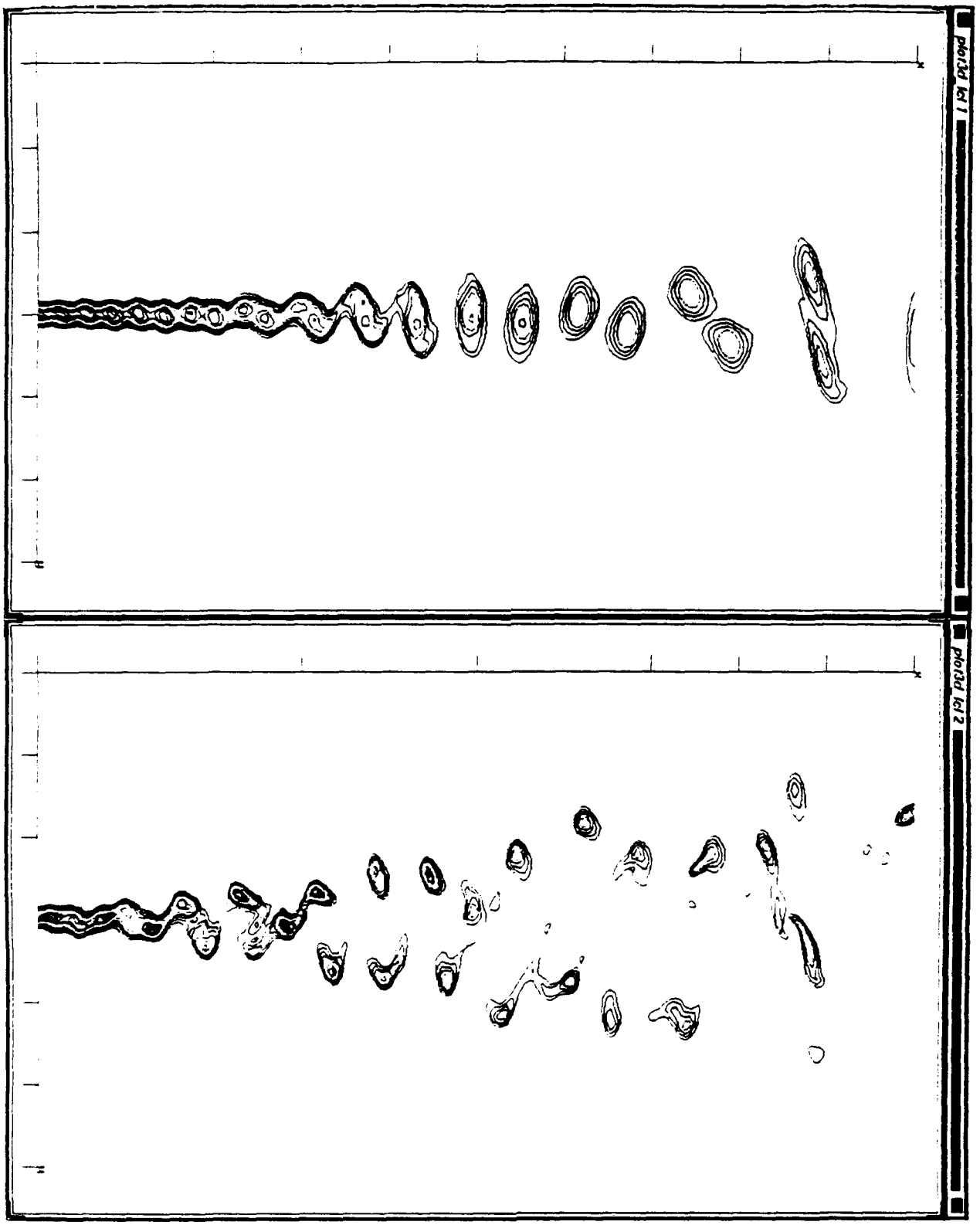

Figure 2. - Spanwise Vorticity Contours in Two- and Three-Dimensional Shear Layers.

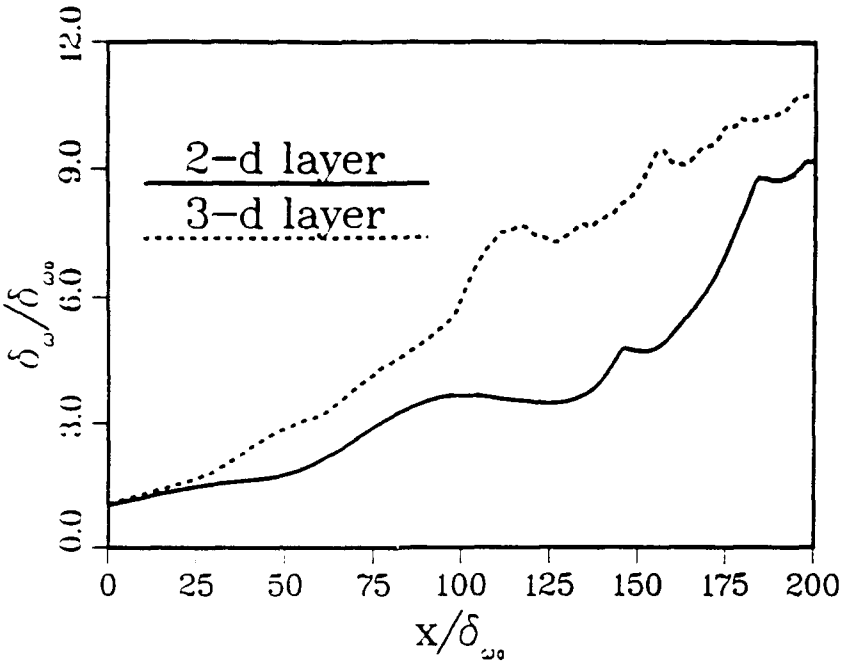

Figure 3. - Initial Shear Layer Growth Rates, M_c=.4.

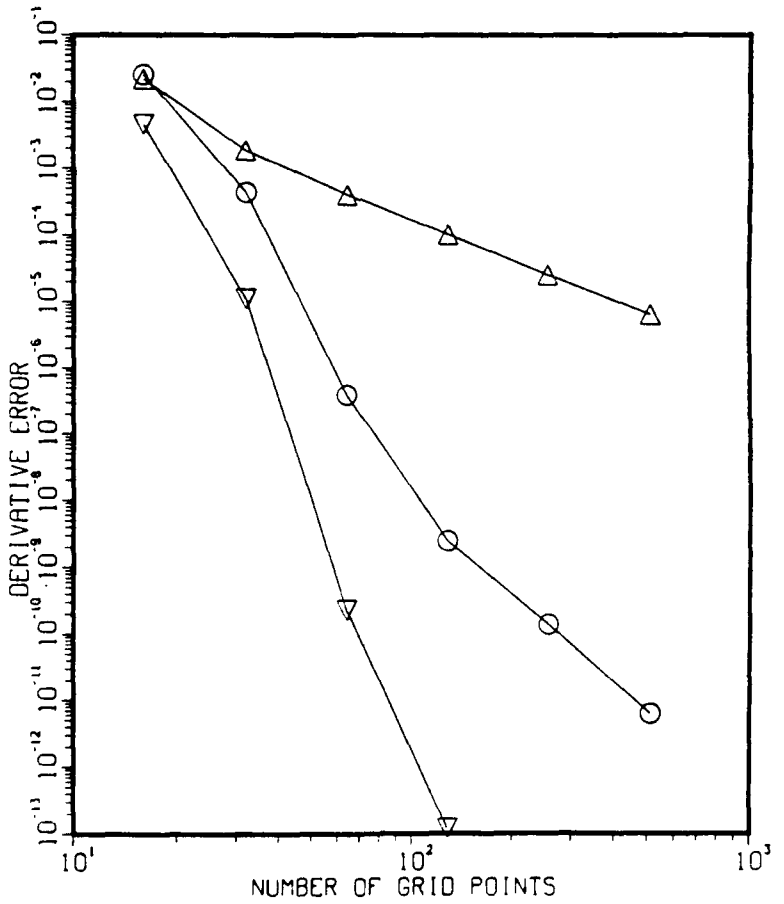

Figure 4. - Error in calculating derivative of sinx when differencing interpolants from Lele's and two NEAR-developed interpolation schemes.

FLOW-TAGGING VELOCIMETRY USING UV-PHOTODISSOCIATION OF WATER VAPOR

AFOSR 2308S101

A. S. Nejad
Advanced Propulsion Division
Aero Propulsion and Power Directorate
Wright-Patterson AFB, Ohio 45433

Summary/Overview: The feasibility of using a flow tagging technique for flow velocity measurement has been studied. The technique is base on photodissociation of water molecules (a natural species in most wind tunnels and combustion devices) resulting in the formation of OH photofragments which is used to mark the flowfield of interest. The displacement of the OH radical was measured as a function of time by laser induced fluorescence as an indication of the flow velocity. The study showed that the OH-photofragment has long chemical lifetime (roughly 150 μsec) to allow measurements of velocity over a wide range. The technique was then applied to study the flow characteristics of three sonic under expanded jets.

Introduction: The need to study high-speed flows encountered in advanced combustion systems (scramjets) has imposed additional constraints on flow diagnostic techniques. Nonintrusive velocity measurement schemes can be classified as follows; 1) particle-based methods i.e., laser Doppler Velocimetry and particle image velocimetry; 2) molecular Doppler-shift techniques (with planar laser-induced Fluorescence detection); 3) flow tagging methods (RELIFE and OH-Flow tagging). Particle based methods have received the most attention in the past because of their ease of applications and measurement accuracy. However, these techniques suffer from seeding problems (not quite nonintrusive!). In supersonic flows particle lag time (velocity slip) can be a great source of measurement error. The second method is base on molecular Doppler shift of a probe gas, which is measured by laser induced fluorescence (LIF) to determine the velocity of the flowfield. Extension of this technique to planar measurements has allowed two dimensional time-averaged velocity measurements. However, because the doppler shift of most gases is relatively small, this technique is good for velocity measurements in access of 100 m/s. Two dimensional measurements is also possible but it requires multiple cameras and laser systems. Although flow tagging technique is not new, it offers an alternative approach for making a wide range of velocity measurements. In its simplest form, flow tagging consists of marking the flow either chemically or radiatively and probing the flowfield at later time for spacial displacement of the tag. Two-photon photodissociation of water vapor to form the OH-radical has recently been demonstrated to be possible. This effort was focused to explore the possibility of using photodissociation to form OH radicals, study its chemical life time, and identify the optimum pump and probe wavelengths for radical production and interrogation.

Photodissociation of water vapor via Rydberg state to form electronically excited OH-photofragments has been studied in the past. Figure 1 is the schematic representation of the four lowest electronic states of water which are involved in photodissociation at energies < 10 eV. The potential energies are plotted as a function of OH-H separation which identifies three distinct dissociation processes. The first involves A^1B1 state at wavelengths longer that roughly 150 nm. The potential energy surface for this system is highly repulsive causing fast and direct dissociation. The OH radicals are in the electronic ground state (rotationally cold however, vibrationally excited). Dissociation processes involving wavelengths shorter than roughly 150 nm where absorption and dissociation proceed via B^1A1 state is also shown. The potential energy surface for this state is more complex than the previous state. The B^1 state is generally less repulsive than the A^1 state. The third photodissociation processes involve wavelengths below 125 nm. This results in direct excitation of the C^1B1 state. Where the C^1 state is strongly coupled to B1 and leads to fast predissociation. Observation of resolvable rotational structures implies predissociation lifetime of picoseconds in range. This opens an alternative channel, bound-free C to A spontaneous emission, which is followed by a fast and direct dissociation via repulsive A^1 state. The lifetimes within the C^1 state evidently are long enough to allow observation of weak emission at 4120 nm. Fotakis was the first to demonstrate that water could be photodissociated via C^1B1 state employing the 248-nm radiation of KrF excimer laser. Subsequent studies have allowed determination of the photodissociation mechanisms in this state by using a tunable excimer laser. Emission from the OH fragment can be directly observed at 308-nm, however this emission is very short lived and is not suitable for flow tagging. Thus the OH fragment is allowed to relax to its ground state and then is probed by LIF.

Experimental setup: The experimental apparatus for making excitation and dispersion scans of water vapor and of the tunable OH-photofragment is shown in figure 2. A tunable Lambda-Physik model 150T MSC KrF laser was used to photodissociate the water molecule. The fluorescence from this molecule was dispersed and recorded with A JY 0.6-m monochromator. Excitation scans were made by incorporating a stepping motor onto the micrometer shaft of the tuning grating of the KrF laser. This allowed the grating angle, (i.e., wavelength) to be precisely tuned from 40200 to 40325 cm^{-1}. For an excitation scan, the monochromator was set to a fixed frequency corresponding to water (420-nm) or the OH photofragment (310-nm). The slit of the monochromator was typically set for one 1 nm resolution during excitation and dispersion scans. The fluorescence signal was detected using a 955QB photomultiplier and amplified and digitized by means of a LeCroy ADC module. Digitized data were collected and processed with a Macintosh IIx computer. Dispersion scans were done by using the same equipment except that the wavelength of the excimer laser was fixed and that of the monochromator was scanned.

Three different nozzle designs.(flat, inner tapered, and outer-tapered) were examined in this study. In all three cases, the fuel tube utilized was straight stainless steel tube, 125 mm long with and I.D. and O.D. of 1.91 and 3.18 mm respectively. The blunt tip thickness of the flat top injector was the same as the tube thickness, roughly 0.5 mm. The inner and outer tapered nozzles had a tip thickness of less than 0.1 mm. Six nitrogen gas bottles were manifolded together to act as a single large high pressure fuel source. The gas pressure was monitored at both the manifold and the inlet side of the tube. An eight inch diameter plenum chamber was

used to condition and preheat the flow prior to injection. This settling chamber was also used to mix the nitrogen gas with water vapor necessary for OH flow tagging.

Preliminary Results and Discussion: Figure 3a shows the experimentally observed intensity of the OH fluorescence as a function of time delay between the pump and probe lasers. Surprisingly, the maximum OH population did not occur at the zero time delay but at 1 to 2 μsec after the pump excitation which was about 50 nsec in duration. The apparent OH concentration decreases in a near-exponential fashion from 1 μsec point and displays an 150 μsec lifetime. The relatively long lifetime of the OH radical allows velocity measurements in low and high speed flows. The chemical lifetime of the OH radical in a premixed propane flame is depicted in figure 3b. Note that the lifetime of the photofragment is nearly identical to that observed in the cold flow conditions. This is an improvement over the RELIEF method where the lifetime of the vibrationally excited O_2 molecules drastically decreases with increasing temperature.

The selection of an optimum time delay between tag formation (pump) and interrogation (probe) is determined by the signal strength (tag chemical lifetime) and flow velocity. Since the lifetime of the OH radical is relatively long, a wide range of time delays is possible to optimize the velocity resolution. In general, the longer the interval between the pump and probe the better the velocity resolution (i.e., smaller m/s per pixel). However, longer time delay results in poorer spatial resolution. In this study a 1-mm maximum spatial displacement was selected translating to 2.5 μsec time delay between pump and probe. By chance, the time delay corresponded to maximum OH signal which caused good signal to noise images for analysis. In figures 4(a-h) images from a typical data acquisition are shown. Figure 4(a) shows the image of the tag line taken in room air without jet flow. The OH radical was not displaced and resulted in a straight line image which served as zero reference line. Figures 4(b-g) show the OH line displacement with the jet in operation. These individual shots can be collected to form a statistical description of the of the velocity field. Figure 4(h) is an example of mean velocity resulting from statistical averaging of 500 images. The average velocity profiles sampled at various downstream locations of the jet flow with flat-tip nozzle are shown in figure 5(a-i).

In conclusion, this study shows the effectiveness of OH photofragmentation for velocity measurement in high speed flows. It appears that OH is a suitable tag with long chemical lifetime (150 μsec). Line measurements of the instantaneous and mean velocities for the jet flows having speeds in excess of 635 m/s were obtained with this technique. It appears that the flat tip nozzle produced better overall mixing while the inner tapered nozzle was able to produce a jet which penetrated the free stream more effectively.

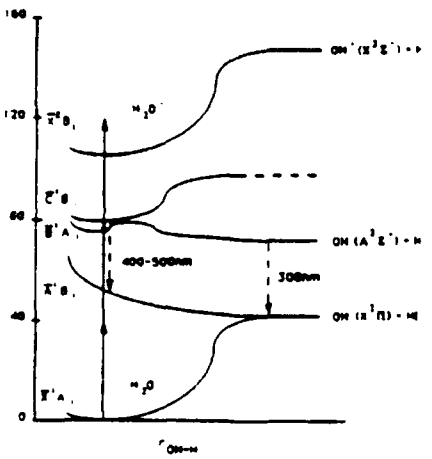

Fig 1. Correlation digram of processes in photodissociation of water

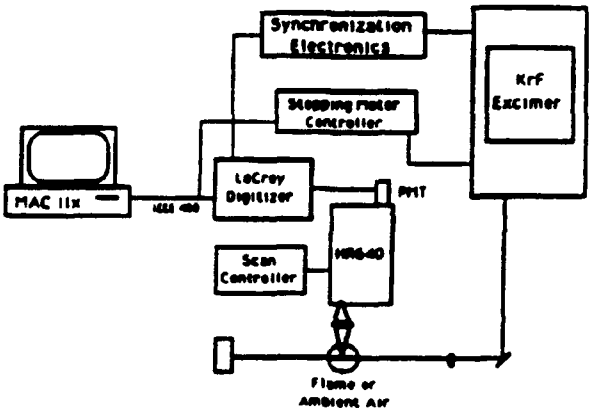

Fig 2. Experimental setup for making excitation and dispersion scans of water

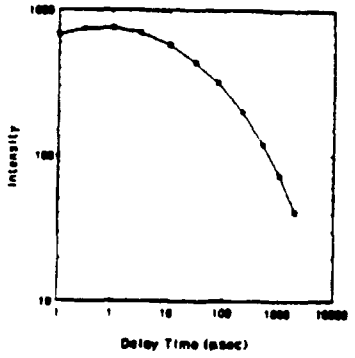

(a)

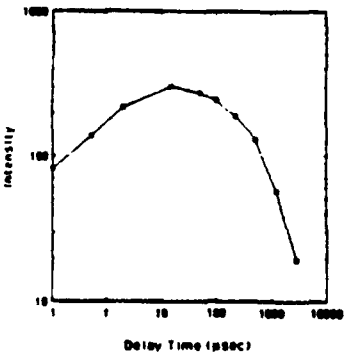

Fig 4. Observed chemical lifetime of OH-photofragment; (a) ambient, (b) flame condition

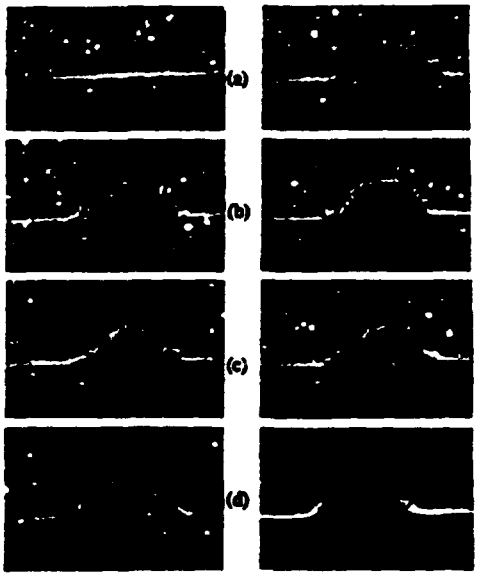

Fig 4. Examples of OH-flow-tagging images

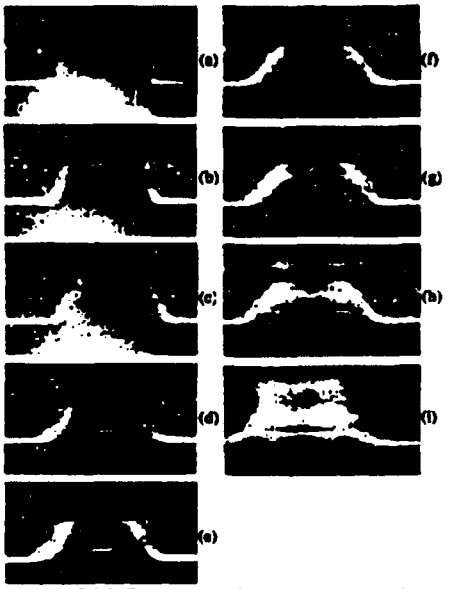

Fig 5. Mean OH-flow-tagging images of jet flow issued from flat tip nozzle

IGNITION AND MODIFICATION OF REACTION BY ENERGY ADDITION: KINETIC AND TRANSPORT PHENOMENA

AFOSR Contract No. F49620-90-C-0070

Principal Investigators: Francis E. Fendell and Mau-Song Chou

Center for Propulsion Technology and Fluid Mechanics
TRW Space and Technology Group, One Space Park, Redondo Beach, California

SUMMARY/OVERVIEW

High-speed air-breathing combustion systems necessitate the complete release of chemical energy during the relatively brief residence time of reactants within combustors of practical length: mixing, ignition, and chemical reaction must be achieved in a relatively short time. We address, from a fundamental chemical-kinetics and fluid-transport point of view, the use of both alternative, photochemical ignition (by laser irradiation) and ignition-promoting additives, in order to alter chemical-reaction pathways to achieve rapid ignition and enhanced combustion rate. We also address the influence of mixture inhomogeneity, and of departure from stoichiometric proportion in fuel/air mixtures, on the processes of ignition, flame development, and flame propagation. Chemical systems of particular interest include hydrogen/air and methane/air, often with trace amounts of carefully selected sensitizers (Chou et al. 1989). We seek to identify optimal circumstances [minimal input energy, minimal amount of sensitizer(s), etc.] for achieving ignition and burnup with currently available optical sources both by irradiating premixtures flowing faster than the adiabatic flame speed, and by carrying out supporting approximate analyses of these experiments.

We also analyze theoretically the use of direct photochemical initiation of a train of very closed spaced spherical detonations, so that an oblique (conical) detonation wave is stabilized in a very-fast-flowing gaseous fuel/air mixture. A combustor within which the flow is everywhere supersonic (except in near-wall layers), and for which relatively small entropy rise occurs, may be based on such a stabilized wave.

TECHNICAL DISCUSSION

We have discussed the stabilization via postulated, temporally continuous sources (plane, line, and point) of nonintrusive energy deposition into the burned gas of a mixture flowing very modestly faster than its adiabatic flame speed (Carrier et al. 1990). A less-energy-demanding flame stabilization would be achieved by the initiation of a train of very closely spaced spherical deflagrations, each evolving from a transient, point-like, ignition-achieving deposition of energy at a fixed site in the flowing unburned mixture. The downwind interaction of the periodically initiated, individual spherical deflagrations results in a burned-gas region enveloped by unburned gas; the "separatrix" is well approximated by the deflagration-wave locus for the just-discussed continuous point source. In connection with the early evolution of a laminar spherical flame from an individual, very localized ignition, we took note of the purported interplay of equivalence ratio, differing diffusivities for reactant species and heat, and

flame curvature in some hydrocarbon-vapor/air mixtures (Strehlow 1984, pp. 390-392). Actually, the oft-cited experimental data (concerning spherical-flamefront deceleration with increasing flamefront radius, for some sufficiently fuel-rich mixtures) seem more likely to be evidence of soot-associated, radiative-heat-loss effects on flamefront propagation speed, rather than evidence of flame-curvature-associated phenomena (Carrier et al. 1991a, 1991b, 1991d).

In any case, the typical value for a laminar flame speed is highly subsonic, and very much less than the speed of the oncoming stream in many practical aerodynamic contexts. A very large number of energy-deposition sources, situated transverse to a stream of fast-flowing premixture, would be required to span that stream with flame, within a modest distance downwind of the plane containing the sources. Furthermore, while the intention might be to initiate nonintrusively the stabilization of a deflagration wave that spans the stream, the inadvertent result might be the creation of a normal detonation wave, which incurs a large rise of entropy. Such a large entropy rise implies the unavailability of much energy to do useful work. Therefore, attention is turned to the use of nonintrusive energy deposition in a supersonically flowing mixture, not to initiate a flame propagation, but rather to initiate a detonation (Carrier et al. 1991c).

As background, we know that a Chapman-Jouguet (CJ) detonation can be initiated directly by a laser-type pulse in a combustible mixture of gases with an appropriate stoichiometry (Lee et al. 1978; Strehlow 1984, pp. 408-409). For certain fuel-air mixtures, we have some preliminary data on the minimum-energy requirements, the pulse-duration requirements, and the deposition-volume requirements (Lee et al. 1978). We think that there is a broad range of pulse parameters (energy, volume, duration) over which the CJ detonation will be initiated and will propagate without transition to either a strong detonation or a weak detonation. We believe that experimentally establishing the just-mentioned pulse-parameter ranges is today the highest-priority result to be sought from research on nonintrusive energy deposition in an air-breathing-propulsion context.

As further background, we know that, in a uniform channel with a gaseous mixture flowing at a speed that is several times the CJ-detonation speed, the weak detonation (for which the downstream flow is uniform and supersonic) implies an entropy rise across the detonation that is greatly in excess of the entropy rise across a CJ detonation in the same mixture; the strong normal detonation (for which the downstream flow is uniform and subsonic) implies an entropy rise that is huge compared with that of the weak detonation. We know that if, in a uniform channel, a periodic succession of CJ detonations leads to a reasonably uniform downstream flow, that flow can be only the uniform flow that would have emerged from either a one-dimensional weak detonation or a one-dimensional strong detonation. We have no reason to expect that, when successive pulses nonintrusively deposit energy (in a uniform supersonic stream of combustible mixture flowing in an axisymmetric container) for the direct initiation of successive CJ detonations, interaction of the spherically expanding detonations with each other and with suitably designed channel walls would lead to the formation of a strong detonation across the channel. We see no reason to doubt that we can select a channel of streamwise expanding cross-section $A(x)$ [with $A'(x) > 0$] so that the downstream flow has the smallest one-dimensional entropy rise, i.e., the entropy rise associated with the weak detonation. In fact, we are confident that a channel with $A'(x) > 0$ can be selected such that the nonuniform flow has an average entropy rise (across the cross-section) that is smaller than the entropy rise associated with the weak detonation.

More explicitly, we envision that of each of the train of periodic pulses deposits sufficient energy [in a uniform supersonic stream (of speed u_o) of combustible mixture, flowing in an axisymmetric container] to initiate directly a spherical CJ detonation. Each detonation expands radially as it is convected downwind. The envelope of detonation-front positions becomes progressively less "scalloped" when the successive spherical CJ detonation waves interact sooner after initiation, because the frequency of pulsing is increased from one fixed finite value to another, larger value. As a consequence of a higher pulsing frequency there is less entropy increase associated with reflected shocks, arising whenever one spherical detonation wave "propagates" into the already-burned mixture encompassed by a neighboring spherical detonation wave. In the limit of indefinitely rapid pulsing, the envelope becomes a standing conical detonation wave, of half cone angle $\beta = \sin^{-1}(u_{CJ}/u_o)$, where $u_{CJ}(< u_o$, by choice of operating conditions) is the CJ-detonation speed for the mixture (Figure 1).

Downwind of the conical detonation wave, the burned gas undergoes a self-similar expansion, describable entirely in terms of the spherical polar angle θ, where $\beta \geq \theta \geq 0$, and the initial ray $\theta = 0$ lies along the axis of symmetry downwind of the energy-deposited site, taken conveniently to be the origin of coordinates. If the (cylindrical) radius σ_w of the container is envisioned for the entry region to be the radius r_o of a circular pipe, then the container must flare with increasing downwind distance x for $x > (r_o/\tan \beta)$, or else entropy-increasing shocks would result from the interaction of the conical detonation wave with the walls of a pipe-type container. For $x > (r_o/\tan \beta)$, a suitable container shape $\sigma_w(x)$ is sought by trial and error via numerical solution, (say) by the method of characteristics, of a (nonselfsimilar) steady axisymmetric isentropic swirl-free supersonic flow. While such a flow model is highly idealized, our successfully finding a suitable shape $\sigma_w(x)$ suggests in principle that the post-detonation flow can be expanded to ambient pressure within a reasonably short, reasonably slender nozzle.

There appear to be at least three advantages of the laser-initiated-oblique-detonation-wave combustor over an alternative design employing an intrusive conical body: (1) the body introduces additional frictional drag; (2) inevitable body jitter and nose curvature result in an at least locally strong detonation, and large entropy rise -- and the consequent upwind propagation of disturbances in the locally subsonic burned gas might result in a broadly normal detonation; and (3) in the absence of a positive ignition device, a long induction time (and hence long streamwise distance) may arise between the site of the conical-body-induced shock and the site of chemical reaction of the high-speed mixture.

There remains a need to establish experimentally that no unforeseen large-entropy-rise phenomena occur in connection with (1) the interaction of two initially distinct spherical detonations, one of modestly larger radius than the other (in accord with the successive initiation in the proposed combustor); or (2) the approach of a spherical detonation to a reasonably rigid wall (including noise, vibration, and upwind propagation of information in a subsonic very-near-wall sublayer). Also, in practice, the opportunities/liabilities for performance associated with imperfect upwind mixing, such that an inhomogeneous gaseous mixture is detonated [so the fuel fraction that persists through the detonation burns in the hot detonation products], require examination. However, we anticipate that the centimeter-scale cellular structure of actual spherical detonations has little practical consequence for the present application, so we do not regard that phenomenon to have high priority in a research agenda.

REFERENCES

Carrier, G., Fendell, F., Chen, K,. and Cook, S. (1991a). Evaluating a simple model for laminar-flame-propagation rates. II. Spherical geometry. Combustion Science and Technology, to appear.

Carrier, G., Fendell, F., Chen, K., and Pallia, C. (1991b). Evaluating a simple model for laminar-flame-propagation rates. I. Planar geometry. Combustion Science and Technology, to appear.

Carrier, G. F., Fendell, F., McGregor, D., Cook, S., and Vazirani, M. (1991c). Laser-initiated conical detonation wave for supersonic combustion. Paper 91-0578, AIAA 29th Aerospace Sciences Meeting, Reno, Nevada. Washington, DC: American Institute of Aeronautics and Astronautics. (Journal of Propulsion and Power, to appear.)

Carrier, G., Fendell, F., Mitchell, J., and Chen, K. (1991d). Deceleration of spherical laminar flames in highly-fuel-rich mixtures by soot radiation. Combustion and Flame, in review.

Carrier, G. F., Fendell, F. E., and Sheffield, M. W. (1990). Stabilization of a premixed planar flame by localized energy addition. AIAA Journal 28, 625-630.

Chou, M.-S., Zukowski, T. J., and Wong, E. Y. (1989). Ignition of $H_2/O_2/NH_3$, H_2/air and $CH_4/O_2/NH_3$ premixed flows by excimer laser photolysis of NH_3. Paper 89-94, Western States Section Fall Meeting. Pittsburgh, PA: Combustion Institute.

Lee, J. H., Knystautas, R., and Yoshikawa, N. (1978). Photochemical initiation of gaseous detonations. Acta Astronautica 5, 971-982.

Strehlow, R. A. (1984). Combustion Fundamentals. New York, NY: McGraw-Hill.

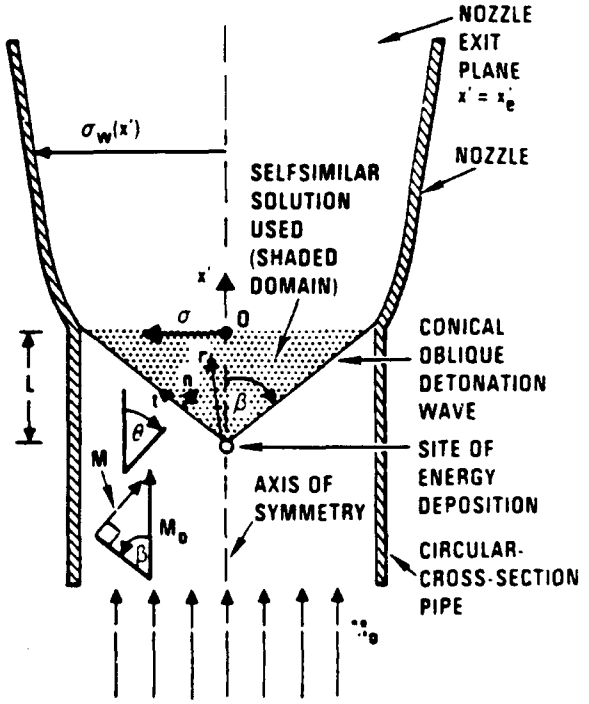

Figure 1. Schematic (not to scale) of a supersonic combustor ($x = x' + L$; n,t are normal, tangential coordinates; $\sin \beta = M/M_o$, $M_o^2 = u_o/a_o$, and $M^2 = u_{CJ}/a_o$, where a_o is the sound speed of the cold mixture). In $L > x' > 0$, $\beta > \theta > 0$, a selfsimilar solution in terms of the polar angle θ holds; r_o is the radius of the pipe section, and $L = r_o/\tan \beta$. The pipe container is flared at the position of intersection with the nearly conical detonation wave, to avoid reflected shocks.

NUMERICAL STUDIES FOR THE RAM ACCELERATOR

AFOSR-MIPR-91-005

Elaine S. Oran, Chiping Li, K. Kailasanath, and Jay P. Boris

Laboratory for Computational Physics, Code 4400
Naval Research Laboratory, Washington, DC 20375

SUMMARY/OVERVIEW

Time-dependent multidimensional Euler and Navier-Stokes simulations have been performed to address the questions of stability of a standing detonation wave on a projectile surrounded by detonable material. The detailed structure of the detonation wave and the effects of the boundary layer are two important elements in determining the detonation stability. These basic elements of complex reactive flows need to be studied numerically with accurate methods and careful analyses of the effects of the approximations used in the study. We are currently using the computations to stud 1) the basic structure of the oblique detonation wave; 2) the structure of boundary layers and the effect of such boundary layers on the oblique detonations in high-speed flows; 3) the impact of other physical and chemical parameters, such as the leading angles of projectile and the heat-release rate, on the detonation structure.

TECHNICAL DISCUSSION

As the strongest, fastest, most efficient form of combustion, detonations increase the flow velocity and the pressure due to rapid conversion from chemical energy to mechanical energy without appreciable expansion. Because of the very rapid conversion of chemical energy to high pressure, some forms of detonation engines present interesting alternatives to usual combustion engines. The RAM accelerator concept is based on the standing detonation. If a detonation wave can be stabilized and maintained at the correct location on an advantageously shaped body, the detonation can impart large thrust to the body and propel it forward. The idea is to keep the detonation peak pressure located near and behind the widest part of projectile to maximize the acceleration.

The problems of achieving detonation stability on a projectile is complex and nonlinear. Whereas many aspects of the steady-state problem may be addressed by theoretical analyses and thermodynamic considerations, the fundamental time-depdendent structure of the complex reactive-flow must be addressed computationally. Thus we have begun to tackle some of these basic problems numerically using the computational tools we have developed for studying the time-dependent behavior of multidimensional high-speed reactive flows. Our approach in this project has been to consider both the fundamental numerical and phsysical issues related to modeling these flows and then to use simulations to study the detailed structure of oblique detonation waves and the effects of viscosity, factors which may be crucial to the stability of a standing detonation.

The fundamental configuration is a supersonic flow impinging on a wedge of varying angle, as shown in Figures 1 and 2. The questions addressed here are both physical and numerical:

- What is the basic structure of oblique detonations under different background and flow conditions?
- What is the effect of viscosity on the shock structures? It should only be important in the boundary layer, which is small in such flows, but does this boundary-layer affect the structure of the detonation waves?
- Given a flow velocity and wedge angle, what amount or rate of energy release produces a stable detonation? What other factors of the reactive-flow or geometry are important in the basic problem?
- What other types of detonation structures, which may or may not be stable, are possible?
- What is the minimum numerical resolution required to obtain the kinds of information we need about stability?

Addressing these questions allows us to begin to assess the fundamental physical issues in detonation stability in RAM accelerators. In this presentation we describe some of the more important and relevant results of these tests.

Nonreactive-Flow Studies

In order to show the effects of viscosity, a set of nonreactive simulations were conducted for a Mach 8 flow over a wedge. Figures 1 and 2 show results from both Euler and Navier-Stokes calculations of a shock impinging on two different wedges. In the small-angle case, where the shock is attached, there are no obvious differences in the computation, which is consistent with the fact that the boundary layer is very thin and there are no recirculation zones in the flow field. The effects of the boundary layer are likely to be confined in the region near the wall. In the detached case, although the basic bowshock structures are similar for Euler and Navier-Stokes computations, the flow structures behind the shocks are significantly different. The effect of viscosity is more visible, possibly due to the large stagnation region and related recirculation zone behind the shock. So far, we have concentrated on the attached case. Some highly resolved computations were conducted to study the structure of the boundary layer behind attached oblique shocks.

Reactive-Flow Studies

The reactive cases focus on the basic structure and stability of oblique detonations. These studies require high enough resolution to resolve the chemical induction region. We find that the detonation wave is stable in some cases and unstable in others, depending on the flow conditions and the amount of heat release. Figures 3 and 4, which show the temperature and induction-parameter contours (the induction parameter represents radical production) for both stable and unstable cases, indicate that the basic structure is similar in both cases. Radicals are produced in a finite induction region behind the shock and above the wall. After enough radicals accumulate, the energy release associated with combustion begins to increase the temperature and strengthen the shock. As long as the after-shock conditions are supersonic, the detonation structure remains steady. However, if the flow is choked behind the shock by the energy rlease, the detonation structure may be unstable and be driven upstream.

Related Detonation Studies

There are a number of other current research projects at NRL with contribute to this project by providing physical insights and numerical technology. These include: 1) Studies of detonation transmission which show us possible dynamics and steady detonation structures that can be achieved and perhaps stabilized; 2) Detailed analyses of detonation cell structures which give us insights into the basic configuration of a gas-phase detonation and provide fundamental tests of the validity of the chemical approximations used; and 3) Studies of flows over complex obstacles which develop computational techniques that will be crucial for modeling entire systems with realistic configurations.

Publications directly related to this project:

A Uniform Algorithm for Boundary and Interior Points and its Application to Supersonic Flow Simulations, C. Li, E.S. Oran, and J.P. Boris, Conference on Parallel Computational Fluid Dynamics, Indianapolis, May, 1990.

A Uniform Algorithm for Boundary and Interior Regions and Its Application to Compressible Flow Simulations, C. Li, E.S. Oran, and J.P. Boris, submitted to the SIAM Journal, 1990.

Numerical Simulation of Gas-Phase Detonation Transmission, E.S. Oran, D.A. Jones, and M. Sichel, AIAA Paper No. 91-0579, American Institute of Aeronautics and Astronautics, Washington, DC, 1991.

The Anatomy of a Marginal Detonation, E.S. Oran, D.A. Jones, and M. Sichel, submitted to *Proc. Roy. Soc.*, 1990.

Structures of Shock and Detonation Waves in Supersonic Flows around Wedges, C. Li, K. Kailasanath, andE.S. Oran, Meeting of the Eastern Section of the Combustion Institute, Orlando, FL, December, 1990.

Structure of Reaction Waves behind Oblique Shocks, C. Li, K. Kailasanath, and E.S. Oran, submitted to the 13th International Colloquium on the Dynamics of Energetic and Reactive Systems, Nagoya, Japan, July, 1991.

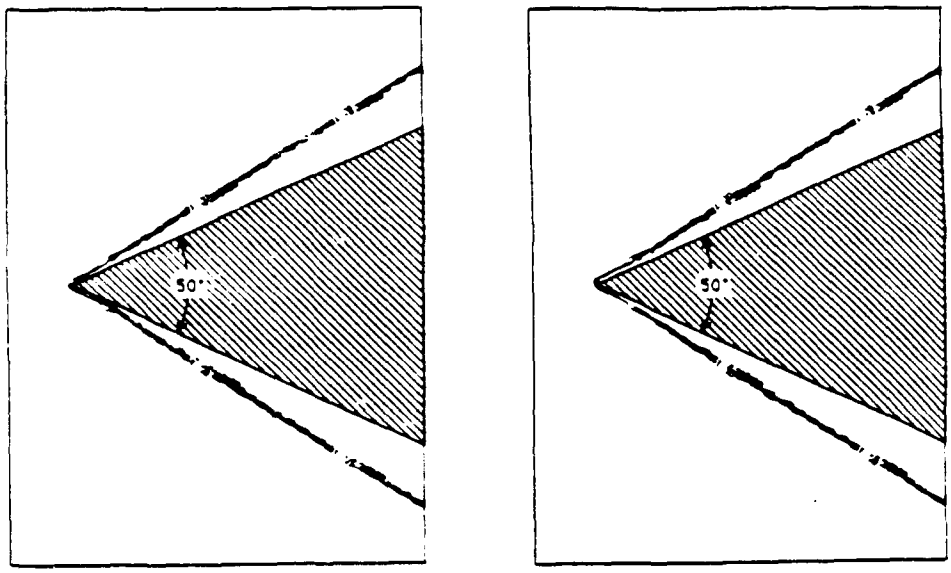

Figure 1. Computed density contours for a supersonic flow passing by a wedge of 50 degrees from inviscid (left) and viscous (right) calculatuions. The inlet conditons: density = 1.117kg/m^3, pressure = 101.3kPa, and Mach Number = 8.

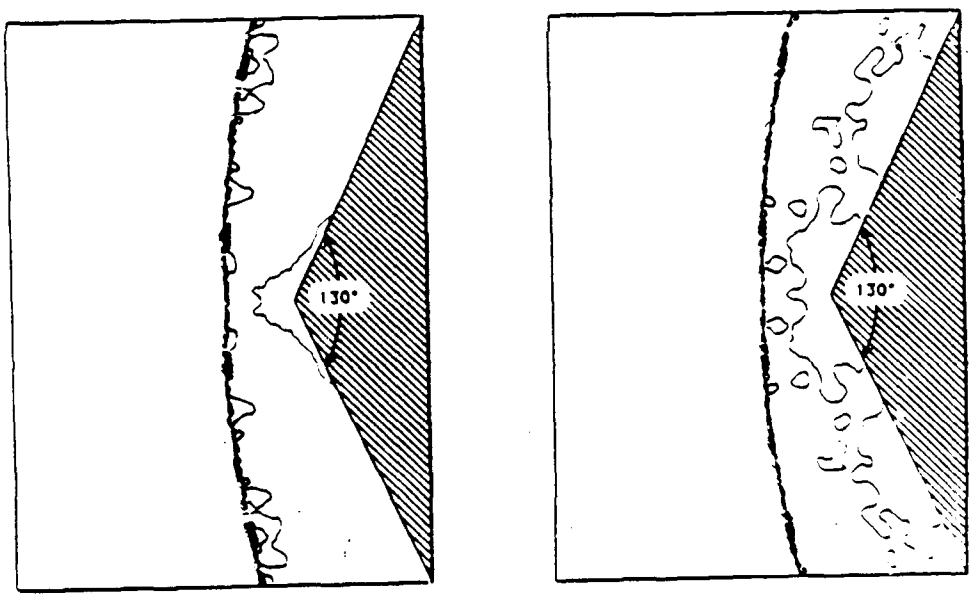

Figure 2. Computed density contours for a supersonic flow passing by a wedge of 130 degrees from inviscid (left) and viscous (right) calculatuions. The inlet conditons are the same as those in figure 1.

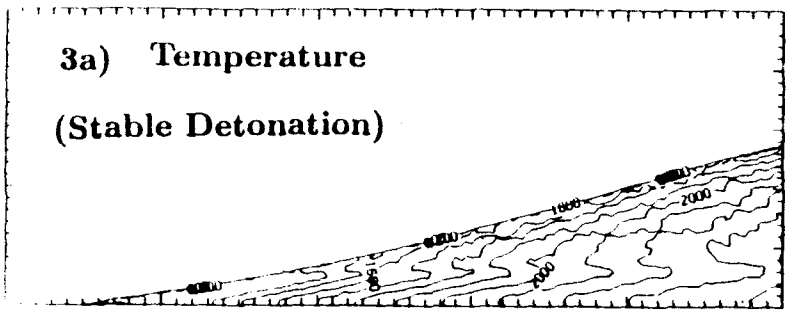

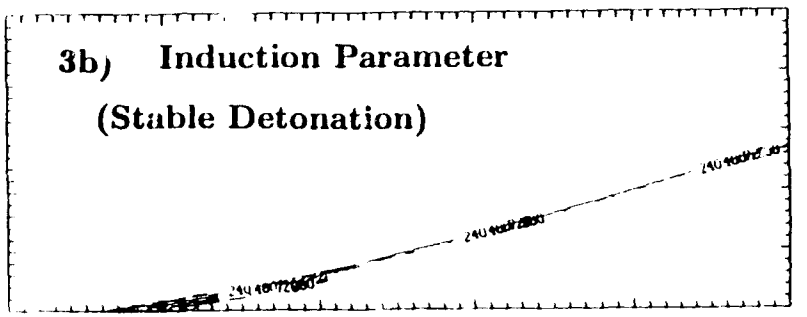

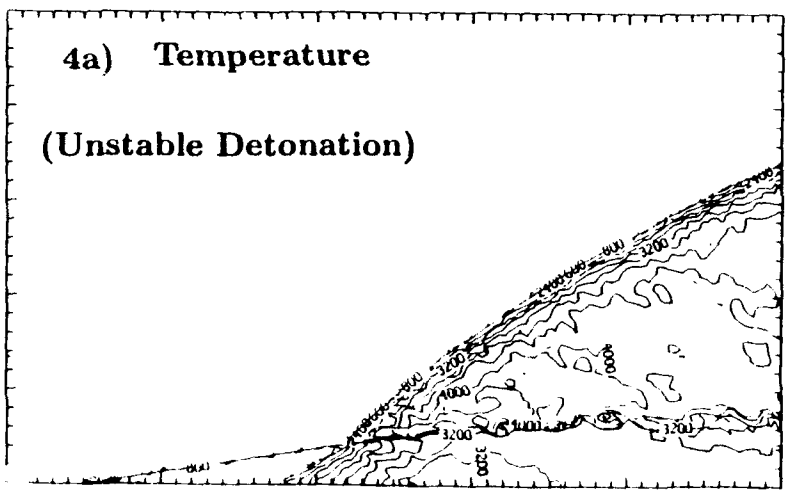

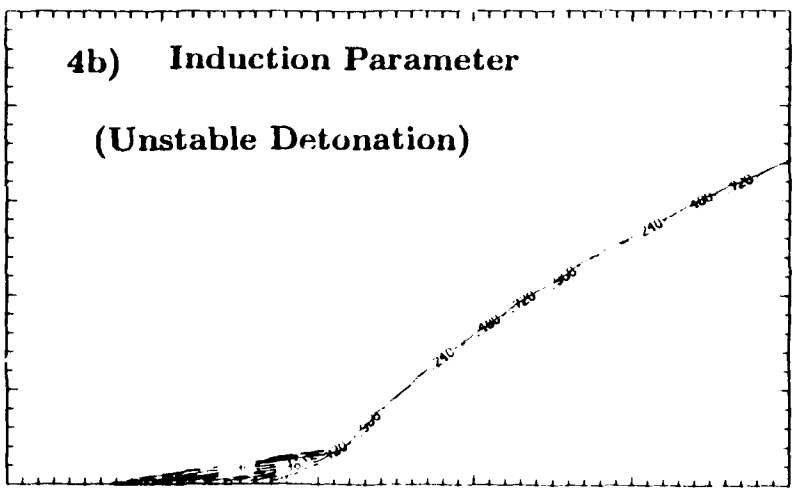

Temperature and induction-parameter contours for two Mach 8 mixtures of H_2, O_2, and N_2 around a 29° wedge.

Figures 3. H_2:O_2:N_2 in the ratio 1.5:1:3.7 resulting in a steady, stable detonation wave.

Figures 4. H_2:O_2:N_2 in the ratio 2:1:3.76 resulting in an unstable detonation wave moving upstream due to the choked condition behind the shock.

MODELING STUDY TO EVALUATE THE IONIC MECHANISM OF SOOT FORMATION

AFOSR Contract No. F49620-91-C-0021

Principal Investigator: H. F. Calcote

AeroChem Research Laboratories, Inc.
P.O. Box 12
Princeton, NJ 08542

SUMMARY/OVERVIEW

The major objective of this study is to delineate the relative importance of the neutral free radical and ionic mechanisms of soot formation in flames by computer modeling. This required the development of a detailed ionic mechanism, estimation of the individual ion reaction rates and the thermodynamics of the large ions involved in the mechanism. It has been demonstrated that an ionic mechanism can be formulated which explains the source of observed ions as due to ion growth from a chemiion. The problem still remains of demonstrating the dominance of one mechanism over the other, especially in flames other than the standard acetylene/oxygen flame.

TECHNICAL DISCUSSION*

A detailed ionic mechanism has been developed for the well-documented acetylene/oxygen flame burning on a flat flame burner at 2.67 kPa. The reaction rates of the individual steps and the thermodynamics of the ions have been estimated.[1]

Frenklach and Wang[2] have run a limited number of computer runs using this mechanism. The early runs showed great differences between experimental and computed ion profiles; as the model was improved the agreement improved. There were no arbitrary alterations of rate constants or of thermodynamics. The major changes were in the choice of reactions and in the isomer used. Without making such choices the number of reactions and reactants becomes excessive.

Some selected comparisons between calculated and experimental ion profiles are presented in Fig. 1. For small ions the agreement is reasonably good. The relationship of the two isomers, $H_3C_3^+$ (cyclopropenium) and $C_3H_3^+$ (propargylium), demonstrates that equilibrium maintains a relatively high concentration of the reactive isomer. One of the arguments against the ionic mechanism was that the stable isomer $H_3C_3^+$ was found experimentally to be nonreactive with acetylene or other small hydrocarbons while the linear isomer was found to be very reactive.[3,4]

The data for larger ions are not in such good agreement. The peak concentrations are reasonably close but the profiles differ markedly. This difference is, however, no greater than the difference for neutral species in the free radical mechanism. One major difference between the ionic model and the Frenklach neutral model is that we have limited the reactants and products to those that have been observed experimentally, and we have required that the model calculate all observed species. The Frenklach model does not have either of these constraints.[2] Thus the neutral model includes cyclopentaphenanthrene which is not observed experimentally, and it does not include phenanthrene and pyrene which are observed experimentally. Further, in the neutral model[2] only five calculated

---

* This report covers a short period of time; the program was unfunded from 1 October 1990 to 18 March 1991.

cyclic compound profiles are compared with experiment; the peak concentration of naphthalene is computed to be 20 times smaller than measured. The ionic model is thus a better fit to the experimental data than the free radical model. Part of the reason for this may be the paucity of data on large neutral species; their concentrations fall with increasing size so they become difficult to detect.

After the fall-off in ion concentration beyond the first peak the calculated ion concentrations increase with distance and the experimental concentrations decrease, Fig. 1. A calculation was carried out in which the temperature profile was fixed at the maximum temperature; the calculated concentrations then decayed slowly. This demonstrates the sensitivity in the computer model to temperature. In another test of the temperature sensitivity, Brown and Pedersen[1] ran our mechanism, using experimental neutral concentrations with the experimental temperature and with a 10% reduction in experimental temperature and observed very large effects on the maximum calculated ion concentrations.

A comparison of the experimentally observed and calculated maximum concentration of ions is presented in Fig. 2. Since the experiments do not distinguish between isomers and there is usually more than one isomer in the computer model, we compare in Fig. 1 the isomer in which the agreement is best between the calculated and experimental concentrations. For most of the large ions, the experimental value exceeds the calculated value. Electron attachment, and thus positive ion-negative ion recombination, has been neglected in the model; inclusion would increase the calculated concentrations. Ions would not be removed from the system as fast as by ion-electron recombination. In an earlier computer test of the model, this was demonstrated by reducing the recombination rate of all recombination reactions. Incidentally, decreasing the rate of recombination would decrease the formation of neutral species which Frenklach incorrectly interprets[2] as a measure of the efficacy of the ion-molecule mechanism.

The neutral species profiles calculated by the free radical mechanism, which is used to calculate neutral reactant species in the ionic mechanism, do not agree well with experimental measurements. Thus at 1 cm above the burner: C_4H_2 calculated exceeds experiment by more than a factor of 6, and C_3H_4 is lower by more than a factor of 6. The experimental measurements have been made by several people with good agreement. The question is thus raised: does the difference between experiment and calculation for the ionic mechanism depend upon problems in the free radical mechanism? This could be readily tested if the experimental neutral species profiles required for the ionic mechanism could be used as input to the computer program, just as the temperature is. Frenklach's program[2] would not handle this so the test was done by Brown and Pedersen at Iowa State.[1] The maximum calculated ion concentrations were many orders of magnitude lower than measured but the profiles were in better agreement. This indicates a great sensitivity in the computer model to the free radical mechanism.

One of the objectives in this program is to compare the rate of neutral and ion species growth. Since these data are not yet available from the computer model, we have compared the rates obtained by calculations from experimental concentration measurements and the rate coefficients employed in the two mechanisms. The calculated rates are very close for the two mechanisms, if one uses for the free radical mechanism the most optimistic measurements and makes the most optimistic assumptions. We have also deduced the rates of ion formation for a large number of ions in the standard flame from the experimental ion concentrations to compare with the observed rate of soot particle formation. The maximum rates for $C_3H_3^+$, $C_{13}H_9^+$ and $C_{21}H_{11}^+$ are thus: 6.5×10^{12}, 3.0×10^{12} and 1.2×10^{12}, respectively. This compares to the maximum measured rate of soot formation of between 4 and 7×10^{12} particles $cm^{-1}\ s^{-1}$.

In future work we plan to modify the Sandia Chemkin-II Code to handle ion diffusion, nonArrhenius temperature coefficients for ion-molecular reactions, and to accept as input neutral species profiles. We will also examine the benzene flame where the relationship between ions and soot is much different, and it is not so clear that soot is derived from ions.

REFERENCES

1. Calcote, H.F. and Gill, R.J., "Computer Modeling of Soot Formation Comparing Free Radical and Ionic Mechanisms," Final Report, AeroChem TP-495, February 1991.

2. Frenklach, M. and Wang, H., "Computer Modeling of Soot Formation Comparing Free Radical and Ionic Mechanisms," Final Technical Report, January 22, 1991.

3. Smyth, K.C., Lias, S.G., and Ausloos, P., "The Ion Molecule Chemistry of $C_3H_3^+$ and the Implications for Soot Formation," Combust. Sci. Techn. 28, 147 (1982).

4. Baykut, G., Brill, F.W., and Eyler, J.R., "Reactions of $C_3H_3^+$ Ions with Aromatic Hydrocarbons and Alcohols and Their Implications for an Ionic Mechanism of Soot Formation," Combust. Sci. Techn. 45, 233 (1986).

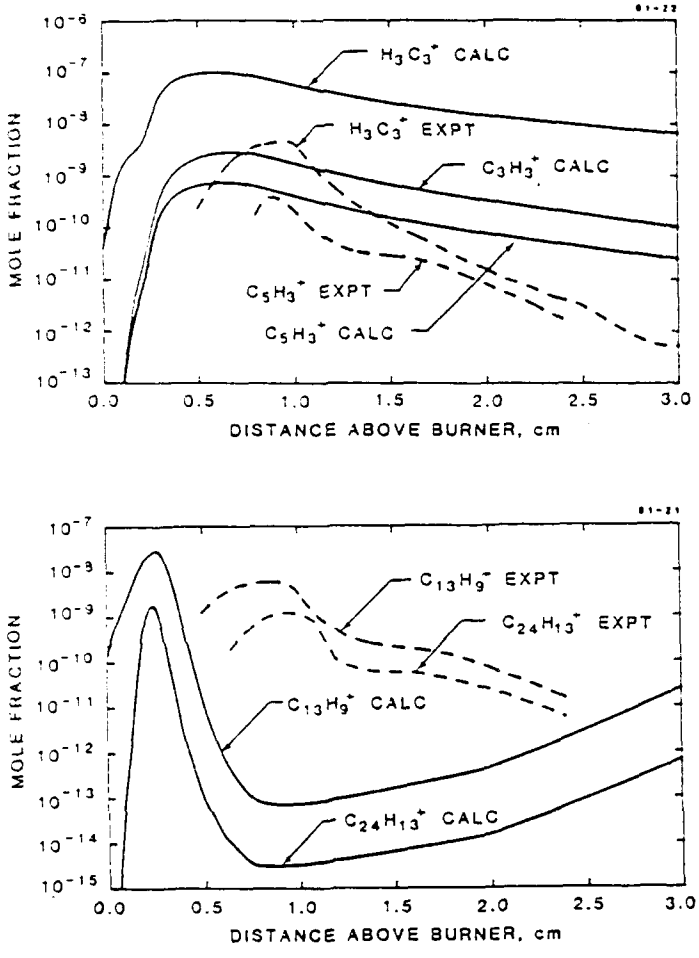

FIGURE 1 COMPARISON OF EXPERIMENTAL AND CALCULATED ION CONCENTRATION PROFILES FOR SELECTED IONS

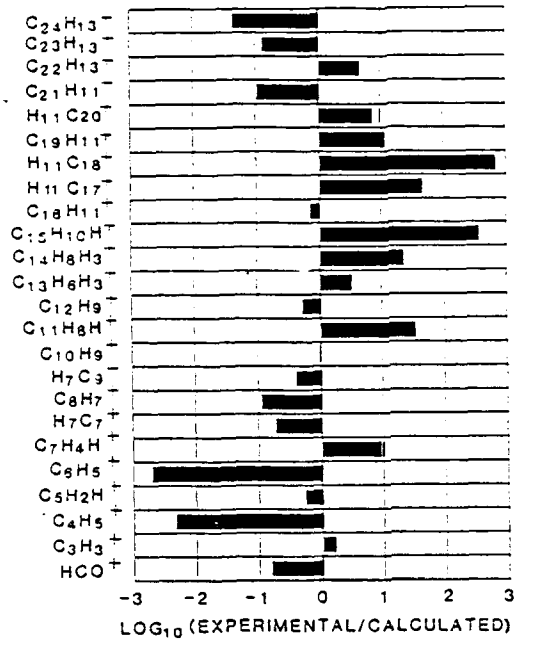

FIGURE 2 COMPARISON OF PEAK EXPERIMENTAL AND CALCULATED ION CONCENTRATIONS

DETERMINATION OF RATE-LIMITING STEPS DURING SOOT FORMATION

AFOSR Contract No. F49620-88-C-0051

Principal Investigator: M.B. Colket, III

United Technologies Research Center
E. Hartford, CT 06108

SUMMARY/OVERVIEW

Soot formation modelling is being carried out which involves coupling flame kinetics predictions of species important to soot formation with an aerosol dynamics analysis of soot spheroid growth. A modified version of a widely-used aerosol dynamics code (MAEROS) has been developed for the latter part of the analysis. While the effort forms the basis for an elaborate, state-of-the-art model, an emphasis of this work has been to investigate simplifications that could make it more useful and efficient for engineering applications. We have found that making simplifying assumptions about the particle inception species results in encouraging agreement with a variety of flame data.

Additionally, during the past three years, a variety of single-pulse shock tube experiments have been completed, including a focus on the comparison between ring formation in pyrolytic and fuel-rich (ϕ=5 to 20) environments. Conclusions from these experimental and related modeling studies have been reported previously. This abstract will focus on recent progress in modeling.

AUTHORS: M. Colket, R. Hall

TECHNICAL DISCUSSION

The soot growth/aerosol dynamics program is based on a sectional representation of the growth equations with provision for inception source terms, surface growth through condensible vapor deposition, and coagulation. The program has been modified in a number of ways for the soot growth problem. Its temperature range capabilities have been extended to the full range of interest in combustion problems by a reformulation of the surface growth sectional coeffient calculations. Provision for an oxidizing, depletible vapor (oxygen) has also been made. The simulations require as input profiles of temperature, condensible and oxidizing vapor concentrations, and the concentrations of certain other flame atomic and molecular species. The input of the aerosol dynamics program has therefore been made compatible with the output of the Sandia pre-mixed, laminar flame kinetics program. The facility to exclude a specified number of small mass spheroids from coagulative processes has also been added. We also have included a calculation of the radiative energy loss from the soot assuming optical thinness and neglecting soot refractive index dispersion.

In the simulations to be described, acetylene is assumed to be the surface growth species, and the growth rate has been calculated using the Harris-Weiner value (Ref. 1) in the appropriate temperature range, or a by modification of the Frenklach-Wang approach (Ref. 2) that calculates the rate based on a steady-state analysis of the surface density of reactive radical carbon sites. The latter requires local values of acetylene and hydrogen atom/molecule concentrations and estimates of rate coefficients for certain kinetic processes, and will hereafter be referred to as the theoretical surface growth model. A 31.8 kcal activation energy was ascribed to the Harris-Weiner expression, although the high temperature dependence is uncertain. Oxidation is assumed to be given by the Nagle and Strickland- Constable expression (Ref. 3), and oxidation by OH by a gas kinetic rate

multiplied by a collision efficiency of 0.13 (Ref. 4). For the soot growth simulations, the size range limits were nominally chosen to be .5 to 200 nanometers (diameter). There is no significant sensitivity to choosing the limits .75 to 300 nm, for example. Cases with relatively low surface growth rates display sufficiently small sensitivity to the number of sections that acceptable results can be obtained with as few as 10 sections. Cases with higher surface growth rates seem to show more numerical diffusion and sensitivity to number of intervals, and have been run with 25 size classes, the maximum currently allowed in this size range. With ten size classes, a growth simulation requires only about 15 sec. CPU on a VAXstation 3100; with 25 classes, the CPU time is about 1. min 30 sec.

One of the key assumptions investigated in the current model is that the benzene molecule (and/or phenyl radical) can be used as a surrogate for the incepting soot particle. By accounting for likely size dependent agglomeration rates, etc., we feel we may effectively simulate the effects observable when assuming larger species as the incepting particle. Kinetic data on acetylene addition to benzene (phenyl radical) compare well with extrapolations of kinetic measurements of acetylene addition to soot. Furthermore, we believe the uncertainties in making accurate predictions of the formation of higher molecular weight species has such a large uncertainty that it is probably premature to have a lot a faith in these predictions. Although benzene predictions can now be made by many authors resonably accurately (within factors of two or better), the state-of-the-art for higher molecular weight species is no better than order of magnitude agreement (conservatively). Hopefully, additional experimental information, modeling efforts, as well as a better understanding of the role of C_5 chemistry will enable workers to enhance this capability. Preliminary results demonstrate the apparent promise of our simplification for using benzene as a surrogate for the incepting particle.

Comparisons have been made with the experimental data of Harris and Weiner obtained with ethylene fuel, and with propane and acetylene-fueled flames investigated by Bockhorn and co-workers (Ref. 5) The experimental conditions thus span a wide range of ambient conditions, with pressures ranging from .12 to one atmosphere, and peak temperatures in the range 1600 - 2000 K. The first step involved simulation of the flame kinetics to provide the needed profiles of the inception species and the C_2H_2, H, H_2, OH, and O_2 profiles needed for the surface growth and oxidation rates. In order to predict these formation rates and concentration profiles, we used the premixed, laminar flame model developed at Sandia. Two kinetics sets were used for predictions, one was developed at UTRC and a second was the (slightly modified) kinetics presented by Harris, Weiner, and Blint (Ref. 6). We used our own thermodynamic data set (which led to some small differences in prediction of species C_4 and larger). The major modification to their mechanism was the addition of some propane reactions and the inclusion of ring forming reactions involving C_3 species for which a lot of information has surfaced during this past year. These reactions double the predictions of benzene formation in the ethylene flames. In addition, for the acetylene flame studied by Bockhorn and coworkers, sensitivity analyses indicate that benzene formation is srongly sensitive to reactions associated with C_3H_3 formation and decay whereas the sensitivity to those associated with C_4 species is insignificant. Numerical agreement between the UTRC kinetics and the modified Harris model were generally fairly good although numerical problems surfaced when attempting to use the 'Harris' kinetics to model some of the Bockhorn flames. Agreement between model predictions and experimental profiles for the several flames (Refs. 1, 5) was generally very good. Consequently, the kinetic model was used to predict benzene profiles (and that for other flame species) for several of the Harris flames for which soot growth profiles were determined but experimental benzene profiles are unavailable. Temperature profiles from these flames were obtained directly from Steve Harris. Benzene profiles calculated for the Bockhorn flames were in excellent agreement with the experimental data (Shown in Fig. 1 for the propane flame). Rapid early formation of benzene

was modeled followed by subsequent decay and (in the case of the acetylene flame) slow growth downstream of the flame front. The initial rapid formation occurs from intermediate temperatures and the existence of high concentrations of decomposition fragments of the fuel. The rapid decay of benzene (and other aromatic species) in these high temperature regimes was found to be linked to the peak temperature of these flames and the fact that at those peak temperatures rapid decomposition of benzene and other aromatic rings occurs. The slow subsequent recovery of benzene (after a temperature drop) is due to long cooking of rich flame gases with the low molecular weight species near to (quasi-) equilibrium conditions.

In the aerosol dynamics simulations, the smallest size class is given a finite source rate, and is regarded as the inception species. This would ordinarily be a higher molecular weight PAH. (Unless there is a strong reason for picking this species, the calculated results should not be sensitive to what is a somewhat arbitrary choice.) Should advancements in the state- of-the-art for higher molecular weight species permit, our kinetics codes could be used to predict the source rate of any such prescribed species. The present comparisons were based, as described, on the zero order assumption that the inception source rate can be approximated by that of benzene. This assumption merely represents the simplest possible implementation of the model; the model is not restricted to it. As will be seen, however, it is possible that the results obtained from it may be just as good as those presently obtainable from more elaborate calculations of the inception species.

Figures 2 and 3 compare the model predictions with the ethylene flame data of Ref. 1. In Figure 2, it can be seen that the theoretical surface growth model and the Harris-Weiner value give similar predictions, in this case for C/O = .8. In Figure 3, it can be seen that the stoichiometric dependence of the flame soot yield is approximated by the theory. No steric factors or other adjustable parameters have been used in these calculations.

Simulation of the Ref. 5 propane and acetylene flames represents a significant extrapolation because of their higher peak temperatures (approx. 1825 and 1975 K, respectively). The inclusion of an acetylene desorption process in our theoretical surface growth expression, with a rate constant assumed to be equal to that for phenyl decomposition, causes the surface growth rate to have a negative temperature dependence for temperatures beyond 1650 K. For the propane flame, the predicted surface growth rate seems still to be somewhat too high (Figure 4), although the disagreement between experiment and theory is only slightly larger than a factor of three at 90 mm. If one is willing to introduce a modest steric factor in the surface growth rate, the agreement could obviously be made much better. For the acetylene flame, the asymptotic agreement is much better, but theory is much too low in the lower regions of the flame. The temperature dependence of the surface growth rate seems to be too extreme for temperatures in the vicinity of 1950-2000K in the present model. The main emphasis in the program now is an attempt to determine the proper high temperature dependence of the surface growth rate.

REFERENCES

1. S.J. Harris and A.M. Weiner, Combustion Science & Technology, 131 155 (1983).
2. M. Frenklach and H. Wang, Twenty-third Symposium (International) on Combustion, Paper 23-247, The Combustion Institute, 1991.
3. J. Nagle and R.F. Strickland-Constable, Proceedings of the Fifth Carbon Conference, Vol. 1, Pergamon Press, 1963, p. 154.
4. Neoh, K.G., Howard J.B. and Sarofim, A.F.: Particulate Carbon: Formation During Combustion (D.C. Siegla and G.W. Smith, Eds.), p. 261, Plenum, New York, 1981.
5. H. Bockhorn, F. Fettig and H.W. Wendt, Ber. Bunsenges. Phys. Chem., 87, 1967 (1983).
6. Harris, S.J. Weiner, A.M., and Blint, R.J., Combust. Flame, 72, 91 (1988).

Fig. 1 Measured and Predicted Species Concentrations
Bockhorn Propane Flame

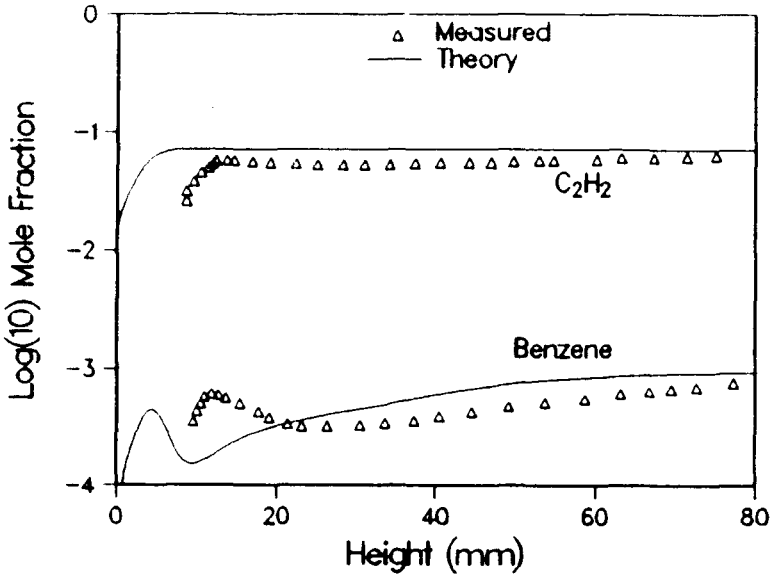

Fig. 2 Calculated Soot Volume Fraction
Harris Flame; C/O = 0.8

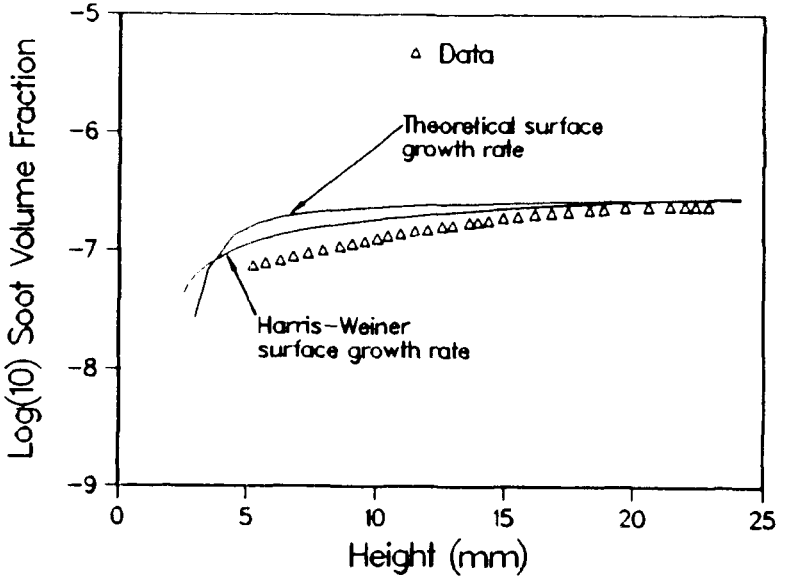

Fig. 3 Calculated Soot Volume Fraction
Harris Flame; Harris-Weiner Surface Growth

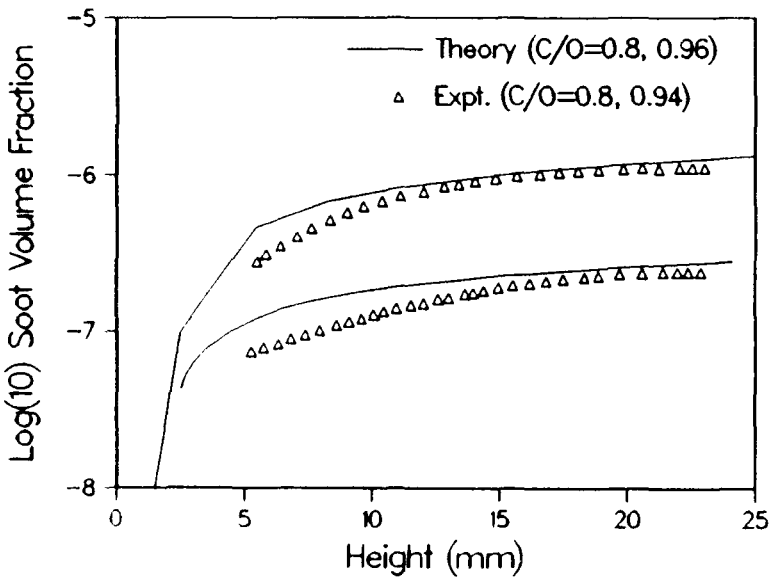

Fig. 4 Calculated Soot Volume Fraction
Bockhorn Propane Flame

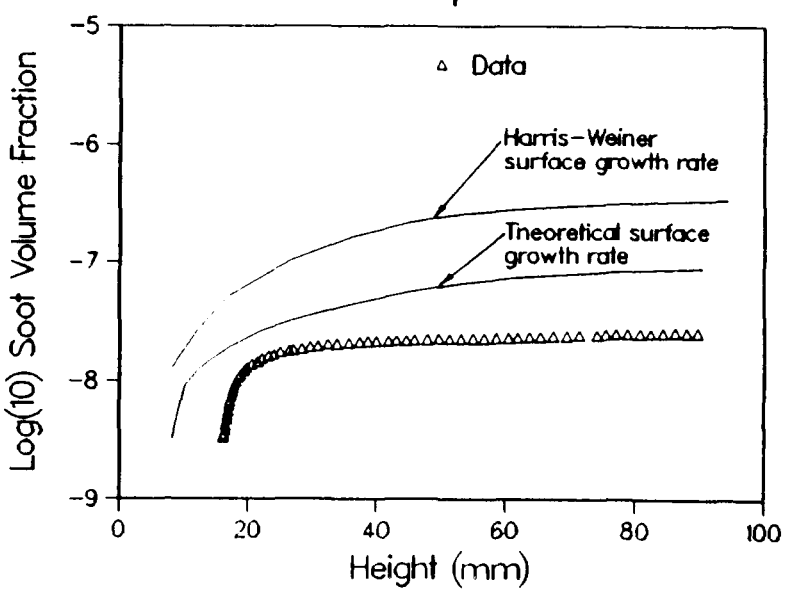

DROP/GAS INTERACTION IN DENSE SPRAYS

(AFOSR Grant No. 89-0516)

Principal Investigator: G. M. Faeth

218 Aerospace Engineering Building
The University of Michigan
Ann Arbor, Michigan 48109-2140

SUMMARY/OVERVIEW

Two aspects of dense sprays are being studied: turbulence modulation, which involves the turbulence field generated by drop motion, and secondary drop breakup, which intrinsically follows primary drop breakup from liquid surfaces. Work completed on turbulence modulation has shown that particle-generated turbulence is strikingly different from conventional turbulence and has provided a means of estimating these turbulence properties. Further progress toward understanding turbulence modulation requires information on particle wake properties in nonturbulent and turbulent flows which is the focus of current work. Work on secondary drop breakup is concentrating on near-limit breakup since these conditions dominate dense sprays. Work completed has provided a flow regime map defining three breakup regimes — bag, multimode and shear breakup — and has shown that large Ohnesorge numbers (representative of near thermodynamic critical point conditions) involves only extended deformation and no breakup. Current work is defining the dynamic properties and outcome of breakup in all but the well-studied shear breakup regime in order to better understand the structure of dense sprays.

TECHNICAL DISCUSSION

Introduction. Processes within dense sprays are not well understood, which hampers progress because the dense-spray region is the initial condition for the rest of the flow (Faeth, 1990). Past work in this laboratory (Ruff et al., 1989, 1991a,b; Wu et al.,1991) has highlighted two aspects of dense sprays that are currently being studied: turbulence modulation, which is the turbulence field generated by drop motion; and near-limit secondary breakup, which is an important rate-controlling step in dense sprays.

Turbulence Modulation. Turbulence modulation is being studied using laser velocimetry in homogeneous particle-laden flows having uniform particle fluxes in stagnant air and water baths so that all turbulence properties are solely due to turbulence modulation. Theory involves extension of Campbell's theorem (Rice, 1954) to obtain a statistical description of continuous-phase properties.

Direct work on turbulence modulation and dispersion was completed and is discussed by Parthasarathy and Faeth (1990a,b) and Mizukami et al. (1991). Both theory and experiment show that turbulence properties are largely controlled by the rate of dissipation, ε, of particle kinetic energy into their wakes. Thus, motivated by the theory, measurements show that r.m.s. velocity fluctuations in the streamwise and crosstream directions, $\bar{u}_i'$ with i = u or v respectively, can be correlated as follows:

$$\bar{u}_i'/U = C_i(\varepsilon d(\theta d)^{2/3}/U^3)^{1/2} \qquad (1)$$

where $C_u = 6.84$, $C_v = 3.42$, d is particle diameter, U is relative velocity and θ is the wake momentum diameter. This degree of anisotropy, 2:1, is extraordinary for a homogeneous turbulent flow — it results from the fact that mean velocities in particle wake contribute to turbulence properties because particle arrivals at a point are random. Thus, while some properties of the flow are similar to conventional turbulence — Gaussian probability

density functions of velocity fluctuations and nearly exponential spatial correlations — other properties are vastly different, e.g., temporal power spectra decay according to frequency to the -1.1 power rather than the conventional -5/3 power.

The stochastic theory predicts many of these trends correctly but fails quantitatively in some instances due to limited information about particle wake properties. Nevertheless, good empirical correlations of critical properties like spatial and temporal integral scales were still achieved. The results are illustrated in Figs. 1 and 2, where streamwise and crosstream spatial and temporal integral scales, L_{ux}, L_{uy}, T_u and T_v, are plotted in terms of the dissipation factor that controls velocity fluctuation levels, see Eq. (1). Thus, present measurements provide a means of computing most turbulence quantities of interest from the dissipation rate of particle kinetic energy: velocity fluctuations, probability density functions, temporal and spatial correlations and spectra.

In order to properly test predictions, particle wake properties in quiescent and turbulent environments must be known better. Thus, a test arrangement involving spheres moving in a glycerol bath has been developed with laser velocimetry used to measure wake properties.

Measurements thus far have been in quiescent baths. The results show that mean velocities decay similar to turbulent wakes for particle Reynolds numbers in the range 50-200, but decay much more rapidly for Reynolds numbers greater than 400. The latter behavior is evidence of effects of unsteady eddy shedding from the spheres. Current work seeks to define wake properties for both quiescent and turbulent bath conditions, and to incorporate these results into the stochastic theory for comparison with our turbulence modulation measurements.

Secondary Breakup. Earlier measurements of the structure of large-scale pressure-atomized sprays (Ruff et al., 1991a, b; Wu et al., 1991) shows that most drops produced by primary breakup are intrinsically unstable to near-limit secondary breakup. Thus, this phase of the investigation is considering secondary breakup.

Breakup of monodisperse drops is observed using a shock tube and flash cinematography, (for overall behavior), and holocinematography, (to resolve the outcome of breakup), see Ruff et al. (1990) for a description of the latter. The first series of tests involved developing a breakup regime map for near-limit breakup. The results are illustrated in Fig. 3. The drop Weber number at breakup, $We_{gp} = \rho_g d \bar{U}^2/\sigma$, is plotted as a function of the Ohnesorge number, $Oh = \mu_f/(\rho_f d\sigma)^{1/2}$, where ρ is density, σ is surface tension, μ is viscosity and subscripts f and g denote liquid and gas properties. Three breakup regimes have been identified: bag, multimode and shear breakup. Large Ohnesorge numbers are seen to prevent all forms of breakup; instead, the particles generally just deform into irregular stringlike shapes: Large Oh occur as drops approach their thermodynamic critical point: assuming that they shatter into small particles at these conditions, due to their small surface tension, is clearly erroneous. Measurements of the bag breakup limit by Hanson et al. (1963), Hinze (1955), Lane (1951) and Loparev (1975) are seen to be in good agreement with present results.

Current measurements are focussing on drop deformation and breakup dynamics below the multimode breakup limit. These measurements are being used to trace drop deformation, drag and bag breakup properties. Overall, it is planned to consider the region up to the well studied shear breakup regime, due to its relevance to secondary breakup in dense sprays.

REFERENCES

Faeth, G.M. (1980) Twenty-third Symposium (Internation) on Combustion, The Combustion Institute, Pittsburgh, in press.

Hanson, A.R., Domich, E.G. and Adams, H.S. (1963) Phys. Fluids 6:1070-1080.

Hinze, J.O. (1955) AICh E J. 1:289-295.

Lane, W.R. (1951) Ind. Engr. Chem. 43:1312-1317.

Loparev, V.P. (1975) Izv. Akad. Nauk SSSR. Mekh. Zhidk. Gaza 3:174-178.

Mizukami, M., Parthesarathy, R.N. and Faeth, G.M. (1991) Int. J. Multiphase Flows, submitted.

Parthesarathy, R.N. and Faeth, G.M. (1990) J. Fluid Mech. 220:485-514; (1990b) Ibid:515-537.

Rice, S.O. (1954) in Noise and Stochastic Processes (N. Wax, ed.) Dover Publications, New York, p. 133.

Ruff, G.A., Sagar, A. D. and Faeth, G.M. (1989) AIAAJ 27:901-908.

Ruff, G.A., Bernal, L.P. and Faeth, G.M. (1990) Appl. Optics 29:4544-4546.

Ruff, G.A., Bernal, L. P. and Faeth, G.M. (1991a) J. Prop. Power, in press.

Ruff, G.A., Wu, P.-K., Bernal, L.P. and Faeth, G.M. (1991b) J. Prop. Power, in press.

Wu, P.-K., Ruff, G.A. and Faeth, G.M. (1991) Atomization and Sprays, in press.

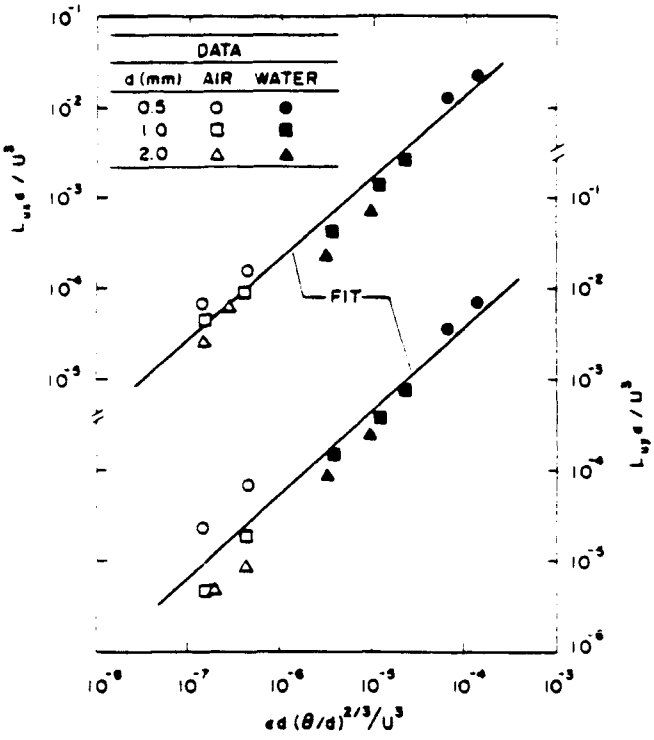

Fig. 1 Integral length scales for turbulence modulation.

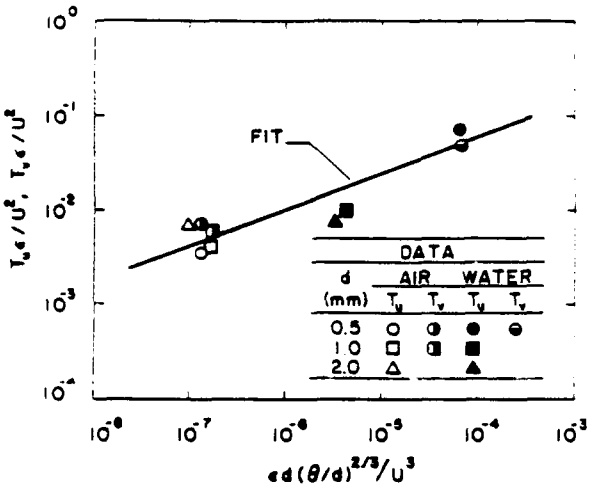

Fig. 2 Integral time scales for turbulence modulation.

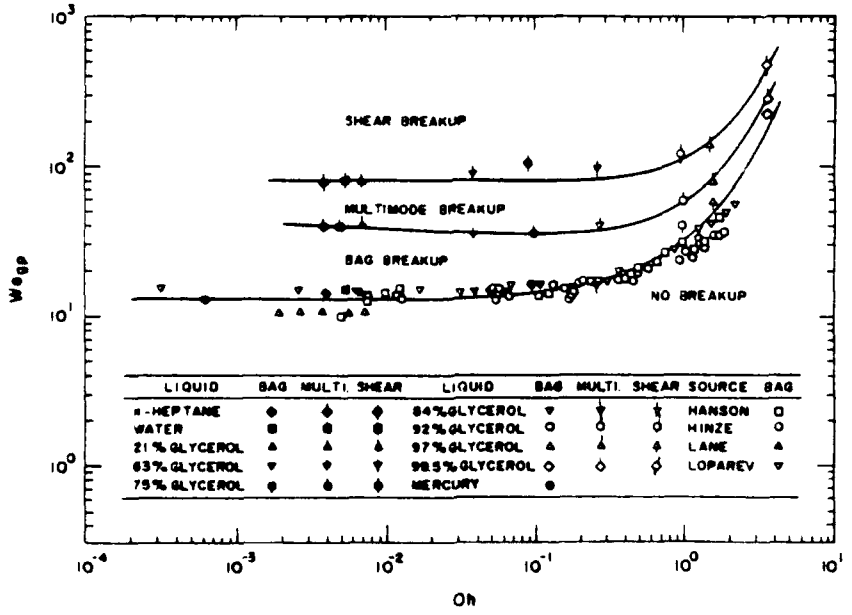

Fig. 3 Secondary drop breakup regimes

DEVELOPMENT OF PREDICTIVE REACTION MODELS OF SOOT FORMATION

(AFOSR Grant No. 91–0129)

Principal Investigator: M. Frenklach

Fuel Science Program
Department of Materials Science and Engineering
The Pennsylvania State University
University Park, PA 16802

SUMMARY/OVERVIEW:

This is a new project on soot formation model development. Following our accomplishments during the previous AFOSR-sponsored project, culminated in quantitative prediction of soot particle formation in several laminar premixed flames of ethylene and acetylene, the objective now is to extend the modeling efforts to computer simulation and analysis of sooting in flames of other fuels and geometries, along with further refinement of the underlying reaction mechanism of soot formation. During the first four months of the project, we developed and implemented an algorithm for calculation of soot particle optical properties; initiated computer simulation of soot formation process in several laminar premixed flames with different stoichiometries; and continued the work on the ionic neutral reaction mechanisms. Some preliminary results are summarized below.

TECHNICAL DISCUSSION

Algorithm for Powder Optical Properties

A computer algorithm was developed that calculates optical properties of an ensemble of particles whose size distribution is given in terms of moments of the size distribution function. This algorithm utilizes the lumping methods[1,2] and corresponding computational codes developed by us to model soot particle formation and growth in flames. It allows us to simulate light absorption and scattering without assuming a functional form for the particle size distribution, and thus to compare directly the numerical predictions of the model to the actual measured properties, such as intensity of scattered light determined by laser diagnostics. The new algorithm was implemented and tested with the lumping code for soot particle formation.

Neutral Mechanism

In a recent review article on chemical kinetics and combustion modeling, Miller, Kee and Westbrook[3] suggested that the cyclization reactions used in our soot formation model, namely

$$n\text{–}C_4H_3 + C_2H_2 \leftrightarrows \text{phenyl} \qquad (1)$$

$$n\text{–}C_4H_5 + C_2H_2 \leftrightarrows \text{benzene} + H\,, \qquad (2)$$

cannot be responsible for the formation of the first aromatic ring because the concentrations of n–C_4H_3 and n–C_4H_5 radicals should be low because the reactions

$$H + n\text{–}C_4H_3 \leftrightarrows H + i\text{–}C_4H_3 \quad (3)$$

$$H + n\text{–}C_4H_3 \leftrightarrows H + i\text{–}C_4H_3 \quad (4)$$

deplete the concentrations of the n–isomers required in reactions (1) and (2). These reactions were not included in our model, because our computational results indicated that the n– and i–isomers are already equilibrated by several other reactions in the system. Nonetheless, to test the Miller *et al.*'s suggestion, we performed additional simulations of the three laminar premixed flames we analyzed previously.[2,4] The reactions (3) and (4) were now included in the simulations assuming rate coefficients 1×10^{14} mol cm^{-3} s^{-1} for the exothermic directions. The results of these simulations for Flame 1 of Ref. 5 are shown in Fig. 1. As can be seen in this figure, the inclusion of reaction (3) and (4) — even with upper-limit rate coefficient values — does not make a difference on the computed profile of benzene. Similar results were obtained with the rest of the simulated flame.

Ionic Mechanism

To evaluate the rate coefficients for some of the key ion-molecule reactions in the AeroChem reaction mechanism[6] suggested for the ionic pathway to soot, potential energy calculations were performed for reaction

$$C_8H_7^+ + C_2H_2 \rightarrow C_{10}H_9^+ .$$

The calculations were performed on various ions using the MOPAC semi-empirical quantum chemical program. For each proposed structure a geometry optimization was performed using the AM1 hamiltonian utilizing a BFGS update technique. A force analysis of the stable geometries, again using MOPAC, confirmed that these were indeed local minima in the AM1 potential energy surface. The force analysis was carried out at 298 K and in the ground state rotational level. In order to find transition states between these structures the SADDLE facility of MOPAC was used that interpolates between given reactant coordinates and product coordinates. Several transition states found in this manner were confirmed to be so by a force analysis showing one imaginary root of the force matrix. Preliminary data, with not fully converged results for some of the transition states, are shown in Fig. 2. Futher calculations are in progress.

REFERENCES

1. Frenklach, M., *Complex Chemical Reaction Systems, Mathematical Modelling and Simulation* (J. Warnatz and W. Jäger, Eds.), p. 2, Springer-Verlag, Berlin, 1987.
2. Frenklach, M. and Wang, H., *Twenty-Third Symposium (International) on Combustion*, The Combustion Institute, in press.
3. Miller, J. A., Kee, R. J. and Westbrook, C. K., *Annu. Rev. Phys. Chem.* 41, 345 (1990).
4. Wang, H. and Frenklach, M., *Modeling of PAH profiles in premixed flames.* Paper presented at the Fall Technical Meeting of the Eastern States Section of the Combustion Institute, Albany, New York, 1989.
5. Westmoreland, P. R., Ph.D. thesis, MIT, 1986.
6. Calcote, H. F. and Gill, R. J., *Computer modeling of soot formation comparing free radical and ionic mechanisms*, Final Report to AFOSR, TP–495, 1991.

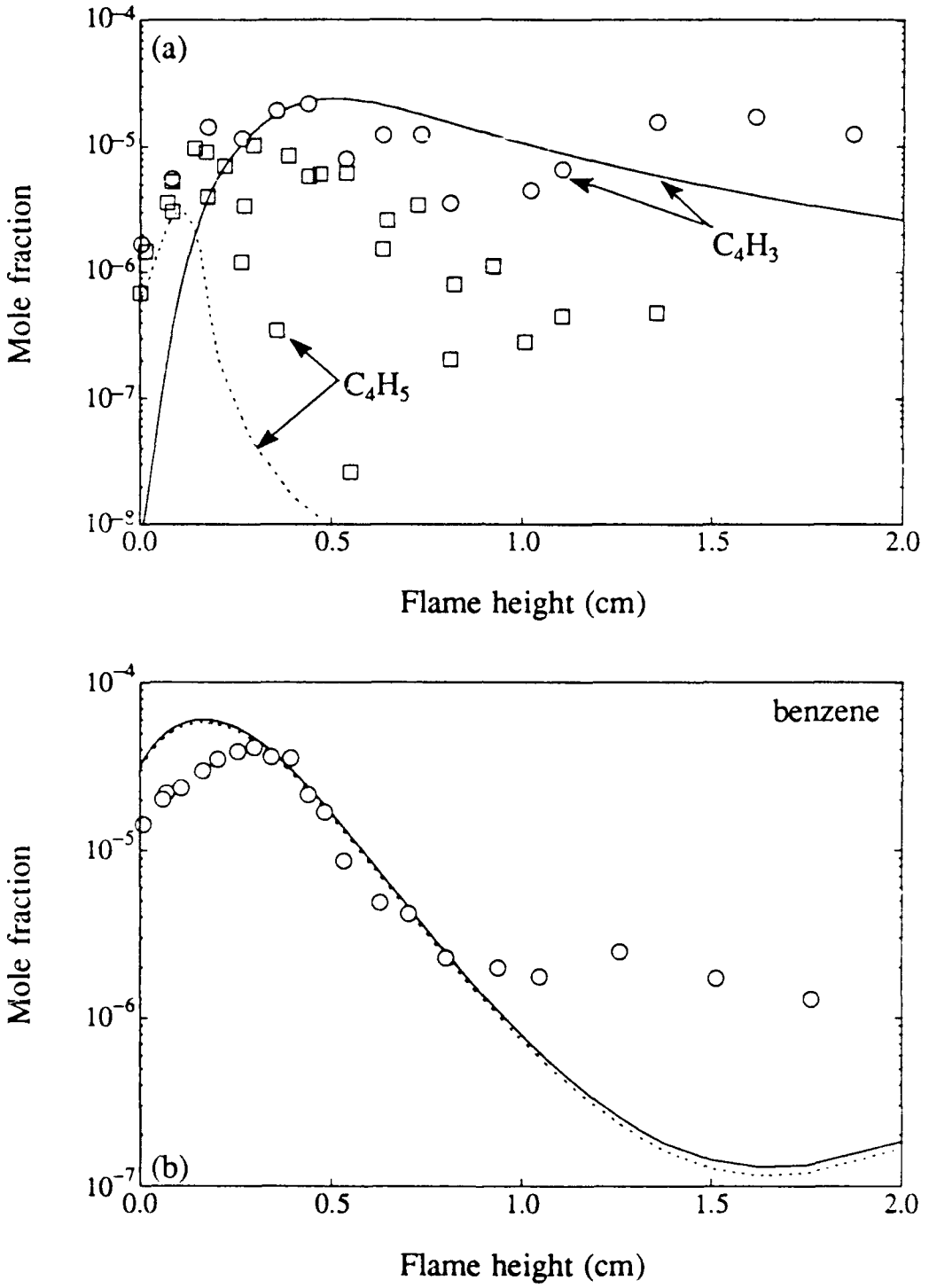

Figure 1. Measured and computed concentration profiles in a 46.5% C_2H_2 – 48.5 % O_2 – Ar laminar premixed flame:[5] (a) C_4H_3 and C_4H_5 radicals, and (b) benzene. The dotted line in (b) is computed with the additon of reactions n–C_4H_3 + H $\rightleftarrows$ i–C_4H_3 + H and n–C_4H_5 + H $\rightleftarrows$ i–C_4H_5 + H with rate coefficient values of 10^{14} cm^3 mol^{-1} s^{-1} for both reactions.

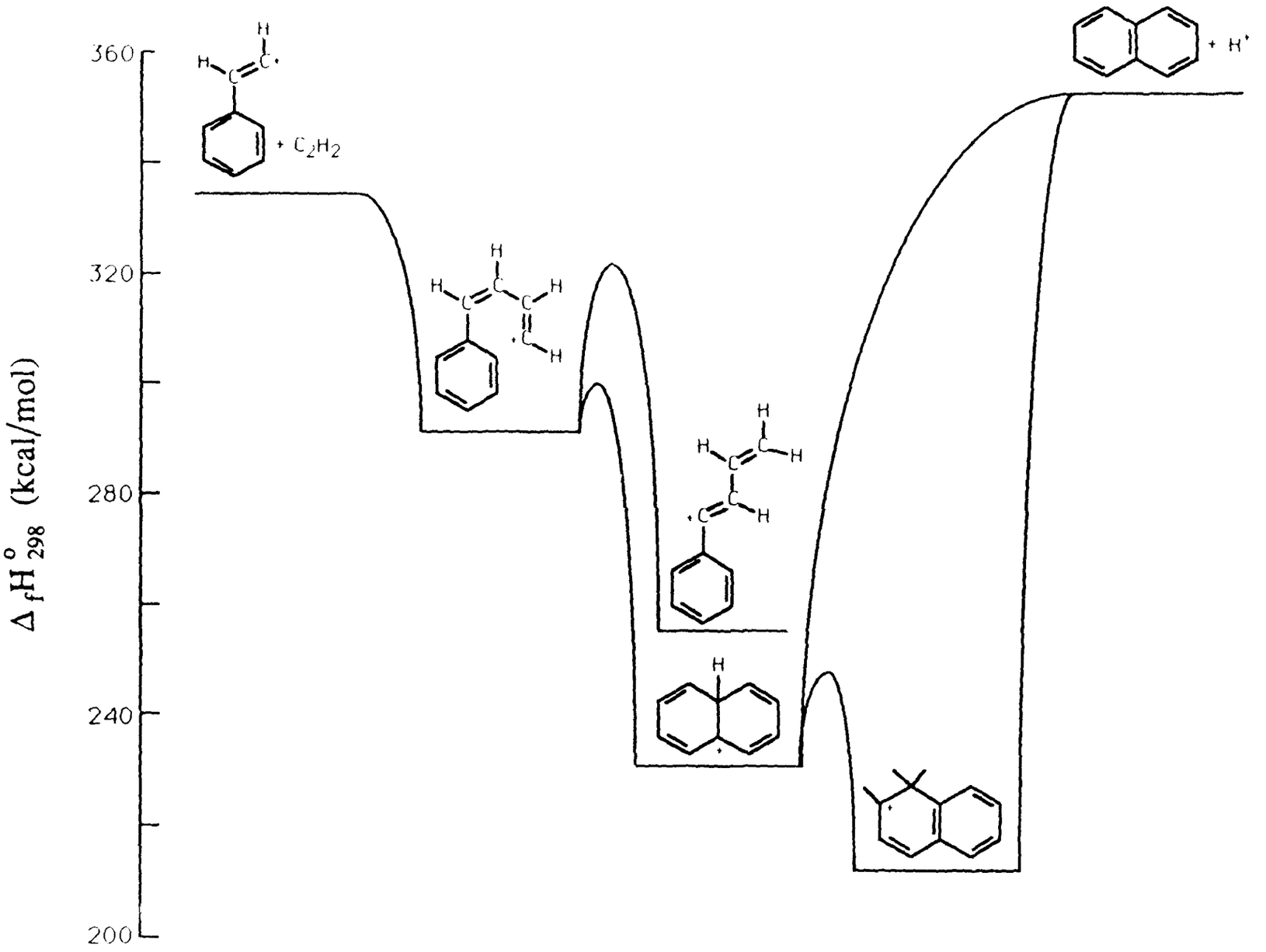

Figure 2. Potential energy diagram for reaction C8H7+ + C2H2 → C10H9+ (preliminary results)

FUELS COMBUSTION RESEARCH

(AFOSR Grant-89-0034)

Principal Investigators: I. Glassman and K. Brezinsky

Department of Mechanical and Aerospace Engineering
Princeton University
Princeton, New Jersey 08544

SUMMARY/OVERVIEW

Progress in understanding soot formation in combustion systems and the effect of fuel type continues. Since results appear to reveal that soot nucleates at approximately the same temperature for all fuels and under all conditions, the present focus of this research is on the possibility that there is a fundamental high activation energy process controlling for all fuels and under all conditions. Corresponding studies of high temperature oxidation of hydrocarbons have concentrated on the aromatic components of jet propulsion fuels. Studies on benzene and mono- and di-alkylated benzenes have been completed. Work is now concentrated on the polynuclear aromatic hydrocarbon oxidation process. Presented here are the results and suggested mechanisms for the oxidation of 1-methyl naphthalene.

TECHNICAL DISCUSSION

Earlier work in this program led to the development of two important aspects of fuel sooting (1). The first was that though the extent of fuel conversion into soot may significantly change from fuel to fuel, there exists a common mechanism of soot formation for all fuels. The second proposal was that there existed a unique temperature for the onset of soot formation, also regardless of the fuel type. This latter proposition implies that there exists a high activation energy chemical rate step which controls soot inception.

The soot inception temperature was measured initially by noting the first appearance of soot on a thermocouple as it moved along the centerline of a diffusion flame. It was realized that this point was not necessarily the true inception point since particles could reach the position by thermophoresis. As well, it is somewhat difficult to make the observation. Therefore a new, unique approach to understanding the soot formation mechanism was devised. In an overall review of soot formation (2), the principle investigator pointed out that sooting from a hydrocarbon diffusion flame could be eliminated by extensive dilution. Such flames appear blue in comparison to the bright orange of a non-diluted hydrocarbon flame. It was argued that if dilution was limited to the condition that the flame would just turn completely blue (specifically along the center streamline) then the temperature of the flame would be the inception temperature of the soot for that particular fuel. The procedure was to establish a 1 cm high luminous diffusion flame for each fuel, then to dilute with nitrogen until the tip of the flame turned blue. The centerline temperature profile was then measured. The value at the observed flame height led to the latest results obtained for various fuels as shown in the following table.

Fuel	Inception Temperature°K
Acetylene	1665
Allene	1586
Ethene	1700
Benzene	1580
1,3 Butadiene	1650
2-Butene	1684
Toluene	1570

There is about 150 K spread in the data. But most interesting is the observation that the temperature variation is oriented so that the least sooting fuel (ethene) has the highest temperature and the most heavily sooting fuel (toluene) has the lowest. Obviously dilution affects the flame somewhat. One is lead to believe that the inception point under non-diluted conditions is close to 1700.

There have been some published results (3,4) that would lead one to believe that nitrogen dilution was more of a concentration effect than temperature effect. The manner in which the investigators conducted their experiments could have affected their conclusions. Since it could be the soot observation technique that could cause the disparity between the investigators' and the early results obtained in this program, it became apparent that an adoption of the completely diluted flame to just eliminate soot which was described above could be a good technique to resolve the question. Experiments were performed in which Ar and CO_2 were used as diluents as well as N_2. To achieve the blue flame with Ar requires greater dilution than N_2. Likewise CO_2 requires less. If dilution were an important effect a different inception temperature would be found for each diluent for each fuel. Fig. 1 reveals that for the four fuels evaluated the same incipient temperature within experimental error is obtained for each fuel.

The current effort on the related aromatic fuels oxidation has concentrated on the oxidation of the polynuclear aromatic hydrocarbons which form an important component of jet fuels. In particular, as reported earlier, the oxidation of 1-methylnaphthalene has been under study. This aspect of the program has been a particularly difficult challenge because of the high molecular weight of the fuel and many of its oxidation intermediates. Condensation in sampling lines have posed very difficult problems. After a thorough experimental analysis of the flow reactor, these difficulties have been resolved and very interesting data are being obtained.

The recent experimental oxidation tests (5) have revealed that naphthalene, indene, phenylacetylene, and benzene were the major aromatic intermediates in the oxidation of 1-methylnaphthalene, with naphthalene reaching a maximum concentration first, then indene, phenylacetylene, and finally benzene (see Fig. 2). The major aliphatics detected were acetylene, methane, ethylene, vinylacetylene, and cyclopentadiene. Significant quantities of 1-naphthaldehyde were found, as well as small concentrations of 1-naphthol and 1,2-dimethylnaphthalene. Just as 1-methylnaphthalene is the doubly-ringed aromatic analog of the singly-ringed toluene, 1-naphthaldehyde, 1-naphthol, naphthalene, indene, and phenylacetylene are the analogues of the major intermediates in the oxidation of toluene, whose mechanism was previously studied in the flow reactor. By analogy then, major mechanistic steps in the oxidation of 1-methylnaphthalene have been proposed (5): once an initiation process has established a radical pool of H, OH, O, and HO_2, the

fuel is attacked by radical abstraction of an H atom from the methyl group, forming the 1-naphthylmethyl radical (see Fig. 3). Displacement of the methyl group by a H atom is probably an additional mechanism of attack of the fuel, and leads directly to the formation of naphthalene. The 1-naphthylmethyl radical, resonantly stabilized to even a greater extent that the benzyl radical in toluene oxidation, undergoes radical-radical reactions with O and HO_2 to form 1-naphthaldehyde. Abstraction reactions with radicals and O_2 break the weak C-H bond of naphthaldehyde, and subsequent unimolecular decomposition yields the 1-naphthyl radical (which quenches to naphthalene in the sample probe) and CO. Reaction of the 1-naphthyl radical or naphthalene with radicals or O_2 gives 1-naphthoxy (observed as 1-naphthol), which rearranges and decomposes to the indenyl radical (observed as indene) and CO. Further radical attack finally ruptures the second aromatic ring and produces the styrene radical, which undergoes β-scission to form phenylacetylene or the phenyl radical (observed as benzene) and acetylene. Support for this mechanism is given by the presence of all of the suggested species (or quenched forms of the radicals), and the lack of any other significant peaks in the GC analysis of the flow reactor runs. Further support is evident in the successive attainment of maximum concentration in the profiles of naphthalene, indene, phenylacetylene, and benzene, consistent with the predictions of the mechanism.

References

1. Gomez, A., Littman, M.G., and Glassman, I., Combustion and Flame 70, 225 (1987).
2. Glassman, I., 22nd Symp. (Int'l.) on Combustion, The Combustion Institute, p. 379 (1988).
3. Axelbaum, R.L., Law, C.K., and Flower, W.L., ibid, p. 379 (1988).
4. Gulder, O.L. and Snelling, D.R., 23rd Symp. (Int'l.) on Combustion, in press.
5. Shaddix, C., Brezinsky, K., and Glassman, I., "The High Temperature Oxidation of 1-Methynaphthalene," 2nd Int'l. Congress on Toxic Combustion By-Products, 1991 (to appear in Comb. Sci. and Tech.).

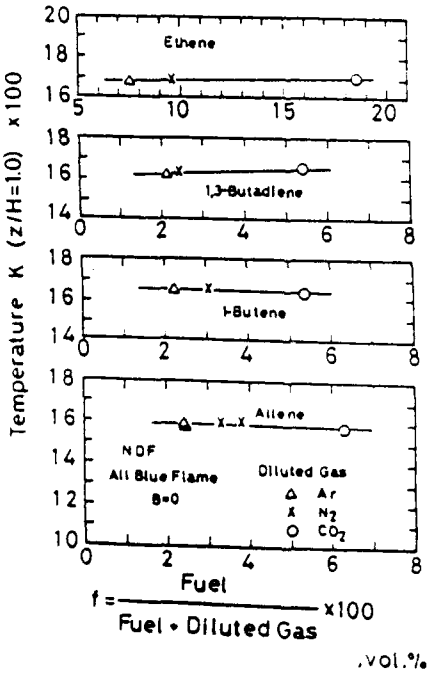

Fig. 1

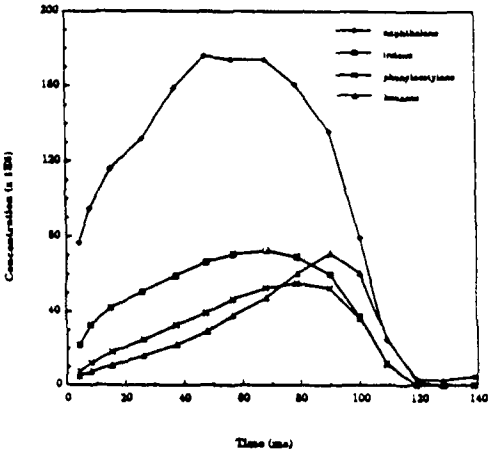

Fig. 2. Time histories of major aromatic intermediates in the flow reactor oxidation of 1-methylnaphthalene, $\phi = 0.47$.

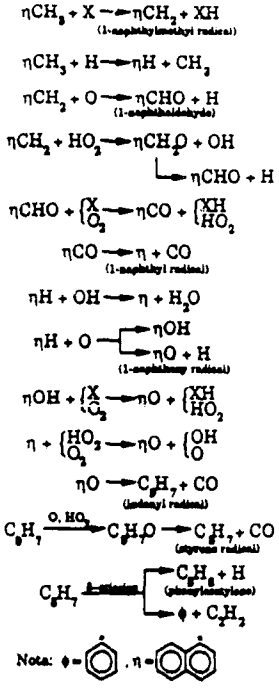

Fig. 3. Proposed mechanism of 1-methylnaphthalene oxidation

PARTICLE DISPERSION IN TURBULENT SHEAR FLOWS

AFOSR Grant No. 89-0392
Principal Investigators: Ian M. Kennedy and Wolfgang Kollmann

Dept. of Mechanical, Aeronautical and Materials Engineering,
University of California,
Davis,
Calif. 95616

SUMMARY:
This joint experimental and numerical project seeks to test and improve our current modelling of droplet scale processes in a turbulent shear flow environment. The experimental approach uses Lagrangian measurements of single droplets in a well characterized turbulent jet to investigate the impact of turbulence on droplet drag and vaporization rates. Comparisons are made with either the results of vortex dynamics calculations or a Large Eddy Simulation in which equations of droplet motion are integrated along with the currently available correlations for drag and vaporization.

TECHNICAL DISCUSSION

Experimental method:

A schematic of the experiment is shown in Fig. 1. A steady stream of monodisperse droplets is generated using a piezoelectric transducer. The droplets are accelerated by the air flow in the nozzle contraction. As each droplet leaves the nozzle it passes through a He-Ne laser beam which is monitored by a photodiode. The diode signal is used as a trigger for the data acquisition system, thereby permitting the individual droplet time of flight to be measured between the nozzle and some downstream location.

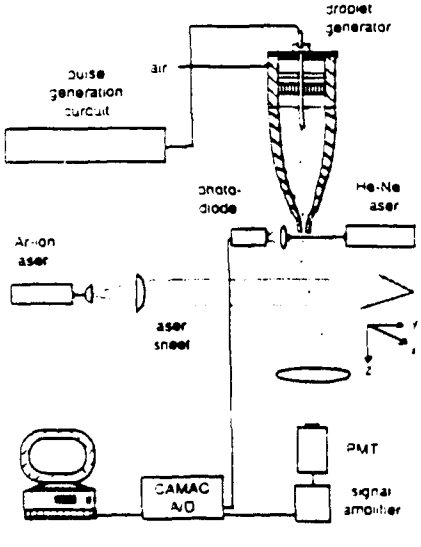

Fig. 1 Experimental Apparatus

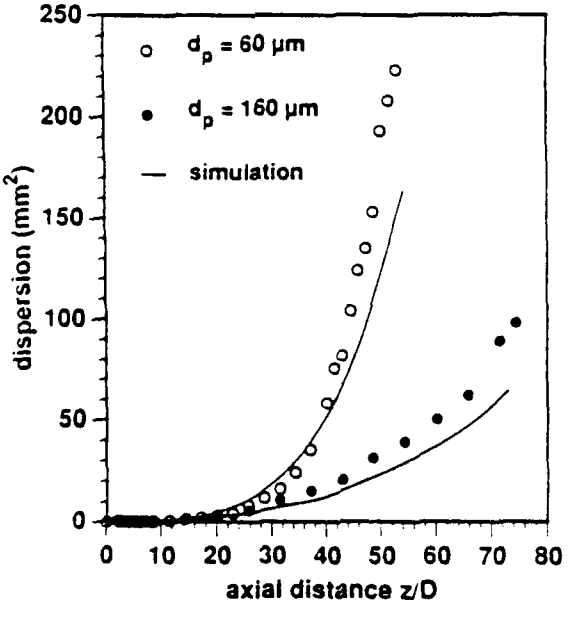

Fig.2 Droplet dispersion as a Function of Axial Location

The droplets are dispersed by the turbulence. Their radial positions at some axial location are measured with a position sensing photomultiplier tube (PMT) that detects light scattered by the particles from a laser sheet. The experiment originally used a photodiode for this purpose but it was found to be too noisy. The PMT gives very high signal to noise ratios (even for the smallest droplets) and its frequency response is sufficiently fast that we are able to track particles as they traverse the sheet of laser light.

As each particle passes through the laser sheet a series of pairs of (x,y) coordinates for its location are obtained. The pairs of data are separated by 50 ms. In order to obtain Lagrangian measurements of dispersion the laser sheet is traversed along the jet axis in finely spaced increments of position. It is then possible to sort the large data set of particle positions into functions of time of flight rather than axial location: the width of each narrow time bin is given by $\Delta t/t \leq 0.04$. By this means we are now able to obtain Lagrangian measurements of droplet dispersion and other statistics such as probability distribution functions (pdfs) of position.

Particle axial velocities are obtained by timing the passage of a droplet through the laser sheet. The timing is performed by determining the width of the scattering pulse on the PMT signal. Work is in progress to obtain radial velocity components by following the position of a particle through either a thickened laser sheet or through multiple sheets.

Results

Figure 2 shows dispersion (mean square displacement from the initial position at the nozzle exit) for two sizes of hexadecane droplets as functions of downstream distance. Also shown in this figure are the results of a stochastic simulation of the particle dispersion which was carried out in the same manner as that used by Faeth and co-workers and others. In the calculation the droplet drag was calculated as

$$C_D = \frac{24}{Re}\left(1 + \frac{Re^{2/3}}{6}\right) \qquad Re < 1000$$

The data are presented as Eulerian statistics. However, the experimental technique permits us to offer an alternative presentation. With the times of flight it is possible to interpret the data in terms of dispersion as a function of time as presented in Fig. 3.

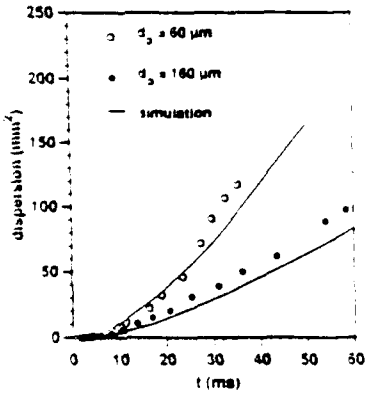

Fig. 3 Droplet Dispersion as a Function of Time of Flight

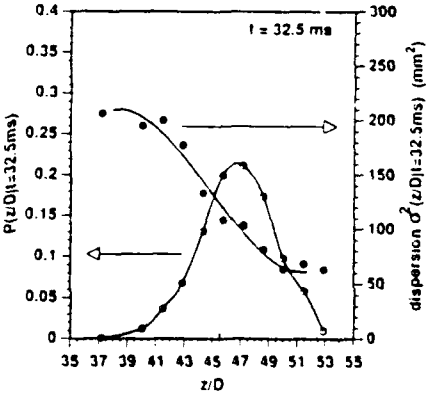

Fig.4 PDF of Axial Location and Dispersion at 32.5 ms from Nozzle Exit

It is also possible to examine conditioned statistics such as the pdf of droplet axial location for a given time of flight or the droplet dispersion as a function of axial location for a given time of flight. These conditioned statistics are shown in Fig. 4.

Effect of Initial Conditions

The results from the previous year's work suggested a significant impact of the initial conditions of droplet velocity on their dispersion. This aspect of droplet behavior has been looked at in greater detail during the past year. The experiment has been modified slightly so as to impart a controllable perturbation to the velocities of the droplets before they leave the nozzle. Figure 5 shows that a secondary air stream is introduced into the tube through which the droplets pass on their way to the nozzle. The impinging air jets cause the droplets to leave the nozzle with a small fluctuation in radial velocity.

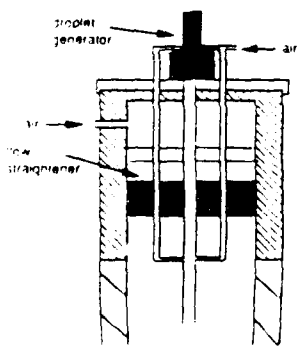

Fig. 5 Modified Droplet Generation and Droplet Delivery System

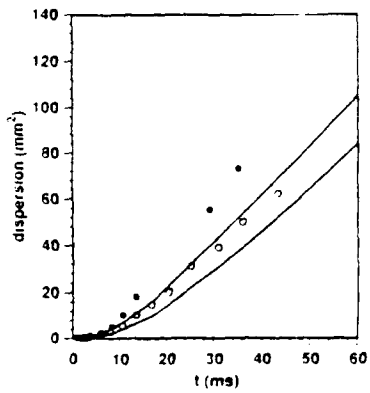

Fig. 6 Dispersion of Droplets with no Initial Velocity Fluctuation (o) and with Initial Fluctuation (•); solid lines are stochastic simulations

The effect of this initial perturbation may be seen in Fig. 6 in which the dispersion of 160 μm diameter droplets of hexadecane is shown. The magnitude of the initial velocity rms fluctuation was determined from detailed measurements of droplet trajectories near the nozzle. Clearly, the initial velocity fluctuations have a significant impact on particle dispersion for large droplets. The experiment was repeated for 60 μm droplets and no measurable difference in dispersion was found.

A second potentially important parameter has been investigated i.e., the location of injection of the particles into the shear layer. A further modification to the droplet apparatus has been used to study this problem. An extended liquid delivery tube and droplet generating nozzle were used to inject the droplets close to the nozzle wall. They ultimately left the nozzle with a displacement of about 1 mm from the axis of the jet. Figure 7 shows that their subsequent dispersion was affected by the position at which they entered the flow. It is likely that the structures generated by the initial shear layer instabilities may affect the downstream dispersion of the droplets.

Droplet axial velocities have also been measured. The mean axial velocities at different axial planes are shown in Fig. 8 for droplets of two sizes. Also shown in the figure are the results of the stochastic simulations which predict the velocities quite well. This figure demonstrates that the larger particles do not adjust to the gas flow quickly; rather, their inertia maintains their velocities well in excess of the gas velocities for a considerable time.

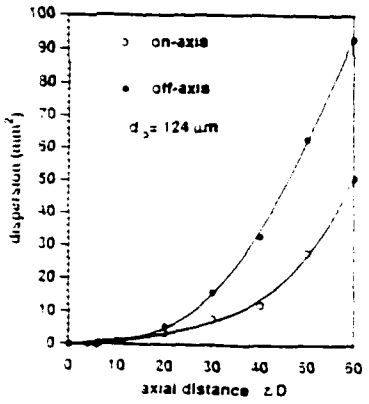

Fig. 7 Influence of Off-Axis Injection on Particle Dispersion in Jet

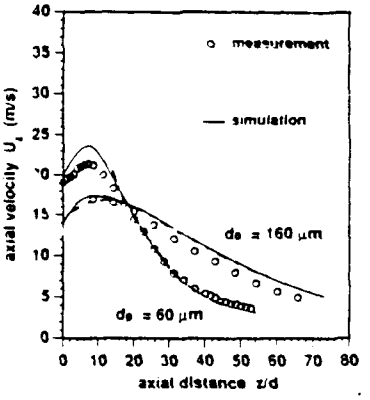

Fig. 8 Droplet Mean Axial Velocities

Numerical Simulations:

The purpose of the numerical study is to develop a flow simulation in which droplet motion may be followed without the modelling that is inherent in other methods such as the stochastic simulation. Work in the previous year was concerned with a vortex dynamics calculation for infinite Reynolds number jet flows. During the past year progress has been made on developing a large eddy simulation for a turbulent round jet at moderate Reynolds numbers. The current effort has gone into identifying and testing the most appropriate numerical scheme for this calculation.

A compact finite difference scheme and a forward time centered space (FTCS) scheme have been evaluated for the viscous Burger's equation as a test case. It was found that the compact scheme was more accurate for flows with large viscosity and small gradients but it offered no advantage over the FTCS method otherwise.

The two techniques have also been applied to a plane 2D jet. This flow was found to offer a good test of the potential methods that may be used in the simulation of the round turbulent jet. Figure 9 shows the velocity field for the 2D jet at Re=4000. Work is proceeding on developing a 3D finite difference code in axisymmetric coordinates; a spectral method will be used in the azimuthal direction to take advantage of periodicity.

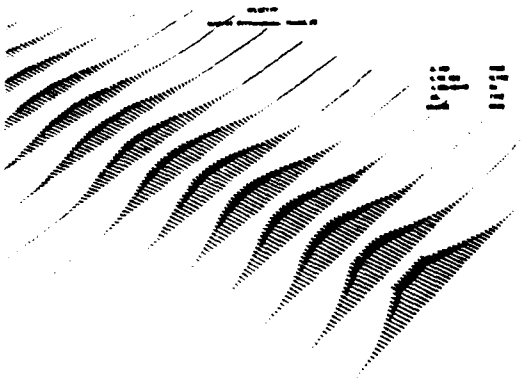

Fig. 9 Velocity Vectors in Plane Jet, Re=4000

INVESTIGATION OF THE APPLICATIONS OF LASER-INDUCED FLUORESCENCE TO FUEL SPRAY AND SINGLE DROPLET VAPORIZATION

ARO Contract No. DAAL03-87-K-0120

Principal Investigator: Lynn A. Melton

Department of Chemistry
University of Texas at Dallas
Richardson, TX 75083-0688

SUMMARY/OVERVIEW:

This report summarizes a variety of techniques for the study of isolated droplets. New results, which indicate partially selective optical sampling of droplets irradiated with a uniform laser beam, are reported for the heating of hexadecane droplets. Techniques under development and/or available now include exciplex fluorescence thermometry, "droplet slicing" and imaging, correction for refraction effects by droplet surfaces, measurement of temperature fields within droplets, and production of monodisperse droplets at high pressures. Not discussed in this abstract is the development of apparatus and techniques for lifetime imaging, which may lead to imaging of the equivalence ratio.

TECHNICAL DISCUSSION:

A. Temperature Measurements in Falling Droplets (UTD)

A previous report described the use of exciplex fluorescence thermometry to measure the (near-surface) temperature of 225 micron droplets, which had fallen 10 cm through a known heated ambient.[1] This work has been extended by (1) reconstructing the apparatus so that the temperature of the droplet could be measured at virtually any point in its 9.5 cm fall through heated nitrogen, (2) increasing the temperature of the ambient to 550 ^{o}C, and (3) using 1,3-di(1-pyrenyl)-propane (PYPYP) as the exciplex fluorescence thermometry dopant, which results in a concentration-independent thermometer useful up to 400 ^{o}C. Other elements of the experiment were substantially similar to the Wells and Melton work. However, in these measurements with 1 x 10^{-4} M P/PYP in hexadecane, the 280 micron diameter droplet was optically thin (absorbance along a diameter = 0.06, as opposed to Wells and Melton results where the absorbance along a diameter was 4). Figure 1a shows the temperature profiles in the fall tube; Figure 1b shows the inferred temperatures of the droplets as a function of fall distance/time. For each curve, the droplet

temperature appears to rise slowly, jump sharply, and then continue a slow rise. The highest temperatures measured for the hexadecane droplets (normal boiling point = 287 ^{o}C) are approximately 200 ^{o}C. Video microscopy measurements showed no evaporation of the droplet.

It is highly unlikely that the temperature of the entire hexadecane droplet jumps 100-120 ^{o}C in 5 ms and then resumes a slow rise. It is much more likely that the excitation process and fluorescence collection process results in selective sampling of the temperature field within the droplet. This "partially selective optical sampling" (PSOS) process has been modeled using geometrical optics. The droplet acts as a lens, which focuses the incoming beam, and through convergence of rays reflected at the backside of the droplet, a "hot spot" is formed at a fractional radius of about 0.75. The programs developed in this work also calculate the fraction of the isotropically emitted fluorescence which is refracted into the detector aperture. Overall, 58% of the total fluorescence originates from the shell between fractional radii of 0.5-0.75, even though this shell accounts for only 30% of the droplet volume. Thus, it is probable that the "temperature jump" records the change of temperature of the selectively sampled portion of the droplet. If radial diffusion is the dominant mechanism for the heating of the interior of the droplets, then the jump records the passage of the thermal wave; if internal circulation is the dominant mechanism, then the jump records the heating of the interior of an internal circulation vortex.

B. Summary of Other Droplet Techniques Used Under Current Contract

1. Correction for Refraction by Droplet (UTD)

The novel work carried out at United Technologies Research Center (UTRC, subcontractor) on "droplet slicing" diagnostics, in which a thin laser sheet illuminates an equatorial plane of the droplet, has stimulated modeling work at UTD to determine how to transform the "camera image" obtained in such an experiment into a "real image", appropriate for analysis by investigators interested in heat and mass transport within droplets, i.e., how to undo the distortions caused by refraction at the droplet/air interface.. It appears that the real image can be accurately recovered out to fractional radii of 0.8-0.9.

2. Droplet Slicing Experiments (UTRC)

a. Measurement of internal circulation using laser-induced oxygen-quenched fluorescence has been demonstrated. Decane doped with naphthalene was used to form droplets which fell a short distance in a chamber filled with nitrogen and a variable amount of oxygen. A thin sheet of ultra-violet light from the fourth harmonic of a Nd:YAG laser illuminates an equatorial section of a droplet, and the resulting fluorescence

is imaged onto a two-dimensional CCD detector. Since oxygen is a strong fluorescence quencher, any liquid volume element which has been exposed to it by surface contact or diffusion will suffer a reduction in fluorescence intensity. Convection from the surface due to internal circulation as well as diffusion cause image regions to appear dark.

b. Methods have been developed which make it possible to determine unambiguously from an experimental image whether the laser sheet did indeed bisect the droplet.

c. Using "droplet slicing" techniques and exciplex fluorescence thermometry, measurements of the temperature field within a droplet have been made. The fluorescence from a single "sliced" droplet, which had fallen into heated nitrogen, was recorded on a color CCD camera. For droplet temperature measurements, the thermometry is carried out by separating the RGB outputs of the CCD camera and dividing the blue intensity by the green intensity pixel by pixel, to obtain a ratio which can be calibrated against the liquid temperature. Thus, signal processing takes the place of complex optical systems with multiple mirrors and separate blue and green filters.

3. Novel Techniques for Monodisperse Droplets (UTRC)

a. Droplet-on-demand generators, which produce droplets reproducibly, can be produced without the use of high-voltage, expensive, tempermental piezoelectric crystals. The 25 mm diameter speaker from a set of personal stereo headphones, driven by a pulse of 2-20 volts, can be used as the driver.

b. Reliable production of uniformly-sized fuel droplets in the 300-1000 micron diameter range at pressures up to 400 psia (27 atm) has been made routine. Data have been acquired of internal flow patterns within droplets as a function of both pressure and time delay.

c. The process of ejecting a droplet through the nozzle of standard droplet generators may induce internal circulation in the same direction as that caused by aerodynamic forces. However, when droplets are ejected into an electrostatic trap where they can be held long enough for any fluid motions due to the droplet formation process to damp out, the influence of aerodynamic forces on internal circulation can be unambiguously identified. Alternately, an aerodynamic droplet generator can be used to produce monodisperse droplets in the core of an axisymmetric jet. The gas flow around the end of a hypodermic needle strips off droplets. Since the gas flow velocity is greater than the initial liquid velocity, any internal circulation due to the droplet formation process will be opposite to that produced by free fall.

1. M.R. Wells and L. A. Melton, "Temperature Measurements of Falling Drops", J. Heat Transfer, **112**, 1008 (1990).

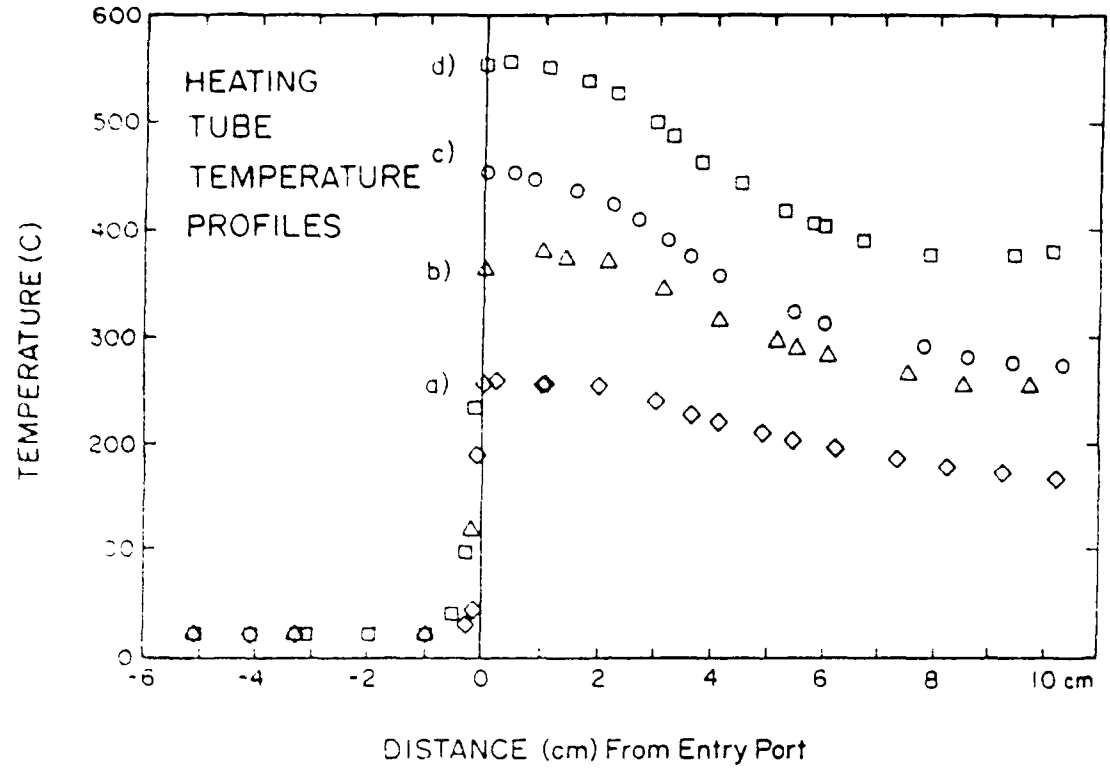
HEATING
TUBE
TEMPERATURE
PROFILES
d)
c)
b)
a)
TEMPERATURE (C)
600
500
400
300
200
100
0
-6
-4
-2
0
2
4
6
8
10 cm
DISTANCE (cm) From Entry Port

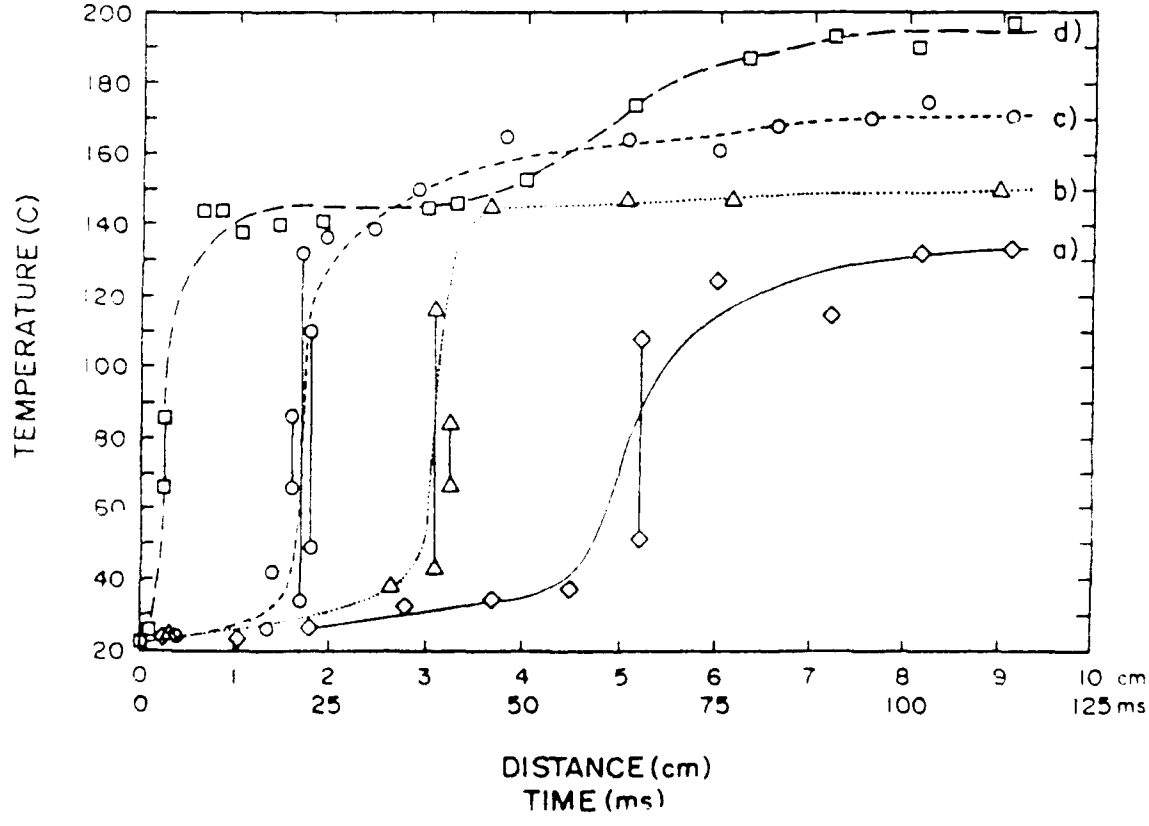
TEMPERATURE (C)
200
180
160
140
120
100
80
60
40
20
d)
c)
b)
a)
0
1
2
3
4
5
6
7
8
9
10 cm
0
25
50
75
100
125 ms
DISTANCE (cm)
TIME (ms)

FUNDAMENTAL STUDIES OF LASER IGNITION AND KINETICS IN REACTIVE GASES

(AFOSR Contract No. 91-0004)

Principal Investigators: Andrzej W. Miziolek
Brad E. Forch

U. S. Army Ballistic Research Laboratory
Aberdeen Proving Ground, MD 21005-5066

SUMMARY/OVERVIEW:

This year our efforts have concentrated on expanding our understanding of uv laser photofragmentation of reactive gases as well as in developing new multiphoton diagnostics for photofragment detection and temperature determination. The main thrusts of our research, that of determining the spin-orbit distributions of oxygen atoms from molecular oxygen using a tunable ArF (193 nm) laser, and the subsequent determination of spin-orbit effects in H_2/O_2 flames, have been delayed due to start-up problems with the laser which have only recently been solved. These experiments are currently underway and a second low pressure burner apparatus has been made operational for this work.

TECHNICAL DISCUSSION

Last year we reported on the wavelength tunable ignition of H_2/O_2 and D_2/O_2 premixed flows in which a distinct H/D isotopic wavelength dependence was demonstrated with the most efficient ignition occurring at 243.2 nm (for H) and 243.0 nm (for D).[1] We also presented results on the fuel molecule-specific microplasma emission resulting from irradiation by a focussed ArF excimer laser beam.[2] In addition, we described the initiation of a laser ignition modeling effort which has been substantially developed but is not yet fully completed.[3]

A. Spin-Orbit Specific Kinetics

The main thrust of our present research is to determine the extent of oxygen-atom spin-orbit specificity in the kinetics of H_2/O_2 flames. The reason we are interested in this is because of our observation of a non-statistical distribution of O-atom ground electronic spin-orbit states following irradiation of molecular oxygen by a broadband unfocussed ArF excimer laser. Our observation of non-statistical behavior, which was reported in a previous year's abstract, was recently confirmed with a reported nascent distribution of the $^3P_2$:$^3P_1$:$^3P_0$ states of 0.47:0.31:0.22,[4] while a thermalized distribution yields a ratio of 0.74:0.21:0.05. Such a high propensity for the formation of the $^3P_0$ spin-orbit state may have implications on the kinetics of H_2/O_2 flames, assuming that there is a significant difference in the elementary kinetic rate constants between the three different spin-orbit states, such as has been observed for other atoms.[5] Our research strategy is relatively straightforward, and that is to establish individual O_2 ro-vibronic photodissociation product spin-orbit ratios using a tunable excimer laser (which can preferentially pump a number of such states) in a low pressure apparatus. Subsequently, we intend to determine the effect of individual ro-vibronic state photolysis in a flame environment. If there are significant differences in O-atom reactivity, depending on which spin-orbit state it is preferentially formed, then one

might expect localized increases/decreases in flame kinetics (heat feed-back) as a result of ArF laser photolysis, particularly in the preheat and primary flame zone. As mentioned before, these experiments are currently underway.

B. UV Laser Photodissociation

While the tunable ArF excimer laser was being made operational, we engaged in further photodissociation studies, but now with a molecule that is somewhat larger that molecular oxygen, and thus having many more photodissociation channels. The molecule we chose, dimethylnitramine (DMNA), is of interest primarily because other researchers have studied it experimentally (although primarily involving the ground potential energy surface) as well as theoretically.[6] Figure 1 shows the prompt emission spectrum following DMNA photolysis at 248 nm (KrF excimer laser). The two prominent peaks (other than the one due to laser scatter) have been attributed to the OH and NO_2 photofragments. Figure 2 shows the nascent rotational population distribution for ground-state OH formed by photolysis of DMNA (open squares) and nitric acid (filled triangles). In both of these cases the rotational "temperature" is rather high (ca. 1400 K). Other results of this study include the determination that the NO_2 A^2B_2, NO_2 X^2A_1, and the OH ground-state are formed via monophotonic, unimolecular pathways, and that the OH excited-state is formed by a two-photon, unimolecular process.

C. Multiphoton Excitation Studies of NO for Flame Thermometry

During the process of determining the primary photoproducts in the above study, we realized the importance of developing diagnostics for species, such as NO, whose single-photon excitation falls far in the ultraviolet region (220 nm) and thus may suffer from the coincident perturbation (photolysis) of other species such as NO_2. This perturbation, of course, leads to artificially high levels of NO. Our approach of two-photon excitation of the NO (A) state at 452 nm was inspired by Professor T.A. Cool of Cornell University, who pioneered this method for flame NO detection. Figure 3 shows a Resonance Enhanced Multiphoton Ionization (REMPI) spectrum of the O_{22} + P_{12} branch taken in a $C_2H_4/O_2/Ar$ flame containing 1% NO.[7] A spectral simulation yields a temperature of 1169+/-50 K, which is in fair agreement with the temperature (1000 K) measured with a coated thermocouple. Figure 4 shows a two-photon LIF spectrum of NO taken at room temperature. As one can see, the spectral best-fit simulation yields a temperature of 326 K. Both the high temperature and room temperature results are encouraging, but indicate that significant improvements are still needed before this approach can be utilized as an alternate/additional flame thermometer. In particular, improvements are needed in spectroscopic constants and in transition probabilities.

1. B.E. Forch and A.W. Miziolek, **Combustion and Flame** (in press) and **Proceedings of the 27th JANNAF Combustion Meeting** (in press).
2. R.J. Locke, J.B. Morris, B.E. Forch, and A.W. Miziolek, **Appl. Opt.**, 29, 4987, 1990.
3. N.M. Witriol, B.E. Forch, and A.W. Miziolek, **Proceedings of the 27th JANNAF Combustion Meeting** (in press).
4. Y. Matsumi and M. Kawasaki, **J. Chem. Phys.**, 93, 2481, 1990.
5. P.J. Dagdigian and M.L. Campbell, **Chem. Rev.**, 87, 1, 1987.
6. M.J. McQuaid, A.W. Miziolek, R.C. Sausa, and C.N. Merrow, **J. Phys. Chem.**, 95, 2713, 1991.
7. R.C. Sausa, S.L. Howard, R.J. Locke, A.J. Kotlar, and A.W. Miziolek, **Fall Meeting of the Eastern Section: The Combustion Institute**, 1990.

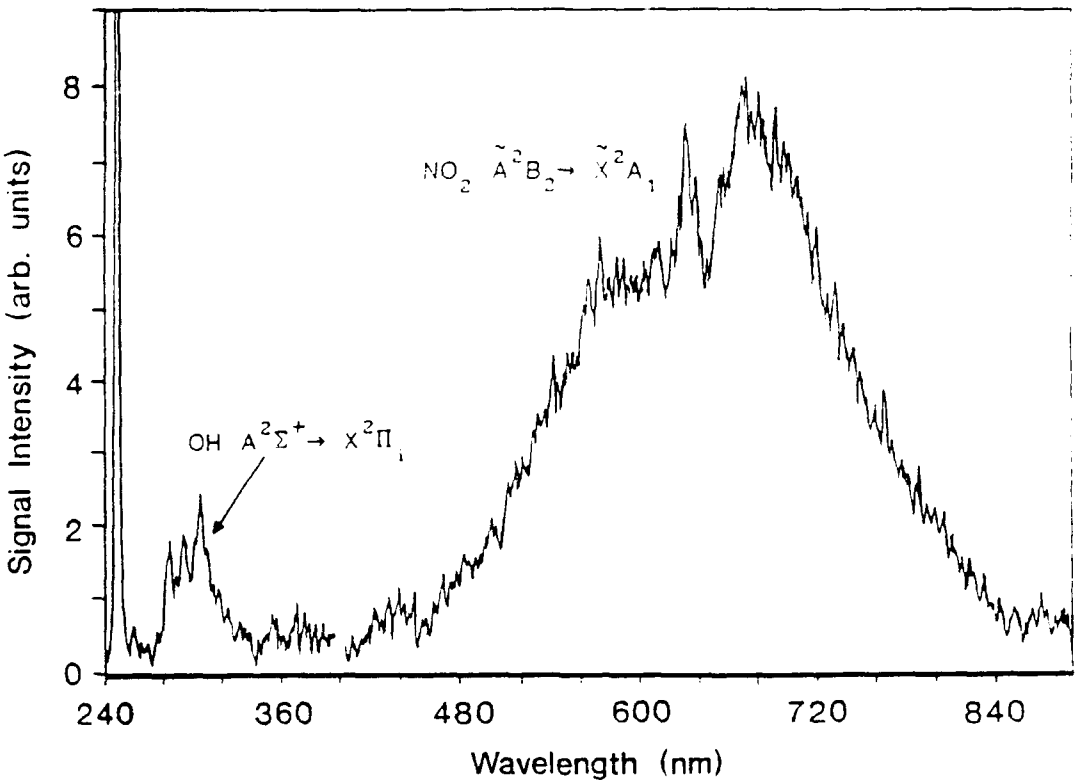

Figure 1. Prompt emission spectrum following DMNA photolysis at 248 nm.

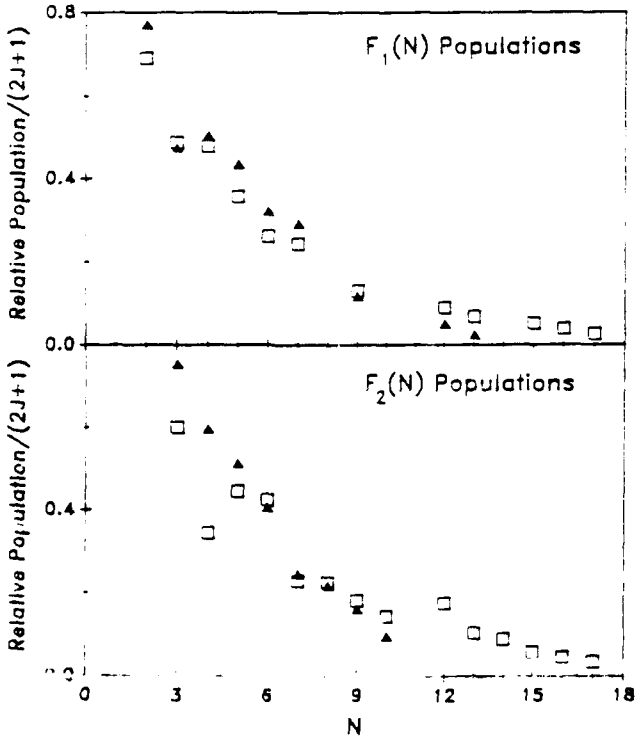

Figure 2. Rotational population distribution of the OH photofragment formed by 248 nm photolysis of DMNA (open squares) and nitric acid (filled triangles)

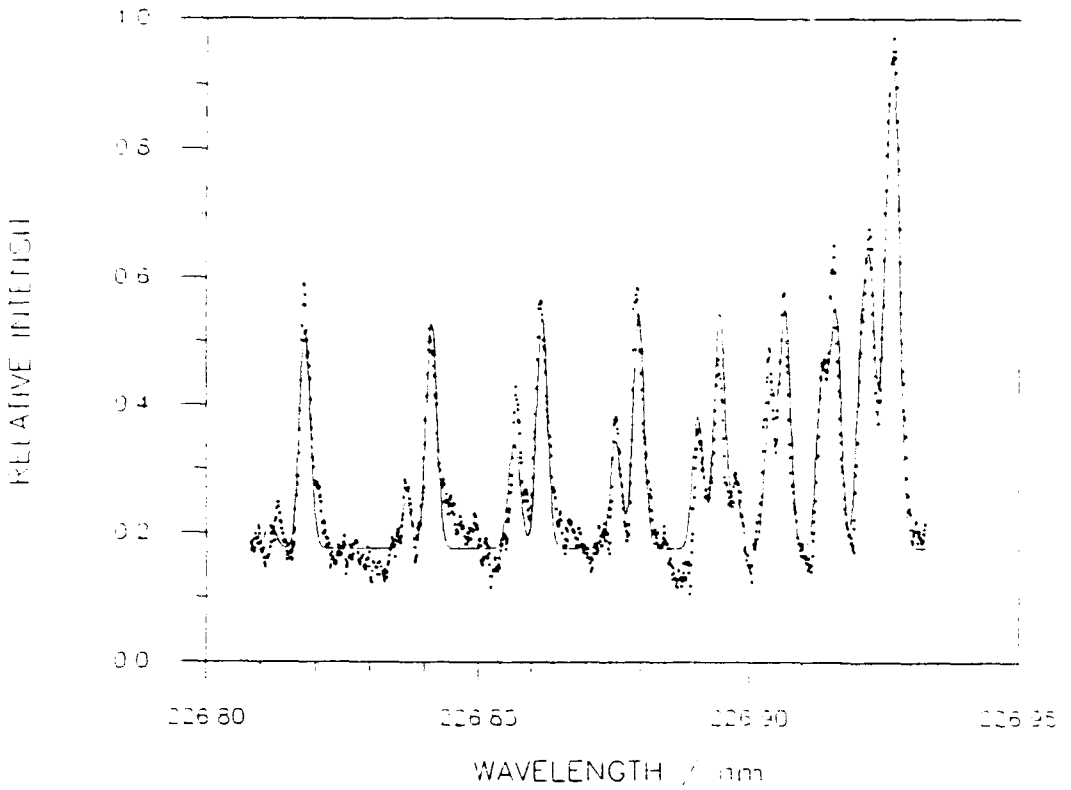

Figure 3. REMPI (2+2) spectrum of the NO O_{22}+P_{12} branch (T=1169+/-50K)

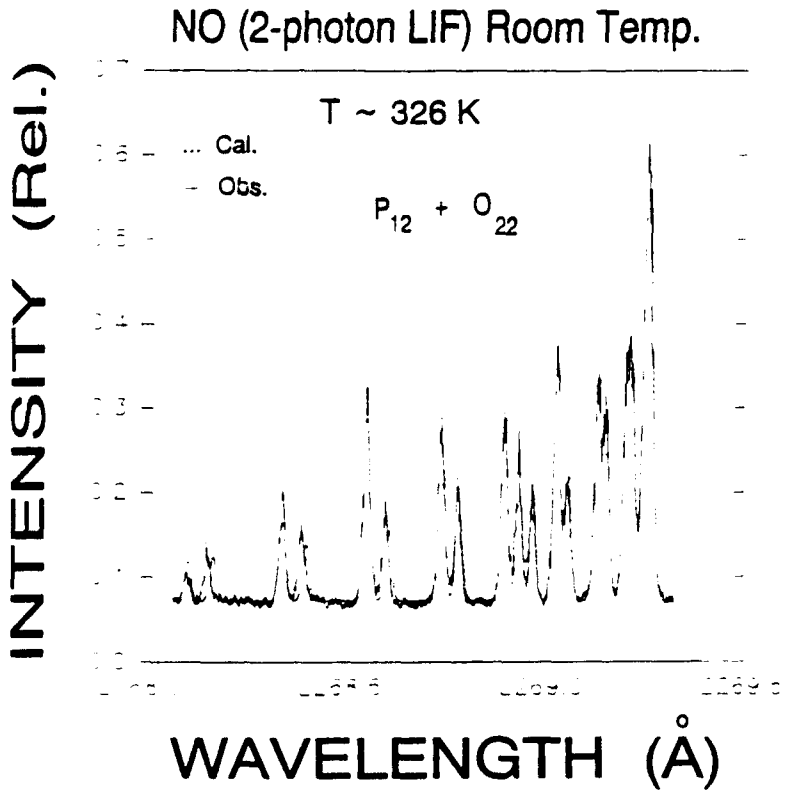

Figure 4. Two-photon LIF of NO at room temperature

TRANSPORT PHENOMENA AND INTERFACIAL KINETICS IN MULTIPHASE COMBUSTION SYSTEMS†

AFOSR Grant No. 89-0223

Principal Investigator: Daniel E. Rosner‡
High Temperature Chemical Reaction Engineering Laboratory
Department of Chemical Engineering, Yale University
New Haven, CT 06520-2159,USA

SUMMARY/OVERVIEW

The performance of ramjets burning slurry fuels (leading to condensed oxide aerosols and liquid film deposits), gas turbine engines in dusty atmospheres, or when using fuels from non-traditional sources (*e.g.*, shale-, or coal-derived), depends upon the formation and transport of small particles, often in non-isothermal combustion gas boundary layers (BLs). Even airbreathing engines burning "clean" hydrocarbon fuels can experience *soot* formation/deposition problems (*e.g.*, combustor liner burnout, turbine blade erosion and "hot" corrosion). Moreover, particle formation and transport are important in chemical reactors used to synthesize or process aerospace materials (turbine blade coatings, optical waveguides, ...). Accordingly, our research is directed toward providing chemical propulsion systems engineers and materials-oriented engineers with new techniques and quantitative information on important particle- and vapor-mass transport mechanisms and rates.

An interactive experimental/theoretical approach is being used to gain understanding of performance-limiting chemical-, and mass/energy transfer-phenomena at or near interfaces. This includes the development and exploitation of seeded laboratory burners (Sections 1,4), flow-reactors (Section 6), and new diagnostic techniques. Resulting experimental rate data, together with the predictions of asymptotic theories (Sections1-6), are then used as the basis for proposing and verifying simple viewpoints and effective engineering correlations for future design/optimization studies.

TECHNICAL DISCUSSION

1. TRANSPORT OF AGGREGATED SUBMICRON PARTICLES

The ability to reliably predict the *thermophoretic* properties of isolated and aggregated flame-generated particles (carbonaceous soot, Al_2O_3, ...) is important to many technologies, including chemical propulsion and refractory materials fabrication. Last year we reported preliminary measurements of the *thermophoretic diffusivity* ($\alpha_T D$) of flame-generated submicron $TiO_2(s)$ "soot" particles using a $TiCl_4(g)$-seeded low strain-rate counterflow laminar diffusion flame technique (Gomez and Rosner, 1991). Inferred ($\alpha_T D$)-values based on *observed* particle-free-zone thicknesses and measured (thermocouple) temperature gradients were well within 10% of values expected using Waldmann's kinetic theory approach *for a dense spherical particle.* Similar conclusions were reached in earlier, rather different experiments on flame-generated submicron "soots", both organic (*eg.*, Eisner and Rosner,1985) and inorganic (Rosner and Kim, 1984). Our current theoretical studies provide an interesting explanation and confirmation for this remarkable and quite useful *insensitivity of (orientation-averaged) $\alpha_T D$ to aggregated particle size and morphology*; viz. addition of a primary particle to an aggregate containing N such particles increases the thermal force and drag by nearly the same amount in both Knudsen number limits. Our results in the near-continuum limit are shown in Fig 1.1 (Rosner *et. al.*,1991) and even smaller departures from unity are found in the free-molecule limit. In marked contrast, it should be emphasized that the Brownian diffusion-, inertial-, and *optical*-properties of such aggregates are quite *sensitive* to size (N) and morphology. We are now exploring many interesting consequences of these differences.

---

† AFOSR Contractors Meeting on Propulsion, Boulder,CO 10-14 June 1991

‡ For research collaborators consult **REFERENCES**

2. HEAT TRANSFER EFFECTS ON COAGULATION DYNAMICS

Our recent studies of submicron particle migration in host-gas temperature gradients and radiation fields (see, *eg.*, Rosner, *et. al.*, 1991, Castillo *et. al.* 1990), Mackowski, D.W.,1990) suggest that even spherical particles thermally out of equilibrium with their local host gas can coagulate with particle-particle encounter rate constants quite different from the usual "isothermal" Brownian values. This leads to *unusual population dynamics*, including the possibility that initially broad coagulating "overheated" particle populations can become *narrower* than ordinary "self-preserving" populations. This is illustrated in Fig. 2.1 (Rosner *et al.* ,1991), which shows the predicted dependence of (log-normal) spread parameter and geometric mean size on dimensionless time for radiatively heated carbonaceous particles in the near-continuum limit. We are also investigating the frequently occuring converse case: *ie.* the strong tendency of radiatively *cooled* large particles to grow still larger by rapidly "scavenging" smaller ones.

3. 'MOMENT' METHODS FOR TRANSPORT PROBLEMS INVOLVING PARTICLE POPULATIONS

Many flow problems involving coagulating and migrating particle populations can be solved conveniently by deriving/integrating a closed set of differential equations for selected "moments" of the particle size distribution (PSD-)function. This is particularly true when the PSD *shape* is relatively simple (eg., single mode log-normal) and does not markedly change as a result of the participating phenomena. One such class of problems occurs in the *theory of aerosol sampling*---ie. correcting PSD instrument data for the systematic effects of wall losses and/or coagulation in the *upstream* sampling tube.We have recently shown that the necessary correction factors can be calculated by direct upstream integration of a closed set of 3 moment equations (Rosner and Tassopoulos,1991).As a representative example, Figure 3.1 shows the correction factor for total particle number density as a function of the scaled length of the sampling system and the spread parameter of the aerosol measured at the instrument (for turbulent gas flow in the absence of appreciable coagulation).

4. MULTIPHASE BOUNDARY LAYER THEORY:THERMOPHORESIS AND INERTIA

Our seeded micro-combustor experiments, and ancillary theoretical calculations on the interesting competition between particle *inertia* and particle *thermophoresis* for the case of laminar gaseous boundary layers on surfaces with streamwise curvature (as for combustion turbine blades) are now essentially complete (Konstandopoulos and Rosner, 1991; Rosner *et. al.* 1991).

5. KINETICS AND MORPHOLOGY OF CVD-MATERIALS

A small impinging jet (stagnation flow) reactor has been designed and built for studying the CVD-rates of refractory films on inductively heated substrates. To help understand the topography of CVD film surfaces in the limit when thermally driven mass transfer *dominates* concentration diffusion we recently completed a linear stability theory (Castillo, et.al.,1991)

Because of the energetic potential of boron as a solid fuel (or fuel additive) and the likely role of *surface* reactions involving the gaseous oxidant $B_2O_3(g)$ in the processes of fine boron-particle ignition, combustion and extinction, we have obtained flow reactor measurements of the intrinsic kinetics of the gasification of CVD-B(s) at surface temperatures between about 1300K and 2100K (Zvuloni *et al.*, 1989 , Zvuloni,1990). While the chemical propulsion implications of these measurements were emphasized in our recent *AIAA-JPP* publication (Zvuloni *et al.*, 1989a) and its chemical propulsion conference companion (Gomez et. al.,1991), the experimental techniques and the mechanistic implications of our results will be emphasized in a full-length manuscript prepared for *J. Phys. Chem* (Zvuloni, Rosner and Gomez, 1990).

6 VAPOR PHASE 'IGNITION' IN CVD BOUNDARY LAYERS

Optimizing the growth rate and properties of CVD films growing on heated surfaces will often require reactor design/flow conditions such that the onset of external diffusion limitations approximately coincides with the onset of homogeneous reactions within the vapor BL (Rosner et.al.,1990,1991). A simple asymptotic theory, which exploits the high activation energy of the homogeneous reactions, allows this to be done (cf. Fig. 6.1, which shows a typical Arrhenius diagram and the surface temperatures corresponding to "vapor phase ignition".

CONCLUSIONS, FUTURE RESEARCH

In our 1990-1991 OSR-sponsored Yale HTCRE Lab research (briefly described above, and in greater detail in the references cited below) we have shown that new methods for rapidly measuring vapor- and particle-mass transfer rates and chemical vapor deposition rates of refractory oxides, combined with advances in transport theory, provide useful means to identify and incorporate important, often previously neglected, mass-transport phenomena in propulsion engineering and materials engineering design/optimization calculations. We are now extending our work on the effects of these new "phoretic" phenomena, 'polydispersed' particle populations and the consequences of highly nonspherical particles (aggregates or macro-molecules).

REFERENCES

Castillo, J.L., Mackowski, D.W., and Rosner, D.E., "Photophoretic Contribution to the Transport of Absorbing Particles Across Combustion Gas Boundary Layers", *Progress in Energy and Combustion Science* **16**, 253-260,(1990)

Castillo, J.L., Garcia-Ybarra, P., and Rosner, D.E.,"Morphological Instability of a Thermophoretically Growing Deposit", *J. Crystal Growth* (in press,1991)

Garcia-Ybarra, P., and Rosner, D.E., "Thermophoretic Properties of Small Nonspherical Particles and Large Nonspherical Molecules," *AIChE J.*, **35**, [1], 139-147 (1989).

Eisner, A.D., and Rosner, D.E., Experimental Studies of Soot Particle Thermophoresis in Non-Isothermal Combustion Gases Using Thermocouple Response Techniques", *Combustion and Flame* **61**, 153-166(1985); see,also: *J PhysicoChemical Hydrodynamics* 7 ,91-100 (1986)

Gomez, A., and Rosner, D.E., "Thermophoretic Effects on Particles in Counterflow Laminar Diffusion Flames " (in preparation, 1991)

Gomez, A., Rosner, D.E. and Zvuloni, R., "Recent Studies of the Kinetics of Solid Boron Gasification by $B_2O_3(g)$ and Their Chemical Propulsion Implications", *Proc. 2d Int. Sympos. on Special Topics in Chemical Propulsion*: **Combustion of Boron-Based Solid Propellants and Solid Fuels**, (in press 1991)

Konstandopoulos, A.G.and Rosner, D.E.,"Inertial Effects on Thermophoretic Transport of Small Particles to Walls With Streamwise Curvature---I. Experiment, II. Theory", Prepared for Submission to *Int. J. Heat Mass Transfer* (Pergamon)

Mackowski,D.W., "Phoretic Behavior of Asymmetric Particles in Thermal Non-equilibrium with the Gas : Two-Sphere Aggregates", *J. Colloid and Interface Science* **140**,(1), 138-1576(1990)

Mackowski, D.W., Tassopoulos, M. and Rosner, D.E.,"Effect of Radiative Heat Transfer on the Coagulation Rates of Combustion-Generated Particulates", Central States Mtg.-The Combustion Inst., 21-24 April 1991, Nashville, TN.; (to be submitted to *Int. J. Heat Mass Transfer* (Pergamon) (1991))

Rosner, D.E , Konstandopoulos, A.G., Tassopoulos, M., and Mackowski,D.W, "Deposition Dynamics of Combustion-Generated Particles: Summary of Recent Studies of Particle Transport Mechanisms, Capture Rates, and Resulting Deposit Microstructure/Properties", *Proc. Engineering Foundation Conference*: **Inorganic Transformations and Ash Deposition During Combustion**, (in press,1991)

Rosner, D.E. and Kim,S.S., "Optical Experiments on Thermophoretically Augmented Submicron Particle Deposition From 'Dusty' High Temperature Gas Flows", *The Chemical Engrg. J.*(Elsevier) **29**,[3].147-157 (1984)

Rosner, D.E., Mackowski,D.W, Tassopoulos,M., Castillo, J.L., and Garcia-Ybarra, P., "Effects of Heat Transfer on the Dynamics and Transport of Small Particles in Gases", AIChE Annual Mtg.-(S.W.Churchill Birthday Symposium), November 1990, Chicago Il; *I/EC-Research*. (in press,1991))

Rosner, D.E., Castillo,J.L., and Tassopoulos, M. "Role of High Activation Energy Homogeneous Reactions in Limiting CVD-Rates and Deposit Quality for Heated Surfaces", Paper 55d, AIChE Annual Mtg., Chicago, IL, November 15, 1990; Prepared for Submission to *J. Electrochem Soc.*,1991)

Rosner, D.E.and Tassopoulos,M.," Direct Solutions to the Canonical 'Inverse' Problem of Aerosol Sampling Theory: Coagulation and Size-dependent Wall Loss Corrections for Log-Normally Distributed Aerosols in Upstream Sampling Tubes", *J. Aerosol Sci.* (in press,1991)

Zvuloni, R., Gomez, A., and Rosner, D.E., "Direct Measurements of the High Temperature Kinetics of Solid Boron Gasification by its Higher Oxide $B_2O_3(g)$: Chemical Propulsion Implications", *AIAA. J. Propulsion and Power* 7 (1) 9-13,(1991)

Zvuloni, R., Rosner, D.E., and Gomez, A., "Role of Water Vapor on the Gasification Kinetics of Solid Boron by its Higher Oxide $B_2O_3(g)$", *AIAA. J. Propuls. Power* (in press (1991))

Zvuloni, R., Rosner, D.E., and Gomez, A., "High Temperature Kinetics of Solid Boron Gasification By its Higher Oxide $B_2O_3(g)$: Flow Reactor Techniques, Rate Measurements and Their Chemical Implications", *J. Phys. Chem.* (to be submitted, 1991)

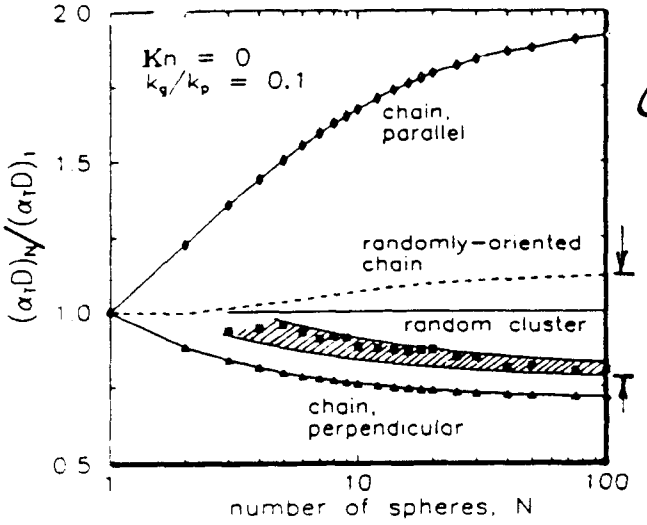

Fig.1.1 Predicted normalized thermophoretic diffusivity of aggregates containing N-primary spheres; near-continuum limit, conductivity ratio=0.1 (after Rosner *et.al.* 1991)

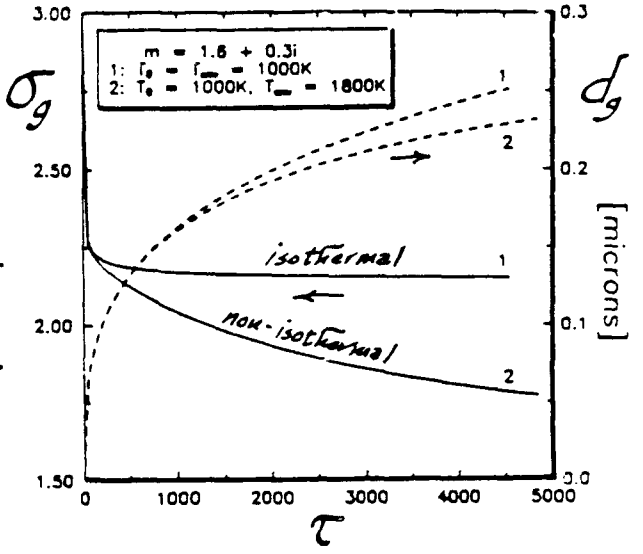

Fig.2.1 Predicted evolution of soot PSD parameters for coagulating populations of carbonaceous spherical particles; effects of particle "overheating" in the high pressure limit (after Mackowski *et al.*,1991, Rosner *et.al.* 1990)

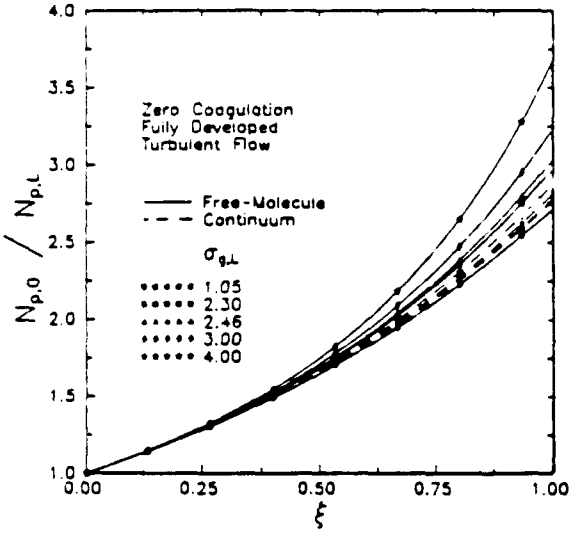

Fig.3.1 Effect of size-dependent particle losses to the walls of an upstream sampling tube; correction factors to be applied to measured total particle number densities using a tube of rescaled L/d. (For turbulent gas flow in both particle Knudsen number limits) (after Rosner and Tassopoulos,1991)

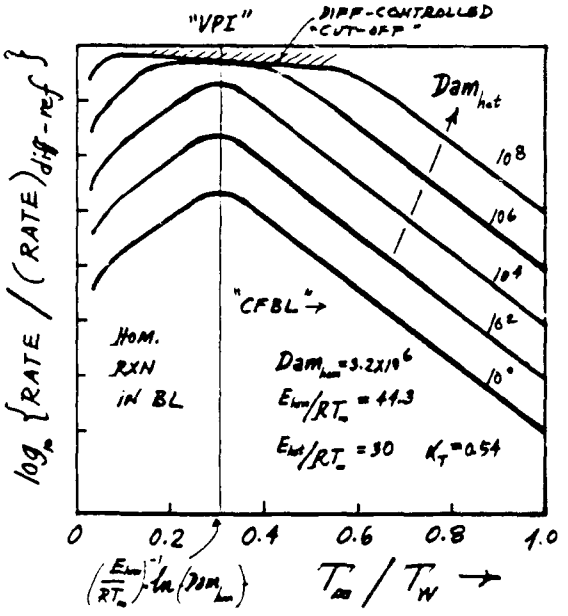

Fig. 6.1 Predicted dimensionless Arrhenius diagram for the chemical vapor deposition of a solid film on a heated substrate. Effects of external diffusion limitations and the abrupt onset of homogeneous reactions in the vapor BL (after Rosner *et al.*,1990,1991)

SOOT PARTICLE INCEPTION AND GROWTH PROCESSES IN COMBUSTION

(AFOSR Contract No. AFOSR-87-0145)

Principal Investigator: Robert J. Santoro

Department of Mechanical Engineering
The Pennsylvania State University
University Park, PA 16802

SUMMARY/OVERVIEW:

The primary objective of the present research program is to provide a fundamental understanding of the processes which control soot particle formation under conditions applicable to future gas turbine engine operation. The current work extends recent studies in laminar diffusion flames on the effects of fuel molecular structure and operating pressure. The emphasis in the present studies is to examine the important gas phase chemistry which is involved in particle inception and surface growth processes. The inception region is of particular interest because it has been argued to be controlling with respect to the ultimate amount of soot formed in the flame. This argument is based on the importance of the initial surface area formed during the inception of the primary soot particles. Present theories conflict on the importance of inception and surface growth in controlling the amount of soot formed during the combustion process. In the present studies, detailed measurements of both the inception and surface growth phases are being undertaken to provide the necessary basis for evaluating the relative importance of these fundamental mechanisms on the formation of soot particles.

TECHNICAL DISCUSSION

The present research program is intended to provide a fundamental understanding of the processes controlling soot particle formation under conditions applicable to future gas turbine engine operation. During the current year of the effort, work has emphasized the effects of concentration and temperature on the formation of soot particles. Through a carefully structured study, the effect of adding a diluent to the fuel stream of a diffusion flame has been studied. Measurements and modeling efforts have shown that differences in the initial concentration of fuel are rapidly mitigated by diffusion. Consequently, local concentration variations are reduced as compared to the initial condition at the fuel tube exit for the undiluted and diluted cases. Furthermore, local temperature measurements indicate that even under equal adiabatic flame conditions, the local temperature in the soot forming region can differ by 40 K between flames involving nitrogen or argon as the diluent. These differences in temperature are argued, based on previous work by other researchers, to be one source for the observed effects on soot formation. Additionally, consideration has been given to residence time effects, largely a result of delays in the onset of soot formation which reduces the effective time for soot growth. Additional work has emphasized the development of sampling and mass spectrometric techniques for measurements in particle laden regions using a new probe developed for conducting such measurements [1].

Background

The formation of soot particles in combustion environments involves a complex series of chemical and physical processes which control the conversion of fuel carbon to carbonaceous particles. Since soot formation is well known to be a chemically kinetic limited process, the effects of temperature and concentration are expected to be important. In the case of concentration effects, it would seem straightforward to expect a direct proportionality between fuel concentration and soot formation rates. However, in many situations, mixing and temperature effects can mask the importance of the fuel concentration variations on the amount of soot formed in the combustion environment.

One means to investigate the effect of fuel concentration is through the introduction of an inert diluent into the fuel stream, which has been observed to reduce soot concentration in laminar diffusion flames. Some workers have argued that the effect of concentration variations resulting from dilution are small relative to the temperature reduction effect [2,3]. Other, more recent studies, have indicated that concentration effects are of greater importance [4-6]. These results imply that the role of temperature in soot formation, commonly believed to be the governing parameter of soot formation rates, is in some situations less important than fuel concentration.

Experimental Setup and Operating Conditions

Investigating the role of temperature and concentration on soot formation requires a careful selection of the experimental approach. Following a method similar to the approach of Axelbaum and Law [6], dilution effects are studied in a series of flames at identical calculated adiabatic flame temperatures, but which have different initial fuel concentrations. The difference in heat capacities of argon and nitrogen permit comparison of flames with identical calculated adiabatic flame temperatures, but different dilutions. Therefore, the effect of concentration is systematically isolated from temperature. Similarly, flame conditions can be selected with identical dilutions, e.g. 50% N_2 and 50% Ar, but different temperatures, thus, isolating the effect of temperature on soot formation.

An atmospheric coannular burner was used to study laminar diffusion flames. A laser scattering/extinction system was used to obtain data on the soot particle field in these flames. The coannular burner consists of an inner brass fuel tube (1.1 cm id) surrounded by an outer tube (10.0 cm id) for the air flow. The fuel or fuel inert mixture is burned in a highly over-ventilated air flow (2.25 SCFM). Studies have been conducted for ethylene and propane over a range of fuel flow rates (2.75-6.58 cm^3/s), fuel concentrations (X_{Fuel} = 0.37-1.0) and operating pressures (0.1 and 0.2 MPa).

Results and Discussion

The effects of dilution of the fuel stream has been assessed through measurements of the total integrated soot volume fraction, F_v. This quantity is related to the local soot volume fraction, f_v, for soot particles in the Rayleigh size limit ($d/\lambda << 1$), through measurements of the extinction (I/I_0) integrated over the appropriate spatial coordinate. The expression for F_v is given as

$$F_v = \int_{-\infty}^{+\infty}\int_{-\infty}^{+\infty} f_v\,dx\,dy = -\int_{-\infty}^{+\infty} c(\lambda,m)\ln\left(\frac{I}{I_o}\right)dy \qquad (1)$$

where x is the direction along the laser beam used for the extinction measurement, y is the direction perpendicular to x, $c(\lambda,m)$ is a constant determined from Rayleigh theory and I/I_0 is a measure of the extinction through the flame. Typical results for the variation of F_v as a function of height in the flame for a series of ethylene/air flames with specified diluent conditions are shown in Figure 1. The nitrogen and argon diluted flames have the same calculated adiabatic flame temperature (2333 K) which is 36 K cooler than the calculated adiabatic flame temperature for an undiluted ethylene flame (2369 K). Thermocouple measurements of the radial temperature profile low in the flame ($z=5$mm) indicate that the maximum temperatures for the two diluted flames are within 10 K of each other. However, at radial locations closer to the center line ($r=5$mm), where soot is first observed to form, temperature differences of between 40 and 60 K are observed, with the nitrogen diluted flames displaying lower temperatures. Previous work has shown that temperature variations of 50 K can result in a factor of two difference in the soot volume fractions observed [9]. Thus, the observed temperature difference can significantly increase the soot formed in the argon diluted flame enhancing the perceived concentration effect.

To gain further insight into the actual concentrations occurring in these flames when diluents are added to the fuel, both model calculations and mass spectrometric measurement studies were conducted. Using the diffusion flame model of Mitchell et al [8], the fuel mole fraction was calculated for diluted and undiluted ethylene flames burning in air. A calculated radial profile of the fuel mole fraction for an

axial location 2.7mm above the fuel tube exit is shown in Figure 2. Comparisons between the diluted and undiluted cases show that differences in the fuel mole fractions in the two flames have been significantly reduced from their initial ratio of two. This is particularly evident in the region where soot is first observed to be formed (r=4-5mm, see ref. 3). Thus, diffusion of nitrogen from the surrounding air rapidly mitigates the initial differences in fuel concentrations introduced by dilution of the fuel stream. To confirm these results, comparisons of mass spectrometric measurements in diluted and undiluted methane flames are shown in Figures 3 and 4. These measurements indicate the same trends observed with the modeling studies. The major combustion species show similar mole fractions in both diluted and undiluted flames in the regions where soot is expected to form. The only species to show significant differences is hydrogen while carbon monoxide shows smaller changes. The implication of these results is that a less than first order dependence on the fuel concentration for soot formation would be expected. In fact, calculations in which F_v was assumed to be related to the fuel concentration as $[Fuel]^b$ yielded values of b between 0.4 and 1.5 with no systematic variation with respect to fuel flow rate.

Residence time effects have also been shown to be important in diffusion flame studies of soot formation (9,10). In fact, a squared or cubed power dependence on the residence time has been observed (10). Thus, changes in residence time which result from addition of the diluent species could affect the soot formation rate. The major observed effect of dilution with respect to residence time is a shift of the location where soot is first observed to higher axial positions. Since the location of the maximum soot volume fraction is largely unaffected by dilution, the total soot residence time is reduced. Note the shift in the location of the initial soot formation region could be a result of temperature, velocity and/or concentration effects. Our preliminary evaluation estimates that between 5 to 20% of the reduction in soot could be a result of the variation in residence time during which soot growth can occur.

The present study of the effects of fuel dilution on soot formation in laminar diffusion flames indicates a number of important effects are present. The lower soot formation rate observed is due to a combination of concentration, temperature and residence time effects. Based on local measurements of the temperature variations in the soot forming regions of the flame, along with previous measurements of the sensitivity of the soot formation process to temperature variation, we argue that temperature is still the most important effect. Our measurements and modeling show that concentration effects are mitigated by diffusion associated with the diffusion flame structure. In particular, diffusion of nitrogen from the surrounding air quickly results in similar concentration fields for both diluted and undiluted flames. Furthermore, dilution appears to increase the time for soot particle inception to occur, resulting in a decreased residence time for soot growth. Our studies indicate that concentration effects can be responsible for some fraction of the observed variation in soot formation as diluent is added. These effects are most important in the soot inception region and appear to decrease in importance as residence time and sooting propensity increase. Additionally, the present studies point to the usefulness of detailed studies to investigate fundamental mechanisms involving soot formation as opposed to global studies.

REFERENCES

1. Puri, R. and Santoro, R. J., "Sonic Probe Sampling in Particle Laden Combustion Flows", Th Fall Technical Meeting, Eastern Section: The Combustion Institute, Orlando, FL, December 3-5, 1990.
2. Glassman, I. and Yaccarino, P., 18 th Symposium (International) on Combustion, p. 1175 (1981).
3. Santoro, R. J. and Semerjian, H. G , 20 th Symposium (International) on Combustion, p. 997 (1984).
4. Kent, J. H. and Wagner, H. G., Combust. Sci. and Tech., 41, p. 245 (1984).
5. Axelbaum, R. L., Flower, W. L. and Law, C. K., Combust. Sci. and Tech., 61, p. 51 (1988).
6. Axelbaum, R. L. and Law, C. K., "Soot Formation and Inert Addition in Diffusion Flames", 23 rd Symposium (International) on Combustion, (in press).
7. Bohm, H., Hesse, D., Jander, H., Luers, B., Pietscher, J., Wagner, H. Gg. and Weiss, M., 22 nd Symposium (International) on Combustion, p.403 (1988).
8. Mitchell, R. E., Sarofim, A. F. and Clomburg, L. A., Combust. and Flame, 37, p. 227 (1980).
9. Santoro, R. J., Yeh, T. T., Horvath, J. J. and Semerjian, H. G., Combust. Sci. and Tech., 53, p. 89 (1987).
10. Honnery, D. R. and Kent, J. H., Combust. and Flame, 82, p. 426 (1990).

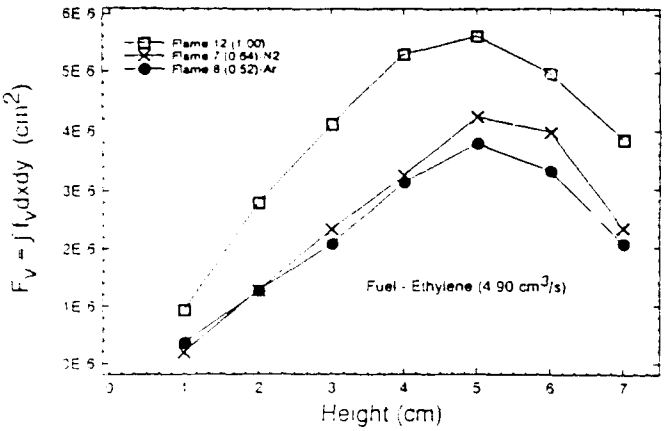

Figure 1. Comparison of the integrated soot volume fraction as a function of height for diluted ethylene flames of equivalent temperature (2333 K) as compared to an undiluted flame (2369 K). The initial fuel mole fractions for the nitrogen and argon diluted flames are 0.64 and 0.52 respectively.

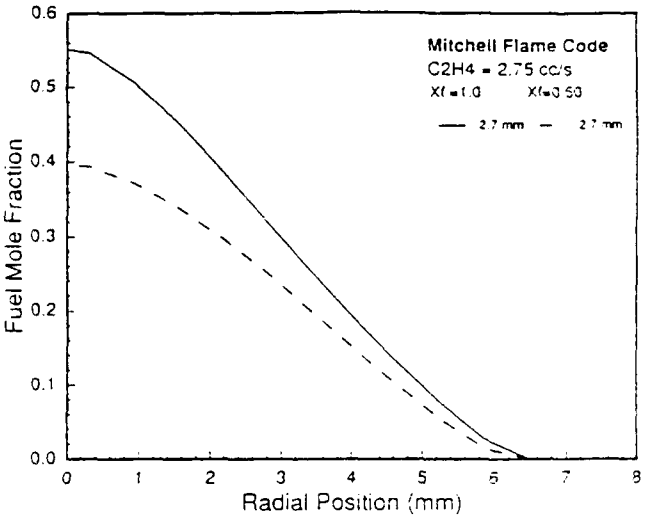

Figure 2. Comparison of the profile of fuel mole fraction as a function of radial position for a diluted and undiluted flame. (axial location - 2.7mm)

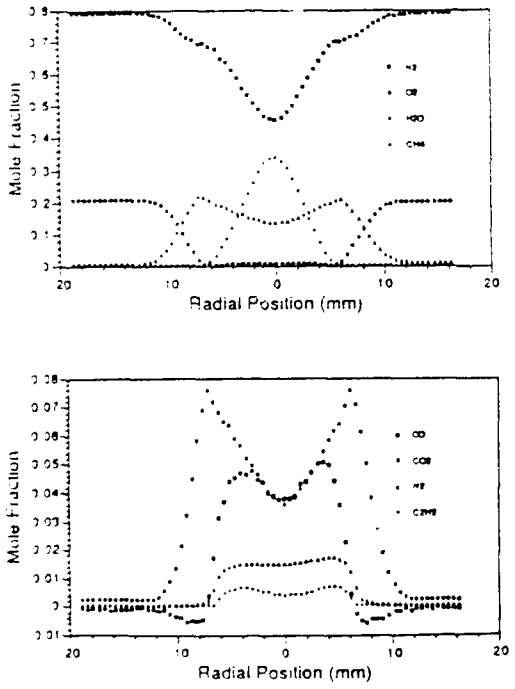

Figure 3. Mole fraction measurement as a function of radial position in an undiluted methane diffusion flame burning in air. The axial measurement location is 12mm above the burner exit. Note negative mole fraction measurements for CO are a result of obtaining CO mole fractions from a differencing procedure involving the mass 28 peak which includes both CO and N_2. The methane fuel flow rate was 5.7 cm³/s.

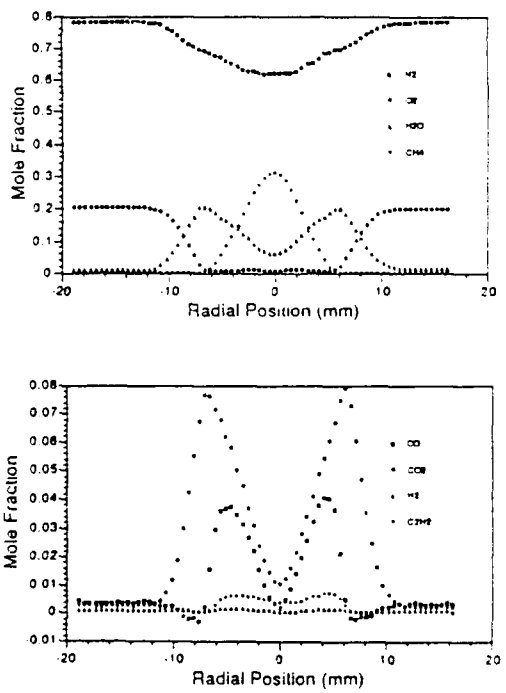

Figure 4. Mole fraction measurement as a function of radial position for a 50% N_2 diluted methane flame burning in air. The axial measurement location is 12mm above the burner exit. Note negative mole fraction measurements for CO are a result of obtaining CO mole fractions from a differencing procedure involving the mass 28 signal which includes both CO and N_2. The methane and nitrogen fuel flow rate were each 5.7 cm³/s.

AFOSR SPONSORED RESEARCH IN AIRBREATHING COMBUSTION

PROGRAM MANAGER: JULIAN M. TISHKOFF

AFOSR/NA
BOLLING AFB DC 20332-6448

SUMMARY/OVERVIEW: The Air Force Office of Scientific Research (AFOSR) program in airbreathing combustion currently is focused on seven areas of study: supersonic combustion, reacting flow, soot, sprays, kinetics, ram cannons, and thermal instability of fuels. An assessment of major research needs in each of these areas is presented.

TECHNICAL DISCUSSION

AFOSR is the single manager for Air Force basic research, including efforts based on external proposals and in-house work at Air Force laboratories. Airbreathing combustion is assigned to the AFOSR Directorate of Aerospace Sciences along with programs in rocket propulsion, diagnostics of reacting flow, and fluid and solid mechanics.

Interests of the AFOSR airbreathing combustion task are given in the SUMMARY section above. Many achievements can be cited for these interests, yet imposing fundamental research challenges remain. The objective of the program is publications in the refereed scientific literature describing significant new understanding of multiphase turbulent reacting flow. Incremental improvements to existing scientific approaches, hardware development and computer codes fall outside the scope of this objective.

Decisions on support for research proposals are based on scientific opportunities and technology needs. Current AFOSR perceptions of scientific opportunities appear in Figure 1, and areas of emphasis are indicated by arrows with positive slopes.

Major emphasis has been given to research on supersonic combustion to support hypersonic airbreathing propulsion technology. Starting in 1987 new research efforts were directed at novel means for achieving ignition, combustion enhancement, and low-loss flameholding in supersonic combustion. 1989 saw new research in interactive control of fluid transport processes. These opportunities reflect a generic interest in interdisciplinary efforts between researchers in control theory and fluid transport behavior. For hypersonic propulsion a particular focus of interactive flow control is the investigation of means to overcome the suppression of mixing which high Mach number flows experience in relation to subsonic flows.

A new area of interest is the behavior of fuels in propulsion systems prior to combustion. Future systems will require fuels to absorb substantial thermal energy, raising fuel temperatures to supercritical thermodynamic conditions. Understanding and controlling fuel properties at these conditions will be crucial for avoiding thermal degradation and for subsequent processes within the combustor.

The purpose of this abstract has been to communicate AFOSR perceptions of research trends to the university and industrial research communities. However, communication from those communities back to AFOSR also is desirable and essential for creating new research opportunities. Therefore, all proposals and inquiries for fundamental research are encouraged even if the content does not fall within the areas of emphasis described herein. Comments and criticisms of current AFOSR programs also are welcome.

Air Force Basic Research

Aerospace Sciences

Airbreathing Combustion

Research Area	Trend	Decrease	Increase
Supersonic Combustion	→		
Reacting Flow	↗		Model Evaluation
Soot	↗		Comprehensive Growth Modeling
Sprays	→		Drop-Turbulence Interactions
Kinetics	↗		Lumping And Reduction Methods
Ram Cannons	↗		AFSC Initiative
Thermal Instability	↗		FY93 Initiative

A STUDY OF ARCING PHENOMENA ON HIGH VOLTAGE POWER SYSTEMS AND THE EFFECT OF ELECTRIC PROPULSION THRUSTER BACKFLOW

(AFOSR-87-0340)

Principal Investigator: Daniel E. Hastings
in collaboration with Torkil Mogstad of McDonnell Douglas Space Systems Company

Massachusetts Institute of Technology
Cambridge, MA 02139

Summary

When high voltage power systems are used in space, serious interactions are known to occur between the exposed conducting surface and the surrounding plasma. The main purpose of the research is to study computationally and theoretically the arcing phenomena on high voltage power systems with specific application to high voltage solar arrays. The aim is to arrive at an understanding which would be useful in engineering design. A study has been done based on a simple model consisting of dielectric material based on negatively biased conductor in a plasma environment. An arcing rate is calculated for a high voltage solar array and good agreement is found with experimental data. The breakdown voltage of the neutral gas over the dielectric surface is also calculated as a function of pressure ranging from semi-vacuum to atomospheric pressure. Future research will be an assessment of effects of repeated arcing on spacecraft operation and applications of the results to other high voltage system in space as a function of thruster parameters.

1. Introduction

In the future, increased activities in space will require a large amount of power, of the order of 100 kW to 1 MW. At this high power level, the loss of power in its transmission inside the spacecraft and the mass of the transmission line can be substantial. High voltage power generation and transmission is one of the solutions which minimize the power loss and the mass of the transmission lines. When the voltage is increased to a high value such as an order of hundred volts, however, we can no longer neglect interactions between the high voltage systems and the surrounding space environment. Arcing is one of the most severe interactions. Arcing has been observed on high voltage solar arrays when the arrays have a negative potential with respect to the surrounding plasma. Arcing is typically defined as a sudden current pulse up to an order of ampere during a time of the order of microsecond or less. In one space experiment arcing was observed to occur at the voltage as low as -200 volt[1]. It causes electro-magnetic interference (EMI) with instruments, enhanced sputtering of the solar cell materials and possible damage to the solar cell. Similar phenomena are expected to occur on any other high voltage system which is surrounded by dense neutral and plasma environment. Such a dense neutral and plasma environment will exist when any type of electric propulsion thruster is used continuously on a

space vehicle. The interactions of the power system with the environment will be especially severe for electric propulsion systems.

The main purpose of the research is to study computationally and theoretically the arcing phenomena on the high voltage systems in space, especially, solar arrays. The basic system we study is shown in Fig. .
It consists of dielectric material placed on a negatively biased conductor in plasma environment. Therefore the results obtained in the research can be applied to any other discharge problem occurring in a similar system. For a solar array, the dielectric material corresponds to the coverglass and the conductor corresponds to the interconnect.

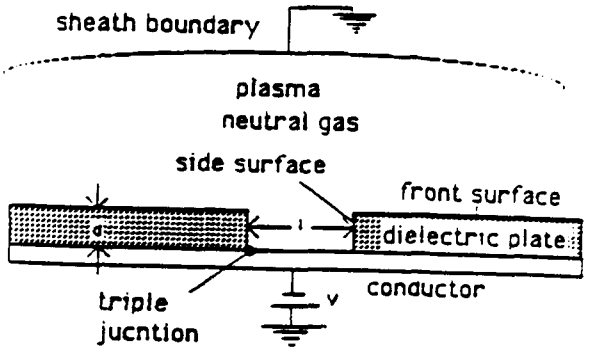

Fig. 1 Schematic View of System

Hastings *et.al.*[2] proposed that arcing occurs by ionization of neutral gas desorbed from the dielectric coverglass due to electron stimulated desorption (ESD) by electrons emitted from the interconnector. Cho and Hastings[3] calculated the dielectric charging processes leading to the build-up of an intense electric field around the triple junction. This can cause significant outgassing from the dielectric surface due to the electrons which are emitted by field emission from the conductor surface.

In this abstract three pieces of work are summarized. One is numerical simulations of the charging processes of the dielectric materials and calculation of arcing rate as a function of the conductor potential V. The second is the calculation of the breakdown voltage of the desorbed neutral gases. The third is the calculation of the backflow from a thruster around a spacecraft.In the following sections, we discuss each work and finally we conclude the abstract discussing the future research topics.

2. Charging Processes of Dielectric Material

The objective of this part is to know

1. To what extent is the dielectric surface charged by charged particles from the space environment?
2. How quickly is the dielectric material charged?

Knowing (1) tells us the electric field under which arcing is initiated. Knowing (2) tells us the rate of arcing for a given solar array. The arcing rate of a solar array is very valuable information when we design a high voltage solar array.

Two types of charging mechanisms are considered. One is the charging due to ions from outside the electric sheath surrounding the solar arrays. Another is the charging due to electrons emitted from the conductor surface by enhanced field electron emission (EFEE). These charging processes are calculated by numerically integrating the particle orbits around the solar cell under the electric field which is consistent with the charging state of the dielectric material.

The major findings are the following three points.

(1) The ambient ions charge the dielectric front surface to the steady state potential $\phi \simeq 5(V)$, where $5(eV)$ is the kinetic energy of the incoming ions with the orbital velocity in the LEO. Therefore, at the steady state given by the ion charging, a strong electric field of $E \simeq V/d$ is created at the triple junction.

(2) After the electric field reached the high value of $E = V/d$ at the triple junction, if there is an emission site with a high field enhancement factor β on the conductor surface near the triple junction, the electrons can charge the side surface. The charging due to the enhanced field emission electron (EFEE) can develop very rapidly because of the exponential dependence of the current on the electric field. When the electric field doubles, the emission current increases by ten orders of magnitude. At the same time, the electrons which impact the dielectric surface increase to more than $10^7(A/m^2)$ for the parameters used in the study. This incident current can desorb a significant amount of neutral gas from the surface and create dense neutral cloud as high as $10^{25}(m^{-3})$ over the surface.

(3) Once we know the charging time of the dielectric coverglass, we can calculate the arcing rate for a given solar array assuming that it takes a negligible amount of time for the ionization of neutral gases. The arcing rate is then defined as the inverse of the time which is necessary to build up the electric field. We calculated the rate of arcing on a solar array with the same parameters as those of the PIX II flight experiment[1] assuming a reasonable distribution of the enhanced field emission site over the conductive surface of the array. The results are shown in Fig.2 with the experimental data.

Fig. 2 Total Arcing Rate vs Bias Voltage

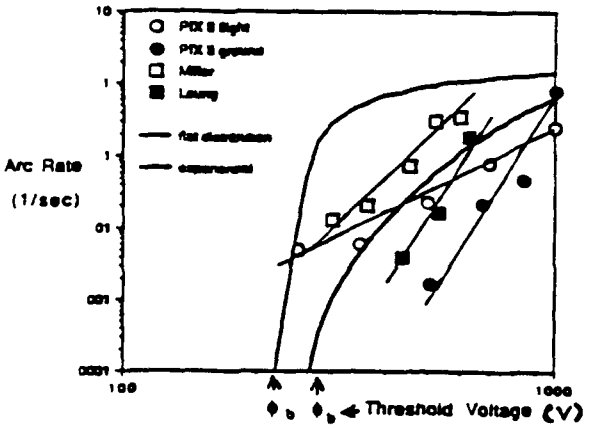

We find we can obtain good agreement between the predicted values and the experimental values. It is noted that a threshold voltage exists if we define it as the voltage which gives the arc rate $R = 1/\tau$ where τ is the experimental waiting time, that is, there is no arc within a time τ at less than this voltage.

3. Semi-Vacuum Gas Breakdown

The neutral gas density over the surface is roughly estimated by dividing the neutral desorption flux by the desorption speed of the neutral particles. The desorption flux Γ_n is given by $\Gamma_n = \gamma j_e/e$ if the neutrals are desorbed due to electron bombardment, where γ is the ESD yield which is defined by the number of neutral particle desorbed by one incident electron, and j_e is the incident electron current. The ESD yields, γ, are seen between 0.01 and 0.1 for most materials and the desorption speed of the neutrals is $10^2 \sim 10^3$ (m/sec) depending on its mass and the surface temperature. Since the electron current varies widely from 0 to $10^7(A/m^2)$ or even higher[3], the resulting neutral density also varies from atmospheric ($10^{25}m^{-3}$) to vacuum.

The length scale of the solar array discharge is $d \leq 0.3(mm)$ if we take it from the thickness of the coverglass. Most of our values of the product pd fall into the region between the Townsend gas breakdown and the vacuum breakdown. Little is known about this region compared to the other two regions. One possible explanation for the gas breakdown in this region is that, if the gap distance d is small enough, a prebreakdown electron current is emitted from the cathode surface by field emission and the feed back effect at the cathode is provided by field enhancement due to the space charge of the incoming ion current[4]. We consider the gas breakdown at low pd based on this hypothesis. For simplicity we consider a one-dimensional system filled with neutral gas of a certain density n_n with two biased electrodes but without any dielectric material. We assume that the field is already enhanced to a certain extent due to a whisker or dielectric impurity of metal at the cathode surface.

The breakdown voltage is calculated analytically by solving one-dimensional equations with a simplified collision model. The results are plotted in the form of a Paschen curve with the Paschen discharge data in Fig. . The semi-vacuum breakdown voltage intersects with the Paschen curve at $p = 40(Torr)$ and $V = 260(volt)$. At pressure higher than this the discharge becomes the classical Paschen discharge. We also show the threshold voltage determined by the charging time of the dielectric material. This has the meaning of the threshold voltage necessary to outgass the neutral gas.

Fig.3 Breakdown Voltage vs Neutral Gas Pressure

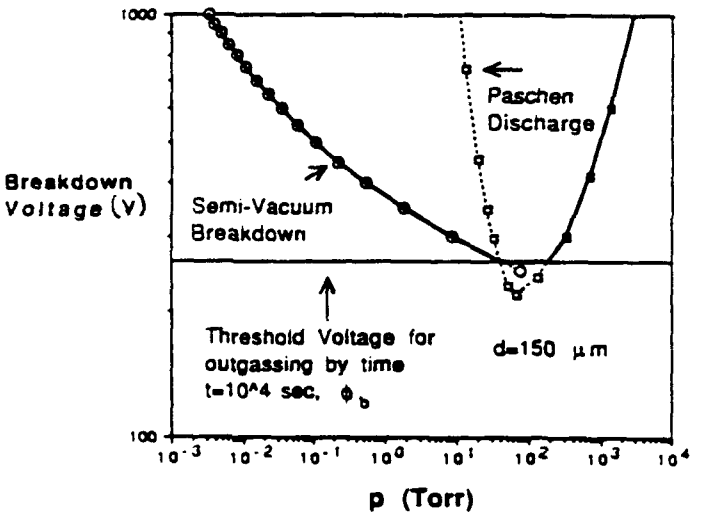

A bias voltage below the threshold voltage cannot create a neutral cloud of enough density to undergo arcing because the electron current incident on the surface is too low. Therefore, when the bias voltage is lower than this voltage, we do not see arcing. When the bias voltage is higher, whether arcing occurs or not depends on whether the bias voltage is higher than the breakdown voltage for a given density of the neutral.

The neutral gas density over a high voltage surface can also be affected by the backflow from a nearby thruster. This has been calculated by a direct simulation Monte Carlo approach for the flow from a hydrogen release. The neutral density is found to be several orders of magnitude above the ambient for some distance from the thruster. This means that the neutral pressure near the thruster exit may be high enough for a classical Paschen discharge to take place.

4. Future Research

In the future research, effects of the neutral density on the arcing rate will be studied more in detail. After determining arc frequency we will asses effects of repeated arcing on spacecraft operation. The sputtering rate of the material and EM radiation form the arcing current are thought to be important from a system designer's point of view. Finally, there will be an application of the results obtained in this study on high voltage solar arrays to arcing phenomena on other high voltage system. There will be a case where there is contamination of the environment around the spacecraft due to the thruster firing. When a thruster is fired in space, there is backflow of the products from the nozzle exit toward the spacecraft. If the neutral gas from the thruster is partially ionized, this ionized gas can interact with the high voltage surface electronically. We will assess plasma density around typical spacecraft configurations as a function of thruster and the possibility of discharge on high voltage surfaces.

References

[1]N. T. Grier Plasma interaction experiment II (PIX II): laboratory and flight results. In *Spacecraft environmental Interaction Technology-1983*, NASA CP-2336, 1983. pp333-347.

[2] D. E. Hastings, G. Weyl and D. Kaufman. A simple model for the threshold voltage for arcing on negatively biased high voltage solar array. *J. of Spacecraft and Rockets.* 27(5), Sept-Oct 1990, pp.535-544.

[3] M. Cho, and D. E. Hastings. Dielectric charging processes and arcing rates of high voltage solar arrays. to be published in *J. of Spacecraft and Rockets* July-August 1991.
[4] W. S. Boyle, P. Kisliuk, and L. H. Germer. Electrical breakdown in high vacuum. *J. Appl. Phys.*, Vol.26, No.6, June 1955, pp. 720-725.

Twenty First Century Propulsion Concept

Robert L. Talley
Veritay Technology, Inc.
East Amherst, New York

ABSTRACT

The Biefield-Brown effect was investigated experimentally under a Phase II SBIR program* to verify and quantify the effect and its alleged capability of converting electrostatic energy directly into a propulsive force in a vacuum environment.

In the 1920s, Dr. Paul Biefield and Townsend Brown claimed that a propulsive force was generated when a large static electrical potential difference was applied between shaped electrodes, fixed with respect to one another by a dielectric. Under these conditions, a net force resulted that acted on the entire electrode/dielectric body and typically caused it to move in the direction of the positive electrode. Brown claimed the forces were proportional to the capacitance of the device, mass of the dielectric, charging potential, spatial divergence of the electric field, and energy density within that field.

This effect has received cursory attention over the many years since its discovery, but it has usually been discounted, the results being attributed to ion wind and corona discharge associated with the applied high voltage. It is probable that ion wind and perhaps corona discharge do contribute to the thrust on test devices when they are operated in air. However, Brown contended:

---

* This work was performed under contract F04611-89-C-0023 with the U.S. Air Force, Astronautics (now Phillips) Laboratory, at Edwards AFB, CA.

> "In a vacuum, the reaction forces appear on solid environmental bodies, such as the walls of the vacuum chamber. The propelling force however is not reduced to zero when all environmental bodies are removed beyond the apparent range of the electrical field."

Further, he noted that the thrust existed under high vacuum conditions, "when there was no vacuum spark."

At the outset of the present investigation, this effect remained inadequately explored, without confirmed operation in a high vacuum, and without an adequate experimental data base to permit the nature and magnitude of its thrust to be determined.

In this investigation of the Biefield-Brown effect, a laboratory test configuration was designed and developed for directly measuring the electrostatically induced propulsive forces on selected experimental devices. This setup utilized a $1.40m^3$ stainless steel cylindrical type vacuum chamber and an expanded 6-inch diffusion pump to achieve air pressures for testing in the range of 10^{-5} to 10^{-7} torr. A vertical, dual, taut torsion fiber measurement system was used for direct assessment of propulsive forces. Two identical test devices, directed horizontally in tandem and mounted on a support structure at equal radial distances from the fiber axis, were suspended by the upper fiber. This unit operated as a torsion pendulum in a dynamic mode. Electrical power to the devices was supplied through the 0.1 mm diameter tungsten torsion fibers. The minimum force detectable with this system was about $2X10^{-9}$ N. Geometrical symmetries were incorporated in the design to minimize the influence of reaction forces, which could arise from nearby bodies including the walls of the vacuum chamber itself.

Most of the devices tested were identical to, or small variations from, those successfully used by Brown in his force generation experiments. Several different electrode shapes and

dielectric types were used in the attempt to explore the parameters that were claimed to influence the induced propulsive forces.

A few attempts were made to drive the test devices with static voltages of 50 kV or more; these voltages were generally limited, however, to about 19 kV or less to avoid electrical breakdown problems across test device elements under vacuum conditions.

Boundary effects arising from the presence of induced surface charges on the walls of the vacuum chamber surrounding the test devices were significant. Considerable care was required to achieve adequate symmetry in the complete measurement configuration so that very small force levels could be detected and measured. Even then, residual boundary and asymmetry effects in the torsion pendulum system had to be taken into account in reducing the force measurements.

Direct experimental results of this investigation indicate that no detectable propulsive force was induced in the test devices by applying a static potential difference up to 19 kV between the test device electrodes under high-vacuum conditions (in the absence of electrical breakdowns). Steady applied voltages up to 33 kV were occasionally obtained during the tests, but there was no indication that any nonlinearities were induced in any of the test devices that would cause propulsive forces to develop using static voltages. Accordingly, the electrostatically generated propulsive force which was claimed to exist by Brown under these conditions was not observed. If such a force still exists and lies below the threshold of measurements in this investigation, then the force may be too small to be attractive for many space propulsion applications.

Near the very end of this investigation, a few brief attempts were made to examine the force-generation effects using

pulsed driving voltages at 19 kV, which was just under the level that caused breakdowns. No significant forces were induced, using pulse repetition rates of 10, 60, 150, 400 and 600 Hz.

Two further tests were conducted to examine the effect on forces generated by test devices in which a ceramic piezoelectric dielectric (lead titanate-lead zirconate) with a high dielectric constant of about 1750 was used in place of acrylic, with a corresponding constant of about 3.0. Under a static applied voltage of 19 kV, slow pulsing electrical breakdowns occurred between electrodes of the asymmetrical test device and over (or through) the dielectric. An anomalous force was associated with the occurrence of these breakdowns. The magnitude of this anomalous force appeared to increase as the rate of breakdown pulsing increased, even though the observed pulsing rates were no more than a few pulses per second. This anomalous force acted in a direction opposite to the direction of the conventional electrostatically induced boundary force (although this may not be true in general). The anomalous force is believed not to be associated with some artifact of current pulses passing through and temporarily altering the properties or calibration of the torsion fiber force measuring system. The origin and nature of this force remains an enigma.

ICRF Plasma Heating Experiment in the Tandem Mirror Rocket

Grant No. AFOSR-90-NA-001

Principal Investigators: F. R. Chang-Díaz*, T. F. Yang

MIT Plasma Fusion Center
Cambridge, Massachusetts 02139

Summary

The ICRF plasma heating experiment has been carried out on the tandem mirror plasma propulsion device at MIT. The radial and axial profile of the wave amplitude agree with theoretical predictions. The axial profile was measured by an array of B-dot probes mounted in the region where the damping would occur from the theoretical prediction. The data showed that the wave was indeed damped when it approached the resonance plane indicating the beach heating effect. This effect is again confirmed by an analytical solution of the wave on a slab model. The time characteristics of electron density, measured by a microwave interferometer, confirm the two types of discharges observed from H_α emission reported previously. The plasma is more stable and has higher density for the type II discharge. From these two results we may choose the type II discharge as the preferred plasma heating method.

Technical Discussion

(1) Introduction

The goal of the first phase experiment is to gain a full understanding of the physics of wave propagation in this device in order to develop a method for achieving high energy conversion efficiency as well as controlling the heating of the plasma. It was reported last year that the numerical simulation of wave propagation in a nonhomogeneous magnetic field predicts that the amplitude of the wave excited in the plasma peaked while it approached the resonance, then damped out. The resonance effect was demonstrated by the drastic increase in amplitude of the wave, and the power absorption was demonstrated by the Fourier spectrum broadening. The absorption is now being observed from the measured axial profile of the wave amplitude this year. It was also reported previously that there were two types of discharge observed from the measured H_α emission. For type I discharge there was initially transient instability at the beginning, followed by stable behavior thereafter. The plasma was quiescent for the type II discharge. Similar phenomena were observed from the electron density measured by a microwave interferometer.

(2) ICRF Wave Experiment

The device is oriented north and south. The double half-loop antenna is located in the north end of the central cell where the field is higher than the resonance field at the midplane of each cell. Therefore the corresponding cyclotron frequency is less than the resonant frequency ($\omega < \omega_{ci}$). The frequency of the rf power is in resonance with the ion cyclotron frequency at the field of the midplane of each cell. When rf radiation was emitted at the antennae, the wave excited in the plasma traveled both radially inward and axially toward the center of each cell.

The electron density of the plasma at two different ICRF frequencies was measured with a microwave interferometer and is shown in Fig. 1. The characteristics of the density results reconfirm the phenomena of the existence of two types of discharges observed from

* Astronaut Office, NASA Johnson Space Center, Houston, Texas

the H_α emission reported previously. Figure 1a is the discharge for $\omega > \omega_{ci}$ and is classified as type I, whereas Fig. 1b is for the discharge $\omega < \omega_{ci}$ and is classified as type II. A type II discharge is more quiescent than type I.

Type I discharges generate densities that are lower than type II discharges. The peak line density obtained from the interferometer is approximately $3.2 \pm 0.85 \times 10^{12} \mathrm{cm}^{-2}$, which corresponds to a plasma density of approximately $1.6 \pm 0.42 \times 10^{11} \mathrm{cm}^{-3}$. The average line density is approximately $2.6 \pm 0.85 \times 10^{12} \mathrm{cm}^{-2}$ or $1.3 \pm 0.42 \times 10^{11} \mathrm{cm}^{-3}$.

The radial profile of B_z of the wave for a type II discharge measured by a single B-dot probe at midplane is shown in Fig. 2. The solid curve shows the numerical results and the open circles with crosses show the experimental data. They are in good agreement.

The axial profile of B_z of the ICRH wave for a type II discharge measured by the B-dot probe array is shown in Fig. 3. It is seen that the wave is damped as it travels toward the resonance plane. The numerical simulation of the wave was presented previously and a trimetric view of the calculated B_z is shown in Fig. 4. The region of the axial profile measured by the B-dot probe array is indicated in Fig. 4 which is the damped region between the peak and resonance plane. The wave is rises to a peak and is then damped toward the resonance plane, in agreement with the experimental data. Such a damping effect is also predicted by the analytic solution discussed in the next section.

(3) ICRF Wave Theory

A refined analysis of the slab model was completed and an efficiency $\mathcal{F}$ was defined as

$$\mathcal{F} \equiv \frac{\int P_{diss} dx}{|\vec{S}|} = 2 \cos\theta_T \sqrt{\frac{S_{Re}}{S_{Re}^2 - D_{Re}^2}} \left[\frac{\cos^2\theta_I}{(\cos\theta_I + \frac{k_0}{k_{pi}} \cos\theta_T)^2 + \frac{D^2}{(S^2 - D^2)^2} \sin^2\theta_I} \right].$$

At the resonance limit it reduces to

$$\mathcal{F} = 2 \sqrt{\frac{S_{Re}}{S_{Re}^2 - D_{Re}^2}} \rightarrow 1.$$

Far from the resonance limit it becomes

$$\mathcal{F} \simeq 2 \left(\frac{\Omega_i}{\omega_{pi}} \right) \cos\theta_T \rightarrow 0.$$

As expected, $\mathcal{F}$ increases as resonance is approached, in agreement with the experimental results of the axial B_z profile.

References

[1] F.R. Chang-Díaz, T.F. Yang, W.A. Krueger, S. Peng, J. Urbahn, X. Yao and D. Griffin, "A Tandem Mirror Hybrid Plume Plasma Propulsion Facility," DGLR/AIAA/JSASS 20th Intl. Elect. Propul. Conf., DGLRA-88-126, Garmisch-Partenkirchen, W. Germany (1988).

[2] T.F. Yang, S. Peng, F.R. Chang-Díaz, "The Propagation of RF Wave in a Tandem Mirror Plasma Propulsion Device," AIAA/DGLR/JSASS 21st Intl. Elect. Propul. Conf., AIAA-90-2638, Orlando (1990).

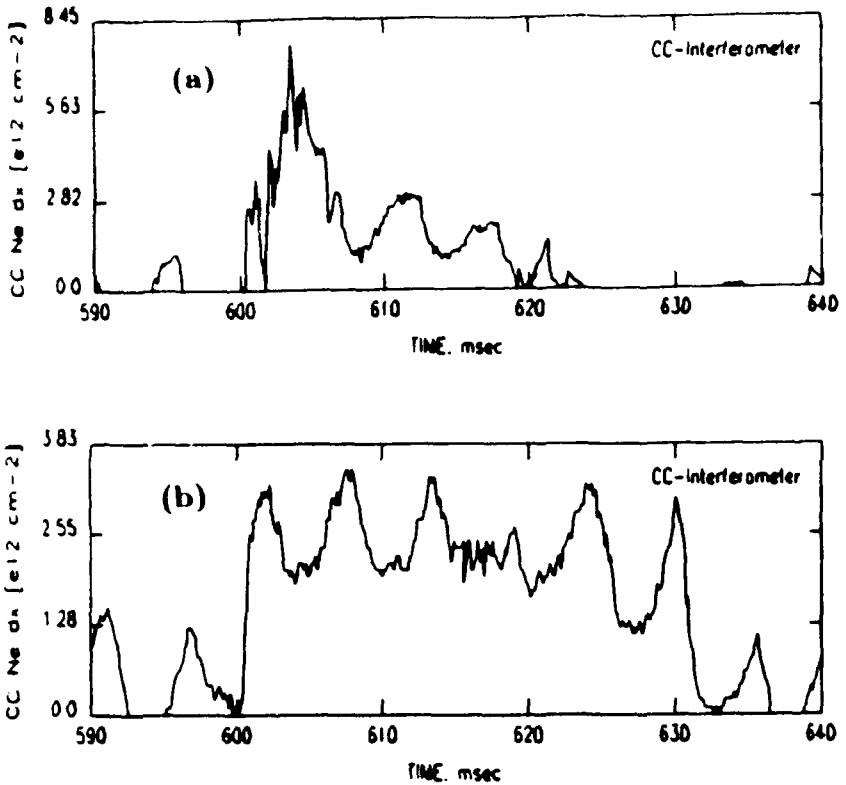

Figure 1: Plasma density measured by interferometer for (a)type I discharge ($\omega > \omega_{ci}$), and (b) type II discharge ($\omega < \omega_{ci}$)

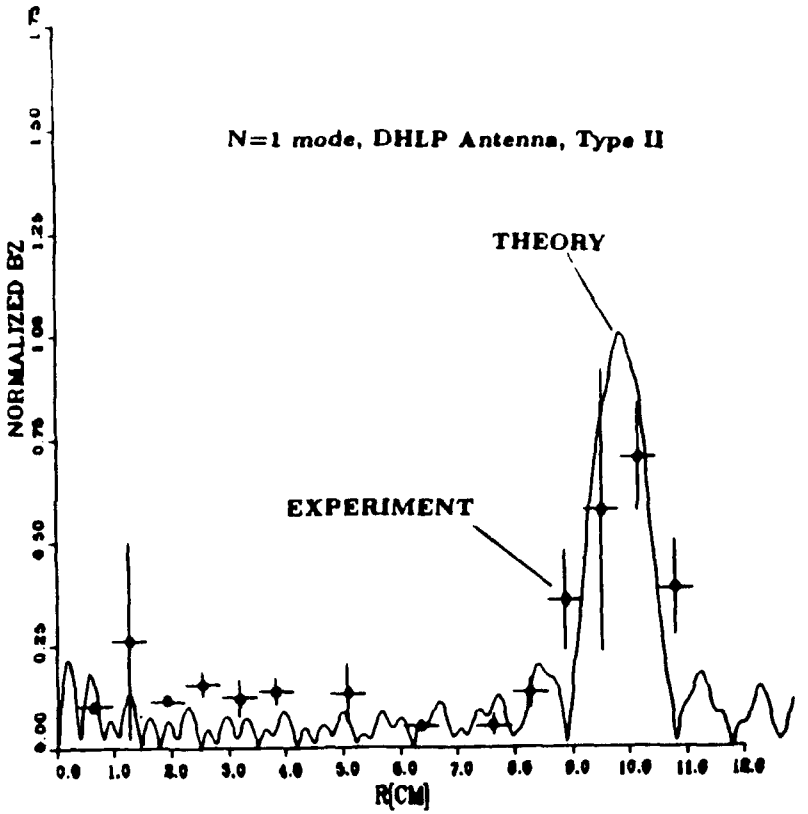

Figure 2: Radial B_z profile for type II discharge. The experimental results closely matches the theoretical prediction.

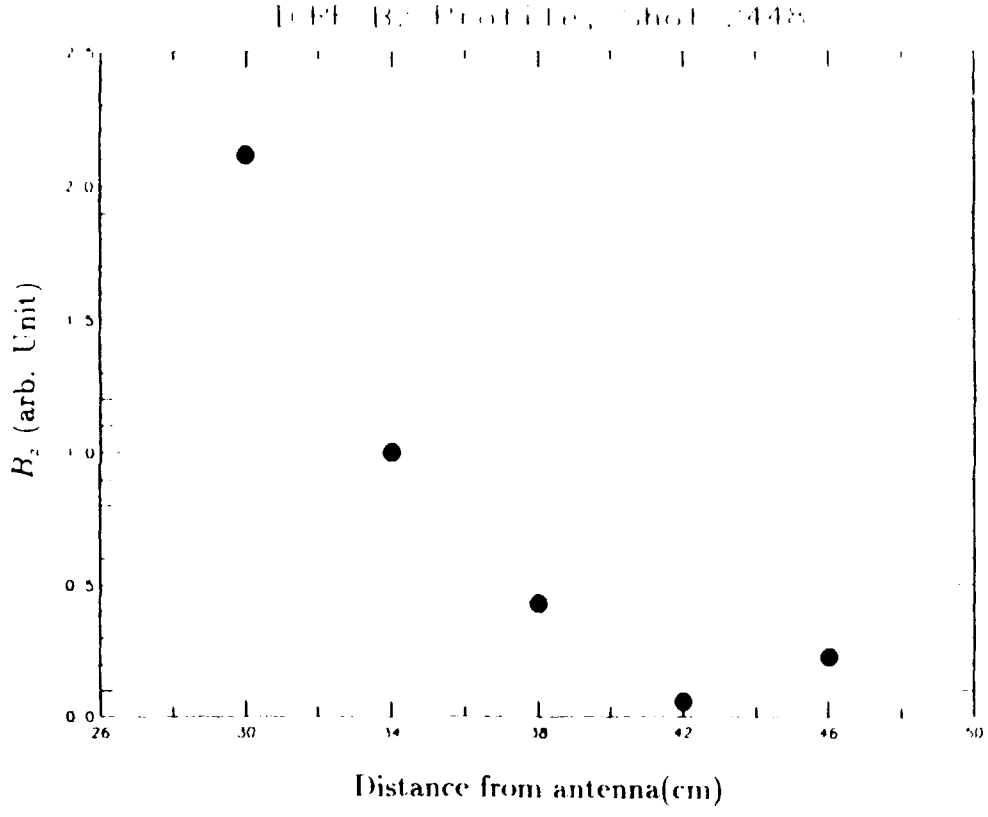

Figure 3: Axial B_z profile for type II discharge. The B_z amplitude decreases indicating damping.

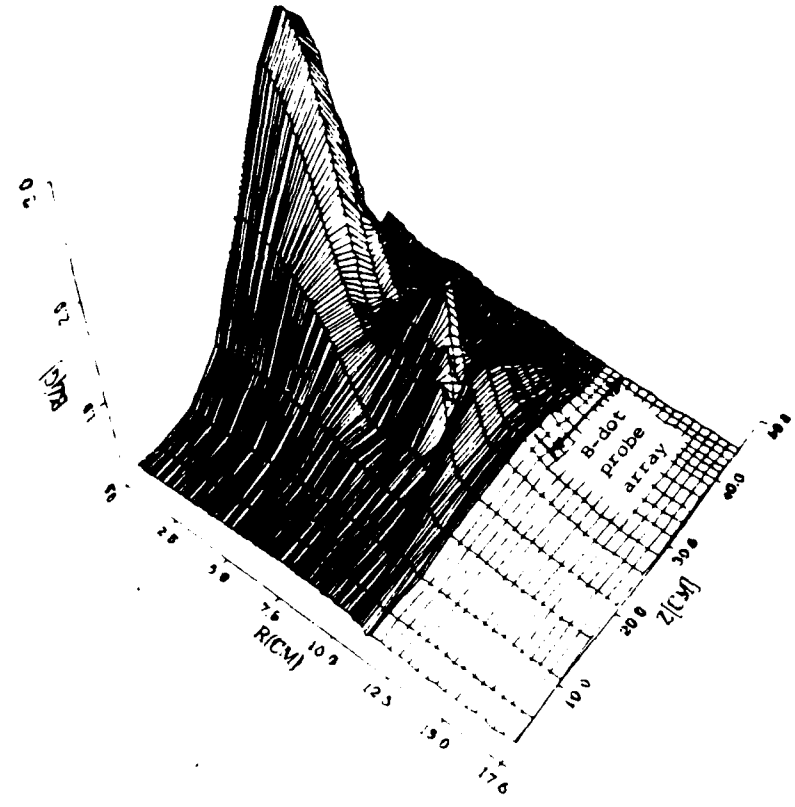

Figure 4: Trimetric view of B_z from numerical simulation. The heavy solid curve corresponds to the B-dot probe array measurement

ECR PLASMA ENGINE RESEARCH

Grant No. AFOSR-87-0205

Principal Investigators:
F. E. C. Culick and J. C. Sercel

California Institute of Technology
Pasadena, California 91125

SUMMARY/OVERVIEW:

The Electron-Cyclotron-Resonance (ECR) plasma engine is an electrodeless electromagnetic plasma accelerator which is being investigated for its potential use in electric propulsion, beamed energy propulsion, and advanced nuclear propulsion. Primary motivation for study of this device vis-á-vis other plasma acceleration schemes is provided by calculations which suggest that the ECR plasma engine has the theoretical potential to deliver moderate to high specific impulse, long life, and high unit power handling capability while processing any of several propellant species, some of which are not useable in other electric thruster concepts (Ref. 1). The theoretical performance of this device matches well with the stated United States Air Force need for more efficient, intermediate thrust propulsion (Ref. 2).

The objective of this research program has been to develop the first quantitative theoretical model of the operation of the ECR plasma engine. To accomplish this objective, both analytical and experimental studies have been performed. A quasi-one-dimensional, steady-state model of the acceleration process has been developed to provide quantitative predictions of physical parameters which are tested experimentally. In addition, a simple two dimensional (axisymetric) model has been formulated to predict the effects of the applied, diverging magnetic field on the plasma flow field. Knowledge of the geometry of the plasma flow field is required to assess potentially important losses such as beam divergence. Tests on a laboratory ECR plasma accelerator have been conducted. Several diagnostic tools, including a gridded energy analyzer, a Faraday cup current density analyzer, Langmuir probes, emissive probes, and a diamagnetic loop have been used to measure physical parameters of interest. While this first theoretical study of the ECR plasma engine concept has met with good success, considerable theoretical unknowns still exist regarding the actual performance potential of this incipient technology.

This research is viewed as the first critical stage in a development program which, if successful, will produce a new type of electric propulsion technology to fill the Air Force's need for efficient, long-life, intermediate thrust propulsion. It is hoped that the theoretical model developed in the present research can be used to design flight-like ECR plasma engines which have the potential to produce the desired performance. In addition, the theoretical models produced in this work are thought to be a prerequisite for the design of test facilities and the interpretation of test data which must be taken to validate this new technology.

TECHNICAL DISCUSSION

As described in previous publications, the theoretical aspect of this research consists of two separate modeling efforts. The first is a two dimensional model used to predict the geometry of the plasma flow field encountered in an ECR accelerator. The second, more extensive study, is the development of a quasi-one-dimensional three-component model which is used to understand non-equilibrium and radiation effects.

Calculation of ECR Plasma Engine Flow Field: We have used a collisionless, steady-state, cold, two-fluid model to predict the trajectory of the ECR plasma as it is accelerated through a diverging magnetic field. Our model allows the calculation of the angle by which the plasma flow field diverges during separation from the magnetic field. The divergence angle is important because the fraction of the momentum of the flowing plasma which is useful for thrust varies as the cosine of the divergence angle.

Our analysis addresses the acceleration of a plasma which is initially at a specified velocity and position in a cylindrically symmetrical system. An applied, strictly longitudinal magnetic field is assumed. Although random thermal energy effects are neglected in the cold plasma approximation, an important effect of the plasma enthalpy is included as the energy and magnetic dipole moment associated with electron Larmor motion perpendicular to magnetic field lines.

The results of calculations based on this model have been published in the open literature (Ref. 3). To summarize, we have found that the ECR plasma accelerator can be used to produce an accelerated plasma beam which detaches from the field of the magnetic nozzle even without collision-induced cross-field diffusion and without ohmic heating of the plasma driven by azimuthal currents. Further, the magnitude of the beam divergence losses can be controlled by adjusting the shape of the field of the magnetic nozzle.

We are now investigating the possibility that the presence of a unique type of current cell, first described by Simon, could cause the actual beam divergence encountered in the ECR plasma accelerator to be less than that predicted by our model (Ref. 4).

Nonequilibrium and Radiation Effects Model: Nonequilibrium and radiation effects are treated using a steady-state, quasi-one-dimensional, three-component model. The three components included are the electron fluid, the ion fluid, and the neutral gas, which is addressed under the assumption of rarified flow. Using this model we can solve for plasma density, gas atom density, axial velocity, and each of two components of the electron temperature (perpendicular and parallel to magnetic field lines). Source terms are present in the model to account for phenomena such as coupling microwave power into the plasma at ECR, collisional energy transfer between the perpendicular and parallel components of the electron temperature, cross-field (Bohm) diffusion, ionization, radiation, and ambipolar diffusion.

The set of equations embodying the model which we are presently working with are presented below:

continuity: $$\frac{d(Anu)}{dz} = A(S_i + S_d)$$

momentum: $$\frac{m_i}{A}\frac{d(Anu^2)}{dz} = F_\mu + F_{drag} + m_i(u\,S_d + u_a\,S_i) - \frac{dP_e}{dz}$$

energy: $$\frac{1}{A}\frac{d(AnuW_\perp)}{dz} = Q_\perp - u\,F_\mu + S_d W_\perp + \lambda\left(\frac{W_\perp}{W_\perp + W_{//}}\right)$$

$$\frac{1}{A}\frac{d(AnuW_{//})}{dz} = Q_{//} + S_d W_\perp + \lambda\left(\frac{W_{//}}{W_\perp + W_{//}}\right)$$

The plasma source terms, S_i and S_d, are the source terms which result from diffusion and ionization of neutral atoms. In this notation, n is the plasma electron number density (assumed equal to the ion number density); u is the plasma flow velocity; z is the axial coordinate; A is the cross sectional area of the plasma beam; m_i is the ion mass; u_a is the gas flow velocity; $W_\perp$ is the mean electron energy perpendicular to field lines; $W_{//}$ is the mean electron energy parallel to field lines; P_e is the the electron static fluid pressure; $Q_\perp$ is the energy flux to the perpendicular component of the electron motion; $Q_{//}$ is the energy flux to the parallel component of the electron motion; F_μ is the electron dipole moment force; F_{drag} is the friction term which accounts for collisions between plasma species and neutrals; and λ is the Spitzer-Harm electron thermal conductivity.

Continuing Work and Plans At present, we are working to incorporate the effects of axial heat transport and vacuum system back pressure into the existing model. Once verified by comparison with our experimental measurements, the present theory can then be used to predict the theoretical performance of the ECR plasma engine. We plan to perform numerical calculations based on the model described above and to compare the results of these calculations with our experimental measurements before publishing the final report for this research effort.

References:

1. Leifer, S. D., Blandino, J. J., and Sercel, J. C., "Electric Thruster Models for Multimegawatt Nuclear Electric Propulsion Mission Design," presented at the Eight Symposium on Space Nuclear Power Systems, January 6-10, 1991/Albuquerque, New Mexico. Proceedings pages 482-492.

2. Birkan, M. A., AFSTC Briefing on Rocket Propulsion, Kirtland AFB, NM, 8 November 1990.

3. Sercel, J. C.,"A Simple Model of Plasma Acceleration in a Magnetic Nozzle," AIAA-90-2667, presented at the AIAA/DGLR/JSASS 21th International Electric Propulsion Conference, July 18-20, 1990/Orlando, FL.

FUNDAMENTALS OF ACOUSTIC INSTABILITIES IN LIQUID-PROPELLANT ROCKETS

(AFOSR Grant No. 91-0130)

Principal Investigator: F.A. Williams

Department of Applied Mechanics and Engineering Sciences
University of California, San Diego, La Jolla, CA 92093-0310

SUMMARY/OVERVIEW

This newly initiated project concerns the mechanisms by which flow, mixing and combustion process are coupled to acoustic fields in liquid-propellant rocket motors. The approach is primarily analytical, with use made of asymptotic methods. Nonhomogeneities in the flow field are taken into account, and attention is focused on both subcritical and supercritical conditions for vaporization, with real chemistry treated through the development of reduced chemical-kinetic mechanisms. It is planned to consider hydrogen-oxygen systems first and storables later. The following is an overview of modeling, prepared for the present meeting.

TECHNICAL DISCUSSION

History and Literature

Liquid-propellant rocket combustion was a topic of intensive research in the 1950's and 1960's, but it experienced de-emphasis thereafter. Since that time, computational capabilities have increased greatly; however, understanding has not. Most of the ideas about steady and oscillatory liquid-propellant rocket combustion were developed during those two decades. Consequently, reviews based on information available at that time, such as [1], provide most of the essential background information. Some updating is obtainable from more recent overviews [2-6]; citations here are restricted mainly to easily available literature or to work not previously cited in reviews.

Mathematical Formulation for Steady and Oscillatory Conditions

To describe the flow in the combustion chamber of a liquid-propellant rocket from a fundamental viewpoint is challenging. A starting point is a deterministic initial-boundary-value problem for a nonideal, chemically reacting fluid with phase changes. Given all the relevant thermodynamics and chemical kinetics, as well as the constitutive relations of Newtonian type relating fluxes and stresses to gradients as in the Navier-Stokes equations, formulation at this level is easy. A perfect computer would solve the problem, predicting atomization, vaporization, combustion, and unsteadiness interpretable as multiphase flow and turbulence. Probably the only such "computer" that will ever be available is the motor itself, from which "output" (velocities, state variables, etc.) is tough to obtain. Therefore, averaging is needed, resulting in conservation equations for multiphase flows [7,8]. Current and future modeling practice deals with such equations. Since different averagings give different accountings, attention to detail is essential in formulation. Appendix A summarizes the equations obtained from one particular approach to averaging.

Describing Steady Motor Operation

In principle, steady-flow equations are to be solved prior to investigating instability. There are a number of different approaches to calculation of steady, multiphase flow. The simplest

descriptions postulate steady, one-dimensional flow and focus either on evolution of droplet probability-density functions, ignoring the gas, or on monodisperse droplet descriptions, including gas effects. There has been some description of area changes in quasi-one-dimensional flow and of transverse mixture-fraction distributions with cylindrical symmetry. Although steady, axisymmetric programs are available even for dense sprays, they are expensive to run and generally not used in rocket applications. It is generally agreed that one-dimensional or axisymmetric descriptions are poor in injection and atomization regions, and although much is known about atomization processes, the information seems too complex to be worked conveniently into models of steady chamber operation, except as upstream boundary conditions. Explicit account of supercriticality also appears lacking in steady-flow modeling. Thus, there are many deficiencies in combustor descriptions even in the absence of instability.

When instabilities are to be addressed, descriptions of steady-state processes are simplified even further. The usual approximation for identifying acoustic modes is that of a chamber without flow and with a single, uniform sound speed. This is successful because the uncertainty in the correct sound speed is large enough that a value can be chosen within the range of uncertainty to match data. The two-phase effects are considered only as perturbations that may influence amplification and attenuation. Although such approximations may be acceptable, they appear to deserve further consideration in possibly masking some instability phenomena.

Describing Combustion Instability

Existing modeling of instabilities is generally patterned after classical descriptions of acoustic instabilities. Time-dependent perturbation equations, linear or nonlinear, are integrated numerically, often without one-dimensional approximations, since standing and traveling transverse modes frequently are significant. Both boundary amplification (e.g. through admittances) and homogeneous amplification (e.g. through a Rayleigh criterion) are considered; the latter especially causes significant complications and uncertainties because of the complexity of the nonuniform multiphase flow. A number of brute-force methods march on time scales short compared with acoustic times. This may seem desirable in that pop-type growth of sharp-fronted instabilities in principle may be described (if the formulation is nonlinear), but in practice correct pop physics is absent in the rough source descriptions, so the advantage is illusory. Multiscale methods [6] that can march on times long compared with acoustic times seem much more efficient and better capable of providing physical understanding.

Even today, the manner in which source amplification or attenuation is handled in practice usually reverts to Crocco's classical time-lag description. The pressure exponent and sensitive time lag are estimated empirically by comparing measured and computed neutral stability boundaries. Although Crocco's contribution was admirable, perhaps the most important in the field, we know that it was devised when the underlying physical processes were unknown and that many mechanisms now are known. It therefore seems better now to put in these mechanisms, one by one, instead of relying on time lags. This might lead to a revolution in modeling of combustion instability.

Amplification Mechanisms

Strahle has identified a number of mechanisms that may be responsible for amplification of instabilities and has evaluated characteristic times for these processes. Some of these processes are listed among others in Table 1, where a few research needs are suggested. Because of the evolution to higher chamber pressures, Strahle's estimates deserve revisitation. Since supercriticality is more prevalent nowadays, it merits closer scrutiny than it has been given with respect to amplification, for both atomization and combustion. A mechanism with correct phasing between vaporization and combustion to amplify acoustics strongly has recently been discovered for planar spray combustion [9]; its potential rocket relevance should be considered.

Research Recommendations

Table 1 lists areas in which further research is needed. In general, studies seem best advised to address real-world chamber conditions, rather than cold flow or reduced pressure, where there are interesting phenomena, to be sure, but not likely the same as in practice. Moreover, in instability investigations it is essential to address phase relationships (as well as characteristic times), since these distinguish amplification from attenuation. If good understanding can be obtained of the new and potentially important amplification and attenuation processes such as those indicated above and in the table, then the important ones can be included in chamber instability modeling to improve capabilities of instability computations.

REFERENCES

1. D.J. Harrje and F.H. Reardon, eds., Liquid Propellant Rocket Combustion Instability, NASA SP-194, U.S. Government Printing Office, Washington, DC, 1972.

2. G.M. Faeth, Prog. Energy Combust. Sci. **9**, 1-76 (1983).

3. W.A. Sirignano, Prog. Energy Combust. Sci., **9**, 291-322 (1983).

4. G.M. Faeth, Prog. Energy. Combust. Sci., **13**, 293-345 (1987).

5. F.A. Williams, Combustion Theory (2nd ed.), Addison-Wesley, Menlo Park, CA, 1985.

6. F.E.C. Culick, Combustion Instabilities in Liquid-Fueled Propulsion Systems – An Overview AGARD 72B PEP Meeting Oct., 1988.

7. S.L. Soo, Fluid Dynamics of Multiphase Systems, Blaisdell, Waltham, MA, 1967.

8. D.A. Drew, Annual Review of Fluid Mechanics **15**, 261-291 (1983).

9. P. Clavin and J. Sun, Theory of Acoustic Instabilities of Planar Flames Propagating in Sprays or Particle-Laden Gases, submitted to Combustion Science and Technology, 1990.

TABLE 1: RESEARCH NEEDS (SHORT LIST)

1. Steady-Flow Descriptions
   a. Better inclusion of atomization processes
   b. Account of both fuel and oxidizer sprays
   c. Explicit consideration of supercriticality
   d. Improved descriptions of mixture-fraction variations
   e. Introduction of turbulence effects
2. Acoustic-Field Descriptions
   a. Account for small-scale flow nonhomogeneities
   b. Consider axial variations and two-phase flow
   c. Address effects of turbulent-combustion noise
3. Instability-Amplification Processes
   a. Atomization response
   b. Mechanical response of liquid sheets
   c. Flames between sheets of impinging jets

d. Droplet wake burning
e. Distributed heat release in nonuniform mixture-fraction field
f. Spray flames with feedback between vaporization and combustion
g. Supercritical mixing with finite-rate chemical heat release

APPENDIX A: CONSERVATION EQUATIONS

Let ρ_{ji} denote the mass of chemical species i in phase j per unit volume of phase j and α_j the volume fraction of phase j. Generally j = g,f,o denotes gas, fuel and oxidizer streams, respectively, although at totally supercritical conditions j = g only, with $\alpha_g = 1$. With N chemical species in the system, the density of phase j is $\rho_j = \sum_{i=1}^{N} \rho_{ji}$, and the total density is $\rho = \sum_j \alpha_j \rho_j$. If $\mathbf{u}_j$ is the mass-weighted average velocity of phase j and $\rho \mathbf{u} \equiv \sum_j \alpha_j \rho_j \mathbf{u}_j$, then overall mass conservation is

$$\partial \rho / \partial t + \nabla \cdot (\rho \mathbf{u}) = 0 . \tag{1}$$

Mass conservation for phase j is

$$\partial (\alpha_j \rho_j) / \partial t + \nabla \cdot (\alpha_j \rho_j \mathbf{u}_j) = -w_j , \tag{2}$$

where w_j is the rate of mass loss per unit volume for phase j, and $w_g = -(w_f + w_o)$. In terms of the diffusion velocity $\mathbf{U}_{ji}$ for species i in phase j, conservation of chemical species i in phase j is

$$\partial (\alpha_j \rho_{ji}) / \partial t + \nabla \cdot [\alpha_j \rho_{ji} (\mathbf{u}_j + \mathbf{U}_{ji})] = \alpha_j w_{ji} + \sum_{j' \neq j} w_{j'} \beta_{jij'} , \tag{3}$$

where w_{ji} is the mass rate of production of chemical species i in phase j, and $\beta_{jij'}$ is the mass of species i added to phase j from phase j' per unit mass loss of phase j'. Vaporization or droplet combustion laws determine w_j and $\beta_{jij'}$, while diffusion equations determine $\mathbf{U}_{ji}$ and chemical kinetics w_{ji}.

Although there are situations in which different phases must be assigned different pressures to avoid inconsistencies, this is probably inessential in liquid-propellant rockets, so that a common pressure p may be adopted; moreover, body forces may be neglected. Overall momentum conservation then becomes

$$\partial (\rho \mathbf{u}) / \partial t + \nabla \cdot \left(\sum_j \alpha_j \rho_j \mathbf{u}_j \mathbf{u}_j \right) + \nabla p = \nabla \cdot \mathbf{T} , \tag{4}$$

where $\mathbf{T}$ is a viscous stress tensor, containing contributions from all phases although often dominated by gas. Momentum conservation for phase j is

$$\alpha_j \rho_j \partial \mathbf{u}_j / \partial t + \alpha_j \rho_j \mathbf{u}_j \cdot \nabla \mathbf{u}_j + \alpha_j \nabla p = \alpha_j \nabla \cdot \mathbf{T}_j + \sum_{j' \neq j} (\mathbf{u}_{j'} - \mathbf{u}_j) \gamma_{jj'} , \tag{5}$$

where $\mathbf{T}_j$ is the viscous stress tensor for phase j, and $\gamma_{jj'}$ is an interphase momentum-transfer parameter, the product of an average local momentum-transfer coefficient with an effective local interfacial surface area per unit volume. Viscous stress equations determine $\mathbf{T}_j$, while drag laws

appear in $\gamma_{jj'}$. It is most usual to use Eq. (5) for j = f,o with α_j small and ∇p and $\nabla \cdot \mathbf{T}_j$ negligible in the equation.

Energy conservation may be written in terms of the total (thermal plus chemical) enthalpy per unit mass for phase j, denoted by h_j. Overall energy conservation then becomes

$$\frac{\partial}{\partial t}\left[\sum_j \alpha_j \rho_j \left(h_j + \frac{u_j^2}{2}\right)\right] + \nabla \cdot \left[\sum_j \alpha_j \rho_j \mathbf{u}_j \left(h_j + \frac{u_j^2}{2}\right)\right] = \frac{\partial p}{\partial t} - \nabla \cdot \mathbf{q} + \Phi, \tag{6}$$

where $\mathbf{q}$ is a heat-flux vector and Φ a rate of viscous dissipation. Often with α_g near unity Φ and $\mathbf{q}$ are dominated by the gas phase, giving $\Phi = -\nabla \cdot (\mathbf{T}_g \cdot \mathbf{u}_g)$ and $\mathbf{q} = -\lambda_g \nabla T_g + \sum_{i=1}^{N} \rho_{gi} h_{gi} U_{gi} + \mathbf{q}_R$, where λ_j denotes the thermal conductivity of phase j, T_j the temperature of phase j, h_{ji} the total (thermal plus chemical) enthalpy per unit mass for species i in phase j, and $\mathbf{q}_R$ the radiant heat-flux vector (Dufour neglected). Energy conservation for phase j is

$$\alpha_j \rho_j \frac{\partial}{\partial t}\left(h_j + \frac{u_j^2}{2}\right) + \alpha_j \rho_j \mathbf{u}_j \cdot \nabla \left(h_j + \frac{u_j^2}{2}\right) = \alpha_j \frac{\partial p}{\partial t} - \nabla \cdot (\alpha_j \mathbf{q}_j) + \alpha_j \Phi_j + \sum_{j' \neq j} (T_{j'} - T_j)\delta_{jj'}, \tag{7}$$

where $\mathbf{q}_j$ is the heat-flux vector for phase j, Φ_j the rate of viscous dissipation in phase j, and $\delta_{jj'}$ an interphase heat-transfer parameter, the product of an average local heat-transfer coefficient with a local interfacial surface area per unit volume. Molecular heat-flux equations determine $\mathbf{q}_j$, while interphase heat-transfer expressions appear in $\delta_{jj'}$. Equation (7) is in a form most directly applicable for j = f,o with α_j small, so that on the right-hand side the last term dominates. This term can assume quite different forms, through different expressions for $\delta_{jj'}$, depending, for example, on the significance of interphase mass transfer and of combustion in thin layers around condensed phases.

After atomization, the condensed phases themselves are conveniently described by spray conservation equations for $f_j(m, \mathbf{v}, \mathbf{w}, \mathbf{x}, t)$, the average number of droplets per unit volume at position $\mathbf{x}$ and time t, per unit range of mass m, of velocity $\mathbf{v}$ and of other parameters $\mathbf{w}$ (such as shape or temperature), having mass in a small range dm about m, velocity in a small range dv about $\mathbf{v}$, and other parameters in a small range dw about $\mathbf{w}$. The spray equation is

$$\frac{\partial f_j}{\partial t} = \frac{\partial (M_j f_j)}{\partial m} - \nabla \cdot (\mathbf{v} f_j) - \frac{\partial (\mathbf{A}_j f_j)}{\partial \mathbf{v}} - \frac{\partial (\mathbf{B}_j f_j)}{\partial \mathbf{w}} + C_j, \tag{8}$$

where M_j is the rate of mass loss of a droplet at $(m, \mathbf{v}, \mathbf{w}, \mathbf{x}, t)$, $\mathbf{A}_j$ is the acceleration of such a droplet, $\mathbf{B}_j$ is the rate of increase of $\mathbf{w}$ of such a droplet, and C_j is the rate of increase of f_j from droplet sources (such as atomization) and from interactions with other droplets (collisions). Analyses of droplet behavior must provide expressions for M_j, $\mathbf{A}_j$, $\mathbf{B}_j$ and C_j. Condensed-phase properties, such as $\alpha_j \rho_j$, are readily expressible as integrals over f_j, and simplified descriptions can be obtained from suitable integrals with delta-function approximations. Given the subsidiary equations that have been indicated to be needed, the system is complete.

ROLE OF UNSTEADY ATOMIZATION IN LIQUID ROCKET COMBUSTION INSTABILITY

AFOSR Grant Number 90-0121

John W Daily, and Shankar Mahalingam

Center for Combustion Research
University of Colorado at Boulder
Boulder, Colorado 80309-0427

SUMMARY/OVERVIEW

Combustion instabilities have been observed in many liquid rocket engines. They are characterized by large amplitude oscillations of various flow quantities (pressure, velocity, etc.), resulting in extensive engine damage. Therefore, there is a need to better understand the processes involved in order to improve prediction ability. In particular, atomization characteristics are completely altered under an oscillatory pressure environment (Reba et al. 1957, Ingebo 1966). However, a complete picture of the interaction between unsteady atomization and combustion process is not available. This research project focusses on the role of unsteady atomization in high frequency combustion instability. A combustor is designed to allow measurement of atomization data under steady state and oscillatory pressure environment. Results obtained will be used to gain understanding of the combustion instability phenomenon and improve stability prediction ability thereby minimizing trial and error testing during the development phase of new engines.

AUTHORS: C. Huynh, A. Ghafourian, P. Johnson, S. Mahalingam, and J. W. Daily

TECHNICAL DISCUSSION

1. Introduction

Experimental studies have shown that atomization characteristics are completely altered under oscillating pressure environment (Reba et al. 1957). Ingebo (1966) measured [illegible] droplet sizes under steady and oscillating pressure environment in a laboratory combustion facility and found that under resonant conditions, the mean droplet diameter decreased by a factor of six, compared to steady state measurements. The length for complete atomization and complete vaporization decreased by factors of two and ten respectively.

Since atomization is the first physical process which takes place in a liquid rocket engine, it is believed that fluctuations in droplet size or velocity, induced by unsteady environment, will significantly influence subsequent processes such as vaporization, mixing, and combustion. As a result, variations in engine performance and stability characteristics are expected. Computer calculations based on the vaporization limited model developed by Priem (1960) support this assertion. To date however, no experimental study aimed at assessing the role of unsteady atomization in liquid rocket instability phenomenon has been performed, as shown by the literature review by Ghafourian (1991). The objective of our research program is to provide a comprehensive picture of the mechanisms for high frequency combustion instability involving unsteady atomization through

a coordinated experimental, analytical and numerical study. Specifically,

- To understand the phase relationship between unstable waves leading to atomization and combustion chamber pressure variations.
- To obtain unsteady atomization experimental data, such as droplet size distributions under oscillatory pressure environment. This information will then be used in a computer program POCCID, provided to us by NASA Lewis, to improve engine stability predictions.

2. Progress to date

We have completed the design of an experimental facility that will allow testing of uni-element injectors of different designs. Mainly, two types of injectors will be studied, shear coaxial and impinging jet type atomizers. Coaxial injectors are studied first. Two methods of excitation have been chosen, to modulate the pressure environment of the atomizing liquid in order to simulate chamber pressure oscillations, as would occur under unstable conditions.

Design considerations

- Similarity numbers and simulant selection:

  Real rocket engines operate at high chamber pressure (1000 psia). Propellants used in the rocket industry are usually toxic or cryogenic. Therefore, it is difficult to reproduce actual engine conditions in a university experimental facility. Hence, an approach based on similarity numbers has been selected. A review on atomization conducted by Ghafourian et al. (1990) identified two main governing parameters: the Reynolds number of the liquid phase, $Re_l = \frac{\rho_l V_l d_o}{\mu_l}$, and the Weber number, $We_g = \frac{\rho_g (V_g - V_l)^2 d_o}{\sigma_l}$. The former has been selected to characterize the turbulence level in the jet as it comes out of the nozzle. This sets the initial amplitude level of disturbances on the jet surface that will subsequently be amplified by aerodynamic interaction with the surrounding gas. The latter takes into account aerodynamic forces, that are the main destabilizing agents for jet atomization. With an appropriate choice of simulants, it has been shown (Ghafourian 1991) that it is possible to operate in the same Re_l-We_g region as in the study by Wanneinen (1966) on a 20000 pound thrust engine without any optical access (see Fig 1). Data obtained on our experimental setup can therefore be compared with real rocket data.

- Excitation methods: Acoustic drivers will be used to excite transverse modes in the combustion chamber. Although transverse modes are frequently encountered in high frequency combustion instability (Reardon et al. 1972), no experimental study has been performed to characterize atomization in a transverse oscillating pressure field. The use of acoustic drivers has been tested in active control of combustion instability applications. Based on the work of Poinsot et al. 1987, Gutmark et al. 1989, Mc Manus et al. 1990, we expect that amplitudes of up to 10 % of mean chamber pressure can be generated.

  In order to excite longitudinal modes and simulate unstable regimes with axially propagating pressure waves as reported by Berman (1957), a mechanical chopper, that periodically closes the exhaust nozzle throat is chosen (Fig 2). This method has been applied successfully by Reba (1957), Ingebo (1966) and Lecourt (1988).

- Chamber geometry and operating conditions: The chamber dimensions were obtained by finding a compromise between two conflicting considerations: the chamber had to be large to ensure complete combustion before the nozzle is reached but small in order to enable high amplitude forcing. Details are given in Ghafourian et al.(1991).

Analytical and numerical developments

In parallel with the experimental design, an analytical model has been developed to study the influence of several destabilizing effects on the atomization process of coaxial injectors. In particular, the velocity profile relaxation as the jet comes out of the nozzle has been identified as a possible mechanism for jet breakup (Reitz et al. 1982). We have completed a study of this effect (Hevert et al. 1991). In the near term, we will examine the interaction between disturbances in the liquid jet and coflowing gas. Results from these investigations will be used in a direct numerical simulation study of atomization that we expect to initiate in the coming year.

REFERENCES

1. Ghafourian, A., Mahalingam, S., Dindi, H., and Daily, J.W., "A Review of Atomization in Liquid Rocket Engines," AIAA 91-0283, 29th Aerospace Sciences Meeting, Reno, January, 1991.

2. Ghafourian, A. , Huynh, C., Johnson, P., Dindi, H., Mahalingam, S., and Daily, J.W., "Combustor Design for Study of Combustion Instability in Liquid Rocket Engines," Paper WSS/CI 91-54 and CCR Report No 91-07, 1991.

3. Ghafourian, A. , Huynh, C., Johnson, P., Dindi, H., Mahalingam, S., and Daily, J.W., "Studies of Liquid Rocket Combustion Instability using Excitation Systems, a Mini Review," CCR Report No 91-08, March, 1991.

4. Heidmann, M.F., Humphrey, J.C., "Fluctuations in Spray Formed by two Impinging Jets," NACA TN 2349, 1951.

5. Hevert, S., Mahalingam, S., and Daily, J. W., "Velocity Profile Effects on the Stability of a Liquid Jet," Paper WSS/CI 91-54 and CCR Report No 91-06, 1991.

6. Ingebo, R. D., "Atomization of Ethanol Jets in a Combustor With Oscillatory Combustion-Gas Flow," NASA TN D-3513, 1966.

7. Lecourt, R, and Foucaud, R. "Experiments on Stability of Liquid Propellant Rocket Motors," 23rd AIAA Propulsion Conference, San Diego, 29 June-2 July, 1978.

8. Priem, R.J. , Heidmann, M.F., "Propellant Vaporization as a Design Criterion for Rocket Engine Combustion Chambers," NASA TR R-67, 1960.

9. Reitz, R. D., and Bracco, F. V., "Mechanism of Atomization of a Liquid Jet," Encyclopedia of Fluid Mechanics, (N.P. Cheremisinoff, Ed.) Vol. 3, Gulf Pub., Houston, 1986, pp.233-249.

10. Wanheinen, J.P., "Effect of Propellant Injection Velocity on Screech in a 20000-Pound Hydrogen-Oxygen Rocket Engine," NASA, TN D-3373, April, 1966.

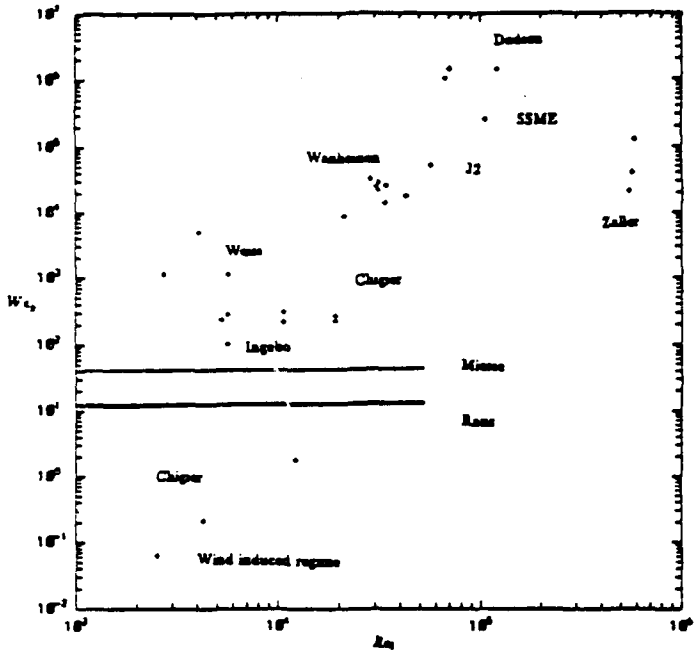

Figure 1: Re_l-We_g Diagram of Some Previous Experimental Studies on Coaxial Injectors

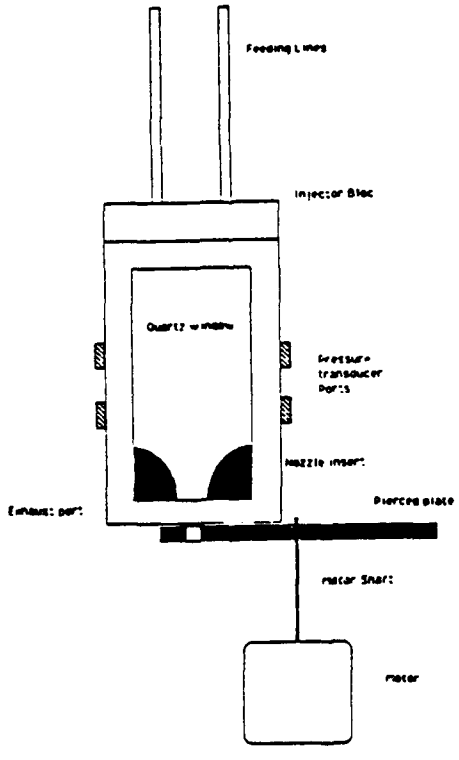

Figure 2: Combustor Sketch for Hot Flow Testing With Mechanical Chopper

ACOUSTIC WAVES IN COMPLICATED GEOMETRIES AND THEIR INTERACTIONS WITH LIQUID-PROPELLANT DROPLET COMBUSTION

(AFOSR Contract No. 91-0171)

Principal Investigator: Vigor Yang

Department of Mechanical Engineering and
Propulsion Research Engineering Center
The Pennsylvania State University
University Park, PA 16802

SUMMARY/OVERVIEW

A focused theoretical program is being conducted to investigate the acoustic wave characteristics in liquid-propellant rocket motors with injector-face baffles. The work primarily addresses the combustion stability behavior of a complicated geometry and the damping mechanisms of baffles -- how does the baffle work in various environments; and what are the physical processes responsible for suppressing unsteady motions in a baffled combustor? In addition, the dynamic responses of liquid-propellant droplet combustion to ambient flow oscillations in the baffle region will be examined in detail. A major goal of this research is to establish a unified framework for treating combustion instabilities in baffled liquid-propellant rocket motors.

TECHNICAL DISCUSSION

Introduction. Because combustion instabilities arise from the mutual coupling between acoustic waves and combustion processes, any realistic study of the motor stability behavior must accommodate a thorough treatment of the wave structure in the chamber. However, to date, no theory exists which can deal with acoustic waves in an entire rocket motor, especially in the baffle region and the convergent section of the nozzle, as shown in Fig. 1. Since injector-face baffles provide the most significant stabilization effects on pressure oscillations, a basic understanding of the oscillatory flow structure in that region and its interactions with propellant atomization and combustion processes appears to be a prerequisite in treating combustion instabilities in liquid-propellant rocket motors. The primary purpose of this study is to develop a comprehensive theoretical analysis within which multi-dimensional acoustic waves in a baffled combustor and their mutual coupling with propellant combustion can be treated properly.

Approach. Baffles may affect the stability behavior of a rocket motor through the following three mechanisms: (1) modification of the acoustic properties of the chamber; (2) damping of acoustic wave energy through viscous friction and mean flow/acoustics interaction; and (3) decoupling of sensitive combustion processes from oscillatory flow motions [1,2]. Thus, a logic approach to this problem is to establish a general framework capable of treating the above mechanisms systematically. The work involves the following three major tasks:

1. development of a three-dimensional analysis for treating acoustic waves in complicated geometries;
2. investigation of acoustic wave characteristics in baffled combustion chambers; and

3. study of dynamic responses of liquid-propellant droplet vaporization and combustion to ambient flow oscillations in the near field of the baffle.

The acoustic field in a baffled combustor can be formulated with the general analysis constructed by the author [3]. Briefly stated, a wave equation governing the flow oscillations is first derived from the conservation equations for a two-phase mixture, with expansion of the dependent variables in two small parameters measuring the Mach number of the mean flow and the amplitude of the unsteady motion. The wave equation can be written in the form

$$\frac{1}{\bar{a}^2}\frac{\partial^2 p'}{\partial t^2} - \nabla^2 p' = -h$$

The function h contains all influences of droplet vaporization and combustion, mean flow/acoustics coupling, and two-phase interaction. It can be correctly modeled as a distribution of time-varying mass, momentum, and energy perturbations to the acoustic field. Boundary conditions are found by taking the scalar product of the outward normal vector with the perturbed momentum equation, and then applying appropriate acoustic admittance functions along the surface of the chamber. To avoid the analytical difficulty associated with the injector-face baffle, a novel solution technique which treats the baffle as a discrete number of fictitious point sources located inside the baffle blades and hub (see Fig. 2) is developed. Thus, the influence of baffle on the motor stability characteristics can be treated explicitly as a source term in the wave equation, and subsequently solved by means of an improved Green's function technique. The major advantage of this approach is the provision of an analytical framework for studying mechanisms proposed as the stabilizing effects of baffles. Furthermore, it alleviates the computational burden associated with conventional numerical techniques, and consequently produces more sweeping results in a more efficient manner.

The second part of the present research is to examine the sensitivities of propellant droplet vaporization and combustion to ambient flow oscillations in a complicated wave environment. Both pressure- and velocity-coupled responses will be considered. The study will be based on the time-dependent supercritical droplet combustion model developed by the author [4,5]. Specifically, the acoustic wave analysis developed in the first part of this project will provide a realistic oscillatory flow condition in the chamber, which will then be incorporated into the droplet model to calculate droplet responses. Results obtained will be used as a source term in the wave equation to calculate the mutual coupling between acoustic waves and droplet combustion responses in a baffled combustor.

The analysis of droplet vaporization and combustion treats the complete conservation equations of mass, momentum, energy, and species concentration for both droplet and ambient gases at Reynolds numbers of practical interest, with a full account of variable properties and vapor-liquid interfacial thermodynamics (see Fig. 3). The model accommodates various important high-pressure phenomena, including ambient gas solubility, thermodynamic non-ideality, property variation, transient diffusion, etc. Because of its completeness. the analysis enables a systematic examination of the droplet vaporization and combustion characteristics in a high-pressure environment. In particular, the underlying mechanisms of droplet vaporization, ignition, and combustion at near- and super-critical conditions, including the transition from the subcritical to the supercritical state, are addressed. Figure 4 presents the instantaneous mass of a n-pentane droplet reacted with air at various pressures. The ambient gas pressure exerts significant control of the droplet gasification and burning processes through its influences on the fluid transport, gas/liquid interface thermodynamics, and chemical reactions.

REFERENCES

1. Harrje, D. T., and Reardon, F. H. (eds.), Liquid-Propellant Rocket Combustion Instability, NASA SP-194, 1972.

2. Oefelein, J. C., and Yang, V., "Liquid-Propellant Combustion Instabilities in F-1 Engines - A Comprehensive Review," AIAA Paper No. 91-2086, presented at the AIAA/ASME/SAE/ASEE 27th Joint Propulsion Conference, June 1991.

3. Culick, F. E. C., and Yang, V., "Prediction of the Unsteady Motions in Solid-Propellant Rocket Motors," to appear in Nonsteady Burning and Combustion Stability of Solid-Propellants, Progress in Astronautics and Aeronautics, eds., L. DeLuca and M. Summerfield.

4. Hsieh, K. C., Shuen, J. S., and Yang, V., "Multi-Component Fuel Droplet Vaporization in High-Pressure Environments, I: Near Critical Conditions," to appear in Combustion Science and Technology.

5. Shuen, J. S., and Yang, V., "Combustion of Fuel Droplets at Supercritical Conditions," AIAA Paper No. 91-0078, presented at the AIAA 29th Aerospace Science Meeting, January 1991.

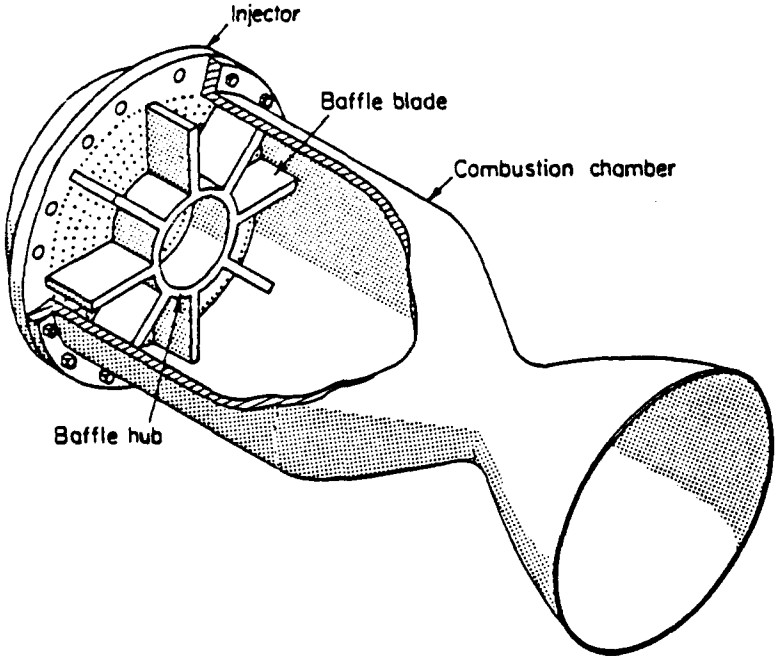

Fig. 1. Schematic Diagram of Liquid-Propellant Rocket Motor with Injector-Face Baffle

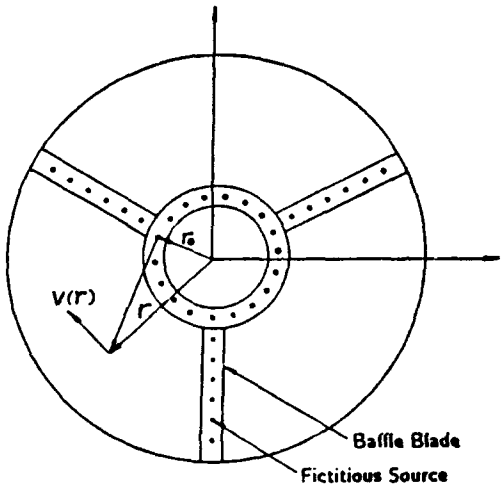

Fig. 2. Schematic Diagram of Fictitious Source Inside Baffle Blade

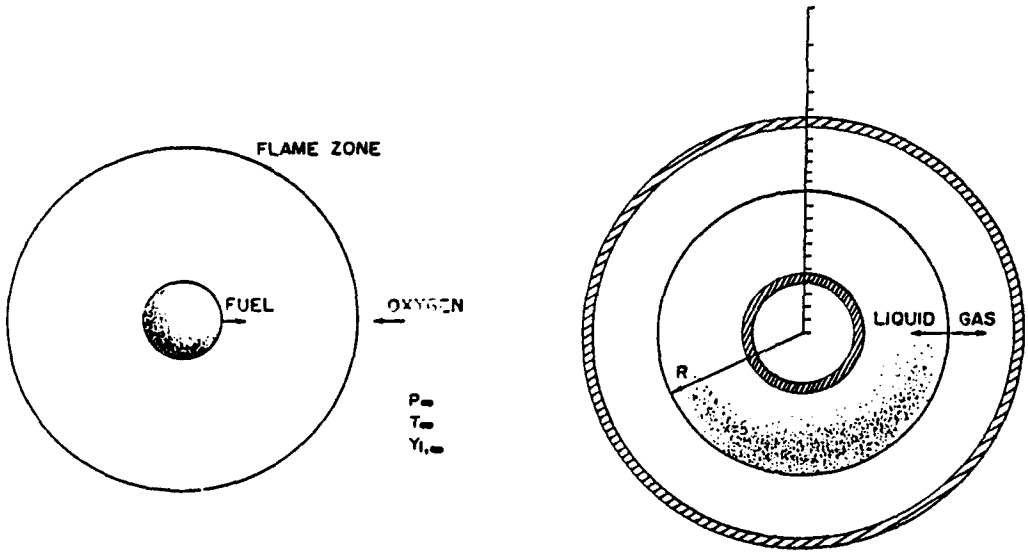

Fig. 3. Grid System for Finite-Volume Numerical Computation of Supercritical Droplet Vaporization and Combustion

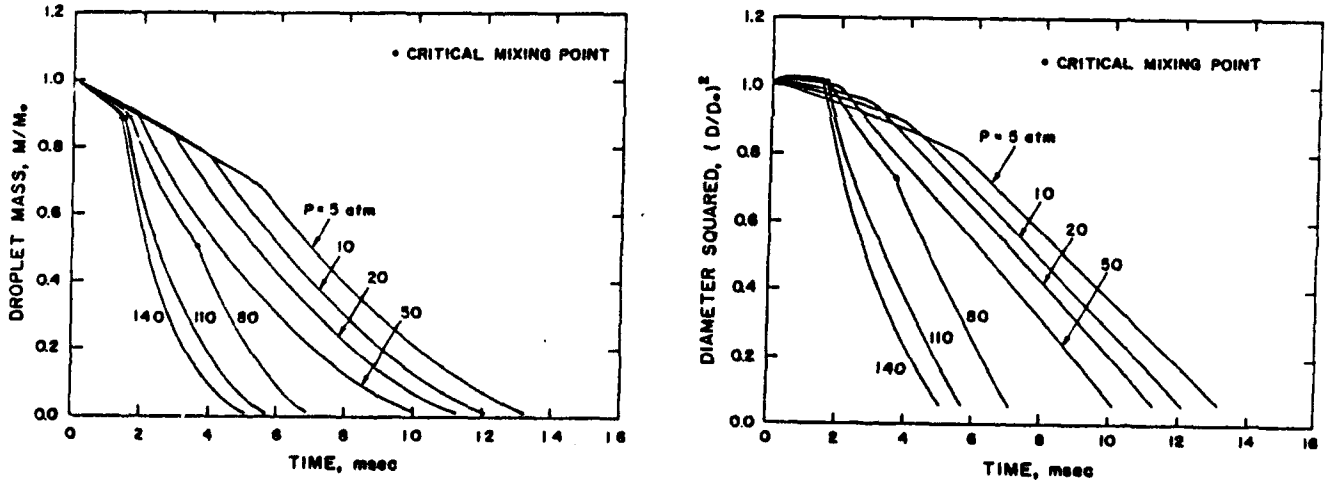

Fig. 4. Time Variations of Fuel Droplet Mass at Various Pressures, n-Pentane/Air System

COMBUSTION INSTABILITY PHENOMENA OF IMPORTANCE TO LIQUID PROPELLANT ROCKET ENGINES

Principal Investigators: W.E. Anderson and R.J. Santoro

Propulsion Engineering Research Center
and
Department of Mechanical Engineering
The Pennsylvania State University
University Park, PA 16802

SUMMARY/OVERVIEW:

A research program has recently been initiated at the Propulsion Engineering Research Center to determine the fundamental physical mechanisms in an impinging liquid jet injector system which control and participate in combustion instability. The impinging jet injector system was chosen for study because of its importance for storable propellants, significance of the problem, and its potential advantages over the coaxial injector system for a LOX/H_2 propellant system. The experiments will emphasize non-intrusive temporal and spatial optical measurements of atomization length and frequency, drop size distribution and trajectories under steady and forced oscillatory conditions. A complementary analytical effort is underway to develop an atomization model for this system; other existing models will also be used in the data analysis. Successful completion of this program will lead to mechanistically-based injector design analysis approaches which can be incorporated into methodologies for future liquid rocket engine design.

TECHNICAL DISCUSSION:

Combustion instability has been widely observed in liquid rocket engines often with catastrophic consequences. Yet, the driving mechanism or mechanisms for this phenomena remain largely unexplained. A number of potential mechanisms have been developed over the course of nearly four decades of research in this area[1]. The most prevalent mechanisms which have been experimentally or analytically studied are the principal component processes of liquid rocket engine combustion: injection, atomization, vaporization, mixing, and kinetics.

No broadly based predictive capability presently exists to identify, even in a general way, the operating conditions and engine configuration parameters which are conducive to the occurrence of combustion instabilities. Given the magnitude of the potential difficulties posed by the occurrence of combustion instability and the cost of including passive damping devices (e.g., baffles and liners), there has been intense periodic interest in furthering the current understanding of the combustion instability phenomena.

In place of a validated, mechanistically-based predictive analysis tool, rocket engine designers have been using empirically-derived guidelines to design injectors since the 1950's. These empiricisms have succeeded to varying degrees. The shear coaxial injector element using the LOX/H_2 propellant combination has been extensively studied, and acceptably performing and stable injector configurations can virtually be assured over the common range of operational conditions. Furthermore, the stabilizing effects introduced into the injector design have been observed to increase performance over the typical operational and design range. Thus, a more complete understanding of shear coaxial combustion processes, although highly desirable in principle, is less critical from a practical viewpoint.

For many missions, the use of either storable propellants or liquid hydrocarbons is mandatory or at least desirable. In these cases, impinging jet injector elements are used to ensure that adequate mixing of the liquid propellants can be achieved. It should also be noted that the impinging injector system has inherent advantages over the coaxial injector system in terms of its design simplicity which translates to lower costs for fabrication, inspection, and maintenance. For this reason impinging injectors are also a desirable system for gas/liquid propellants.

Unfortunately, the state of injector design for impinging injectors is not nearly as well developed as

it is for coaxial injectors. This is due in part to the many possible injector configurations (e.g., like-on-like doublets, triplets, etc.) which can be used; however, of greater significance is the lack of basic knowledge regarding the fundamental atomization mechanisms of impinging jets and their subsequent mixing and combustion processes. This lack of knowledge is exacerbated by the fact that, unlike the coaxial system, design and operational effects on stability and performance for impinging injectors typically act in opposite directions, i.e., improved performance is achieved usually through sacrificing high frequency stability margin, and vice versa. To take full advantage of the benefits of impinging injectors, it is essential that a fundamental understanding of their atomization mechanisms and their relationship to stability and performance be attained.

For a process to contribute to a combustion instability occurrence, the characteristic time for that process must generally match the characteristic response time of the combustion chamber. The use of a combustion response methodology to analyze rocket engine combustion instability has recently received widespread acceptance throughout the industry and may be regarded to represent the current state of the art in engineering practice. This methodology was the basis for a recent Air Force program[2] and has also been integrated into an interactive design analysis by NASA Lewis[3]. The essential elements of this approach consist of a chamber response, dependent on chamber geometry and gas properties, and a combustion response, dependent on combustion characteristics primarily determined by injector design, propellant type and operating conditions. The concept is shown qualitatively in Figure 1. The response functions are plotted as a function of frequency; in areas of overlap, an instability may grow in amplitude exponentially. Currently, injection and vaporization processes are accounted for in terms of a response function.

In order to assess the likelihood of particular operative mechanisms on combustion instability, a characteristic time analysis has been performed for two very different engines of interest to the Air Force: the XLR-132, a N_2O_4/MMH propellant-based engine being developed for upper stage applications; and the Advanced Launch System (ALS) engine, which uses the LOX/H_2 propellant combination. A summary of the analysis is given in Figure 2.

The XLR-132 nominal chamber pressure is 1500 psia and has a chamber diameter of about 2 inches. The ALS nominal chamber pressure is 2250 psia and has a chamber diameter of about 21 inches. The range of acoustic times shown in Figure 2 correspond to an "open loop" first tangential instability at the high end of the time scales (f_{1T}^{-1}), and a "closed loop" third tangential mode instability at the low end of the time scales ($2f_{3T}^{-1}$). Generally, it is believed that closed-loop processes are more common in high frequency combustion instability. The first through third tangential instabilities were considered because they are the most prevalent in high performance rocket engines today.

A review of Figure 2 can be used to discriminate between potential coupling mechanisms. For the XLR-132 case, kinetics, gas phase mixing, droplet response, drop and jet shattering, atomization and injection all have appropriate characteristic times. For the ALS case, similar potentially important phenomena emerge. One surprising observation is that droplet vaporization does not appear to couple effectively as a driving mechanism. This result is potentially misleading in that the calculation is based on a mean droplet size. However, the actual spray atomization process results in a distribution of droplet sizes. Thus, small droplets present in the distribution can still couple effectively. Additionally, large droplets, which have long characteristic times, are prime candidates for secondary atomization processes, which do possess characteristic times of the proper magnitude to drive combustion instabilities. Thus, the spray atomization process can indirectly represent a driving mechanism even for a large droplet sizes.

The above characteristic time analysis does not identify a single mechanism as potentially dominant for driving combustion instability. However, it does justify investigations for particular phenomena as potentially contributing to combustion instability and argues for a combustion response which can account for different processes as illustrated in Figure 3. Individual elements of the analysis need to be critically evaluated and focused experiments need to be performed for further understanding of this critical area.

A schematic of the impinging jet system, which is the topic for our studies, is shown in Figure 4. At typical rocket operating conditions, Reynolds numbers based on diameter are on the order of 10^5 to 10^6 and pressure drops are from about 5 to 30 atmospheres. There is an extreme lack of existing fundamental data for this system. Heidmann and Humphrey experimentally studied the atomization characteristics of a series of configurations operating in the high Reynolds number regime (10^5), varying impingement angle, orifice diameter, and injection velocity[4]. A very significant result, in the context of combustion instability, is that the atomization frequency, manifested in their experiments as waves of droplets, was on the order of several thousand Hertz, clearly putting it into the realm of typical tangential instability. The atomization frequency was found to be linearly dependent on injection velocity, with

minor dependence on impingement angle and orifice diameter.

The most fundamental study of turbulent impinging jets was performed by Dombrowski and Hooper[5], whose study extended to Reynolds numbers of 12000. Their major conclusions were that, above a critical liquid Weber number of about 150, the primary mechanism of spray generation was related to the formation of hydrodynamic impact waves at the point of impingement; these waves then caused the liquid sheet to disintegrate into bands of droplets, similar to Heidmann and Humphrey's observations. At lower than critical Weber numbers, aerodynamically-induced waves were the predominant breakup mechanism. Finally, the mechanism of disintegration and the resultant drop size were principally dependent upon the velocity profiles across the jet, and their angles of impingement. This must be regarded as the present state of our knowledge of impinging jet injector system.

To understand the physical processes which control the stability characteristics of the impinging jet injector system more completely, a research program has recently been started at the Propulsion Engineering Research Center at Penn State University in collaboration with Aerojet Propulsion Division. The research program is primarily experimental, but also contains a theoretical element to develop an atomization model for the impinging jet system.

The experiments emphasize laser-based techniques to obtain quantitative determinations of the temporal and spatial characteristics of the spray formed by the impinging jets under "stable" and "unstable" conditions. Conditions for characterizing the regimes of stable and unstable operation are based on actual engine development experience and represent a key link between these studies and practical engine design implementation. The like-on-like impinging jet system with realistic geometries and operating conditions will be the focus of the study. An empirically-derived stability parameter for these injectors will be used to define the stable or unstable test condition. The temporal measurements are aimed at determining how changes in the stability parameter affect the dominant frequency characterizing a specific process while the spatial measurements will investigate how spatial location aspects of the processes are affected by the variation of the stability parameter. Contrasting the behavior of the stable and unstable conditions will provide a means for establishing which processes play a role. An externally-forced oscillation will be imposed on the system and amplification and decay mechanisms will be investigated. The analytical portion of the study will focus on effects in the orifice region, which have been badly neglected in most if not all the previous atomization work, on development of a model for impact waves if proof of their presence is found, and on a critical review of current atomization modeling approaches. Finally, the results of these studies will form the basis for incorporating new methodologies into injector design procedures to provide low-cost, stable and high performance impinging injector elements.

REFERENCES:

1. Harrje, D.T. and Reardon, F.H., Liquid Propellant Rocket Combustion Instability, NASA SP-194, 1972.

2. Muss, J.M. and Pieper, J.L., "Performance and Stability Characteristics of Lox/Hydrocarbon Injectors", AIAA-88-3133, AIAA/ASME/SAE Twenty-fourth Joint Propulsion Conference, Boston, MA, July 1988.

3. Klem, M., Pieper, J.L. and Walker, R.E., "Combustor Design Analysis Using the Rocket Combustor Design (ROCCID) Methodology", AIAA-90-2240, Twenty-sixth Joint Propulsion Conference, Orlando, FL, July 1990.

4. Heidmann, M.F. and Humphrey, J.C., "Fluctuations in a Spray Formed by Two Impinging Jets", NASA TN2349, 1951.

5. Dombrowski, N. and Hooper, P.C., "A Study of Spray Formation by Impinging Jets in Laminar and Turbulent Flow", J. of Fluid Mech., 18, 3, 1963.

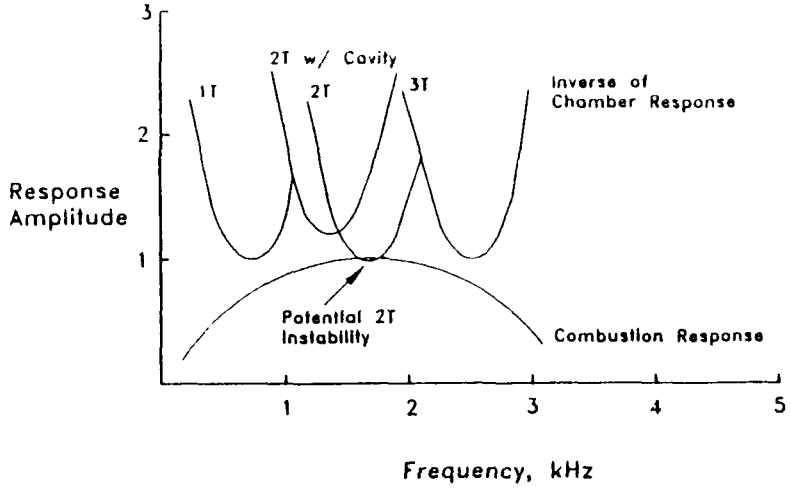

Figure 1. *Illustration of Combustion Stability Response Analysis*

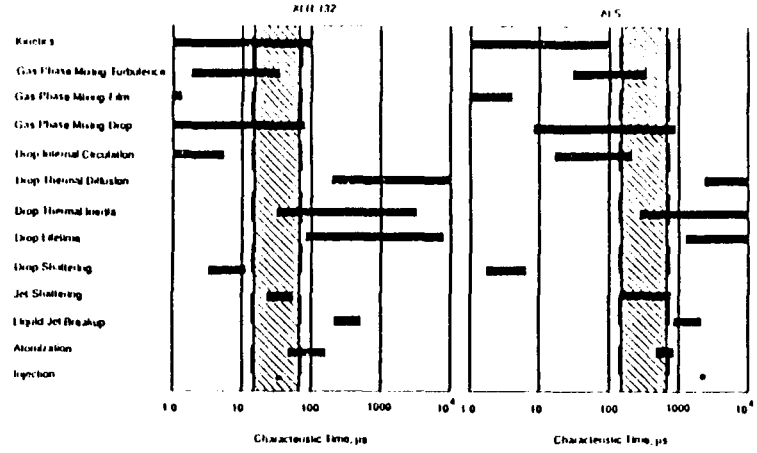

Figure 2: Comparison of Characteristic Times for XLR-132 and ALS engines. Shaded area represents range of pertinent acoustic timescale.

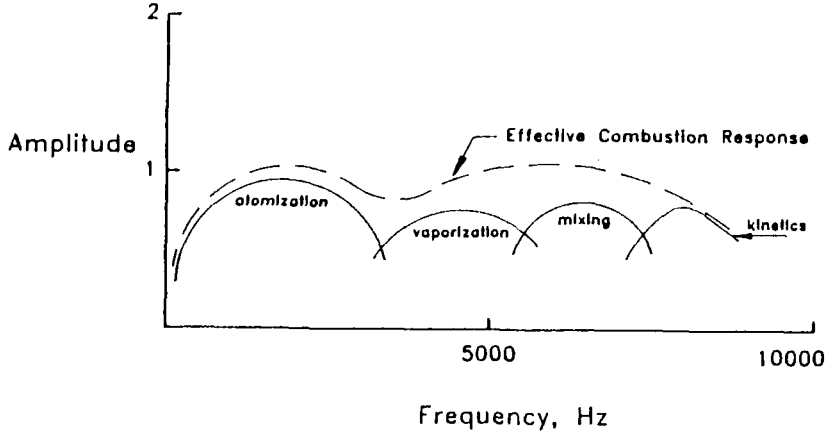

Figure 3. Multi Component Combustion Response

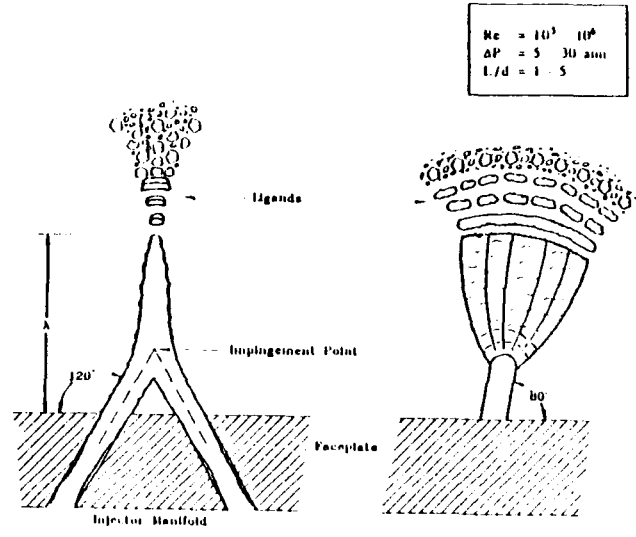

Figure 4: Schematic of Liquid Propellant Spray Formation from Impinging Liquid Jets

FUNDAMENTAL STUDIES OF DROPLET INTERACTIONS IN DENSE SPRAYS

AFOSR Grant/Contract No. 90-0064

PRINCIPAL INVESTIGATOR:

W.A. Sirignano

Department of Mechanical and Aerospace Engineering
University of California
Irvine, CA 92717

SUMMARY/OVERVIEW:

The research addresses interaction amongst droplets in a dense spray via a fluid dynamical computational approach. Flow fields, transport details and droplet lift, drag, torque, trajectories, and vaporization rates are determined. Three major tasks are included. Three dimensional interactions of droplets moving side-by-side are examined. In another task recently completed, three fuel droplets moving in tandem are studied by axisymmetric calculations. In the third task, liquid oxygen droplets are studied including axisymmetric interactions with another fuel or oxygen droplets.

AUTHORS

C.H. Chiang
S.E. Elghobashi
I. Kim
W.A. Sirignano

TECHNICAL DISCUSSION

1. Three-Dimensional Interactions of Droplets

A numerical simulation of three-dimensional fluid-dynamic interactions between two spheres has been performed to obtain basic information concerning the two phase flow in dense sprays. Calculations for the interaction of two solid spheres held fixed in the transverse direction against the uniform stream were first performed for the nondimensional spacing distance (the distance between two spheres normalized by the sphere diameter) $1.5 \leq d_o \leq 25$ at Reynolds numbers 50, 100, and 150. The two spheres repel each other strongly through lift forces when they are close and attract weakly each other at intermediate separation distances as shown in Figure 1. Eventually, the lift vanishes when $do \geq 21$. The two droplets experience positive torque when near and negative torque at intermediate distances as shown in Figure 2. Eventually, the torque vanishes when $d_o \geq 21$. Note that the torque acting on the spheres is relatively small and less than 1% of the drag coefficient. The drag also becomes larger when the distance becomes shorter than 4. It slightly increases in the intermediate region, but eventually converges to that of a single sphere when $d_o > 21$ as shown in Figure 2.

Calculations for the interaction of two spherical droplets were also performed for the nondimensional spacing distance $1.5 \leq d_o \leq 25$ and the viscosity ratio 25 and the density ratio 300 (interior

to exterior) at Reynolds number 50, 100, and 150. The overall physical phenomena in the gas phase of the droplets are quite similar to those of the solid spheres due to the high viscosity ratio. The gas phase velocity vectors indicate a deviation from an axisymmetric flow in the liquid phase is small due to the weak torque but observed clearly near the front and rear stagnation points. Since the calculations for the interactions of two fixed droplets were done, we have been extending the code for the interactions of two moving droplets in a stationary fluid medium, where the droplets experience change in their directions as well as retardation due to the drag and lift forces.

2. Axisymmetric Calculations of Three-Droplet Interactions

This research addresses the interaction of three vaporizing droplets moving collinearly which represents a model of an injected stream of fuel droplets. The purposes of this study are to study the wake effect of the lead droplet on the downstream droplets and to examine the effects of initial spacing on the total system.

The effects of variable thermophysical properties, transient heating and internal circulation of liquid, deceleration of the flow due to the drag of the droplet, boundary-layer blowing, and moving interface due to surface regression as well as relative droplet motion are included. The results are compared with those of an isolated droplet [1] as well as those of the two-droplet system [2] to investigate the effect of the presence of the third droplet. The interaction effects from the downstream or upstream droplet are identified. Then the behavior of trailing droplets, which follow the first two or three droplets, can be estimated from that of the first two or three droplets on account of the periodical nature of linear droplet arrangements.

Here, we illustrate the variations of trajectory with time and drag coefficients vs. instantaneous Reynolds number for the cases of different initial spacings in Figure 1. Results of Case 1 with large initial spacing (D12=D23=12) indicate that the drag coefficient is smaller for the second droplet than for the lead droplet and still smaller for the third droplet. The drag coefficient of each droplet is reduced from the isolated droplet value. The major decrease in drag occurs in the first two droplets. In Case 2, the drag coefficients of the lead and the second droplets are significantly reduced (comparing curves 7 and 10, and 8 and 11, respectively) due to the strong interactions when the first two droplets are spaced only two diameters away. Similar trends occur for the downstream droplet pairs of Case 3 (comparing curves 8 and 14,and 9 and 15, respectively). The third droplet in Case 2 has a higher drag coefficient than that of the second droplet since the second droplet is better shielded by the droplet before it. The D23 thus increases with time. Also, note that the drag coefficient of the third droplet, which is spaced far away from the second droplet, seems to be independent of D12 as indicated in curves 9 and 12. However, it strongly depends upon D23 as illustrated in curves 9, 12 and 15.

Results for the cases of sufficiently large spacing (above approximately 6 droplet diameters) show that the flow field of each droplet is qualitatively similar to that of an isolated droplet, although the transport rates are reduced along the downstream direction due to the cascade effect of the wake. The major drops in transport rates occur in the first two droplets. For the cases of small droplet spacings (less than approximately 3 droplet diameters), the flow field of downstream droplets can be significantly altered due to the interaction effects from the upstream droplets. Usually, the second droplet has the lowest drag coefficient since it receives interactions from both neighboring droplets. However, the difference in transport rates between the second and the third droplets is not significant since both droplets are fully protected by the wake of the first droplet. The effect of D23 on the behavior of the first droplet is insignificant. However, depending upon the values of D12 as well as D23, the effect of D23 on the behavior of the second droplet may become significant. The general qualitative conclusions drawn from the two-droplet study [2] can be applied to two neighboring droplets in the three-droplet analysis. The correlations for heat transfer and droplet

dynamics have been developed and are applicable in a one-dimensional droplet spray calculation. More details are available in [3].

3. Interacting LOX-fuel droplets research

The first stage of this project involves an axisymmetric analysis of a cold LOX droplet suddenly introduced into the hot methane fuel-vapor stream. The effects of variable thermophysical properties, real gas behavior, transient heating and internal circulation of liquid, deceleration of the flow due to the drag of the droplet, boundary-layer blowing, and moving interface are included. A primitive-variable formulation with an implicit finite-difference scheme has been developed to solve the complete set of Navier-Stokes, energy, and species equations. The results are presented for the low pressure case. The interesting phenomena due to the large surface blowing and surface boiling are examined.

We have learned in all calculations that the LOX droplet surface very quickly reaches the boiling temperature, which is about 120 k for the case of 10 atms ambient pressure. However, the droplet core remains cold since the conductivity is low and, at the early time, the circulation strength is not strong enough to convect much energy. All the available heat transfer from the gas phase is used to heat the surface and also utilized for the latent heat of vaporization. The surface boiling persists throughout the droplet lifetime. The very rich and cold oxygen vapor surrounding the droplet is depicted in Figure 4. The large gradient occurs at the front stagnant region as we expect. The LOX droplet would require much of energy for the heat of vaporization rather versus the heating the internal fluid. As a result, the transient droplet heating is responsible for the unsteady thermal behavior of the LOX droplet. The high surface blowing velocity has a significant effect on the flow structure and modifies the flow separation angle and wake length, etc. The drag coefficient, Nusselt and Sherwood numbers are reduced to below their corresponding stagnant values [4].

The interactive computation in the next stage will be concentrated on three basic configurations: (1) a LOX droplet following in the wake of another LOX droplet, (2) a LOX droplet following in the wake of a fuel droplet, and (3) a fuel droplet moving in the wake of a LOX droplet. Fuels are selected to be hydrocarbons and alcohols. The results of vaporization rates, gas-phase composition, gas-phase mixing rates, drag coefficients, Nusselt numbers and Sherwood numbers are to be reported. The dependencies of the above quantities upon the droplet Reynolds numbers, droplet spacings, and transfer numbers will be determined.

References

[1] C. H. Chiang, M. S. Raju and W. A. Sirignano, *AIAA Aerospace Sciences Meeting*, Paper 89-0834. (1989). Also to appear in *Int. J. Heat Mass Transfer* (1991).

[2] C. H. Chiang and W. A. Sirignano, *AIAA Aerospace Sciences Meeting*, Paper 90-0357 (1990). Also submitted to *Int. J. Heat Mass Transfer.*

[3] C. H. Chiang and W. A. Sirignano, paper accepted for presentation at the Fifth International Conference on Liquid Atomization and Spray Systems, Gaithersburg, MD U.S.A., July 15-18, 1991.

[4] C. H. Chiang and W. A. Sirignano, AIAA Aerospace Sciences Meeting, Paper AIAA-91-0281, (1991).

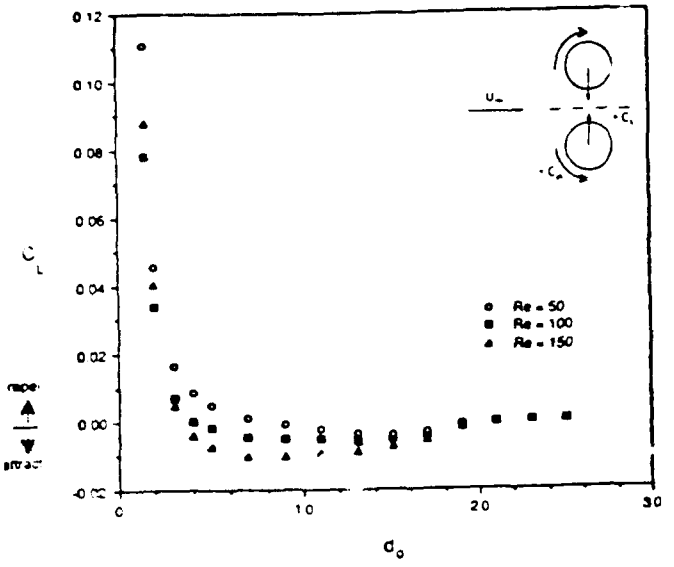

Figure 1. Lift coefficients as a function of distance for solid sphere at Re=50, 100, and 150.

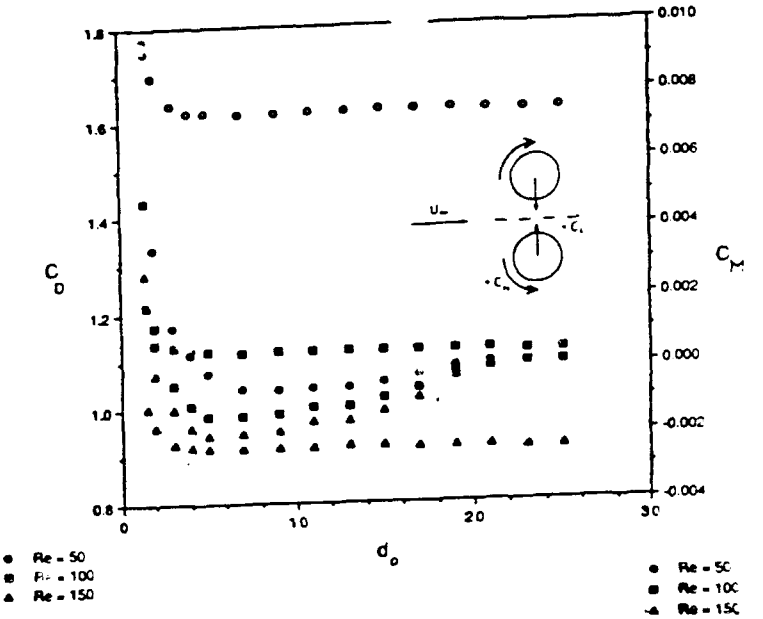

Figure 2. Drag and moment coefficients as a function of distance for solid sphere at Re=50, 100, and 150.

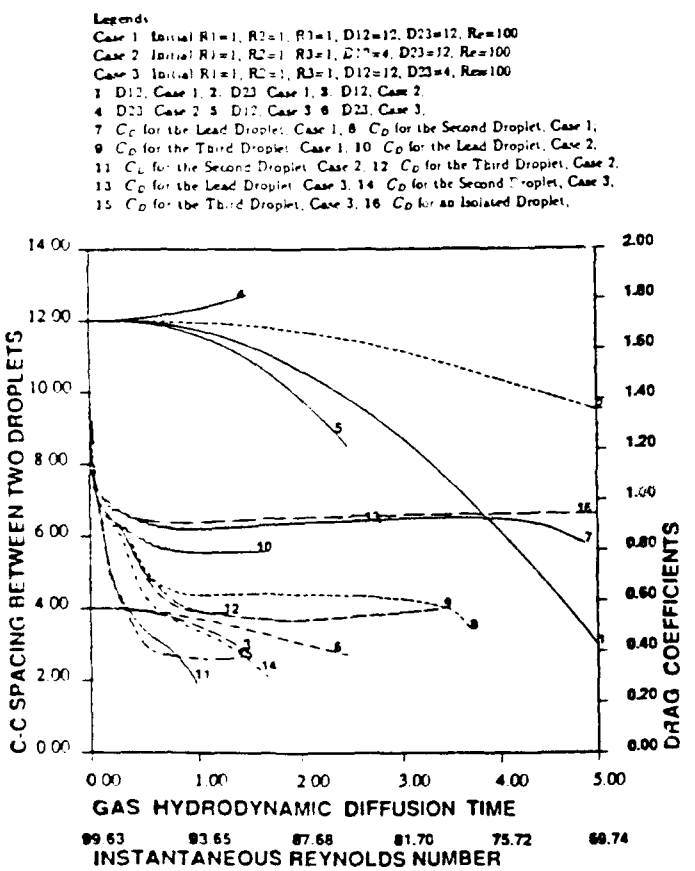

Figure 3. Time variation of droplet drag coefficients and droplet spacings for the cases of large initial droplet spacings. (Cases 1, 2 and 3)

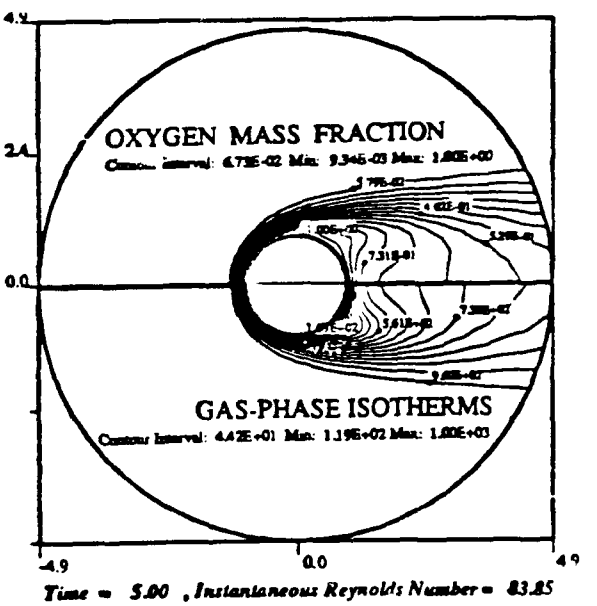

Figure 4. Oxygen mass-fraction contours and isotherms.

INVESTIGATION OF FLAME DRIVING AND FLOW TURNING IN AXIAL SOLID ROCKET INSTABILITIES

(AFOSR Grant/Contract No. AFOSR-84-0082)

Principle Investigators: B. T. Zinn, B. R. Daniel, and U. G. Hedge

School of Aerospace Engineering
Georgia Institute of Technology
Atlanta, GA 30332

Summary/Overview:

This research program investigates the driving and damping of axial instabilities in solid propellant rocket motors by gas phase solid propellant flames and 'flow turning', respectively. The response of premixed and diffusion flames, stabilized on the side wall of a duct, to imposed axial acoustic waves has been investigated earlier under this program. The focus of the present investigation is the development of a greater understanding of the damping of combustion instabilities due to 'flow turning'. Initial attempts, based upon a state-of-the-art theoretical approach, to measure the flow turning loss failed to show any measurable effect. An ensuing theoretical investigation of this problem revealed that the original experimental procedure may have neglected terms of the order of the local 'flow turning' loss, therefore giving erroneous results. This theoretical investigation developed a model which is in some respects more general than the previous approach and is developed in terms better suited to experimental verification. This model is currently being used to guide the development of a new experimental approach which will account for all relevant terms in the measurement of the 'flow turning' loss. This experimental investigation will determine the contribution of the 'flow turning' loss to the stability of solid propellant rocket motors.

Technical Discussion:

The elimination or reduction of the occurrence of combustion instabilities in solid propellant rocket motors requires that the processes which add or remove energy from the waves be accounted for in a stability analysis. An understanding of the mechanisms which control these processes must then be developed. It is generally accepted that the energy required to initiate and maintain the acoustic instability is supplied by the combustion process, and significant insights into the flame driving mechanisms have been developed in previous phases of this program. It is also generally accepted that nozzle damping, viscous dissipation, heat transfer, and 'flow turning' are processes which remove energy from the acoustic field. The

current phase of this program is concerned with understanding and quantification of the damping provided by the 'flow turning' process.

In an initial experimental investigation of the 'flow turning' loss under this program the classical acoustic energy flux, Real (p'u'), was measured and integrated over the surface of a control volume. Since no other sources or sinks of acoustic energy were present within the investigated control volume, any measured net loss of acoustic energy would represent the flow turning loss. This procedure was unable to measure any acoustic energy loss larger than experimental errors. This stimulated an analytic investigation to explain the result. A one-dimensional acoustic stability equation was developed from an energy balance approach, similar to that used by Cantrell and Hart. The analysis was based on explicit considerations of mass, momentum, and acoustic energy fluxes at the control volume boundaries. It involved considerations of the first and second order perturbations of the acoustic quantities. The consideration of second order quantities is necessary for proper evaluation of terms of the order of the acoustic energy. Basically, the energy equation was expanded to second order in acoustic perturbations and the perturbed forms of the mass and momentum conservation equations were used to modify the energy equation. An expression for the acoustic growth rate α was derived which by careful manipulation was shown to be independent of any terms involving second order perturbations. The resulting stability equation is similar in form to Culick's result.

In order to provide a model suited to experimental investigation, the analysis was then redone by expanding properties in terms of time averaged and time varying quantities, as opposed to expanding in powers of acoustic perturbations as done before. The form and nature of the result was basically unchanged. However, the new model is readily amenable to experimental investigation. This result is valid for a constant height control volume with constant mean density ρ_o, no residual burning, and no particles. The developed stability equation contains terms that were not accounted for in previous treatments. It is more general than previous treatments in the sense that the acoustic oscillation need not be a natural acoustic mode of the duct, which allows forced oscillations to be studied.

A new experimental procedure is being developed using the information gained in the analytical study. The flow turning term has been identified in the one-dimensional acoustic stability equation discussed above as

$$\text{Flow Turning Loss} = < \int_0^L \frac{u'^2}{H} [m_{bo}]_0^H \, dx > \qquad (1)$$

This will allow the flow turning loss term to be measured directly, instead of the indirect approach utilized earlier under this program. The other terms of the one-dimensional acoustic stability equation will also be measured to provide a check for both the flow turning loss and stability equation itself.

The developed experimental setup (see Fig. 1) consists of a 2.5 meter long, 3.75 x 7.5 cm^2 duct with the multi-diffusion flame burner (MDFB) shown in Fig.2 installed on the bottom wall. Though initial experiments will be performed using cold flow, the MDFB can be used to simulate the behavior of a gas phase solid propellant flame. The MDFB consists of 1537 hypodermic tubes arranged in a 29 x 53 matrix. During hot flow experiments, oxidizer flow is supplied through the hypodermic tubes, simulating the flow of combustion products from burning oxidizer particles (e.g., ammonium perchlorate) in a composite solid propellant, and the fuel is supplied through the spaces between the hypodermic tubes, simulating the flow of pyrolysis products from the fuel binder. In cold flow experiments, room temperature air is supplied through both the tubes and the surrounding spaces. Two acoustic drivers attached to opposing duct walls just upstream of the exit plane are used to excite a standing longitudinal acoustic wave in the duct, simulating an axial instability in an unstable rocket motor. Flow is injected at the upstream end of the duct to simulate the core flow in a rocket motor. This head end injector is made of a porous plate that behaves as an acoustically 'hard' termination. The location of the MDFB relative to the acoustic field can be changed by axial translation of the porous plate. Pressure transducers mounted on the wall above the MDFB are used to characterize the excited acoustic field and the location of the flow turning region with respect to the standing wave.

In order to evaluate the terms of the one-dimensional acoustic stability equation, detailed velocity and pressure measurements will be performed in the flow turning region of the system. Mean and fluctuating velocities in both the axial and transverse directions will be measured simultaneously using a 5-watt Coherent argon-ion laser and a TSI 9100-7 dual beam forward scatter LDV system. Acoustic pressures will be measured with a piezoelectric pressure transducer attached to a probe. Measurements will be obtained for a range of operating conditions by varying the mass injection rate, the frequency and amplitude of the acoustic oscillations, the core flow velocity, and the location of the side injection with respect to the standing wave.

The measured data will be used to determine the magnitude of the flow turning loss in a control volume by direct computation of the flow turning term shown in Eq. 1. The remaining terms of the acoustic stability equation will be found similarly. Comparison of these results should provide a check of the validity of the one-dimensional acoustic stability equation derived under this program, as well as determine the magnitude of the flow turning loss.

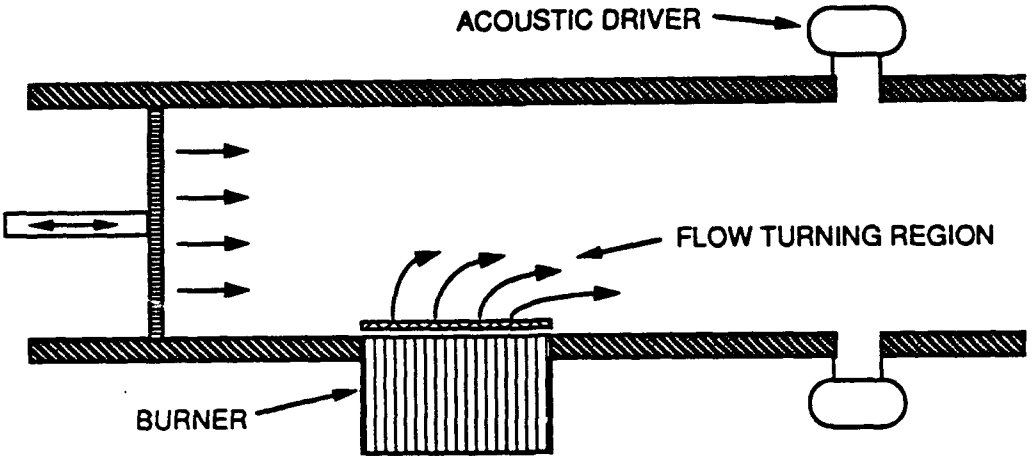

Figure 1. A schematic of the experimental setup.

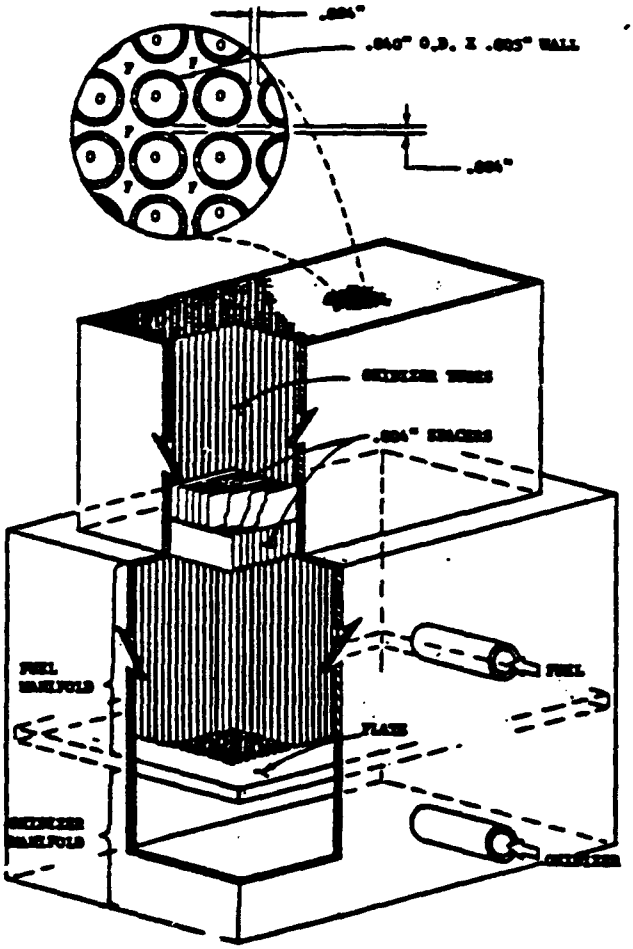

Figure 2. Schematic of the developed multi-diffusion flame burner.

MODELING OF ACOUSTIC PHENOMENA IN SOLID ROCKET ENGINES

(AFOSR Grant No. 89-0023)

Principal Investigator: **David.R. Kassoy**

Mechanical Engineering Department
Center for Combustion Research
University of Colorado
Boulder, CO 80309-0427

SUMMARY:

Predictive capability for the response of a solid propellant combustion chamber mean flow to acoustic disturbances generated by burning rate transients can improve system safety and performance. Systematically developed mathematical models are employed to study the interaction between a specified mean flow in a semi-confined geometry (the chamber) and acoustic disturbances arising from explicitly defined conditions on the chamber walls. In contrast to modeling based on stability theory, our results predict the initiation and evolution of linear and nonlinear acoustic waves arising directly from boundary forcing, refractive interactions that cause the appearance of oblique propagating modes, as well as the influence of axial, transverse and oblique wave reflections within the chamber geometry. Analytically based studies demonstrate that chamber pressure response at any specific location can be surprisingly irregular due to the simultaneous passage of axial, transverse and oblique traveling waves as well as the transient bulk response of the chamber gas. These waves can induce undesirable mechanical stresses in the chamber structure, excess heat transfer to the propellant surface, as well as unpredictable propellant combustion, particularly if the waves nonlinearize into weak shocks that create relatively large pressure transients during boundary reflection. Results of this type suggest that engine stability and design codes should have the capability of analyzing nodal point data so that traveling acoustic/shock wave propagation can be identified explicitly!

AUTHORS: **D.R. Kassoy and Meng Wang**

TECHNICAL DISCUSSION

1. Small Amplitude Travelling Wave Evolution in a Shear Flow

A systematic analysis has been performed to discover the effect of a low Mach number (M) shear flow on acoustic wave propagation in a planar duct. We study the response of a steady shear flow to acoustic disturbances arising from velocity disturbances imposed at a given duct cross-section. The mathematical analysis is carried out when the characteristic shear flow Mach number $M \approx 0.1$, and the wavelength of the fundamental acoustic mode is comparable in magnitude with the duct width.

Two types of velocity disturbances, i.e., $O(M^2)$ and $O(M)$, relative to the $O(M)$ mean flow velocity, are considered. Our initial effort has been focused on the smaller $O(M^2)$ disturbance

type corresponding to acoustic pressure variations that are 1% of the mean flow pressure. This is characteristic of pressure transients observed in well-behaved solid rocket engines. In this case the nonlinear convective terms affect the pressure at the level of 10^{-2}% while the acoustic-shear flow interaction (refraction) processes have a 0.1% influence.

Solutions are developed in terms of Fourier series summations, which provide a unified description of both short-time acoustic transients and the quasi-steady wave field long after the passage of the acoustic wavefront. Refraction arising from the shear flow velocity gradient causes the $O(M^3)$ planar acoustic pressure wave to have transverse structure. In addition, dispersive acoustic transients of the same size are generated that evolve into a number of quasi-steady, propagating oblique modes and an infinite number of non-propagating modes that die out rapidly away from the plane acoustic source. The number of propagating modes increases with the driving acoustic frequency, and affects the $O(M^3)$ acoustic pressure in a drastic way (cf. Fig. 1). Non-resonant solutions are valid for extended time periods. Resonance occurs in a single refractive acoustic mode when the duct width is an integer multiple of the the driving acoustic wavelength, in which case the refraction effect is greatly enhanced. The solutions are correct for a disturbance function period. At low frequency, when the driving acoustic wavelength is greater than the duct width, the only propagating mode is planar, and the solution agrees with the classical planar wave solution [1].

Viscous acoustic boundary layers are shown to affect less than 1% of the duct width. A smooth transition of the acoustically induced velocity to the no-slip condition occurs in this narrow zone. The horizontal velocity component for each acoustic mode exhibits Richardson's annular effect.

More details of this work have been reported in [2].

2. Small Amplitude Standing Wave Evolution in a Shear Flow

A related study involving standing wave interaction with a low Mach number shear flow has been conducted and reported in [3]. The model problem deals with the evolution of an initially imposed standing wave disturbance (1% of the mean flow pressure) trapped in a rectangular cavity bounded by impermeable duct walls parallel to the flow direction and special perpendicular acoustic reflectors that permit the passage of the mean flow. This idealized model problem allows us to study the effect of multiple wave reflections during the acoustic-mean flow interaction process, which is crucial in practical rocket configurations.

Fourier-based solutions show that the imposed purely longitudinal acoustic field is altered by about 10% as a result of convective and refractive corrections. The bulk convection of the fluid is responsible for periodic, longitudinal wave form deformations. Additionally, transverse and oblique standing acoustic waves as well as forced bulk oscillations arise from the refraction of the longitudinal acoustic wave by the mean flow velocity gradient. A particularly interesting finding of this study is that a linear combination of the various refraction generated acoustic modes can give rise to irregular pressure signals at a given location (see Fig. 2).

3. Wave Nonlinearization and Weak Shock Formation

The traveling and standing wave studies discussed above involve relatively small acoustic amplitudes, so that the waves remain linear on the time and length scales that are of importance in solid rocket combustion chambers. When the imposed pressure disturbance is 10% of the mean pressure, then the corresponding velocity disturbance and the mean flow value are both $O(M)$, a condition which can be encountered in rocket engines experiencing acoustic instability. Nonlinear accumulation effects become prominent when the wave travels a few acoustic wavelengths. This can be of practical interest to slender solid rocket motors.

A multiple-scale analysis is being performed to study the formation and propagation of weak shocks in the shear flow field following the wave nonlinearization process. Results to date show that the nonlinear deformation of the leading order planar traveling wave is unaffacted by the mean shear flow field, except for a slightly modified propagation speed due to bulk convection. However, the physical characteristics of the refractive acoustic pressure (1% of the mean pressure) depend strongly upon the leading order wave shape, and are thus affected in a fundamental way by the wave steepening into a weak shock. This work is currently in progress.

4. Acoustic Processes in an Inviscid Rotational Flow

The basic flow field in a solid rocket engine chamber is induced by gaseous products of propellant burning. The combustion zone gases are thought to move normal to the propellant surface. However, chamber confinement causes the gas velocity to turn toward the axial direction, flow downstream and exit through the nozzle. Acoustic phenomena in the induced chamber flow are thought to arise from burning transients on the propellant surface.

An elementary model of chamber acoustics driven by burning rate transients is constructed in terms of controlled mass addition from the sidewall boundary of a long, relatively narrow duct closed at one end. Steady mass addition with an injection Mach number $M = O(0.01)$, induces an axial value $M = O(0.1)$. An analytical solution can be obtained to the low Mach number inviscid, rotational describing equations. The solution satisfies the no-slip boundary condition for arbitrary distributions of boundary mass addition.

Acoustic disturbances to the steady induced chamber flow are generated by specifying a spatial distribution of transient mass addition of a magnitude equal to that of the original steady value. The injection transient induces an acoustic pressure response which is about 10% of the mean pressure value and a factor of ten larger than the pressure field associated with the steady state flow field. The short time acoustic response (relative to the axial acoustic time scale) is a transverse wave of variable axial strength propagating away from the injection surface. After multiple wave reflections from the lateral surfaces, an axial pressure gradient is set up which relaxes into axial and oblique traveling acoustic waves and a bulk mode response. If the boundary transient is oscillatory, the latter is characterized by the forcing frequency. There is a critical resonance in the induced axial mode for a specific low frequency, and for explicitly defined higher frequencies each of the oblique modes resonate. Sufficiently high frequency resonance is associated with oblique modes that are nearly transverse. These waves can be a source of instablity that is trapped in the chamber because their propagation speed in the axial direction is very small relative to the speed of sound.

Consider the example for a duct of length $L = 100cm$, width $D = 20cm$, and an axial acoustic time $t_a = 2 \times 10^{-3}s$. We find that the axial mode resonates at $125Hz$, while the first oblique mode is resonant at $160Hz$. The tenth oblique mode resonates at $1000Hz$.

This study, based on linear acoustic theory in a semi-confined geometry, is quite independent of the shear flow associated with the steady inviscid rotational solution. Previously described results imply that refraction effects arising at a higher order will be the source of even more wave complexity in terms of generating another set of transverse, axial and oblique traveling waves. The analysis shows clearly how sidewall boundary transients can be the source of axial and oblique traveling waves in a model of a rocket chamber. The resonant solutions suggest a specific cause-effect relationship between explicitly defined boundary disturbances and unstable acoustical behavior in the chamber, a result that cannot be obtained from a stability analysis of the inviscid rotational solution.

Solutions valid on time scales longer than t_a must be found for resonant cases in order to

examine the gradual nonlinearization of reflected wave fronts and the appearance of weak shocks in the chamber.

REFERENCES

[1] D.C. Pridmore-Brown, "Sound propagation in a fluid flowing through an attenuating duct", *J. Fluid Mech.*, 4, 393–406, (1958).

[2] M. Wang and D.R. Kassoy, "Transient acoustic processes in a low mach number shear flow", submitted to *J. Fluid Mech.*, (1990).

[3] M. Wang and D.R. Kassoy, "Standing acoustic waves in a low Mach number shear flow", submitted to *AIAA Journal*, (1991).

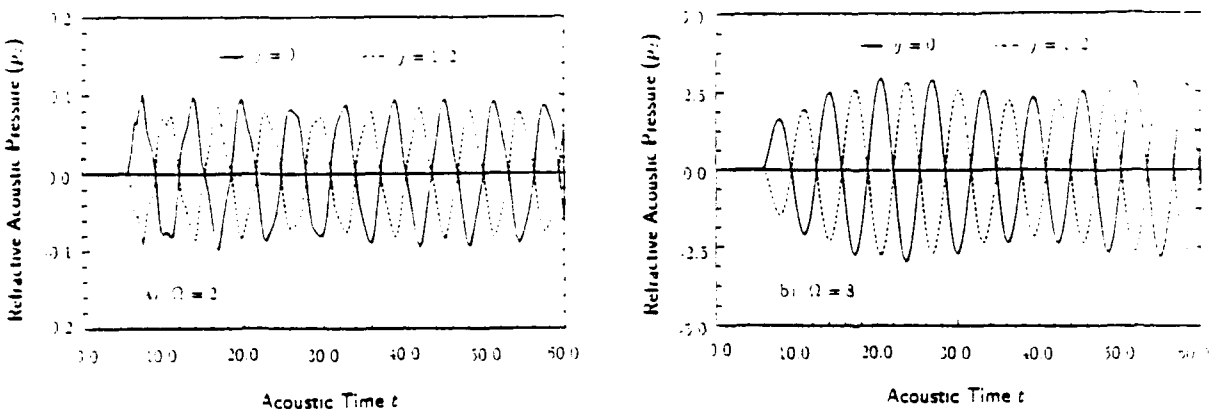

Figure 1: Time variations of the second order acoustic pressure due to refraction on the duct wall ($y = 0$) and center-plane ($y = 1/2$) one wavelength downstream the disturbance source. The acoustic waves are generated by a specified velocity perturbation $\hat{u}(x = 0) = \sin(t)$ in the shear flow field $U = 4y(1 - y)$. The maximum mean flow Mach number $M = 0.1$. Case (a) Only the planar mode is present (dimensionless frequency $\Omega = 2$); case (b) the planar mode and the second oblique mode are present ($\Omega = 8$).

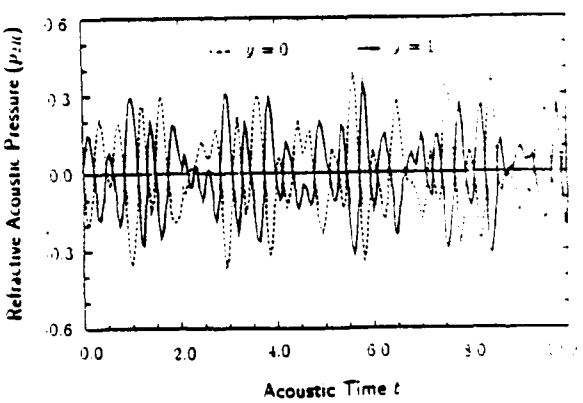

Figure 2: Irregular acoustic pressure signals due to refraction on the center-plane ($y = 0$) and duct-wall ($y = 1$), next to an acoustic reflector ($x = 0$). The refraction effects are generated as the initial acoustic disturbance $\hat{u}(t = 0) = \sin(2\pi x)$ relaxes in the shear flow described by $U = 1 - y^2$. The duct length to width ratio = 2.

CHEMICAL PHENOMENA AT BURNING SURFACES DETERMINED BY EXPERIMENTAL SIMULATIONS

AFOSR-89-0521

Principal Investigator: Thomas B. Brill

Department of Chemistry
University of Delaware
Newark, DE 19716

SUMMARY/OVERVIEW:

A chemical and physical description of the surface reaction zone during propellant burning is essential to any advanced model of combustion. Because chemical details have not been obtainable during actual combustion, two simulation experiments have been developed to determine the kinetics and mechanisms. The burn rate is predicted by the measured kinetics. The observed gas products, therefore, very probably initiate the first stage of the flame zone.

TECHNICAL DISCUSSION

New high energy rocket propellants formulated without metal fuels present an enormous challenge to the rocket propulsion community. Instability, safe ignitability, and tailorability are all potential problems that have to be surmounted. Modeling will play a major role in guiding development because of the expense of large scale testing.

The ultimate goal of modeling combustion and combustion stability of rocket propellants requires, among other inputs, a chemical and physical description of the reacting surface at the microscale level. Such detail has not been forthcoming from direct measurements during combustion. This is because the surface is transient, heterogeneous, non-equilibrium and is obscured by the flame. Therefore, it is necessary to design experiments that simulate the condensed phase and surface during combustion, but release the gases into a cool unreactive atmosphere where they are quenched and detected immediately.

The burning surface can be imagined to be a film of material 20-100μM thick in which a phase change occurs driven by chemical reactions and heat transfer. In effect, it is a "thin-film" reaction zone that regresses through the condensed phase on one side leaving gas products behind on the other side. Therefore, an instantaneous simulation of this reaction zone would be a thin film of sample experiencing a heating rate in the 100-2000°C/sec range at a pressure of atmospheric or higher. The choice of the heating rate of 100-2000°C/sec is based on recent work of Sakamoto and Kubota with thermocouples imbedded in HMX propellants. Their measurements indicate that dT/dt in the condensed phase (foam) reaction zone is 1000±500°C/sec.

Two approaches to the reaction zone simulation have been developed: Fast-Heat-and-Hold/FTIR Spectroscopy (also called T-jump/FTIR) and Simultaneous Mass and Temperature Change/FTIR Spectroscopy (SMATCH/FTIR). Measurement of both high rate kinetics and the gas products released is important because it needs to be demonstrated that the kinetics predict the burn rate in order to have confidence that the gas products observed are the ones that feed the dark zone of the combustion region.

The Fast-Heat-and-Hold/FTIR method is designed to permit heating of a sample at 2000°C/sec to a preselected final temperature. In this way, most of the interfering chemical processes that are operative in decomposition studies at slow heating rates and that result from "cooking" are minimized. Figure 1 shows a diagram of the method. The thermal response trace of the sample is obtained from the control voltage of the circuit that maintains constant resistance of the Pt ribbon filament. The gas products are evolved into a cool argon atmosphere where they quench and are identified and quantified by absorbance of the IR beam of a rapid-scan FTIR spectrometer. Figure 2 shows the composite of these data for HMX heated at 2000°C/sec to 300°C. The ignition exotherm is the sharp negative spike in the control voltage.

The fact that gas products are detected in advance of the exotherm is strong evidence that autocatalysis is operative in HMX. The fact that NO_2 and N_2O appear in advance of the fuels (CH_2O and HCN) indicates that these fuel and oxidizer-producing reactions are not coupled. That is, NO_2 and HCN are not produced in the same elementary reaction and N_2O and CH_2O are not produced in the same elementary reaction. Instead, N_2O and NO_2 are released and CH_2O and HCN are then produced in later stage degradation of the residue. The fact that the gas product concentrations are not changing through the exotherm implies that the mechanism of decomposition before the exotherm and during the exotherm is essentially the same throughout. More of the HMX is simply decomposing.

The most useful new data from this experiment so far are gas product ratios as a function of temperature. The N_2O/NO_2 ratio shown in Figure 3 reflects the ratio of rate constants for the two global decomposition paths of HMX: the $N_2O + CH_2O$ branch and the NO_2 + HCN branch. At lower temperature the $N_2O + CH_2O$ branch dominates, while at higher temperature the NO_2 + HCN branch dominates. Temperatures in the range of 350°C are believed to exist on the surface of burning HMX propellants. Thus, Figure 3 gives the ratio of the rate constants for the two "feeder" reactions that should be used as inputs in models of the gas phase during the ignition of HMX.

The SMATCH/FTIR technique enables the dynamic weight change of the sample to be recorded as a function of time and temperature as the sample is rapidly heated. From this, a kinetics simulation of the burning surface is obtained. Simultaneously, the near surface gas products are recorded by rapid-scan FTIR spectroscopy.

Recently, it has been found that the Arrhenius constants from SMATCH/FTIR studies of thin films accurately predict the burn rate ($\dot{r}$) measured in the same pressure and temperature range. Figure 4 shows the simultaneously acquired weight-loss, temperature increase and near surface gas product data for 13%N nitrocellulose. A non-isothermal kinetics model was applied. The Arrhenius constants obtained and the known sample thickness predict $\dot{r}$ = 0.3 mm/sec. The value is in excellent agreement with the experiment $\dot{r}$ of 0.4 mm/sec for a double base propellant (80% nitrocellulose) determined under the same pressure conditions. The SMATCH/FTIR data for glycidylazide polymer (GAP) predict $\dot{r}$ = 1.35 mm/sec compared to the experimental value of 1.7 mm/sec under the same pressure conditions. The similarity of the predicted and measured $\dot{r}$ gives confidence that the gas products and concentrations measured by SMATCH/FTIR are the reactants for the flame were a flame to be present. The gas products from SMATCH/FTIR are essentially the same as those measured by the Fast-Heat-and-Hold/FTIR method and all of our previous fast thermolysis/FTIR studies. As a result, the connection between the chemical composition of a material and its ultimate flame characteristics is beginning to be made.

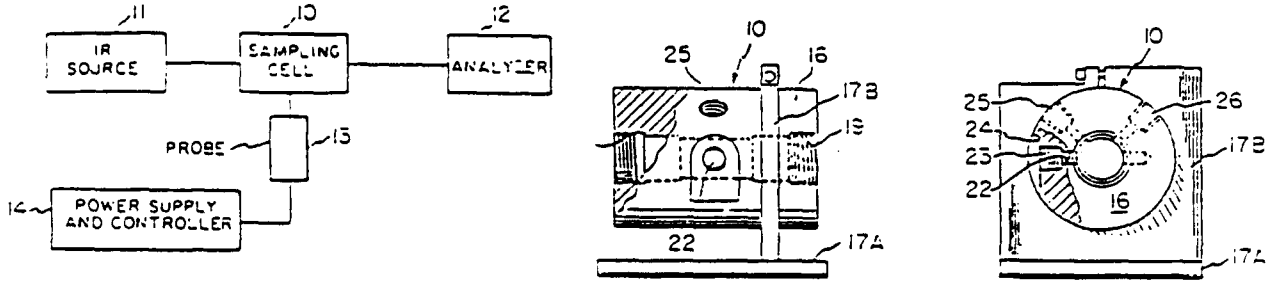

Figure 1. The physical layout (left) and cell design for the Fast Heat and Hold/FTIR experiment. A thin film of 200μg of sample is placed on a Pt ribbon filament and inserted through the cell wall at site 22.

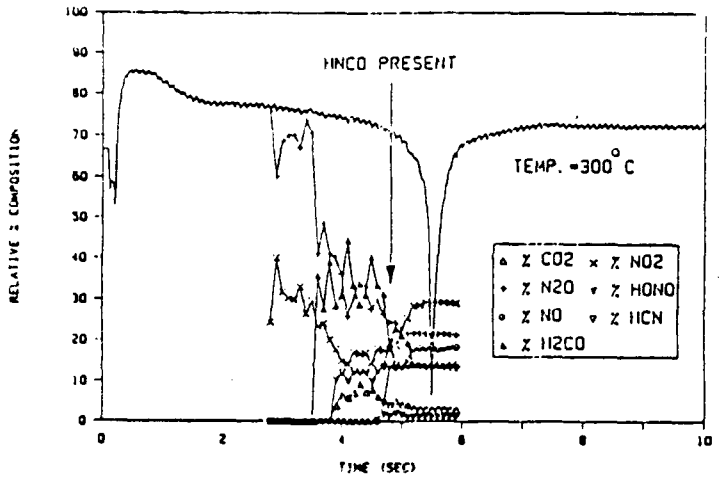

Figure 2. The control voltage response of the Pt filament superposed on the quantified gas products from 200μg of HMX. The heating rate was 2000°C/sec to a constant temperature of 300°C. The negative spike is the exotherm of HMX. See text for more details.

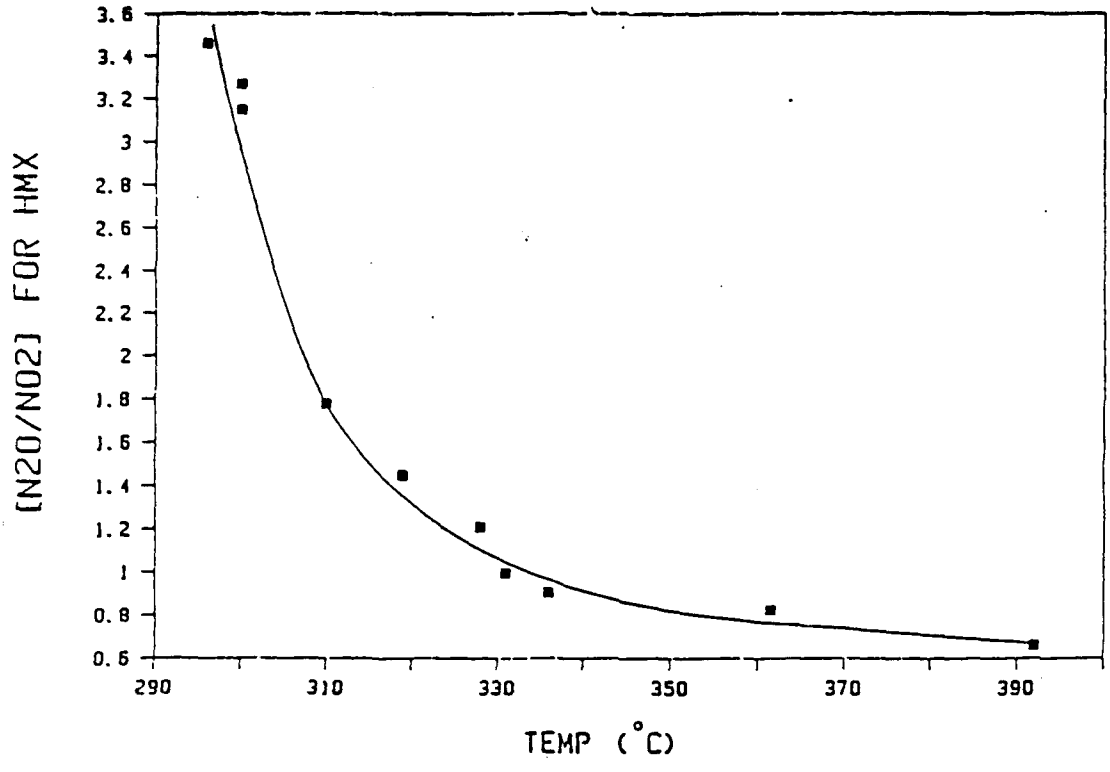

Figure 3. The N_2O-CH_2O/NO_2-HCN branching ratio of HMX as a function of temperature. The rates of these two reactions are approximately equal at the burning surface temperature of HMX (340-360°C).

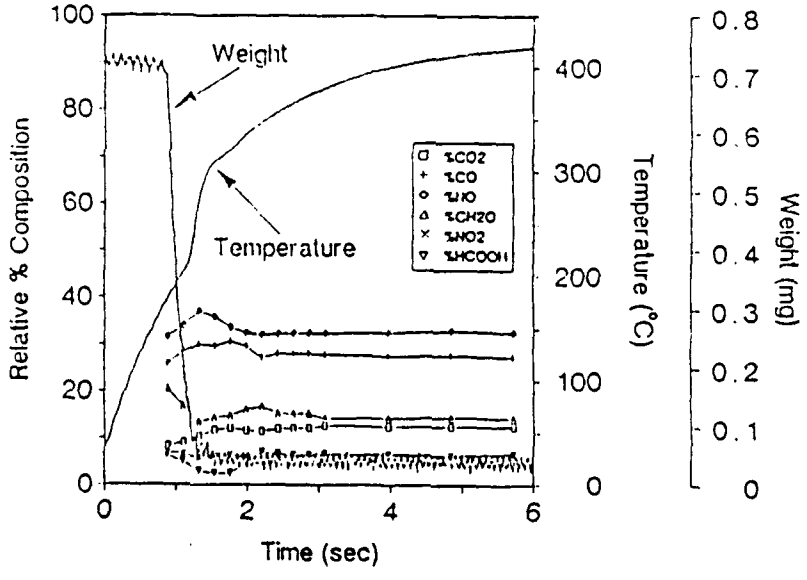

Figure 4. SMATCH/FTIR data for a 30μM thick film of 13%N nitrocellulose showing the dynamic weight change, temperature change and near surface gas products. The mass change and temperature profile enables a non-isothermal kinetics model to be applied. The gas products are the species that leave the surface under this simulated combustion situation.

KINETIC STUDIES OF METAL COMBUSTION IN PROPULSION

AFOSR Grant No. 89-0086

Principal Investigator: Arthur Fontijn
Research Collaborator: Peter M. Futerko

High-Temperature Reaction Kinetics Laboratory
The Isermann Department of Chemical Engineering
Rensselaer Polytechnic Institute
Troy, NY 12180-3590

SUMMARY

The transfer of engineering data, on rocket chamber and plume combustion, from present to advanced propulsion systems, requires understanding and knowledge of individual B and Al species reactions. Experiments with our unique HTFFR (high-temperature fast-flow reactor) technique have shown a wide variety of ways by which temperature affects the rate coefficients. This emphasizes the need for accurate measurements on further B and Al reactions, which should be included in rocket combustion models. Moreover, a framework needs to be established to allow estimates on yet other reactions. Here we report new measurements and a correlation function which unifies activation energies for a series of BCl and AlCl reactions and can be extended to further series of homologous reactions.

TECHNICAL DISCUSSION

Relevance and Scientific Approach

We have made kinetic (i.e., temperature dependent rate coefficient and product identification) measurements in the 300 to 1900 K temperature range. The major reactions investigated in the context of current propellants with Al as metallic and NH_4ClO_4 as oxidizer component are those of Al, AlCl and AlO oxidation by O_2, CO_2 and HCl. Groups specializing in modeling should now incorporate these results into models, which allow comparison to actual performance data. These models should allow the construction of models for advanced systems, by addition (and sometimes substitution) of further kinetic data. For such advanced models we have already measured a series of reactions of BCl and intend to measure BO, BO_2 and B and AlF reactions. For a B/O/H/C system (boron-hydrocarbon slurries) a kinetic model already exists,[1] but it lacks the measured k(T) data that our program would provide. Additionally, we plan to study both Al and B species reactions with H_2O, the one major rocket oxidant not yet covered in our work.

Recent Experiments

The following k(T) measurements, expressed in $cm^3molecule^{-1}s^{-1}$, have been completed:

$$AlCl + CO_2 \rightarrow OAlCl + CO \qquad T = 900\text{-}1790\ K \qquad (1)$$
$$k(T) = 3.6 \times 10^{-23}\ (T/K)^{3.0}exp(-3630\ K/T)$$

$$AlCl + N_2O \rightarrow \text{Products, see below} \qquad T = 700\text{-}990\ K \qquad (2)$$
$$k(T) = 6.1 \times 10^{-11}exp(-7460\ K/T)$$

An attempt to measure AlCl with SO_2 was unsuccessful, due to interference of SO_2 fluorescence and the extreme slowness of this reaction. The reason for studying reactions (1) and (2) was the correlation scheme discussed in the next section. We had studied reaction (1) previously from 1175 to 1775 K.[2] However, the scatter in those results was such as to preclude its inclusion in the correlation scheme. In Fig. 1 we compare the previous to the present measurements. It is interesting to note that the best fit to the older measurements does not differ in a major way from the new measurements, though the scatter is now significantly reduced. The technique modifications that have allowed this improved accuracy have been described.[3]

This year we have established a new technique for introduction of radicals from refractory species. As used, an upstream removable evaporator produces gaseous $AlCl_3$ entrained in Ar. The mixture then passes through a microwave discharge zone, where AlCl is produced, and finally flows into the HTFFR. The discharge step is similar to our BCl production from BCl_3 directly from a cylinder.[3] The results shown in Fig. 1 were in part obtained by this new method, in part by the original method,[2] i.e., evaporation of Al inside the reactor and entrainment in an Ar flow containing traces of Cl_2; the agreement between the measurements from the two methods is excellent. The new method should be especially useful for future studies of species not otherwise readily introduced into the reactor, such as BO_x.

Correlations in Homologous Reaction Series

By expressing the rate coefficients for the reactions of AlCl with O_2 and BCl with O_2, CO_2, SO_2 and N_2O in the form $k(T) = AT^nexp(-E/RT)$, and fixing n, e.g. at 3.0, we noted at last years meeting that a correlation between the E-values, existed. By including the result from the CO_2 reaction (1) and literature values over more limited temperature ranges for the BF + O_2 and BH + O_2 reactions,[4,5] we have now established that the following relationship exists

$$E = a + b\ D(M\text{-}X) + c\ (IP_{MX} - EA_{OXIDANT}) \qquad (3)$$

which is illustrated in Fig. 2. In this equation a, b and c are constants, with the values, -72.74 kJ mol^{-1}, 0.07987 and 0.04893, respectively. D and IP are the bond energy and ionization potential of the B or Al compound and EA stands for electron affinity, all expressed in kJ mol^{-1}. Moreover, we can show that this relation can be derived from standard Pauling resonance theory. The same

treatment leads to equally good correlations for several other series of homologous reactions, e.g., our recent observations on metal-atom N_2O reactions under an NSF grant.

The only exception we have seen to the trends of Fig. 2 is reaction (2). Expressed in the same formalism it has a much higher E-value than that figure would predict. However, it also has a pre-exponential larger than BCl + N_2O, whereas we find for oxidation by O_2, CO_2 and HCl that the BCl reactions have an about factor 10 larger pre-exponential then the AlCl reactions.[3] The correlation of Fig. 2 suggests that the reactions given there have a similar mechanism, i.e., direct O atom abstraction. Apparently the AlCl + N_2O reaction follows a different path. Peculiarities in N_2O reactions have been noted sometimes in other studies.[6,7]

These observations show that it is possible to make predictions for series of similar metallic species reactions by measuring a few of its members. This allows faster model development, but as reaction (2) illustrates experimental confirmation remains desirable.

References

1. R.A. Yetter, H. Rabitz, F.L. Dryer, R.C. Brown and C.E. Kolb, "Kinetics of High-Temperature B/O/H/C Chemistry", Combust. Flame, 83, 43 (1991).

2. D.F. Rogowski and A. Fontijn, "An HTFFR Kinetics Study of the Reaction Between AlCl and O_2 from 1175 to 1775 K", Chem. Phys. Lett., 132, 413 (1986).

3. A.G. Slavejkov, P.M. Futerko and A. Fontijn, "High-Temperature Fast-Flow Reactor Kinetics Study of the Reaction Between BCl and CO_2 From 770 to 1830 K", Twenty-third Symposium (International) on Combustion, in press.

4. G.C. Light, R.R. Herm and J.H. Matsumoto, "Kinetics of Some Gas-Phase Elementary Reactions of Boron Monofluoride", J. Phys. Chem., 89, 5066 (1985).

5. N.L. Garland, C.T. Stanton, J.W. Fleming, A.P. Baronavski and H.H. Nelson, "BH Reaction Kinetics Studied with a High-Temperature Reactor", J. Phys. Chem., 94, 4952 (1990).

6. J.M.C. Plane, "A Kinetic Study of the Reaction Li + N_2O: Non-Arrhenius Behavior Over the Temperature Range 363-900 K", J. Phys. Chem., 91, 6552 (1987).

7. P. Marshall, A. Fontijn and C.F. Melius, "High-Temperature Photochemistry and BAC-MP4 Studies of the Reaction Between Ground-State H Atoms and N_2O", J. Chem. Phys., 86, 5540 (1987).

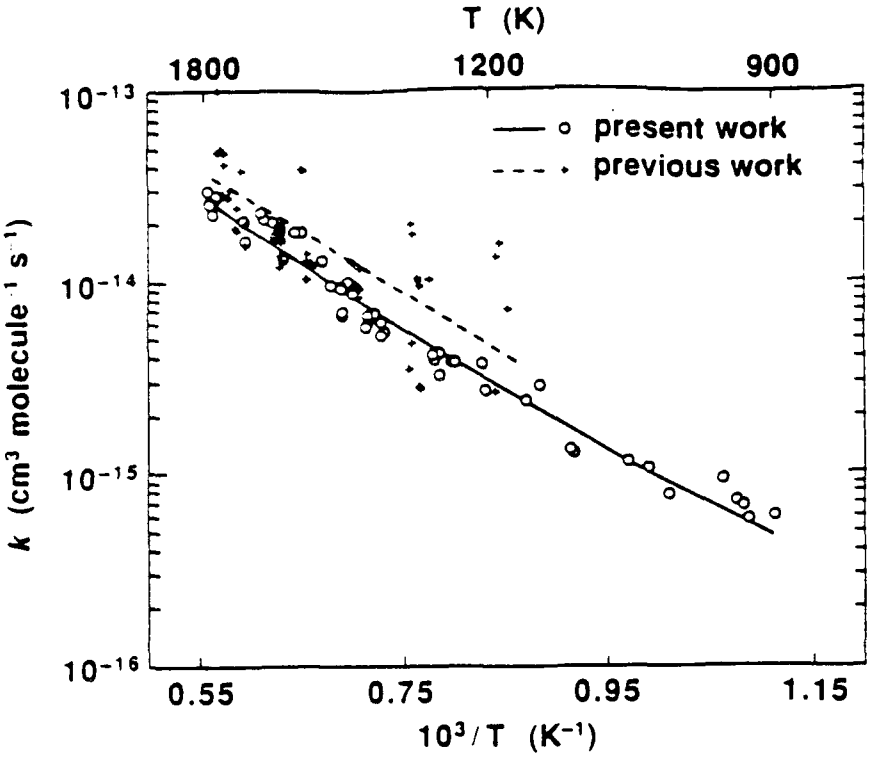

Figure 1. Rate Coefficients for the AlCl + O_2 Reaction

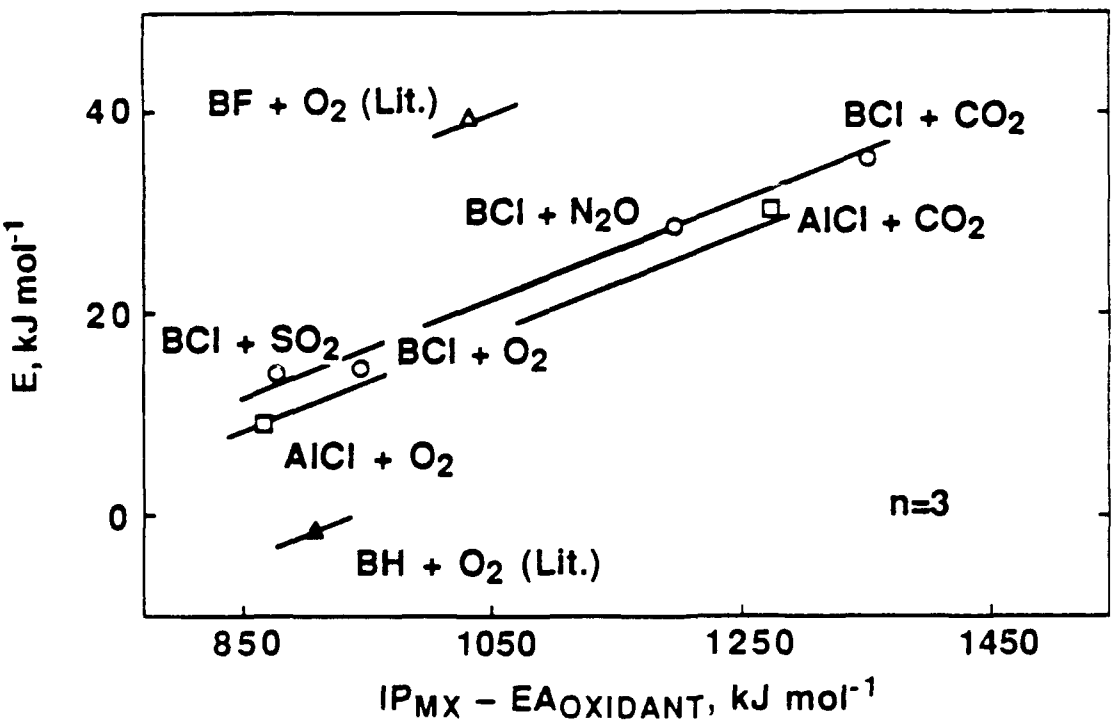

Figure 2. Correlation of the Activation Energies of the Reactions of Several B and Al Radicals with a Number of Oxidants.

Measurements and Chemical Kinetic Simulation of the Structure of Model Propellant Flames

AFOSR Grant Number AFOSR 90-0121

Melvyn C. Branch and Hasan Dindi
Center for Combustion Research
Mechanical Engineering Department
University of Colorado
Boulder, Colorado 80309-0427

SUMMARY/OVERVIEW:

The combustion of solid rocket propellants and other energetic materials is a complex multidimensional and multiphase process involving a wide variety of chemical species. The very high pressure and temperature conditions of practical rocket combustion chambers are at present inaccessible by most conventional diagnostic techniques. The study of these coupled phenomena in situ, therefore, has not been possible in sufficient detail to develop a complete understanding of the chemistry and physics of the combustion process. A coordinated research program has been initiated by JANNAF to study separate aspects of the overall process in an effort to provide a comprehensive understanding of the combustion mechanism. This study is one component of that coordinated investigation and has as its focus the gas phase reactions associated with the combustion of these solid fuels.

TECHNICAL DISCUSSION:

The purpose of this report is to summarize the current status of studies we have undertaken of model gas phase flames associated with the combustion of nitramine based solid rocket propellants. These studies consist of measurements of the structure of stable and unstable species concentration profiles and temperature in laminar, premixed, flat flames of fuel/NOx mixtures at low pressure. The experimental measurements are then compared to calculations of the concentration profiles using a one dimensional flame code which models the transport processes and chemistry of the flame. The transport processes include species diffusion and thermal conduction through the flame and the chemistry is modeled by a detailed chemical kinetic reaction mechanism. The flames which have been studied thus far are supplied with CH_4, CH_2O, CO or H_2 as fuel and NO_2, N_2O or O_2 as oxidizer. The recent results are presented below and conclusions of the flame modeling are discussed.

<u>CO-N_2O Flames:</u> Low pressure, laminar, premixed flames of CO-N_2O have been stabilized over a rectangular flat-flame burner. Laser-induced fluorescence spectroscopy was used to establish the absence of CN, CH, NH, NH_2, and OH in these flames. Gas chromatographic sample analysis was used to determine the CO, CO_2, N_2O, NO, N_2, and O_2 concentration profiles for three CO-N_2O flames having equivalent ratios of 1.00, 1.32, 1.50. Lean flames could not be stabilized. Temperature profiles for all three flames were measured using R type thermocouples. Measured temperature profiles were corrected for radiation losses. These flames are considerably lifted above the burner and contain a single luminous zone. The main feature of these flames is the absence of any reactive intermediates except oygen atom.

A chemical kinetic mechanism containing 27 elementary reactions was presented. This mechanism was used as an input to a flame code developed at Sandia National Laboratories to calculate the concentration profiles of major species. The calculations supported the absence of any reactive intermediate but O atoms. There was excellent quantitative agreement between the measured and the calculated concentration profiles for all three flames. The elementary

reaction contribution and sensitivity analyses showed that the reaction mechanism could be reduced to four elementary reactions. The bimolecular reaction $CO + N_2O \rightarrow CO_2 + N_2$ was the dominant elementary reaction. The reaction rate parameters for the four-step mechanism were determined and were compared with literature data. Because the free radical pool of these flames is very poor, addition of trace amounts of hydrogen-containing compounds significantly alters the structure of these flames.

We believe that the four-step mechanism derived above satisfactorily describes $CO-N_2O$ flames. The kinetic parameters reported in this work for these four reactions can be used with confidence for other kinetic calculations involving these reactions.

H_2-NO_2 Flames: In a manner similar to that described above, flames of H_2-NO_2-Ar have been stabilized on a flat flame burner at 25 torr. Measurements of the composition of stable species were by probe sampling and mass spectrometric gas analysis. The composition profile of OH was measured by linear LIF and the temperature determined by measuring the OH rotational temperature. Modeling was again done with the Sandia premixed flame code using the chemical kinetic data in the review by Miller and Bowman. The results show good agreement between the modeled and measured results for stable species and for OH. The global reaction can be represented by $H_2 + NO_2 = NO + H_2O$ with no N_2 being detected.

CH_4-N_2O Flames: Measurements of composition and temperature in laminar premixed flat flames of CH_4-N_2O-Ar and CH_4-O_2-Ar were made in near stoichiometric mixtures at 30 torr by molecular beam sampling and mass spectrometrc sample analysis. All major stable species and many important unstable species were measured by this technique, many species being identified in the flame with N_2O as oxidizer for the first time. Calibration of the concentration profiles was accomplished by the use of calibration gases for stable species and by comparison of the mass spectrometer signal in the well characterized CH_4-O_2-Ar flame with signals in the CH_4-N_2O-Ar flame and by partial equilibrium for the hydrogen-oxygen system. The measurements have identified the presence of NCO, HCN and HNCO as reaction intermediates and the importance of these species in the reaction mechanism is discussed. Detailed flame modeling is in progress.

PUBLICATIONS:

M.C. Branch, A. Alfarayedhi, M. Sadeqi and P.J. Van Tiggelen, "Measurements of the Structure of Laminar Premixed Flames of $CH_4/NO_2/O_2$ and $CH_2O/NO_2/O_2$ Mixtures," *Combustion and Flame*, in press.

M.C. Branch, M.A. Habeebullah and F.N. Alasfour, "Flame Structure of CH_4/N_2O and CH_2O/N_2O Laminar Premixed Flames," *23rd Symposium (International) on Combustion,* in press.

H. Dindi, H.M. Tsai and M.C. Branch, "Combustion Mechanisms of Carbon Monoxide-Nitrous Oxide Flames," *Combustion and Flame,* in press.

J.V. Volponi and M.C. Branch, "Flame Structure of H_2-NO_2-Ar Laminar Premixed Flames," Paper No. WSS/CI 90-02, *Western States Section/Combustion Institute,* October 1990.

J. Vandooren, P.J. Van Tiggelen and M.C. Branch, "Measurements of the Structure of CH_4/N_2O/Ar and CH_4/O_2/Ar Flames by Molecular Beam Sampling and Mass Spectrometric Analysis," Paper No. WSS/CI 91-16, *Western States Section/Combustion Institute,* March 1991.

TABLE 1

Reaction mechanism for carbon monoxide–nitrous oxide flames.
Rate Coefficients are in form $K(T) = AT^n \exp[-E/(RT)]$.
The units are moles, cm^3, seconds, K, and cal/mole.

No.	REACTION	A	n	E	Ref.**
1*	$N_2O + CO \rightarrow N_2 + CO_2$	1.25E+12	0.0	1.73E+04	†
2	$CO + NO_2 \rightarrow CO_2 + NO$	1.20E+14	0.0	3.16E+04	12
3	$CO + O + M \rightarrow CO_2 + M$	6.17E+14	0.0	3.00E+03	8
4	$CO + O_2 \rightarrow CO_2 + O$	2.50E+12	0.0	4.78E+04	31
5	$CO + CO + O \rightarrow CO_2 + CO$	5.30E+13	0.0	-4.54E+03	31
6	$CO_2 + N \rightarrow NO + CO$	1.90E+11	0.0	3.40E+03	8
7*	$N_2O + M \rightarrow N_2 + O + M$	3.50E+14	0.0	5.16E+04	†
8*	$N_2O + O \rightarrow N_2 + O_2$	1.00E+14	0.0	2.82E+04	†
9*	$N_2O + O \rightarrow NO + NO$	1.00E+14	0.0	2.82E+04	†
10	$NO_2 + M \rightarrow NO + O + M$	1.10E+16	0.0	6.60E+04	8
11	$NO_2 + O \rightarrow NO + O_2$	1.00E+13	0.0	6.00E+02	8
12	$O + O + M \rightarrow O_2 + M$	1.89E+13	0.0	-1.79E+03	8
13	$N + NO \rightarrow N_2 + O$	3.27E+12	0.30	0.00E+00	8
14	$N + O_2 \rightarrow NO + O$	6.40E+09	1.00	6.28E+03	8
15	$C + NO \rightarrow CN + O$	6.60E+13	0.0	0.00E+00	8
16	$C + O_2 \rightarrow CO + O$	2.00E+13	0.0	0.00E+00	8
17	$CN + O \rightarrow CO + N$	1.80E+13	0.0	0.00E+00	8
18	$CN + O_2 \rightarrow NCO + O$	5.60E+12	0.0	0.00E+00	8
19	$CN + O_2 \rightarrow NO + CO$	5.60E+12	0.0	0.00E+00	8
20	$CN + NO_2 \rightarrow NCO + NO$	3.00E+13	0.0	0.00E+00	8
21	$CN + N_2O \rightarrow NCO + N_2$	1.00E+13	0.0	0.00E+00	8
22	$CN + NO \rightarrow N_2 + CO$	1.07E+14	0.0	8.00E+03	32
23	$CN + N \rightarrow C + N_2$	1.04E+15	-0.5	0.00E+00	8
24	$NCO + O \rightarrow NO + CO$	2.00E+13	0.0	0.00E+00	8
25	$NCO + N \rightarrow N_2 + CO$	2.00E+13	0.0	0.00E+00	8
26	$NCO + NO \rightarrow N_2O + CO$	1.00E+13	0.0	-3.90E+02	8
27	$NCO + M \rightarrow N + CO + M$	3.10E+16	-0.50	4.8E+04	8

* Reaction included in the final mechanism.

** Number in this column refers to the number of the reference of the paper.

† This study.

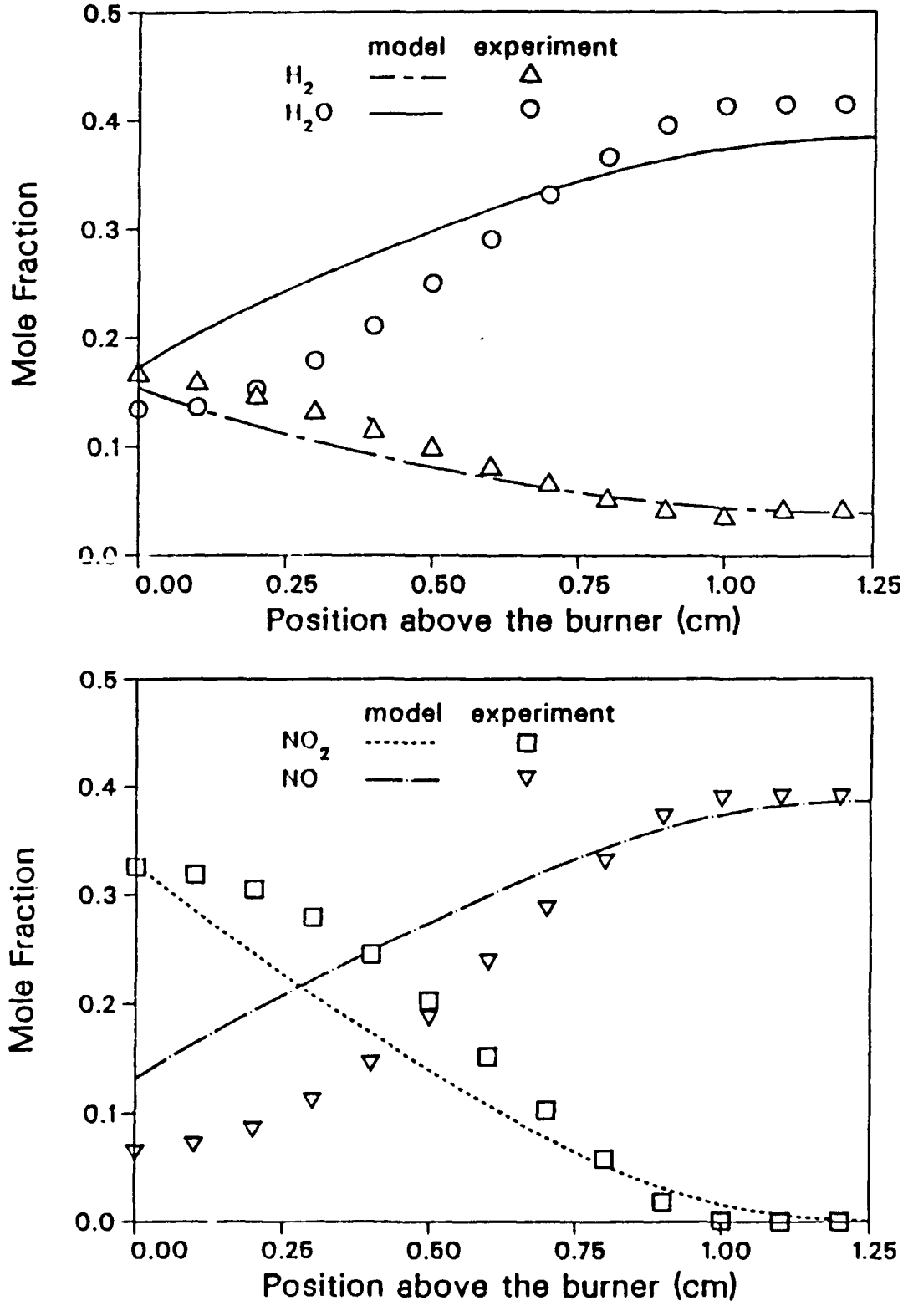

Figure 1. Comparison of experimentally measured and calculated flame structure for 25 torr H_2-NO_2-Ar flame at an equivalence ratio of 1.08. Total gas flow rate is 5.47 slm.

PLUME INVESTIGATION OF A 1 KW ARCJET USING LASER INDUCED FLUORESCENCE
(AFOSR TASK NO. 2308M4)

Ronald A. Spores
OL-AC Phillips Laboratory, Edwards Air Force Base 93523-5000

Daniel A. Erwin
University of Southern California 90089-1191

SUMMARY/OVERVIEW:

The primary goal of this work is to accurately clarify the flow field of a 1 KW arcjet plume. Non-intrusive velocity measurements will be made at pointwise locations in the arcjet plume using Laser Induced Fluorescence (LIF). The arcjet will be tested using both hydrogen and ammonia propellants over a range of power and mass flow settings. For ammonia, both the atomic hydrogen and nitrogen velocity profiles will be obtained from the Doppler-shifted absorption peak. This project will also obtain information about the electron density and atomic temperature via careful measurement of the absorption lineshape.

TECHNICAL DISCUSSION:

Efficiencies of current arcjets are on the order of 30-40% with the major energy loss mechanisms being frozen flow losses from the plume expansion and viscous losses throughout the nozzle region. Viscous losses, along with a highly peaked centerline temperature, result in exit velocity profiles that are likewise strongly peaked along the centerline. If a more uniform exit velocity profile could be generated, the overall efficiency, and thrust, of arcjets would be enhanced. However, before an extensive design modification effort is undertaken to improve the exit velocity profile, it is important to gain further knowledge about the present profile. LIF is considered the best technique for nonintrusively probing this low pressure, high temperature plasma environment. This work will provide strong guidance towards improving the fundamental design of next generation arcjets (in particular the nozzle region) in order to enhance performance.

The principal objective of this work is to generate a velocity map of the plume region for a 1 KW class arcjet. Axial velocity profiles will be compared between the 1 KW arcjet results of this study and the 30 KW class arcjet tested by Pham-Van-Diep, Deininger and Erwin (1990) which was a proof of concept for this LIF technique on arcjets. The principle

of the LIF velocity measurements is the Doppler shift of the atomic transition wavelength peak; for hydrogen, the Hα (λ= 656.3 nm) transition line will be used. The control volume is defined as the intersection of the focussed laser beam and the focal region of the photomultiplier tube (PMT) collection optics which are positioned for 90^{o} collection of the incident laser light. The experimental set up, which gives an actual control volume size of approximately 200 x 200 μm, can be seen in Figure 1. The output wavelength of the tunable dye laser is then scanned over the spectral region of an atomic transition wavelength to be investigated with the PMT output giving the absorption profile. By comparing wavelengths of the measured Doppler-shifted absorption peak with that of a stationary source, one can determine the mean velocity of control volume gas.

The center wavelength of an atomic transition will be shifted proportionately to the velocity of the atom in the direction of the light source for the case of absorption, or in the direction of the detector for emission. The relationship between velocity and wavelength shift is given by,

$$\upsilon = \frac{\Delta\lambda}{\lambda} c$$

where $\Delta\lambda$ is the shift of the center wavelength of the lineshape with respect to the center wavelength for v=0, λ is the pump (laser) wavelength, and c is the speed of light. Exit velocities of arcjet plumes are on the order of 20 Km/sec, which corresponds to a transition lineshift of approximately 0.4 Å .

For the case of ammonia, a detailed comparison will be made of the velocity difference between the nitrogen and hydrogen atoms. In multispecies propellants, the components with the heavier atomic weight are expected to have a substantially lower mean velocity than the lighter atoms due to the transfer of less translational energy per collision. In the work of Pham-Van-Diep, Deininger and Erwin(1990), which is shown in Figure 2, only the atomic hydrogen was investigated for ammonia propellant.

Although this effort will focus on the axial velocity component, the radial and azimuthal components will also be investigated. Both of these secondary components are indicators of the plume spreading and expansion process. The results from this portion of the effort will be compared with those of Pivirotto, Deininger and Seidel (1987) who indicated extremely high azimuthal velocities, over 20% of the axial values. In addition to the obvious decrease in axial thrust that is due to radial gas expansion, there is also the important factor of spacecraft contamination caused by propellant expansion back towards the satellite. This contamination can cause problems with satellite sensors, antennae, and solar arrays. In order to measure these secondary velocity components, the experimental set up must be modified in order to bring the laser beam in at 90^{o} to the arcjet axis.

Another major effort of this project will be to carefully measure the overall absorption lineshape and deconvolute this lineshape into its various components. The primary components will be the gaussian-shaped Doppler broadening and the lorentzian-shaped Stark broadening. By least squares fitting the lineshape wings, one should obtain the lorentzian profile which can then be deconvolved from the total lineshape to give the gaussian component. An important concern will be that the laser intensity is low enough to avoid saturation broadening. The goal of this lineshape investigation is to extract electron density profiles from the Stark broadening mechanism of the $H\beta$ line and determine atomic temperatures from the Doppler broadening mechanism.

After the plume region has been successfully mapped, this technique shall be used to obtain velocity measurements inside of the nozzle and thus enable one to obtain information about the internal flow field and expansion process. Internal measurements can be made by collecting light at an angle of less than 90^{o} or by creating small optical access holes through the nozzle body perpendicular to the incident laser beam.

References

1. Pham-Van-Diep, Gerald C., Deininger, William D., Erwin, Daniel A., "Velocity Mapping in the Plume of a 30-kW Ammonia Arcjet", AIAA-90-1476, 21st I.E.P.C., July 18-20, 1990.

2. Pivirotto, T., Deininger, W., Seidel, D., "Velocity measurements in the plume of an arcjet engine", AIAA-87-1063.

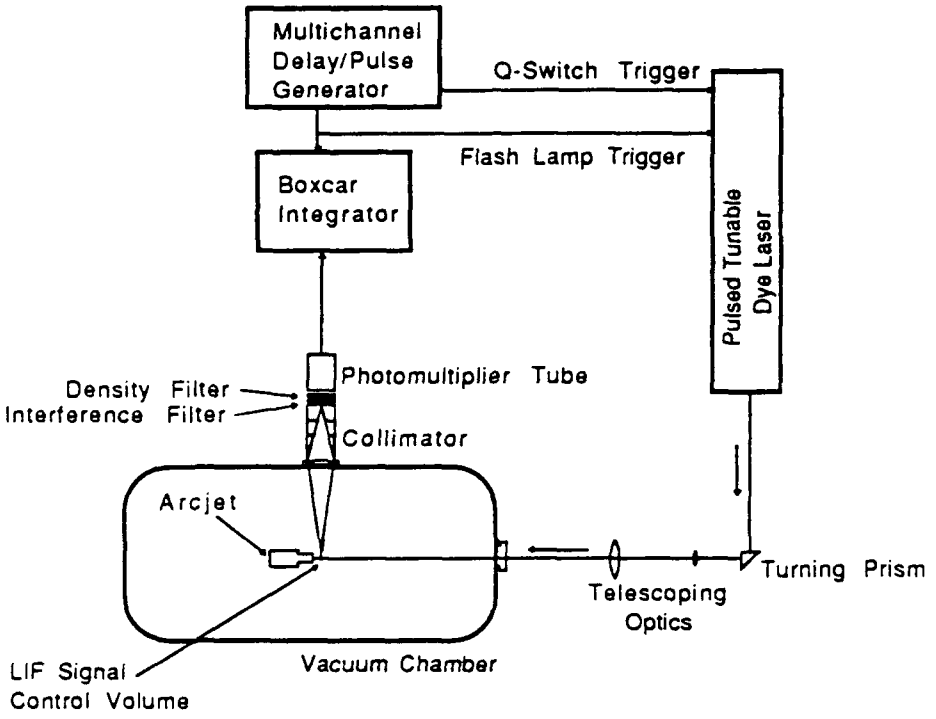

Fig.1 Schematic of LIF Setup for Arcjet Diagnostics

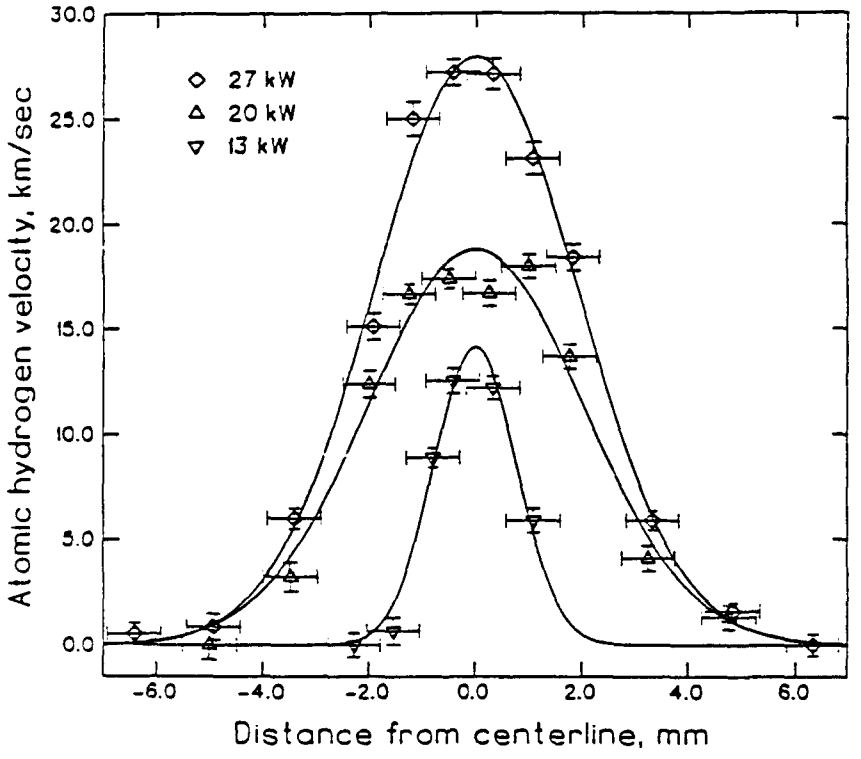

Fig.2 Velocity of Hydrogen Atoms vs. Radial Distance for a 30 kW Class Arcjet

THE INLET IONIZATION PROBLEM

M MARTINEZ-SANCHEZ, MIT

(1) Relevance

The inlet relaxation problem has been one of the most important and difficult areas of uncertainty in plasma devices. Non-equilibrium MHD generators suffer global instabilities due to this problem[1]. Our own experimental MPD thruster[2] failed to produce azimuthally uniform plasma when the inlet electric field was too weak due to a convergent-type design. Japanese experiments[3] showed that Hydrogen would ionize very weakly and with large delays in a thruster in which Argon showed no such difficulties. The gas enters these devices with no ions or free electrons, and a rapid process of electron multiplication must take place, starting with a few back-diffused or photoionized electrons. As the case of Hydrogen vs. Argon shows, the details of the kinetics of intermediate "radicals" can control the whole process, in analogy with the ignition delay problems in high speed combustors.

References

1. Lin, B.C. and Louis, J.F. "Stability of Non-equilibrium MHD Disk Generators". AIAA 26th Aerospace Science Meeting, Jan. 1988.

2. Heimerdinger, D.J., Kilfoyle, D.B. and Martinez-Sanchez, M. "Experimental Characterization of Contoured MPD Thrusters", AIAA-88-3205, 24th JPC, Boston, Ma. 1988.

3. 2-D Kuriki Experiments.

2. Scientific Approach

One type of injector which is potentially important for steady-state MPD thrusters is a ceramic porous plate. This is one limiting configuration which can be analyzed as a one-dimensional structure. In previous work, we have studied the dynamics of such an inlet layer assuming full ionization. We now extend this by including kinetic equations for ionization and species diffusion. Radiation and excitation kinetics may also play a role, and will be assessed.

A more common configuration involves discrete injector holes. Here, the diffusion of electrons into the fresh gas is mainly across streamlines, rather than against the flow, and the structure resembles a 3-D diffusion flame. The study in the three dimensional case is very difficult, and we will attempt to simplify it by using its slenderness to treat it as a submerged reacting jet.

In either case, the results should indicate the length of the inlet relaxation zone, and also the threshold conditions below which no plasma ignition occurs. Both of these items are important design information for plasma devices.

(3) Progress

Significant results have been obtained for the one-dimensional case. Because of the presence of the insulating (hence electron-repelling) back plate, the electron heat flux must be small in the ionization layer, and hence a constant Te approximation is made. Assuming also a constant flow speed through the layer (an assumption to be removed later), one can integrate the convection-diffusion - ionization equations between a wall condition relating diffusive ion flux to Bohm velocity times local density and a downstream asymptotic plasma state. It is found that no attached ionization layer can exit bevond a flow velocity (which increases strongly with electron temperature). When an attached ionization layer does exist, its thickness varies as $(\text{velocity})^{0.6}$ and decreases exponentially with T_e. For $T_e \geq 1$ eV and reasonable conditions, in Argon, the layer thickness is found to be a few mm. or less. The near-back plate electron density is found to be high enough to support strong electron thermal conductivity, hence validating the $T_e \equiv$ constant assumption. These results are summarized in the attached viewgraph.

Work is in progress on the effect of simultaneous acceleration and ionization, as well as on the effect of small T_e variations. The two-dimensional case is in the formulation stage.

Argon Ionization Distance and Maximum Inlet Speed

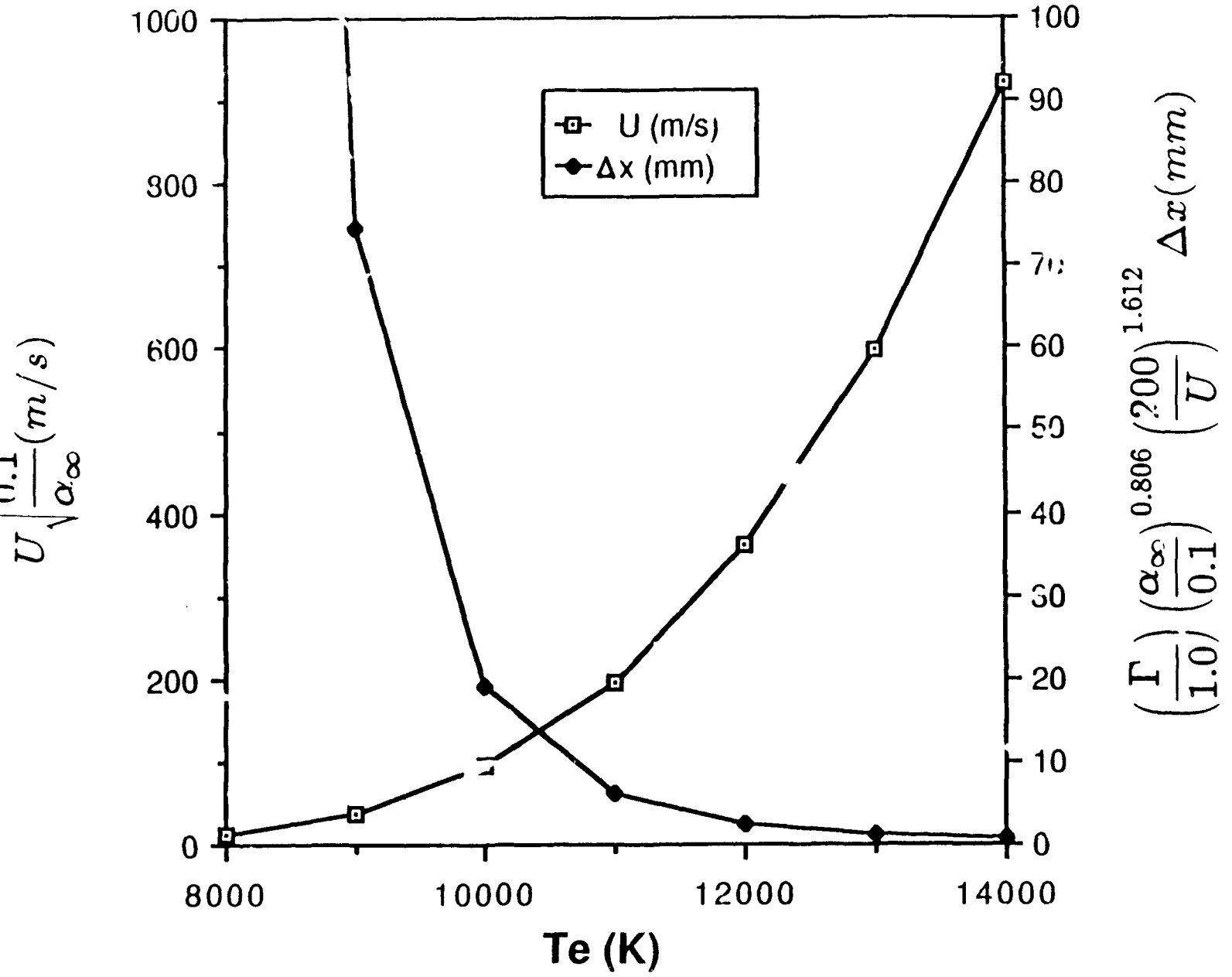

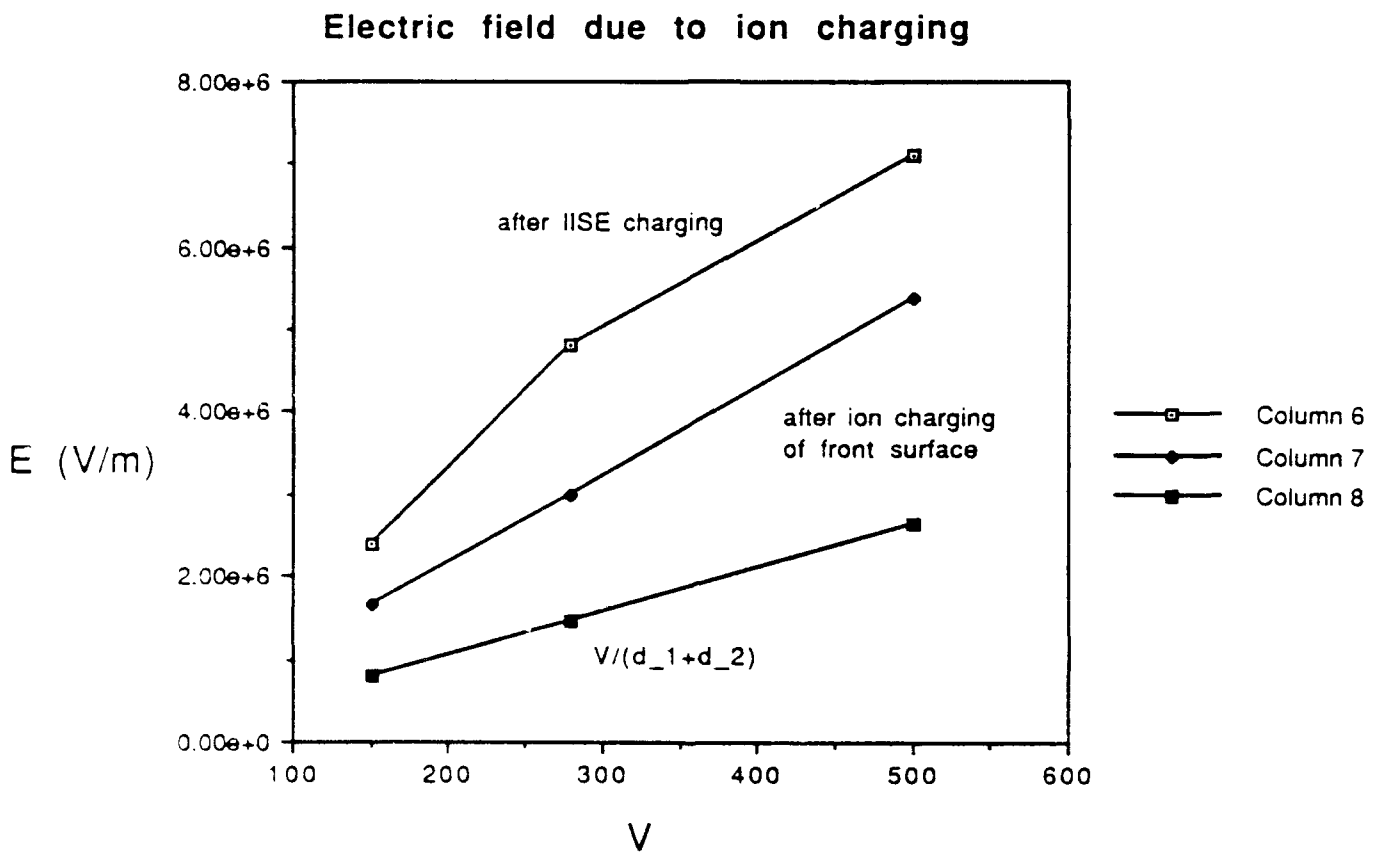
Electric field due to ion charging
8.00e+6
6.00e+6
4.00e+6
2.00e+6
0.00e+0
E (V/m)
after IISE charging
after ion charging
of front surface
V/(d_1+d_2)
100
200
300
400
500
600
V
Column 6
Column 7
Column 8

LASER SUSTAINED PLASMAS IN NON-LTE FOR BEAMED ENERGY PROPULSION

AFOSR Grant No. 89-0274

Principal Investigators: Herman Krier and Jyoti Mazumder
Ph.D. Candidates: David K. Zerkle and Ayhan E. Mertogul

Department of Mechanical and Industrial Engineering
University of Illinois at Urbana-Champaign

SUMMARY/OVERVIEW:

This research is aimed at understanding the fundamental energy transfer mechanisms in laser sustained plasmas (LSP's) for application to rocket propulsion. The fraction of incident laser power absorbed by gases in the plasma and the fraction converted to useful enthalpy are considered the key performance parameters. The usual assumption of local thermodynamic equilibrium (LTE) is not used in this research; thus the thermodynamic state of the plasma is determined more accurately. Non-LTE based values for emission and absorption coefficients, as well as for the transport properties are used. The laser absorption coefficient is closely related to the plasma electrical conductivity. The investigation includes both experiments and detailed modeling. For comparison to the analyses global laser absorption is measured using cone calorimetry and the thermal conversion efficiency is determined by measurements of the gas temperature. Emission spectroscopy is used to determine electron number density and atomic excitation temperature, which are used as input to a numerical algorithm for determining non-LTE parameters such as electron and heavy particle kinetic temperatures and heavy particle number density.

Generalized non-LTE calculations are being performed which rely on collisional-radiative modeling to provide source terms in the gas flow conservation equations. It is expected that the experimentally linked model will reproduce the global absorption and thermal efficiency measured directly, and that the generalized model will be able to match those results as well as the spectroscopically determined electron number density and atomic excitation temperature. The generalized model could then be used with confidence to predict the performance of LSP's as laser power approaches one megawatt. The ultimate goal of this research is the accurate prediction of LSP performance at the pressure, mass fluxes, and megawatt laser powers likely to be found in a full scale laser propulsion system.

TECHNICAL DISCUSSION:

Introduction

The central issue in the study of laser sustained plasmas for thermal rocket propulsion is the accurate prediction of plasma performance at operating conditions likely to be required in practice. That is, laser power of one to ten megawatts or higher, chamber pressures of two to five atmospheres or higher, and propellant (hydrogen) mass flux to achieve optimum performance. High laser power will be required to produce a practical thrust level, and the performance advantages of elevated pressure (above one atm.) and mass flux are well documented [1-4]. Predictions can be made by the application of an appropriate numerical model, and through the measurement of plasma properties at conditions available in the laboratory from which trends are identified.

Before reliable predictions can be made, the fundamental energy transfer mechanisms within the laser sustained plasma must be clearly understood. The absorption of laser power by the electrons via inverse bremsstrahlung (and other minor

absorption mechanisms), the subsequent transfer of energy to the surrounding heavy particles, the convection and conduction of energy out of the plasma,the diffusion of particles within and out of the plasma, and the radiation of energy within and out of the plasma must all be included in this understanding. The performance of an LSP as defined by its global absorption (percentage of incident laser power absorbed on the whole) and thermal conversion efficiency (percentage ending up as thermal energy in the plasma exhaust gas) must be related to the internal plasma processes and understood on those terms.

As outlined in the summary, this investigation relies on several independent diagnostic techniques in order to characterize the LSP. The primary tools have been calorimeter measurements of transmitted laser power and (thermocouple) temperature measurements of plasma exhaust gas. The transmitted power is related to the absorbed power and the bulk gas temperature increase through the plasma is related to the thermal conversion efficiency. These techniques have been used to experimentally map the performance of argon LSP's as functions of laser power, gas pressure and mass flux, beam focusing geometry, and multiple plasma separation [1-3]. In recent experiments nydrogen plasmas have exhibited similar performance trends, but with much improved thermal conversion efficiency [4,5].

Non-LTE Emission Spectroscopy

In determining the thermodynamic state of the plasma, it is important to understand the concept of plasma temperature and the partitioning of energy. The energy content of the plasma gas is taken up by various modes. These include the kinetic energy of the free electrons and the heavy particles (neutral atoms and ions), the ionization energy of the ions, and the electronic excitation of the heavy particles. To a good approximation, the distribution of the energy in each of these modes can be characterized by a temperature parameter associated with Maxwell-Boltzmann statistics. The degree of ionization in the plasma can be similarly characterized by temperature (through the Saha equation). If the plasma is in thermodynamic equilibrium then the thermodynamic state is completely determined by the values of any two properties such as pressure and temperature. In thermodynamic equilibrium Boltzmann's formula for the distribution of excited electronic states, Maxwell's law for the distribution of particles velocities (energies), and Saha's equation describing the plasma composition are all associated with the same temperature parameter.

As mentioned the past LSP research has been directed toward measuring their performance in terms of global laser absorption and thermal conversion efficiency. In order to better understand these results on a physical level it is important to be able to measure temperature and densities inside the plasma. Absorption of laser energy and radiation from the plasma at each point in the plasma will depend on these plasma conditions, thus enabling an understanding of the global results on a local level.

It is a goal of this research to arrive at correct values for absorption and emission coefficient based on the measured or calculated value of number densities and temperatures. It is expected that this will lead to a fundamental understanding of the laser energy conversion process and to more accurate determinations of global absorption and thermal conversion efficiency. This part of the work is comprised of both experimental and theoretical/numerical analysis of laser sustained gas plasmas. The goal is to determine the thermodynamic state of the laser sustained plasma independent of an assumption of local thermodynamic equilibrium. An accurate assessment of the plasma state allows a more reliable determination of global plasma laser absorption, and the conversion efficiency of laser power to gas thermal energy.

A 10 kW continuous wave CO_2 laser is used in this work. Both argon and hydrogen plasmas are being studied. Argon is important because it is inert, with sufficient studies in laser sustained plasmas (and arcjets) already performed under the assumption of local thermodynamic equilibrium; hydrogen is important because it is the propellant of choice for laser propulsion missions. Defining the plasma state entails measuring or calculating the plasma constituent particle number densities and kinetic temperatures,

as well as several atomic excitation temperatures [6]. The experimental portion of this work involves emission spectroscopy. Using an optical multichannel analyzer, both spectral and spatial information can be obtained simultaneously. The emission profile of the hydrogen Balmer series alpha line is measured for the determination of electron number density through Stark broadening theory. In argon plasmas a small amount of hydrogen is added for this purpose. In addition other spectral lines are measured and their integrated intensities used to determine upper atomic level excitation temperature. The excitation temperature is extrapolated to the lowered ionization limit to determine the population of the effective highest bound state. All data must be Abel inverted in order to back out volumetric emission from the measured line-of-sight integrated emission.

The two measured quantities, electron number density and highest bound state population, are used as input to a numerical algorithm. An iterative scheme is used to solve an axisymmetric flow field In this approach axial and radial velocities and pressure are calculated directly. Electron kinetic temperature is then solved for from an electron energy equation involving these velocities and pressure. Heavy particle number density and kinetic temperature, and total excitation temperature are then updated after each iteration. The updating requires three algebraic relations. These are an equation of state, the total Boltzmann distribution, and a non local thermodynamic equilibrium Saha-type ionization equation.

An implied input to the numerical scheme is the laser power profile. Absorbed laser power is treated as a source term in the electron energy equation. As the laser profile interacts with the plasma flowfield the power absorbed at every grid location can be calculated. This results in an accurate determination of global laser absorption. Finally the kinetic temperatures derived from the algorithm along with the velocity fields allow a calculation of inlet and exit gas enthalpies. The difference between the two quantities when compared to the inlet laser power gives a measure of the plasma thermal conversion efficiency. These quantities are then available for direct comparison to experimental determination of absorption and thermal efficiency as a verification of the numerical calculations.

Generalized Non-LTE LSP Model

The goal of a generalized non-LTE model is to predict results for global absorption and thermal efficiency of high pressure hydrogen laser sustained plasmas (LSP's) at very high powers. The approach taken to such a prediction can depend on a priori knowledge of the thermodynamic state of the LSP. If it is known that the LSP is in LTE, then only *one* temperature is necessary for a complete thermodynamic description. In this case the solution algorithm also becomes somewhat simplified. However, in general LSP's cannot be assumed to be in LTE. In the non-LTE case a separate temperature could be assigned to each energy mode of each species, for example the translational temperature of the electrons could be different than that of the neutrals or any of the ions, or the neutral excitation temperature. The non-LTE case greatly complicates the solution process with the introduction of several new variables (the new temperatures). In addition, radiation can play an important role in the production and destruction of species in a non-LTE LSP which is not collisionally dominated. A new technique must be introduced to account for the coupling of the particles and radiation.

The prediction of global absorption and thermal efficiency can be considered to be a macroscopic prediction that requires the accurate prediction of LSP thermodynamic and transport properties including the species number densities of H_2, H, H^+, e^-, H^-, H_2^+, and H_3^+ at each point within the LSP. In addition, for a non-LTE LSP some method of accounting for the coupling between radiation and particles must be applied to each point in the LSP as well as across the LSP from one point to another. Finally, the macroscopic velocity, pressure and temperature fields for the entire LSP must be solved via the conservation equations using an iterative algorithm.

The calculation of species number densities is well documented for hydrogen plasmas in LTE [7]. The basic method is to first identify the reactants and products for

each equilibrium reaction taking place. Then, setting the chemical potential of the reactants equal to that of the products, equations can be arrived at relating particle number densities to particle partition functions. These equations involve the equilibrium temperature, and are relatively easy to solve using an iterative process. The case of non-LTE species number densities requires a modification of the basic equilibrium solution algorithm and necessitates the introduction of additional particle-mode temperatures. These temperatures would be supplied by other portions of the overall solution algorithm, and the equations can again be solved iteratively [8]. In addition, a scheme to account for the production or destruction of species through the interaction with radiation (a collisional-radiative) model must be included in these calculations.

Once the species fractions are known, the thermodynamic properties, specific heat and enthalpy, and the transport properties, viscosity, thermal conductivity and electric conductivity can be calculated. In addition, the absorption of the incident laser beam can be calculated through the calculation and combination of several absorption coefficients including the electron-ion, electron-neutral and electron-molecular inverse bremsstrahlung coefficients, as well as the photoionization of neutrals, the photodetachment of electrons from negative ions, and the resonance absorption of neutrals, if any. Most of the relations that determine these quantities are applicable to both LTE and non-LTE cases with only a slight modification of the input quantities. Next the velocity fields for the heavy particles are solved using an iterative algorithm, as well as the pressure field and temperature fields for the entire LSP.

Current plasma models used to predict results for hydrogen are limited to usage at only 1 atm gas pressure for LTE LSP's with peak temperatures below 30000K [9]. The model uses tabulated thermodynamic and transport coefficient data which are interpolated between. The logical approach to a generalized non-LTE model is to calculate all necessary properties as they are needed, thereby eliminating the need for tabulated data. This is an important feature of our ongoing research.

References

1. Zerkle, D.K., Schwartz, S., Mertogul, A., Chen, X., Krier, H., Mazumder, J., "Laser-Sustained Argon Plasmas for Thermal Rocket Propulsion," *J. Propulsion and Power*, Vol. 6, No. 1, pp. 38-45, Jan.-Feb. 1990.
2. Mazumder, J., Krier, H., "Experimental and Numerical Studies of Laser Sustained Gas Plasmas," Final Technical Report under Grant No. AFOSR-88-0129, April 1989.
3. Schwartz, S., Mertogul, A., Eguiguren, J., Zerkle, D., Chen, X., Krier, H., Mazumder, J., "Laser-Sustained Gas Plasmas for Application to Rocket Propulsion," AIAA paper 89-2631 presented at the 25th Joint Propulsion Conference, Monterey, CA, July 10-12, 1989.
4. Krier, H., Mazumder, J., "Experimental Studies of Laser-Sustained Argon and Hydrogen Plasmas," Annual Technical Report under Grant No. AFOSR-89-0274, March 1990.
5. Mertogul, A., Zerkle, D.K., Krier, H., Mazumder, J., "CW Laser Sustained Hydrogen Plasmas for Thermal Rocket Propulsion," AIAA paper 90-2637 to be presented at the 21st International Electric Propulsion Conference, Orlando, FL, July 18-20, 1990.
6. Eddy, T.L., "Low Pressure Plasma Diagnostics Methods," AIAA paper 89-2830, presented at the 25th Joint Propulsion Conference, Monterey, CA, July 10-12, 1989.
7. Patch, R. W., "Components of Hydrogen Plasma including Minor Species," NASA TN-D-4993, 1969.
8. Cho, K.Y., Ph.D. Thesis, Georgia Institute of Technology, 1988.
9. Eguiguren, J.V., M.S. Thesis, University of Illinois at Urbana-Champaign, 1989.

PLASMA INSTABILITIES AND TRANSPORT IN THE MPD THRUSTER

AFOSR Contract No. AFOSR-91-0162

Edgar Y. Choueiri, Arnold J. Kelly an Robert G. Jahn

Electric Propulsion and Plasma Dynamics Lab.
Princeton University
Princeton, NJ. 08544

1 Summary

Computer models of the MPD[1] thruster rely on the numerical solution of the magnetohydrodynamics (MHD) equations to predict the performance and aid in the design of higher efficiency thrusters. Current MHD models of the accelerator include only classical transport[2] (i.e. transport due to collisions between particles) and overpredict the performance of the experimental prototypes. The inclusion of anomalous transport (i.e. transport due to "collisions" of particles with the oscillating fields of unstable waves in the plasma) is expected to greatly enhance the validity and applicability of such models. To assess the nature and importance of anomalous transport a sound understanding of the mechanisms controlling the stability of the plasma is necessary. This study addresses the problem by studying the various instabilities the plasma can sustain, and modelling their effects on transport. The resulting models are formulated in terms of transport coefficients that can be readily included in any MHD computer code.

[1]Throughout this abstract the term MPD thruster refers to the coaxial, self-field, high-current, gas-fed MagnetoPlasmaDynamic thruster.

[2]Throughout this abstract, "transport" refers to the following processes: electrical conductivity, particle diffusion, viscosity and thermal conductivity.

2 Technical Discussion

2.1 Motivation

The Magnetoplasmadynamic (MPD) thruster is an electromagnetic plasma accelerator that is a promising spacecraft thruster because of its simplicity, thrust scaling, high thrust density and high specific impulse. The MPD thruster can be seen as a plasma accelerator whose performance is dictated by the competition between current-driven acceleration, which constitutes the prime acceleration mechanism in the device, and current-driven dissipation. This competition between two processes driven by the same source, the current, is manifested in the low thrust efficiency (below 30% for argon) of the present devices.

Computer models based on the MHD equations are the ultimate tools for the design of higher efficiency thrusters. Most of the few codes that already exist for the MPD thruster do not include include the effects of finite non-equilibrium rates (i.e. rates of excitation, and deexcitation of internal and translational modes, ionization and recombination) and plasma instabilities (i.e. effects of turbulent transport enhancement due to the existence of unstable waves in the plasma). Consequently, existing codes, although useful for the undesrtanding of various flow features and pecularities, provide little predictive competence when describing the disspative processes dictating the overall performance. Such codes usually predict thrust efficiencies well in excess of the experimentally measured values. The usefulness of these codes can be substantially boosted if they are supplied with transport coefficients that correctly represent the various dissipative mechanisms at play.

3 Approach

Our research has permitted us to identify two distinctly different approaches by which increased propulsive efficiency can be obtained. The first approach is to try to recover the dissipation losses by making the recovery and acceleration time scales comparable. This approach is exemplified by the hybrid electrothermal/electromagnetic accelerator. To achieve an equilibrium between acceleration and enthalpy recovery, the chamber pressure must be considerably larger than the 10 Torr typical of the MPD thruster. This, in turn, translates into an increase in the required power, since the mass flow has to be effectively ionized in order for the electromagnetic and electrothermal thrust components to be comparable. In other words, the realm of the hybrid electrothermal/electromagnetic device is one of higher pressure and higher power than existing MPD devices.

The second approach is to investigate the physical basis of turbulent dissipation with the ultimate goal of defining means for its suppression or diminution. This approach is obviously more beneficial for a frozen flow device like the one currently in our laboratory since it directly deals with the *source* of dissipation

unlike the first approach which addresses the problem of *recuperating* dissipated energy, a problem rendered more difficult by the highly non-equilibrium nature of the flow. The second approach may thus permit us to attain respectable efficiencies without having to use the high pressures which would be undoubtedly required by the first approach (to raise collisionality and lower the equilibration rates) and which will necessitate operation at unrealistically higher power levels (to maintain the ionization degree required by the electromagnetic acceleration process).

The methods of turbulent suppression which may encompass active techniques like using r.f. antennae to couple with and destroy the unstable modes or various changes in the operation and configuration of the benchmark thruster will *not* be attempted in this study. The future implementation of such techniques, however, will be conditioned by the characterization of instability-induced transport which is the actual goal of our research.

3.1 Current and Future Work

The existence and importance of current-driven plasma instabilities have been established through theoretical and experimental work at our laboratory during the past four years as documented in refs. [1,2] and [3]. It is clear, by now, that their ubiquity and impact on the performance are such that no realistic model of the MPD thruster can afford to neglect them.

The Plasma Wave Experiment (PWX) and Plasma Characterization Experiment (PCX) along with the linear wave kinetic theory (all described in [1]) constitute the tools needed for the identification and characterization of the active instabilities. Comparisons (cf. Fig. (1) of measured dispersion relations[3] with predictions from our recent stability models have identified the dominant instability in the MPD plasma as the lower hybrid current-driven instability (LHCDI). The instability, the details of which are presented in refs. [2,3], can account for the type of over-heating and over-ionization that are ubiquitous features of the MPD thruster.

Our current work is concerned with extending the instability analysis to study the effects of the identified instabilities on transport using non-linear plasma theory. The resulting models will be cast in terms of transport coefficients that depend on macroscopic quantities and communicated to other workers in the field who can test them in their MHD codes. A two-dimensional MHD code[4] has been developed in our laboratory under NASA support and is currently being refined. This code will also be used in-house to test the improved transport coefficients.

[3]The dispersion relation is the relation between the frequency and wavelength (or wavenumber) of electric field oscillations.

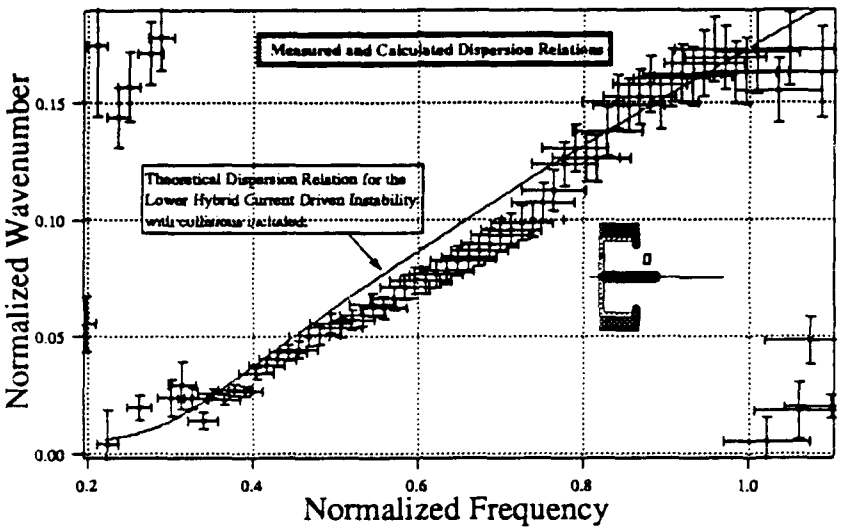

Figure 1: Measured dispersion relation of unstable waves in the MPD thruster compared to our most recent stability model. The schematic in the inset is a cross-section of the device with a small rectangle denoting the region where the measurements were made.

References

[1] E. Y. Choueiri, A. J. Kelly, and R. G. Jahn. Current-driven instabilities of an electromagnetically accelerated plasma. In 20th *International Electric Propulsion Conference*, Garmisch-Partenkirchen, W. Germany, 1988. AIAA-88-042.

[2] E.Y. Choueiri, A. J. Kelly, and R. G. Jahn. Current-driven plasma acceleration versus current-driven energy dissipation part I : Wave stability theory. In 21st *International Electric Propulsion Conference*, Orlando, Florida, 1991. AIAA-90-2610.

[3] E.Y. Choueiri, A. J. Kelly, and R. G. Jahn. Current-driven plasma acceleration versus current-driven energy dissipation part II : Electromagnetic wave stability theory and experiments. In 22nd *International Electric Propulsion Conference*, Viareggio, Italy, 1991.

[4] G. Clado, E.Y. Choueiri, A. J. Kelly, and R. G. Jahn. An MPD code with anomalous transport. In 22nd *International Electric Propulsion Conference*, Viareggio, Italy, 1991.

PICOSECOND LASER BREAKDOWN THRESHOLDS IN GASES

AFOSR Grant No. AFOSR-86-0317

Principal Investigator: Dennis Keefer

Center for Laser Applications
University of Tennessee Space Institute
Tullahoma, TN 37388
615 455-0631

SUMMARY/OVERVIEW

Continuous plasmas were sustained by a sequence of 10 ps pulses from a free electron laser (FEL) in experiments we performed at Los Alamos. These experiments showed an unexpected difference in breakdown threshold intensity for argon as compared to hydrogen or nitrogen. Our present understanding of these processes suggests that the observed difference in breakdown thresholds was due to gasdynamic expansion during a multiple pulse cascade to breakdown. The more massive argon atoms absorb energy from electron collisions more slowly than the lighter atoms and it also has a slower gasdynamic expansion. Theoretical calculations and laboratory experiments utilizing sub-picosecond probe pulses are being performed to develop a better understanding of the optical breakdown processes in the picosecond time regime.

TECHNICAL DISCUSSION

Laser or microwave energy beamed to a space vehicle can provide plasma propulsion systems which have significantly higher specific impulse than comparable chemical rockets. Orbital maneuvering missions which employ these high specific impulse motors can result in significantly lower launch costs for a given mission payload.

The objective of this research is to develop an understanding of the basic physical processes which control the interaction of plasmas sustained by laser beams in a flowing propellant gas. Previous experimental and theoretical studies have provided a reasonable understanding of these processes in flowing plasmas sustained by continuous lasers, and have shown that the absorption efficiency and radiation losses can be controlled through a combination of optical geometry, pressure and flow configuration. Practical beamed laser propulsion systems may require laser powers greater than one megawatt, and current laser development for other applications suggests that lasers capable of delivering average powers at these levels will be free electron lasers (FEL). The power from these free electron lasers will be pulsed, rather than continuous, and we have successfully sustained quasi-steady argon

plasmas using the RF linac free electron laser at Los Alamos National Laboratory (LANL). The RF linac free electron laser at LANL produces a burst of mode-locked micropulses having a duration of approximately 10 ps at a wavelength of 10.6 micrometers and a peak power of approximately 50 MW. These micropulses are spaced 46 ns apart in a burst (macropulse) lasting for 100 to 300 microseconds.

We also attempted to initiate plasmas in both nitrogen and hydrogen using the same experimental procedures as for argon. These attempts were not successful, even though the pulse energy was an order of magnitude larger than our observed threshold for argon. This result is somewhat surprising, since predicted breakdown thresholds using 10.6 micron wavelength and 10 ps duration pulses for hydrogen and nitrogen are essentially the same as for argon. The threshold intensity required for laser breakdown is inversely related to the pulse length for pulses shorter than a microsecond. At the intensities characteristic of our FEL experiments it is likely that breakdown did not occur at the first 10 ps pulse, but cascaded through absorption of subsequent pulses in the plasma electrons remaining from previous pulses.

We are developing a theoretical model to investigate the question of breakdown threshold for the long wavelength, short pulse regime of our experiments. During the 10 ps duration of the laser pulse, there are only approximately 250 optical cycles and only approximately 10 electron-atom collisions. Between collisions, the electron oscillates in the optical electric field gaining "quiver" energy. During an elastic collision the electron changes direction and gains additional energy from the optical electric field. The electrons rapidly gain energy from the optical field and then can produce additional electrons by impact ionization.

During the time between pulses the high energy electrons continue to produce additional electrons by inelastic collisions which also reduce the average energy of the electron distribution. Elastic collisions between the electrons and the heavy particles during the time between the laser pulses will heat the gas and lead to a reduction in density through gasdynamic expansion. The next pulse interacts with all the electrons created by the previous pulse which remain within the focal volume, and the number of electrons may cascade over several pulses to breakdown. However, if the gasdynamic expansion is strong enough, the cascade may reach a limiting electron density below breakdown. The computational code utilizes a particle in cell (PIC) method to calculate the electron distribution during and for a short time after the laser pulse. Between pulses a one-dimensional gasdynamic code is used to calculate the reduction in the electron density due to expansion of electrons out of the focal volume.

The combination of pulse length and wavelength used in the LANL experiments are unique to that FEL. However, we have undertaken an experimental study of picosecond pulse breakdown using single pulses produced by a neodymium-YAG laser at wavelengths of 530 nm and 1.06 μm. These experiments have been used to develop diagnostic methods for the study of optical breakdown on picosecond time scales and to develop insight into the growth of ionization. At these wavelengths, unlike the experiments with the FEL, multiphoton ionization processes play an important role in the breakdown process.

However, experiments performed at different pressures and wavelengths may enable us to separate the effects of electron impact and multiphoton ionization.

The experimental technique used to observe the buildup of ionization during a single 60 ps laser pulse is shown in Figure 1. The method uses a pump-probe technique, where a beam of one wavelength is used to create the breakdown, and a beam of a different wavelength is used to observe the plasma formation. In Figure 2 the green (530 nm) 60 ps pulse creates the plasma breakdown and the absorption of the red (590 nm) < 1 ps pulse is used to detect it. It is difficult to resolve picosecond times electronically, and an optical delay line is used to vary the timing between the < 1 ps probe pulse and the 60 ps pump pulse. A 150 μm movement of the prism will vary the delay by 1 ps, and by scanning the delay line the transmitted pulse energy will produce a transmission curve as indicated in the figure. Variation of the power of the pump pulse or the pressure within the test cell will shift the breakdown time and alter the characteristics of the transmitted signal. The probe pulses consist of a modelocked sequence of pulses spaced at 13 ns, and the longer term decay of the plasma can be probed on a nanosecond time scale.

The laser pulse is Gaussian in time and multiphoton ionization is proportional to the intensity raised to a power. This results in a growth of electron density given by an error function. However, if electron impact ionization occurs, then the ionization rate is linear with laser intensity, but proportional to the number density of the electrons, leading to an exponential increase in electron density. Figure 2 shows the probe pulse transmission through the plasma for experiments in helium at pressures from 0.54 to 8.5 atm with a pulse energy of 9.5 mj. Data have been obtained for argon, helium and nitrogen at pressures ranging from 0.1 Torr to 8.5 atm. The decay of the plasma can be seen from Figure 3. The first pulse is transmitted without absorption prior to breakdown. The second pulse is almost completely absorbed at 200 ps after the breakdown pulse, but subsequent pulses are transmitted with decreasing absorption as the plasma decays. A numerical code is being developed to simulate the temporal and spatial growth of electrons for both multiphoton and impact ionization as an aid in the interpretation of the experimental results.

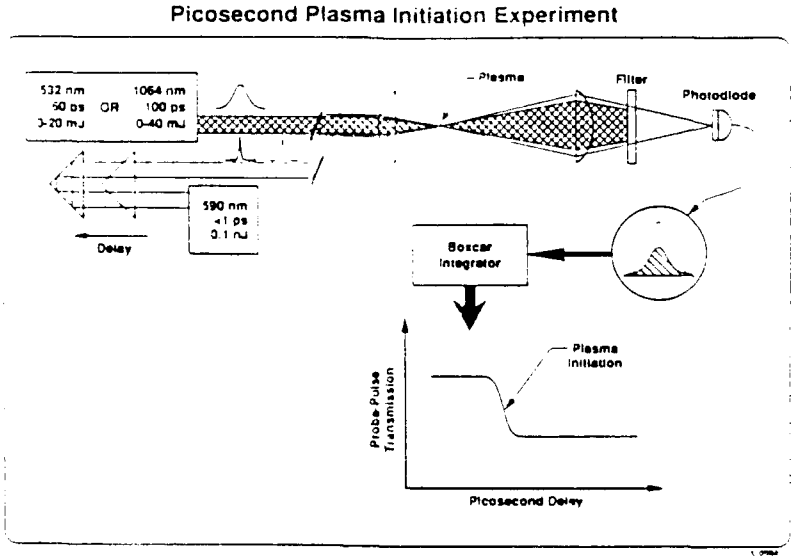

Fig. 1 Pump-Probe Laser Experimental Arrangement

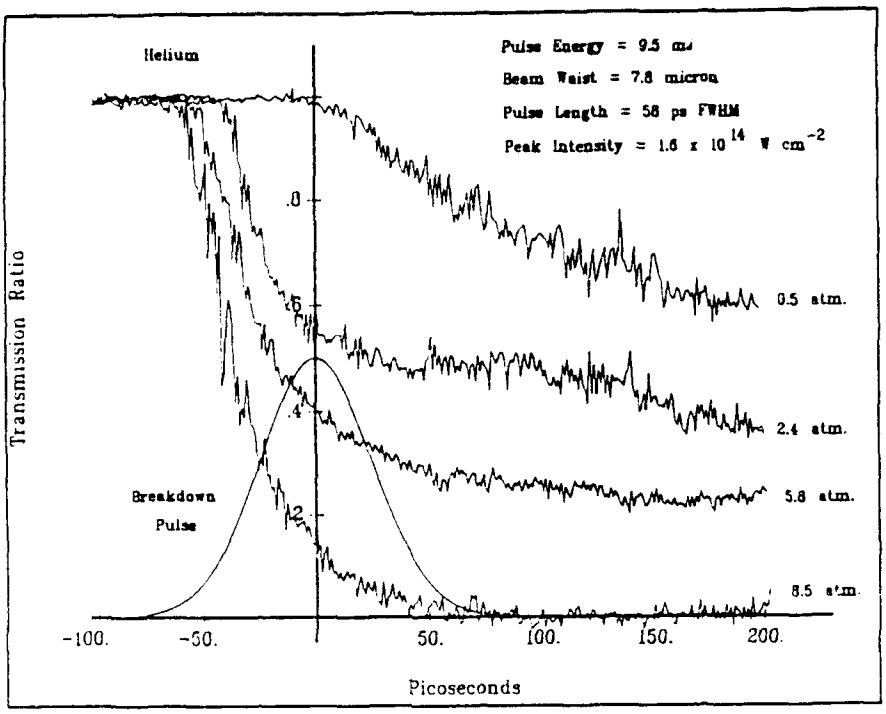

Fig. 2 Probe-Pulse Transmission Through Helium Plasma

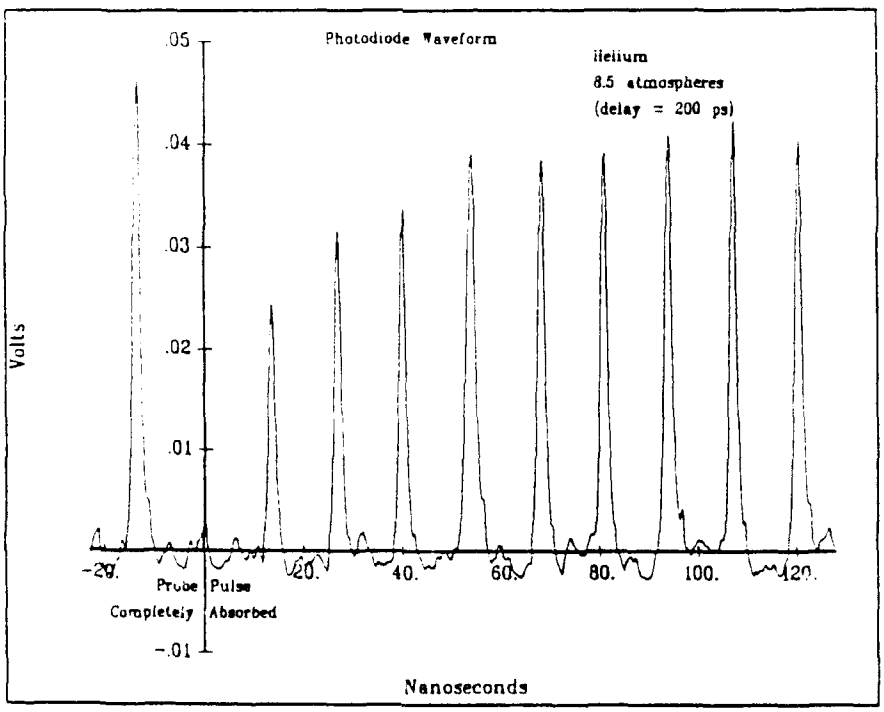

Fig. 3 Probe-Pulse Transmission Showing Plasma Decay

Basic Process of Plasma Propulsion

AFOSR Grant No 86-0337

Principle Investigator: Herbert O. Schrade

Institute for Space Systems
University of Stuttgart
Pfaffenwaldring 31
D- 7000 Stuttgart 80
FRG

Overview: In order to improof performance, lifetime and reliability of plasma thrusters one has to understand and assess certain fundamental processes and problem areas like nonequilibrium magnetoplasmadynamic flows, plasmastability and electrode erosion effects. Here two problem areas are discussed: a) the stability of a current carrying plasma channel and b) the erosion mechanism of a spotty cathode arc attachment.

Author: Herbert O.Schrade

Technical Discussion

a) Plasmastability: Onset Phenomenon explained by Run-Away Joule Heating

One of the most critical limiting effects of self-field MPD-Thrusters is the so-called "Onset- Phenomenon", a plasma instability which causes a severe degradation of the thruster performance as soon as for a given mass flow rate a critical current is exceeded. The onset condition can be characterized by a threshold like increasing voltage fluctuation combined with an intolerable ablation of thruster components, when the measurable parameter, as given by current square divided by mass flow rate, surpasses a critical value. Several different explanations have been put foreward so far and to a great extent reviewed by several authors [1, 2, 3]. In this paper another explanation is presented which also bears the merit to explain qualitatively and quantitatively this onset-phenomenon. It is based on a run-away Joule heating process caused by the self-magnetic field of a current carrying plasmachannel which drastically decreases the radial conduction heat loss. This is the case if the product cyclotron frequency times average collision time, $\omega_e \tau_e$ for the electrons reach values which cannot be ne-

glected any more with respect to unity. At first the heat conduction coefficient for the electrons is calculated by means of a perturbation approach for the electron velocity distribution function taking into account an azimuthal magnetic field. It turns out that the heat conduction coefficient becomes a tensor and that the classical radial heat flux of the electrons must be multiplied by a factor $| sin\omega_e\tau_e | /\omega_e\tau_e$. This factor has the consequence that for $\omega_e\tau_e$-values which are not small compared to one the radial heat conduction losses decreases. Simultaneously the temperature within the discharge channel must increase and as can be shown with the temperature also the quantity $\omega_e\tau_e$ increases, what again should lead to a further lowering of the conduction losses and an even further heating. This run-away heating effect may eventually be stopped by a disturbance of the rotational symmetry of the discharge channel leading to a more dissipative helical configuration (see Fig. 1) which can cause an increased voltage fluctuation. It is shown that the observed onset occures at $\omega_e\tau_e$-values, which cannot be neglected besides one and that the maximum $\omega_e\tau_e$ within a discharge channel is proportional to $\frac{\rho^{1/3}}{m}$ which agrees quite well with experimental observations.

References

[1] Hügel, H: Zur Funktionsweise der Anode im Eigenfeldbeschleuniger. DFVLR-FB 80-30, 1980.

[2] J.W. Barnett and J.R. Jahn, :Operation of the MPD - Thruster with stepped Current Inputs , Dissertation for the Degree of Philosophy by J.W. Barnett, Mechan. and Aerospace Engeneering Princton Univ. April 1985. and J.W. Barnett and R.J. Jahn : Onset Phenomena in MPD Thrusters AIAA 85 - 2038, Oct 1985

[3] J.S. Sovey and Mautenicks: Performance and Lifetime Assesment of MPD- Arc Thruster Technology NASA Tech. Memorandum 101293, AIAA - 88 - 3211, 24th Joint Propulsion Conf. July 1988

Cathode Erosion Mechanism

Pulse- discharge experiments with rectangular current pulses of ca 1400 A for 2 ms duration taking thoriated thungsten cathodes show an almost threshold like increase of the erosion rate by lowering the ambient (Nitrogen) pressure from about 1000 Pa to about 100 Pa. This effect can be explained by means of the previously developed arc spot instability theory and by applying the Prandtl- Mayer jet deflution theory to the cathode jet. Based on the arc spot theory the main electron emitting cathode surface area consists of one or more micro spots of very high current- density (up to $10^{11} A/m^2$ and even higher) which causes locally extremly high heat loads leading to strong evaporation and micro craters from which current- carrying plasmajets propagate. The theory now shows that the erosion rate due to evaporation is directly proportional to the average spot current and that the spot discharge becomes unstable if the pressure difference, spot pressure minus ambient pressure falls below about three times the magnetic pinch pressure at the crater orifice. By lowering the ambient pressure this

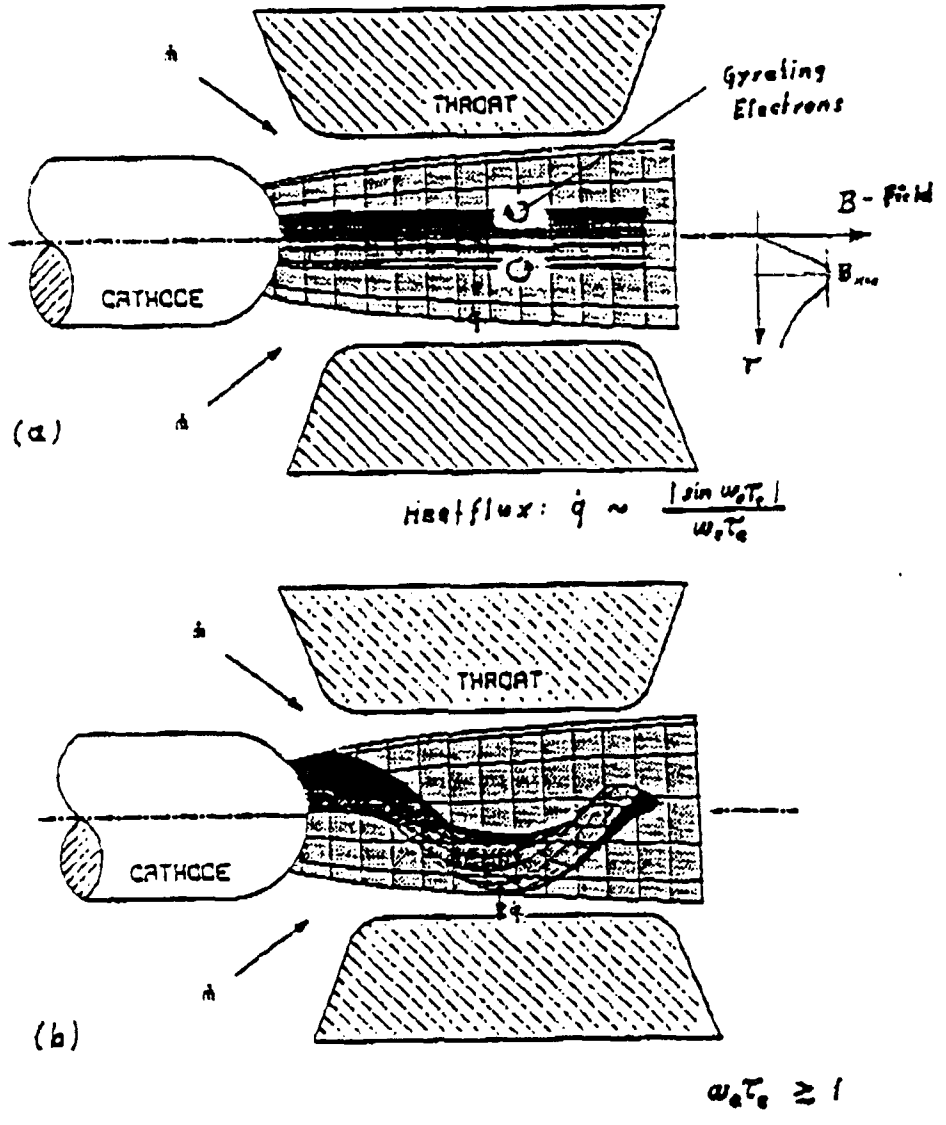

Figure 1: Illustration of Run Away Heating as a Consequence of the $\omega_e \tau_e$-Dependent Radial Heatflux. a) Rotational Symetric b) Distributed Current Carrying Plasmachannel

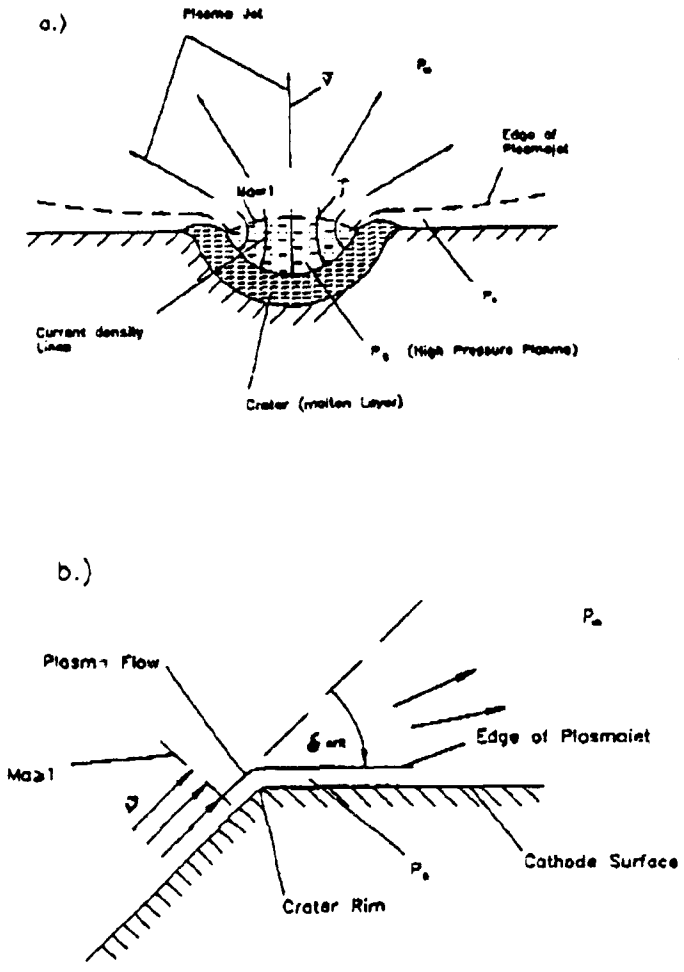

Figure 2: Illustration of a) Arc Cathode Spot with b) the Plasmaflow Arround the Crater Rim with Prandtl- Mayer Deflection Angle, δ

pressure difference gets smaller and the spots become already at lower spot current unstable.

Hence, by lowering the ambient pressure the erosion rate due to evaporation decreases what is in agreement with experimental findings. The threshold like increase now can be explained by the Prandtel Mayer deflection. If the ambient pressure or the pressure ratio, ambient- devided by spot pressure decreases below a certain value, the deflection angle exceeds a critical angle (see Fig 2). The jet plasma can hit the cathode surface outside the crater and evaporates additional cathode material and eventually increase the spot size and hence the average spot current.

EXAMINATION OF CHEMICAL APPROACHES TO STABILIZING COMPOSITE PROPELLANT COMBUSTION

AFOSR Contract No. F49620-90-C-0067DEF

Merrill K. King
R. H. W. Waesche

Atlantic Research Corporation
5945 Wellington Road
Gainesville, VA 22065

RELEVANCE OF RESEARCH

Over the years, the appearance of combustion instabilities in solid rocket motors, in developmental stages and even in operational systems (as the propellants age, with changes in burning characteristics) has cost hundreds of millions of dollars in developmental and refurbishment costs as well as leading to performance compromises associated with "fixes" to these instabilities. (Such acoustic instabilities, occurring over a wide range of frequencies, are generally intolerable in that they can lead to unacceptable interactions with control systems, structure, and/or payload and, in some cases, to catastrophic motor failure.) Before approximately 1960, instabilities occurred quite frequently in solid motors, particularly tactical motors where natural resonant frequencies are typically in the 1 Khz and higher regime. A fortuitous "fix" to many (though not all) of these instabilities was found to be addition of large amounts of metal additives to the propellant formulations, with the resulting condensed-phase products producing large amounts of damping of oscillations due to velocity lags dissipating large amounts of acoustic energy. (In fact, large amounts of metal were first added to propellants just for this effect, before it was found that such metal addition also provided significant performance gains.)

However, increasingly stringent mission requirements (with increased energy density) have led to increased incidence of instabilities in modern rocket motors, even with large amounts of metal additive. In addition (and probably more important), there is a major recent shift to a requirement for "reduced smoke" propellants for tactical missiles to improve survivability (by reducing detectability) of the missiles and their launch platforms, e.g., aircraft. This requirement precludes inclusion of more than very minor amounts of metal particles in propellant formulations, leading to a considerable increase in the occurrence of instability problems due to removal of a major accoustic energy sink (damping term) associated with the condensed-phase products. Accordingly, it is important that an alternative approach to alleviating instability problems, namely reduction of driving (acoustic energy source) terms be addressed. One major source term (generally the most important source) is associated with interaction of an acoustic wave with the solid propellant combustion processes. Both pressure and flow oscillations associated with an acoustic wave can cause solid propellant burning rate (energy release rate) oscillations which in turn can feed energy into the acoustic wave.

The relationship between burning rate oscillations and pressure oscillations is referred to as the pressure-coupled response function (a complex variable) of the propellant, while that between burning rate oscillations and velocity oscillations is referred to as the velocity-coupled response function

(although the latter is generally agreed not to be an intrinsic propellant property, depending strongly on the structure of the local mean flowfield). Attention here will be restricted, at least for the time being, to the pressure-coupled response function; it is easily shown that the real part of this complex response function is the important quantity as regards driving of acoustic waves, with relationships between the growth constant for oscillations and the pressure-coupled response function being presented and discussed in numerous references, most notably CPIA Publication 290, "Combustion Instability in Solid Rocket Motors." For typical scenarios, it is found that the pressure-coupled response is a major contributor (driver) in the acoustic energy balance.

Accordingly, development of means of reducing the amplitudes of the pressure-coupled response functions of a wide range of solid propellants, leading to significant reduction of the driving terms in acoustic energy balances for motors, should lead to major reduction or elimination of instability problems in motors utilizing such propellants. Thus, it is apparent that development of a systematic approach (principle) to reduction of the magnitude of composite propellant pressure-coupled response functions would be of tremendous potential importance to the solid rocket field.

TECHNICAL APPROACH

For many years, analysts have attempted to estimate pressure-coupled response functions for composite propellants using theoretical approches (in general, equivalent to the well-known Z-N approach) which are strictly applicable (at best) for homogeneous propellants. As shown by King in the early 1980's (utilizing very simplified composite propellant combustion models), composite propellants provide an additional potential destabilizing mechanism beyond those treated by the Z-N type approaches. This mechanism involves production of oscillations in the oxidizer/fuel ratio of "slugs" of propellant gases leaving the propellant surface (and thus oscillations in the gas-phase heat release) accompanying oscillations in surface temperature, due to different activation energies for the fuel and oxidizer surface ablation processes. Based on the existing literature, it appears that the ablation of ammonium perchlorate oxidizer has a somewhat higher activation energy than the ablation of typical HTPB binders (by approximately 5 Kcal/mole). Thus, upward perturbations in surface temeprature will be accompanied by similar upward perturbations in oxidizer/fuel ratio of "slugs" of gas leaving the propellant surface; since AP/HTPB formulations are generally fuel-rich, thus will in turn lead to increases in gas-phase heat release with increases in surface temperature, a destabilizing mechanism as shown numerically by King in the aforementioned study utilizing simplified gas-flame models. Most important, this reasoning suggests a possible significant fundamental approach to development of a class of AP-composite propellants which will burn stably in a much wider range of motor conditions than do current formulations; this approach is centered around development of means of increasing the temperature sensitivity of fuel ablation or decreasing that of oxidizer ablation, thus lowering $E_{OXIDIZER} - E_{FUEL}$, the effects of which are depicted in the following figure.

CURRENT RESEARCH STATUS

At this time (late March 1991), an analytical modeling study of the effects of differential activation energies of ablation of fuel and oxidizer in composite propellants on pressure-coupled response functions is underway. A complex steady-state model of unimodal-oxidizer composite propellant combustion (derivative of the classic BDP approach) developed by King and used

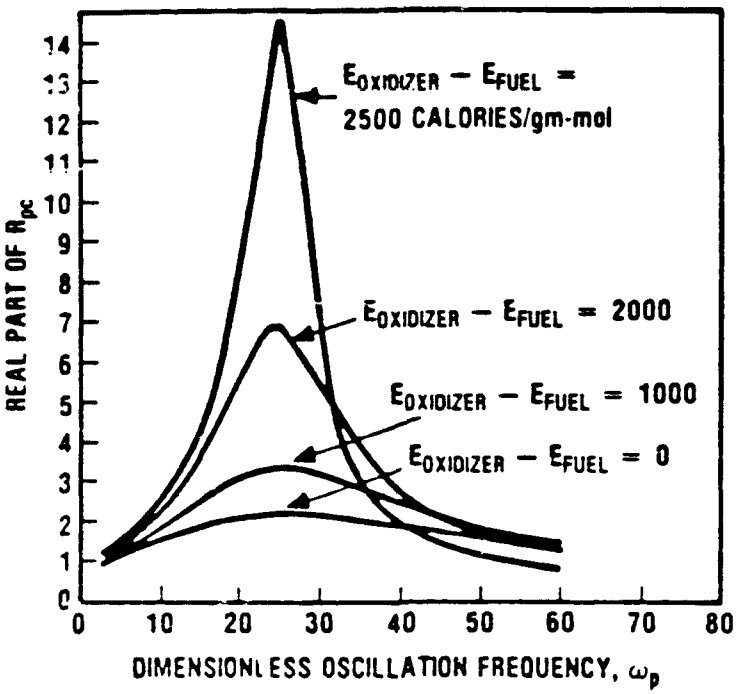

EFFECT OF ALLOWANCE FOR DEPENDENCE OF OXIDIZER/FUEL RATIO OF GASES LEAVING THE SURFACE ON SURFACE TEMPERATURE.

successfully as part of an erosive burning study has been modified to eliminate a discrepancy present in most, if not all, of the BDP-type models. [In these models, the relative surface areas of oxidizer and fuel are calculated on geometrical considerations, with the ratio of the area of the fuel to the planar oxidizer surface area being assumed to be equal to the volumetric ratio of fuel to oxidizer in the formulation; as a result, due to different volumetric ablation fluxes of fuel and oxidizer (in general) mass is not conserved. That is, the mass ratio of oxidizer and fuel ablation is not in general equal to the mass ratio of these ingredients in the propellant.] This deficiency has been corrected in the modified steady-state model in which a trial-and-error approach regarding calculation of fuel surface area associated with a given oxidizer planar surface area is utilized to ensure that the ratio of the products of areas and mass fluxes of oxidizer and fuel is equal to the mass ratio of these ingredients in the propellant. This revised model has been calibrated against an extensive database for AP-composite propellant strand burning rates at various pressure for various AP/HTPB formulations developed as part of the aforementioned erosive burning study.

Currently, a perturbation analysis of this steady-state model consisting of a Fourier analysis of the solid proellant subsurface region plus a quasi-steady-state analysis of surface and gas-phase processes, including allowance

for gas composition perturbations is underway. It is anticipated that by the time of the Contractor's Meeting the unimodal oxidizer analysis will have been completed and extension to treatment of multimodal oxidizer formulations will have been initiated. As part of this study, the effects of partial adjustment of the oxidizer and fuel areas to oscillations in ablation fluxes is being treated and will be examined parametrically. (For very rapid oscillations, there will be no time for such adjustments, while for slow oscillations, approacning zero frequency, such adjustment will be total. Estimates of the degree of response of relative surface areas to mass flux oscillations will be made based on the ratio of oscillation period to the time required to burn through a propellant thickness equal to the oxidizer diameter.) Results of these studies, demonstrating the theoretical potential for reduction of pressure-coupled response functions by lowering of the oxidizer ablation activation energy or raising of the fuel ablation activation energy will be presented.

FUTURE RESEARCH

If the theoretical studies indicate promise for the proposed approach to control/reduction of pressure-coupled response functions of AP-composite propellants, an experimental program to test the concept and, hopefully, to eventually lead to reduction of sensitivity of composite propellant burning rate oscillations to imposed pressure oscillations through tailoring of differential sensitivities of oxidizer and fuel ablation to surface temperature will be initiated. This aspect of the research will consist of two major phases. In the first phase, various approaches to decreasing the temperature sensitivity of oxidizer ablation/decomposition and/or increasing the temperature sensitivity of fuel ablation/decomposition will be examined. At this time, it appears that the most promising approaches to modifying the oxidizer ablation characteristics would involve occlusion of possible catalysts in the oxidizer crystals or co-crystallization of mixed oxidizers (such as ammonium perchlorate and hydroxyl-ammonium perchlorate, for example). With respect to modifying the temperature sensitivity of fuel ablation, various approaches including use of catalysts, substitution of various moieties on the basic polymer chains, and variation of crosslinker type and level are available. In this phase of the work, techniques developed by Tom Brill (University of Delaware) for simultaneously measuring ablation rate and surface temperature of the ingredients at extremely high heating rates will be employed.

After ingredients (fuel and oxidizer) with a range of sensitivities of ablation rate to temperature have been developed, combinations yielding a range of values of ΔE will be chosen for determination of R_{pc} versus frequency characteristics in standard T-burner testing. From these tests, corroboration or refutation of the postulated mechanism of control of response function characteristics will be established. If the approach offers significant promise, further refinement of the analysis will be carried out with guidance from the experimental results and further development of means of controlling the relative temperature sensitivities of fuel and oxidizer ablation, with consideration of other practical formulation constraints and objectives, will be pursued.

EFFECTS OF VORTICITY TRANSPORT ON COMBUSTION STABILITY

AFOSR Grant No. 90-0159

Principal Investigator: Dr. G. A. Flandro

Georgia Institute of Technology
School of Aerospace Engineering
Atlanta, GA 30332-0150

SUMMARY

Cold-flow experiments have verified the important role played by vorticity transport in major processes involved in rocket motor combustion instability. Many of these processes such as the coupling of the acoustic field to time dependent combustion of the propellant are strongly affected by the velocity and pressure distributions within the combustion chamber. The experiments and the analyses carried out in this research have shown that vorticity transport strongly affects the velocity distributions in critical regions of the chamber. For example, it produces a velocity overshoot near the burning surface approximately twice the amplitude of the centerline acoustic velocity amplitude. The phase angle relative to the pressure wave differs dramatically from the simple plane axial acoustic wave model used in virtually all current combustion instability models. Representations of combustion instability effects based on simple velocity distributions are therefore highly suspect. Analyses of particle damping, velocity coupling, and pressure coupling interactions depend crucially on the geometry and phase of the waves. The work described here is part of a collaborative effort with United Technologies Chemical Systems Division (CSD) to greatly expand the understanding of this phenomenon and to incorporate it properly into predictive motor stability calculations.

VORTICITY TRANSPORT IN COMBUSTION INSTABILITY

Vorticity is produced when combustion gases are produced at the burning surfaces of a solid rocket motor combustion chamber; the entire field is dominated by rotational flow effects. The importance of vorticity in controlling the mean flow characteristics is well-known[1,2]. Since the boundary conditions require that the gas flow enters the chamber in a direction normal to the surface, there is a strong shear effect caused by the axial flow through the chamber leading to vorticiy production. Analogous effects should be expected in an unsteady flow superposed on the rotational mean flow. Cold-flow experiments involving axial acoustic waves in a porous tube with injection show that this is indeed the case[3,4]. The measured velocity field exhibited a velocity overshoot near the porous surface approximately twice the amplitude of the centerline acoustic velocity amplitude. The phase relative to the pressure wave departs greatly from the simple plane axial acoustic wave model. Representations of combustion instability effects based on simple velocity distributions are therefore highly suspect. For example, analyses of particle damping, velocity coupling, and other surface interactions depend crucially on the geometry of the waves.

This research shows that inclusion of vorticity transport accounts for the observed effects. The velocity overshoot is caused by a traveling shear wave that is generated at the surface and propagates radially at the mean flow speed. Its amplitude diminishes because of viscous damping and because the radial mean flow component approaches zero at the chamber axis. The shear wave results from vorticity introduced because the flow must enter the chamber in a direction normal to the surface. It is not necessary to invoke the effects of viscosity directly in order to account for the main features of the flow.

The theoretical maximum velocity overshoot is twice the amplitude of the acoustic wave, and the unsteady velocity perturbation is very nearly in phase with the pressure at the injection surface

instead of 90 degrees out of phase as assumed in much combustion instability modeling. The depth of penetration of the shear wave into the chamber, its wavelength, and overshoot amplitude are controlled by two Reynolds numbers based, respectively, on the injection speed of the mean flow and the acoustic wavenumber. For low-order axial modes in rockets, the rotational perturbations dominate the flow. They also exhibit a strong axial dependence that modifies the apparent combustion response in a manner similar to that usually attributed to the classical velocity coupling mechanism.

APPROACH

The problem is being analyzed at several levels in this research. A simple, inviscid model demonstrates all major features of the observed flow in the vicinity of the injection surface. However, unlike the rotational mean flow analog, it is necessary to account for viscous losses explicitly to accurately represent the unsteady field throughout the chamber. A similarity solution of the complete problem including the axial dependence has been completed. In regions of the chamber not dominated by turbulence agreement with the cold flow data is quite good. Although these analyses provide clarification of many of the interactions, it is necessary to resort to a complete numerical simulation of the flow field to produce a complete representation of the vortical gas motion. Therefore, an important part of the research has centered on a complete solution of the three-dimensional time-dependent Navier-Stokes equations including the effects of turbulence. Cold-flow experiments are being conducted by CSD to provide a much more detailed set of measurements of the velocity and pressure distributions in a realistic simulation of a rocket motor. The analytical and numerical solutions have been configured so that they can be readily applied to any geometry. One of the numerical grids is an exact representation of the CSD porous tube experiment. The validity of the numerical solutions will be established by direct comparison to the new experimental data as it becomes available.

EXPERIMENTAL DATA

Recent cold-flow experiments[3] have dramatically demonstrated that the simplified models of time dependent gas flow used in virtually all current combustion instability analyses cannot represent a correct portrayal of the flow field under the conditions described. The experiments were executed as part of a study of velocity coupling. The apparatus consists of a porous tube with mean gas flow (nitrogen) entering normally through the surface and exiting through a choked nozzle; axial acoustic waves are excited by a rotating valve at the nozzle end. Of central interest here are the hot wire measurements of axial acoustic velocity distributions. Figure 1 shows data points from six separate tests carried out under identical thermodynamic and geometrical conditions. The measurements were made at the first axial mode resonance (84 Hz). Data are normalized to the center-line reference velocity. Figure 2 is the corresponding phase angle distribution relative to the pressure fluctuations. Measurements were taken by traversing a two-axis hot-wire probe radially at a location several inches from the closed end of the chamber.

The time-dependent velocity and phase distributions are grossly different than those expected on the basis of linearized acoustic theory. There is large radial dependence of both the wave amplitude and phase with largest deviations from the acoustic plane wave near the sidewall. Deviations apparently decrease as the chamber axis is approached. The expected plane wave behavior is limited (for the conditions of the test) to a small volume near the axis of the chamber. In the absence of a correlating theory, the plots suggest that there are large radom errors in the measurements. However, at any given radial position there seems to be reasonably good reproducibility suggesting that an organized behavior is responsible for the deviations.

The normal mean influx boundary condition, which applies to both the steady and unsteady gas motions, leads to the generation of vorticity that affects the entire field since it is generated at the surface and is convected with the mean flow. The fluctuating velocity normal to the surface must "turn" so that it merges smoothly with the axial acoustic motions in the volume of the chamber. Since the fluctuating component must satisfy a no-slip boundary condition (the oscillating mass flux must enter the chamber at 90° to the surface), then an oscillatory component of vorticity must also be generated.

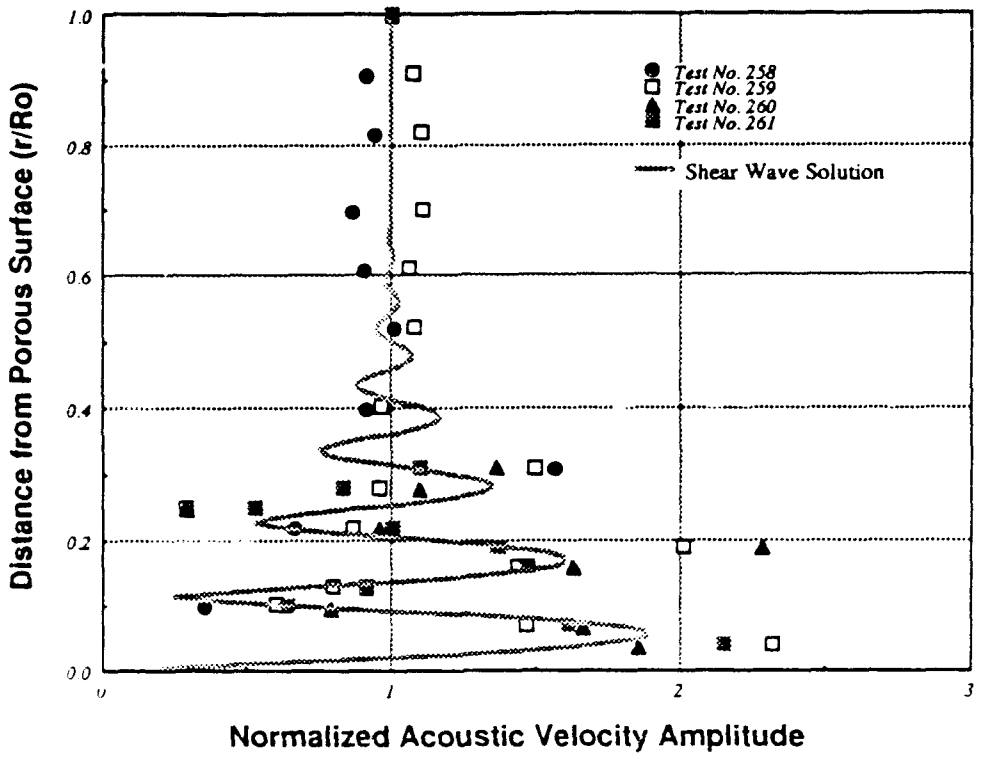

Figure 1. Measured Wave Velocity Amplitude vs Distance from Surface

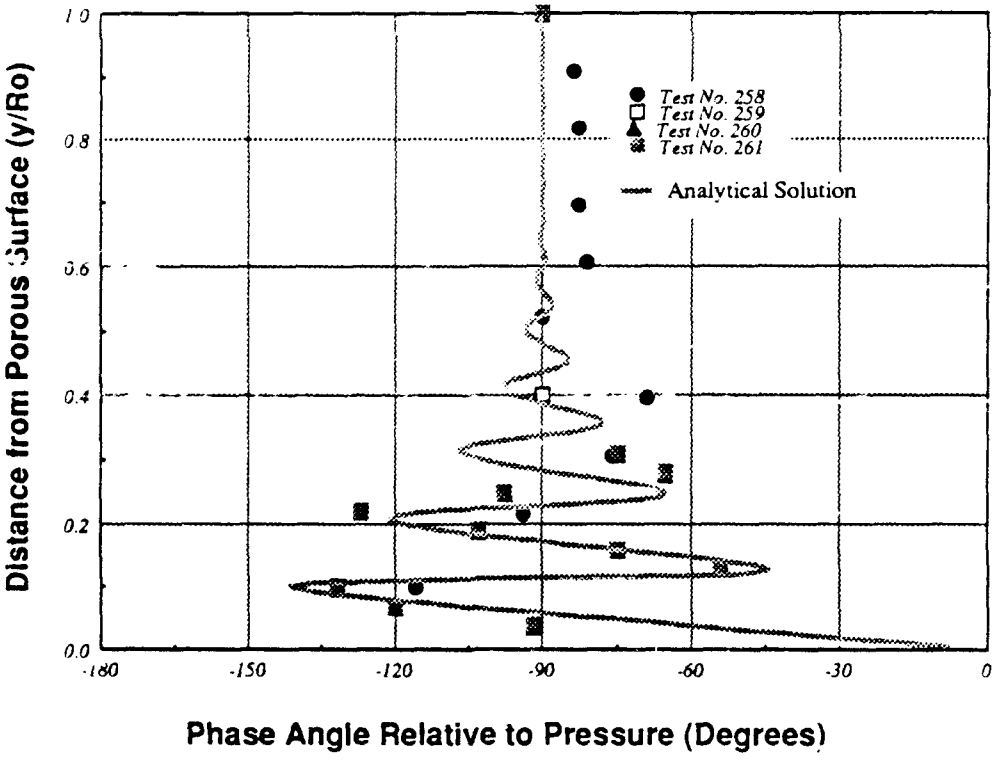

Figure 2. Measured Phase Angle vs Distance from Surface

CURRENT STATUS OF THE RESEARCH

The analysis has three main goals: (1) to determine the role (if any) played viscosity in determining the time-dependent flow field in the vicinity of a burning propellant surface and throughout the chamber, (2) to ascertain the basic dependence of rotational flow effects on chamber geometry and the physical characteristics of the gas flow, and (3) to establish the proper direction for further evaluation of the effects of the time-dependent shear effects on motor stability assessment procedures. The cold flow data offer a unique opportunity to validate the theoretical results directly and to expose any weaknesses therein. Two analytical approaches have been used. In the first, and simplest one, viscous forces are ignored completely. In the second, viscous forces are retained along with the associated mathematical complications. A numerical approach is required in evaluating the results. A full computational (CFD) attack is also used in order that all flow interactions including turbulence and realistic mean flow and chamber effects can be accounted for.

The analyses show that effects of vorticity transport markedly affect the time-dependent velocity distributions in rocket motor flows. The motion consists of perturbations to the assumed axial acoustic plane waves caused by traveling shear waves generated at the surface. These waves are generated because the flow must enter the chamber radially; vorticity is thereby introduced. This is the direct analog of the corresponding rotational mean flow effects.

The existence of the disturbances does not require the presence of viscous forces in the volume of the chamber (other than those implied in the normal injection process). However, the viscous shear forces induced in the time-dependent case are of the order of inertial forces and cannot be neglected in mathematical modeling. They act to damp the shear waves as they propagate toward the axis. Additional effective damping results from the interaction with the radial mean flow. The result is a set of rapid radial fluctuations in the amplitude and phase of the time-dependent flow; the expected plane wave motion is confined to a region near the chamber axis.

The penetration depth of the perturbations depends on two Reynolds numbers, one related to the injection speed of the gases, the other to the acoustic particle velocity or frequency. For longitudinal modes of oscillation, these effects dominate the gas motions. Near the injection surfaces or burning propellant, the velocity magnitude overshoots that of an acoustic plane wave by a factor of up to two. There are also significant phase distortions. The phase angle near the surface is nearer a lag of 0° than the 90° assumed in simple theories.

For low-order axial modes and injection speeds typical of rocket combustion, the shear waves fill the chamber. The influence on particle damping and other combustion stability elements obviously requires attention. Effects on particle damping, velocity coupling and pressure coupling response are being evaluated using the results of the analysis. These are in a form directly applicable in providing corrective procedures for motor stability computations. Inclusion of these effects significantly improves both physical understanding and predictive capability in combustion instability problems.

REFERENCES

1. Culick, F.E.C., "Rotational Axisymmetric Mean Flow and Damping of Acoustic Waves in a Solid Propellant Rocket," AIAA J. 4:8, 1462-1464, August 1962.

2. Dunlap, R., Willoughby, P.G., and Hermson, R.W., "Flowfield in the Combustion Chamber of a Solid Propellant Rocket Motor", AIAA J. 12:10, 1440-1442, Oct. 1974.

3. Brown, R.S., and Blackner, A.M., Willoughby, P.G., and Dunlap, R., "Coupling between Velocity Oscillations and Solid Propellant Combustion", AIAA Paper 86-0531, AIAA 24th Aerospace Sciences Meeting, Jan. 1986.

4. Dunlap, R., et al, "Internal Flow Field Investigation," AFRPL TR-86-104, March 1987.

5. Flandro, G.A., "Solid Propellant Acoustic Admittance Corrections", J. Sound and Vibrations 36:3,297-312, March 1974.

6. Flandro, G. A., "Nonlinear Combustion of a Solid Propellant with Velocity Coupling," Paper No. 83-1269, AIAA 19th Joint Propulsion Conference, June 1983.

Fundamental Research on Erosion in Magnetoplasmadynamic Thrusters

(AFOSR Grant No. 87-0360)

Principal Investigators: V. V. Subramaniam and J. W. Rich

Department of Mechanical Engineering
The Ohio State University
Columbus, Ohio 43210

SUMMARY/OVERVIEW:

The purpose of this research is to understand and quantify the mechanisms responsible for erosion in steady state magnetoplasmadynamic (MPD) thrusters. This is an important step in being able to predict thruster lifetimes. A major if not dominant erosion mechanism in the diffuse mode, is evaporation. This analytical work aims to understand this mechanism in particular, its limits, and to provide quantitative models in order to estimate the electrode lifetimes.

TECHNICAL DISCUSSION

Erosion processes depend on a complex coupling between plasma discharge characteristics, plasma-wall interactions, and electrode phenomena. In particular, erosion rates depend on whether the current conduction is through localized spots, or via a diffuse (distributed) mode. Spots are detrimental to the electrode material because of their high erosion rates. Therefore, it is important to understand how and under what conditions they may be formed, and exactly when diffuse mode behaviour ends. Much of the focus of this research is on the cathode, although the anode has also been studied. The thermal response of the electrodes at steady state has been studied and for the first time, been coupled to existing models of the flowing plasma[1-5]. These will be briefly reviewed next, followed by a short summary of ongoing and planned research.

Recently developed simple models of the electrode-adjacent sheath have revealed a thermal runaway mechanism that can limit diffuse mode operation[1,2]. The thermal runaway is caused by a positive feedback between electron bombardment and thermionic emission. This is predicted to occur at high total currents for a given mass flow and thruster geometry, for both the anode and the cathode. Limits have been derived for both the minimum sheath voltage drops as well as the maximum local surface temperatures at which this thermal runaway occurs. The predicted critical surface temperatures for tungsten and thoriated tungsten (approximately 3200 K and 2850 K respectively) are well below the melting temperature. In addition to identifying limits to steady state operation, electrode surface temperatures and evaporative erosion rates have been predicted for a given steady state

operating point. The steady state electrode surface temperature is related to the global parameters such as electrode material, geometry, discharge current, and propellant mass flow rate. Once these quantities are specified, the profiles of current density, charged particle number density, and temperature versus distance along the electrode can be computed for the core flow far away from the walls. These are computed by solving the quasi one-dimensional non-equilibrium ionizing MPD equations[3,4], which subsequently serve as boundary conditions to an approximate two-temperature non-equilibrium ionizing viscous boundary layer model[5]. This boundary layer model is then able to predict the charged particle number densities near the electrode surfaces. Finally, coupling these solutions to the electrode-adjacent sheath serves to simultaneously determine the sheath voltage drop as well as the surface temperature.

Recently, there have been reports of tests being conducted at the University of Stuttgart on steady state, coaxial, self-field MPD thrusters[6]. The results of these tests showed severe cathode damage in the middle as opposed to the ends of the cathode (see schematic in Fig. 1). It appears that the cathode melted and exploded from within suggesting that the internal temperatures far exceeded the surface temperatures. The authors of ref.[6] report that they believe the damage to be caused by ohmic heating in selected regions of the thoriated tungsten cathode. However, this phenomenon can and will occur at Onset according to our theory, and is intimately linked to the recently reported thermal runaway. Based on the mass flow rate, total current, and geometry of the Stuttgart DT2 and ZT1 thrusters, we have attempted to model the Stuttgart test. The results are displayed in Fig. 2 where the surface temperature and centerline temperature profiles versus distance along the cathode are shown. Indeed, as observed in the Stuttgart tests, the maximum temperatures occur *within* the cathode and in the middle regions rather than at the ends. This is easily understandable since both ends of the cathode are cooled and the centerline in an axisymmetric geometry is a line of symmetry and hence an adiabat. The exact location an extent of the damaged location cannot be compared between theory and experiment because other necessary details such as the amount of heat removal at the base of the cathode in the test were not reported. It is encouraging however, that (1) the damage predicted by the theory occured at the operating conditions in the experiment, and (2) the approximate location of the maximum temperature and melting damage occured away from the ends of the cathode as predicted by our theory.

Despite the apparent successes of our approximate models, two weaknesses remain. First, the behavior of the cathode sheath at conditions where the current densities are high (above $10^5\ A/m^2$) and the number densities are low (below $10^{20}\ m^{-3}$) is presently unknown. It is expected that the electron velocity distribution function will be substantially different from the Maxwellian distribution since the characteristic energy relaxation time is far greater than the momentum relaxation time. Consequently, the electrons in the near sheath region consist of two groups. These are the "slow" plasma electrons, and the "fast" electrons thermionically emitted from the electrode surface that gain substantial energy from the cathode fall. Based on this, a mechanism for enhanced ionization near emitting electrodes is being proposed and investigated. It is suggested that re-absorption of resonance radiation from the bulk of the flowing plasma produces a high density of excited states near the electrodes. These excited atoms are then subsequently ionized by electron impact from the thermionically emitted electrons when the sheath voltage drops reach levels on the order of the difference between the ionization potential and the energy of the first excited state. Second, the presence of these "fast" electrons in a region where only a few collisions take place, can excite large longitudinal oscillations[7]. This can lead to unsteady behavior in the terminal voltage which

is observed at Onset. Future research is therefore aimed at studying transport of resonance radiation in the MPD plasma, incorporating transient response in the sheath models, and multi-dimensional modelling of the MPD flow field with full finite rate ionization/recombination kinetics.

References

(1) V. V. Subramaniam, and J. L. Lawless, "Thermal Instabilities of the Anode in an MPD Thruster", *J. Propulsion & Power*, Vol. 6, No. 2, pp. 221-224, March-April 1990.

(2) K. S. Hoyer, V. V. Subramaniam, and J. L. Lawless, "Limits on Steady Diffuse Mode Operation of the Cathode in an MPD Thruster", accepted for publication in *J. Propulsion & Power*.

(3) J. L. Lawless, and V. V. Subramaniam, "Theory of Onset in Magnetoplasmadynamic Thrusters", *J. Propulsion & Power*, Vol. 3, No. 2, pp. 121-127, March-April 1987.

(4) V. V. Subramaniam, and J. L. Lawless, "Onset in Magnetoplasmadynamic Thrusters with Finite Rate Ionization", *J. Propulsion & Power*, Vol. 4, No. 6, pp. 526-532, November-December 1988.

(5) V. V. Subramaniam, and J. L. Lawless, "Electrode-Adjacent Boundary Layer Flow in Magnetoplasmadynamic Thrusters", *Phys. Fluids*, Vol. 31, No. 1, pp. 201-209, January 1988.

(6) M. Auweter-Kurtz, B. Glocker, H. L. Kurtz, O. Loesener, H. O. Schrade, N. Tubanos, T. Wegemann, D. Willer, and J. Polk, "Cathode Phenomena in Plasma Thrusters", paper AIAA-90-2662 presented at the 21st International Electric Propulsion Conference, Orlando, Florida, July 18-20, 1990.

(7) V. V. Subramaniam, and W. F. Hughes, "A Macroscopic Interpretation of Landau Damping", *J. Plasma Phys.*, Vol. 36, part 1, pp. 127-133, August 1986.

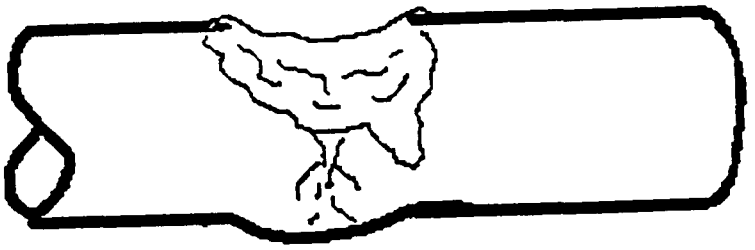

Fig.1:Schematic of the type of damage sustained by the DT2 and ZT1 thrusters after sustained steady state operation at 6500 A and 8000 A respectively. The total argon propellant flow reported was 2 g/s. For further details, please see reference [6].

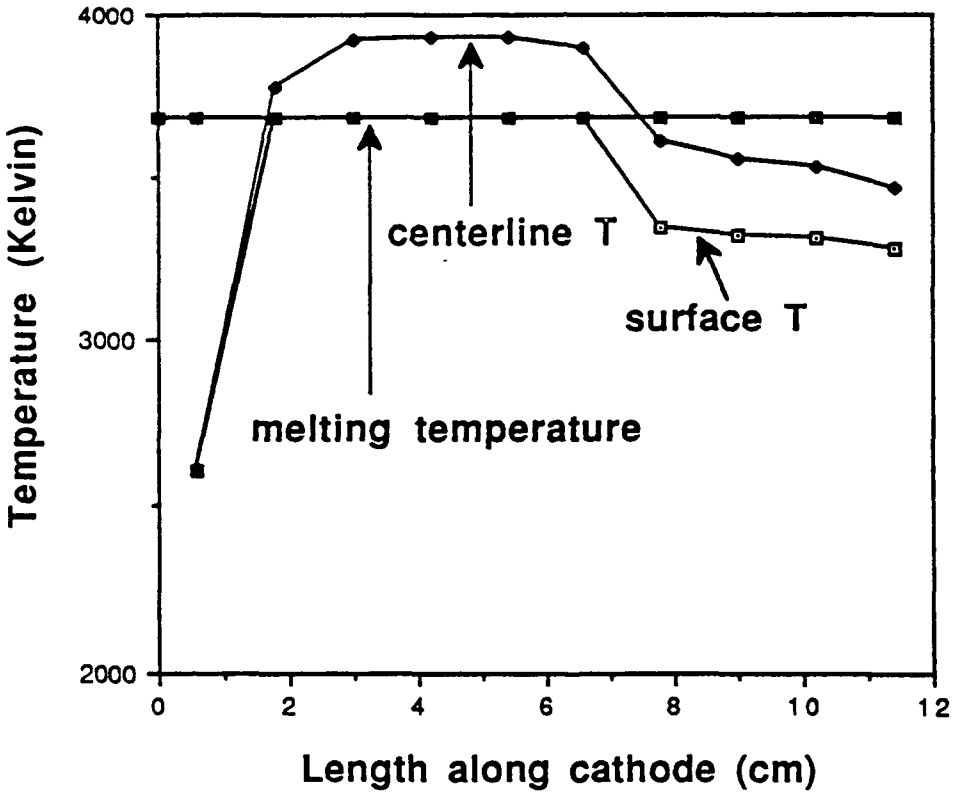

Fig.2:Shown here are calculated surface and centerline temperature profiles versus distance along the cathode for the Stuttgart ZT1 thruster. The horizontal line at 3680 K denotes the melting temperature of tungsten. Temperatures above this value cannot be taken seriously from the theoretical predictions, since the theory does not account for phenomena once melting has occurred. However, as the model suggests and as shown in this figure, the centerline temperature has exceeded the surface temperature in the select region thereby explaining the exloded cathode observed in the Stuttgart test.

DISTRIBUTED COMBUSTION IN SOLID PROPELLANTS

AFOSR Grant No: AFOSR-91-0152

Principal Investigators: M.W. BECKSTEAD, and
M. QUEIROZ

BRIGHAM YOUNG UNIVERSITY
PROVO, UTAH

Technical objective: Identify and develop a quantitative understanding of the mechanism of distributed combustion.

Approach: The current work is aimed at developing both an experimental and analytical basis for determining the mechanisms of distributed combustion. A Rijke burner has been developed at BYU and preliminary testing has been done to characterize the burner. Particles are added to the burner through a gas inlet and are then ignited by the flame. Preliminary data with aluminum and ZrC shows that the aluminum apparently interacts with the acoustics at more than twice the level that ZrC does. This burner will continue to be used to study the combustion of particles in both oscillatory and steady flow.

June 1991

COMBUSTION INSTABILITY
IN
SOLID PROPELLANT ROCKET MOTORS

The basis of current linear stability acoustic codes for solid rockets was developed by Culick and has been incorporated into the SSP code that is commonly used to make motor stability predictions for solid rockets. The analysis is based on the conservation equations for an acoustic cavity. A perturbation analysis is performed to put the equations into the form of a wave equation, which is then integrated, giving the acoustic contributions of the various physical mechanisms operating within the rocket motor.

The acoustic damping mechanisms that are usually accounted for include: particle damping, flow turning, nozzle damping, structural damping and wall damping. The predominant driving mechanisms are pressure and velocity coupled driving. Response function values for the pressure and velocity coupled driving must be obtained either from calculations or from measurements in a laboratory device (usually a T-Burner). The third driving mechanism considered is distributed combustion, but the theoretical foundation for determining distributed combustion is not well established, and there is no corresponding experimental measurement device available.

To calculate the stability conditions of a rocket motor, the effect of the dominant acoustic mechanisms must be determined by integrating over the entire surface (and corresponding volume) of the motor cavity. The net sum of the various contributions determines whether the motor is stable or unstable and must be determined as a function of the burn time. Because this procedure involves taking the difference of several mechanistic contributions to determine the stability margin, the final number may contain a considerable amount of uncertainty dependent on the magnitude and uncertainty of the various mechanisms.

The current work is aimed at developing both an experimental and analytical basis for determining distributed combustion, and will therefore focus on those physical mechanisms that contribute to distributed combustion.

COMBUSTION INSTABILITY IN SOLID PROPELLANT ROCKET MOTORS

Data from T-Burners

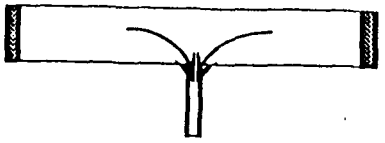

or

Calculate Response Function

Propellant Response Function
= f (n, A, B,Ω)

STANDARD STABILITY PROGRAM (SSP)

INPUT FOR MOTOR CALCULATIONS

Motor Geometry
Physical Properties
Propellant Properties
Acoustic Properties
- Particle Damping
- Flow Turning
- Nozzle Damping
- Velocity Coupling
- Distributed Combustion

Integrates acoustic mechanisms over motor geometry

If $\alpha > 0$
motor is unstable

If $\alpha < 0$
motor is stable

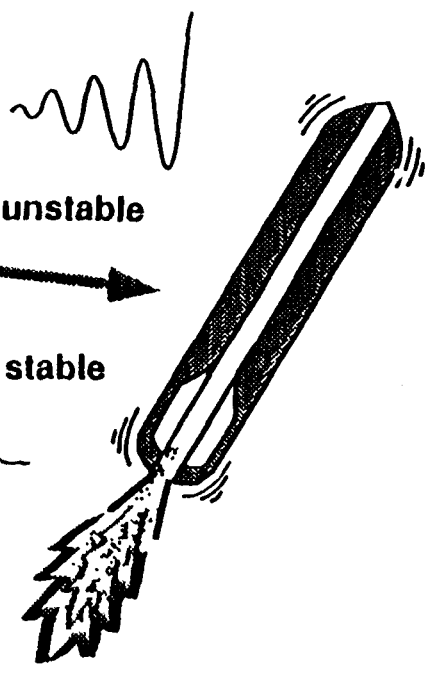

MOTIVATION: Distributed Combustion is a critical mechanism of combustion instability which lacks understanding

APPROACH: Study Distributed Combustion to give a broader overall understanding of combustion instability

MEASUREMENT OF DISTRIBUTED COMBUSTION

Acoustic suppressants have been added to low smoke and smokeless propellants for the past decade. For many years aluminum was a panacea for combustion instability. However, as the motivation to eliminate visible smoke in rocket exhausts has increased, aluminum began to be eliminated from propellant formations. In an attempt to avoid combustion instability, ingredients were sought that would act as acoustic suppressants. For the past decade, the suppressants most often used in tactical motors have been ZrC and graphite flake.

There are three predominant mechanisms whereby additives influence or suppress an acoustic wave:

(1) Viscous energy dissipation due to particle drag,

(2) Combustion response modification due to interaction of the additive with the burning surface (i.e. dynamic catalysis), and

(3) Distributed combustion of combustible additives as they burn through the volume of the motor.

As a particle leaves the propellant surface, it becomes a source of viscous drag and contributes damping according to the established laws of particle damping. Most particles currently used as additives can also be oxidized, and therefore, will ignite and burn. As they do so, the energy released by the particle combustion can drive the acoustics as distributed combustion, which can be either a positive or a negative contribution to the acoustic wave.

Within the concept of distributed combustion, there appear to be two predominant physical mechanisms that contribute to the acoustic interaction with a variable energy release. The first is the amount of energy released and the second is the rate of the combustion reaction (which is proportional to particle size). Studying different additives and different particle sizes should help in identifying the relative importance of the different mechanisms.

A Rijke burner has been developed at BYU and preliminary testing has been done to identify the mechanisms that lead to acoustic interaction (suppression or driving) by burning particles. Preliminary data with aluminum and ZrC shows that the aluminum apparently interacts with the acoustics at more than twice the level that ZrC does.

This burner will continue to be used to study the combustion of particles in both oscillatory and steady flow. The overall approach has been summarized in the attached figure. Particles are added to the burner through a gas inlet and are then ignited by the flame.

MEASUREMENT OF DISTRIBUTED COMBUSTION

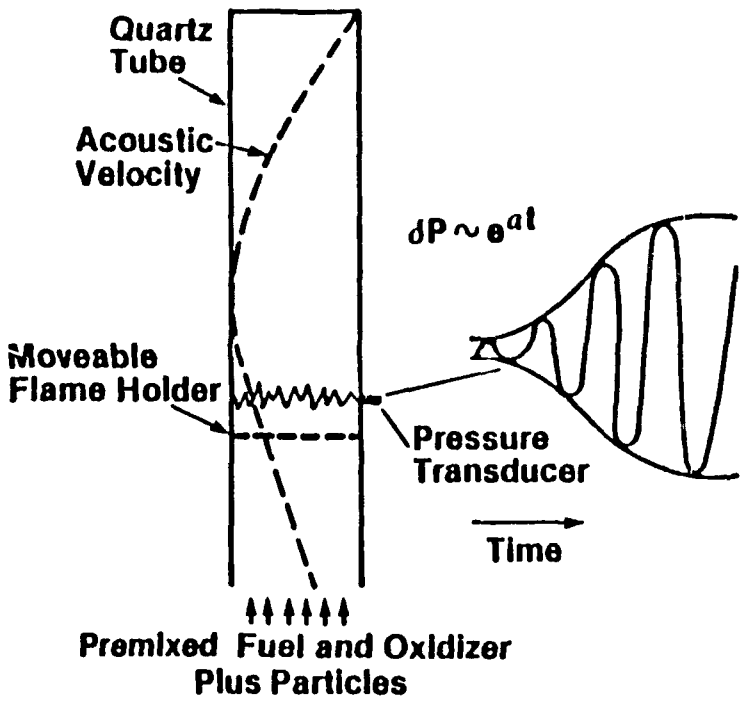

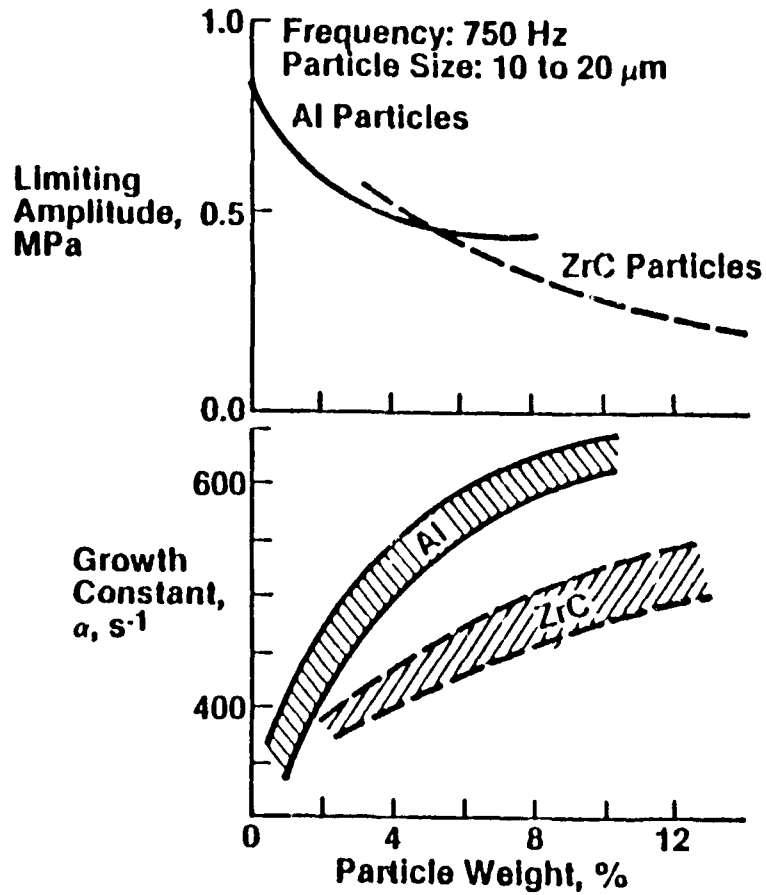

Research

- Establish Laboratory Burner Which Deploys Reacting Particles in Combustion Driven Wave.
- Model Energy Exchange Between Particles and Combustion Gas.

PARTICLE COUNTER-SIZER-VELOCIMETER (PCSV)

Particle Counter Sizer Velocimeter (PCSV) is a recently developed laser diagnostic technique for combustion systems with the potential of on-line, real-time, simultaneous measurement of particle size, absolute concentration, and particle velocity which typically requires less than a minute to process. PCSV performance has been demonstrated in diverse applications such as pulverized coal combustion, coal-water slurry atomization studies, and liquid sprays.

A PCSV has been obtained at BYU and will be available for use on this program. The PCSV's measurement principle is based on analysis of forward scattered light. Particle speed is determined directly using a transit timing technique. Both particle size and velocity depend on the optical system sample volume intensity distribution. The instrument has a wide dynamic range for particle size (0.2 - 200 microns), concentration (up to 10^7 for sub micron particles), and velocity (up to 200 m/s). The potential to make in situ measurements of absolute particle concentration, size, and velocity allows a much more complete analysis of the entire combustion process.

Different sizes of the aluminum will be tested to vary the surface area available for reaction and the combustion time as both should have a very significant influence on distributed combustion. The recently acquired BYU PCSV is particularly suited to obtain such data. Quantifying the effect of particle size will be very important in isolating dominant mechanisms. Utilizing a less reactive particle, such as zirconium carbide, aids in identifying the effect of heat release on the acoustic wave. Data from the previous study shows that the more reactive Al does show a greater acoustic interaction than the ZrC.

Testing will be performed using the PCSV to obtain fundamental particle combustion rates varying a variety of test parameters, such as:

1. particle type--Al and ZrC
2. Al particle size--- 19 μm, and > 30 μm
3. O/F ratio-- 0.9, 1.02, 1.10
4. gas temperature-- 3 values

NON-INTRUSIVE PARTICLE COUNTER-SIZER-VELOCIMETER • PCSV

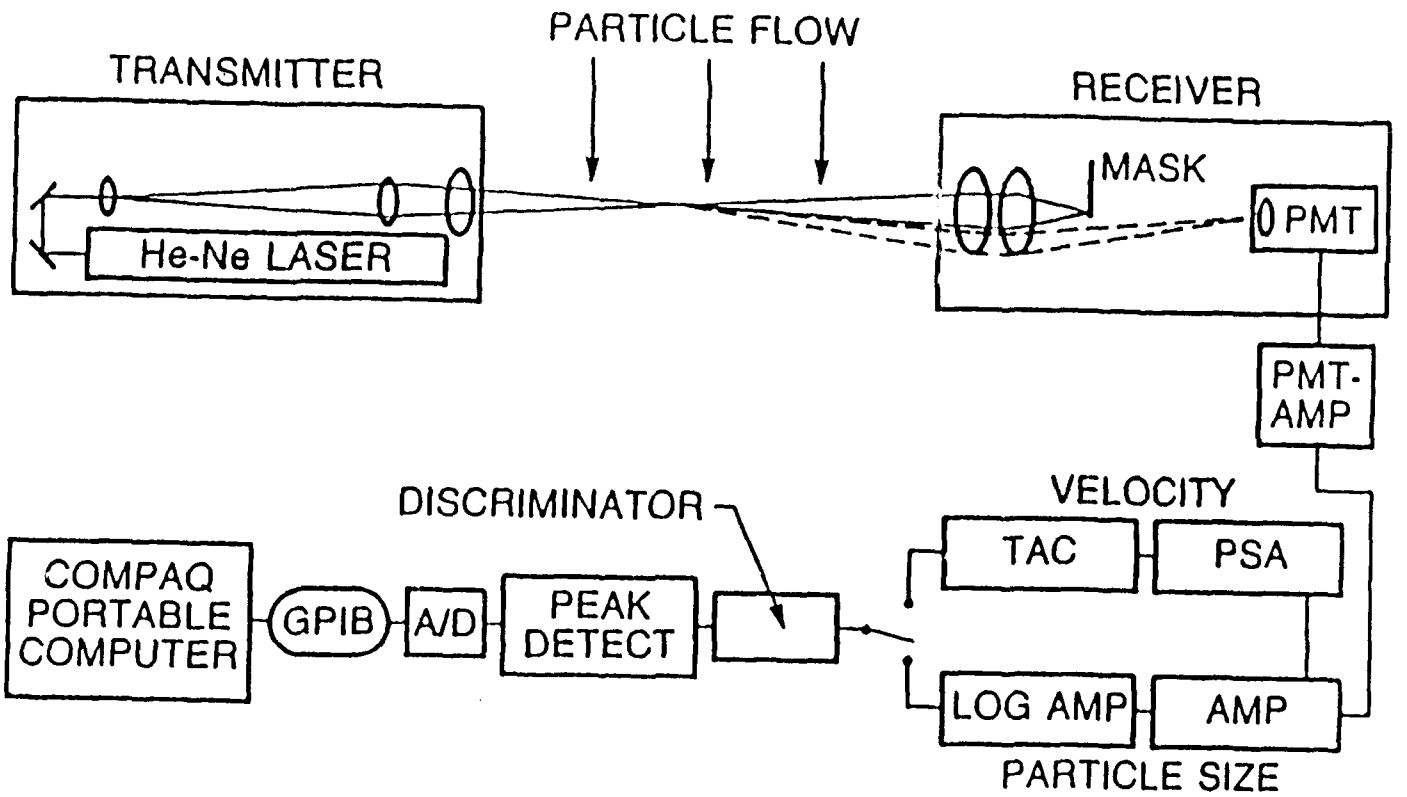

Schematic of PCSV-E showing Optics, Signal Processor and Computer.

FUTURE WORK

The technical objective of this program is to identify and develop a quantitative understanding of the mechanisms whereby acoustic suppressant additives burn and modify an acoustic wave (i.e. the mechanism of distributed combustion).

To aid in focusing on fundamental mechanisms, three types of particles will be studied. The baseline test condition is aluminum because it is known to burn vigorously. Zirconium carbide will be tested as a less reactive particle. A third inert material such as Al_2O_3 or SiO_2 will also be selected for testing.

Each of the particles to be studied will be tested at a few baseline conditions, but the aluminum will be tested at a variety of conditions, varying frequency, concentration, temperature, and O/F ratio. Although testing at varying particle concentrations is important, most testing will be done at relatively dilute levels (~1 to 5% additive) in order to minimize particle cloud effects.

Data to be obtained will consist of precombustion particle size distributions, gas flow rates, particle flow rates, acoustic pressure amplitudes (at 2 or more locations), and particle combustion tracking (using the PCSV).

Data analysis will include acoustic growth rate measurements, acoustic mode shape reconstruction, particle combustion times, viscous particle damping calculations, etc. The data will be recorded directly into a minicomputer, and data reduction will be performed digitally with the minicomputer.

The previously developed theoretical analysis of the Rijke Burner will be applied to the gas/particle system. The analyses will be applied to the various test configurations both with and without particles. The temperature data will be used to evaluate the convective heat transfer within the analysis allowing the determination of the overall system losses. Similarly, pressure measurements will be used to evaluate the acoustic mode shape which will, in turn, be used in evaluating the overall system response. A reaction model for the particles (i.e., a simplified response function) will be developed and included to allow for the dynamic response of the particles through the acoustic wave. The reaction model will be developed considering both vapor phase combustion (e.g. Al) and heterogeneous reaction at the particle surface (e.g. ZrC).

FRACTAL IMAGE COMPRESSION OF RAYLEIGH, RAMAN, LIF AND LV DATA IN TURBULENT REACTING FLOWS

(AFOSR Contract No. 88-0001)

Principal Investigators: Warren C. Strahle and Jechiel I. Jagoda

School of Aerospace Engineering
Georgia Institute of Technology
Atlanta, GA 30332

SUMMARY/OVERVIEW:

This experimental and analytical program is designed to provide a data base and computational methods for a flow of extreme technological importance-that of a turbulent reacting recirculatory flow behind a step. The experiment simulates the flame stabilization region in a solid fueled ramjet. There has never been a detailed probing of such a flow to test its predictability. Two components of velocity are measured by laser velocimetry while species concentrations and temperature are determined by Rayleigh scattering and Raman spectroscopy. The flow is modeled by a two equation turbulence model. Fractal based methods of data analysis are being developed in order to enhance the data reduction process. This will speed up the data acquisition process in the face of the low repetition rate laser used for Raman scattering. These methods are general, however, and should be of use to the turbulent reacting flow community at large.

TECHNICAL DISCUSSION:

The flowfield of interest is generated in a subsonic windtunnel with a backward facing step in which the solid fuel is simulated by injecting hydrogen plus a diluent (argon or nitrogen) through a porous plate on the floor behind the step. The tunnel is shown in Fig. 1. The porous floor is divided into three sections. The first part is blocked off, hydrogen and diluent are injected into the second section and pure diluent is injected into the third section to keep the wall cool.

The main effort during the past year was to completely map the mean and fluctuating velocity (two components), the nitrogen concentration and the temperature throughout the flowfield. The velocities are measured by laser velocimetry. This hot flow work followed earlier maps of the cold flow velocities, some of which were redone this year for consistency checks. The mean velocities are best illustrated by the streamline plot shown in Fig. 2. The difference between the hot and cold flows is readily apparent; combustion lifts the recirculation zone because of the density decrease and the reattchment point is moved downstream. For reference, the mean tunnel velocity at the step is 70m/s.

Representative turbulence intensities are shown in Fig. 3 for hot flow, where the dashed line is for cold flow. The turbulence levels are quite high in the recirculation zone, and combustion reduces them somewhat.

Nitrogen concentrations are measured by the intensity of the nitrogen Stokes line generated by the Raman spectroscopy laser. The mean concentrations are shown in Fig. 4, on the left. The bottom figure shows the result when nitrogen is substituted for argon in the diluent. The lack of any change shows that there is very little injectant in the flow and that the dominant source of nitrogen is the air. This fact has been exploited to infer the temperature. Under the assumption of unity turbulent Lewis number, the presence of a two feed system, and equilibrium chemistry the nitrogen density is a direct measure of the temperature for weak mean pressure variations, as occur here.

Temperature obtained from these observations through the perfect gas law is shown in the middle column of Fig. 4. Verification that the requisite assumptions are valid is shown by the dashed line in the figure fourth from the top. This line is the temperature obtained from thermocouple measurements, seen to be identical to that infered by Raman spectroscopy. The root mean square temperature fluctuation is shown in the right column of Fig. 4. The temperature fluctuations are quite high, and the greatest values occur in the shear layer region containing the maximum mean temperature gradient, as expected.

The two equation turbulence model used in conjuntion with the numerical prediction code has in prior years worked well in cold flows. Some difficulty is seen in prediction, however, in this hot flow. Second from the top in the middle column of Fig. 4 is shown the predicted (dashed line) temperature distribution compared with the experimental result. The analytical method predicts the "flame" to be too close to the floor of the tunnel. This problem was known last year, and several efforts to find the reason for this have not yet yielded an explanation. Efforts are continuing to find the root cause of the problem.

Several laser maintenance problems have delayed the final phase of the program, where joint measurements of temperature and velocity are to be gained. The covariance of the vertical velocity and temperature represents turbulent heat transfer in the (primary) vertical direction. Prediction of this quantity is considered a severe test for any analytical method. The joint measurements are currently underway and will be completed by the end of the current program year.

The joint measurements represent a good testing ground for the application of hidden variable fractal interpolation, a method which has undergone significant development this year. The laser repetition rate is low (.1 sec) for the Raman laser and the signal is, therefore, uncorrelated from point to point. The velocity data, however, are closely spaced in time. Using the experimental fact that the fractal dimension of both traces is the same (about 1.7) it is possible using the velocity trace as the basis to augment the temperature data by fractal interpolation. This reduces the run time necessary to gain a good covariance between temperature and velocity, just as has been shown earlier in this program for single variable fractal interpolation. Current development of the hidden variable (two variable) technique is complete and is awaiting the joint data, and application of the method will be made before the end of this program year.

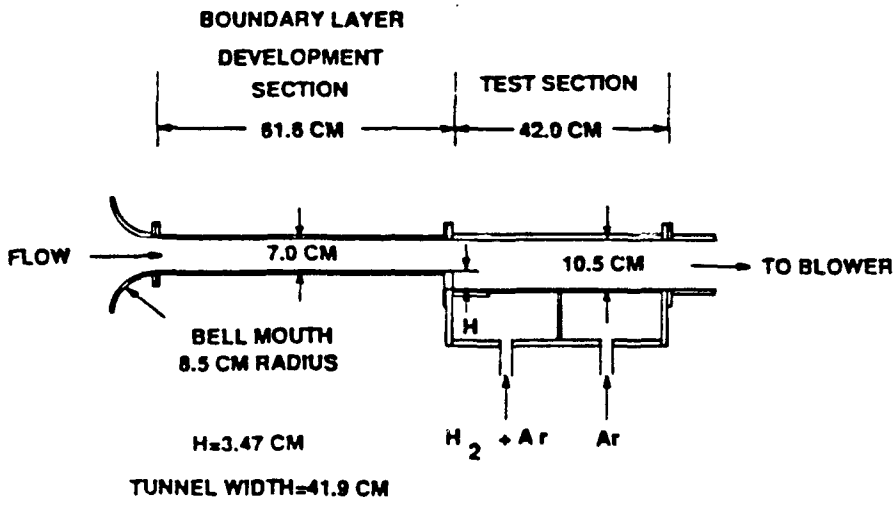

Figure 1. Windtunnel schematic.

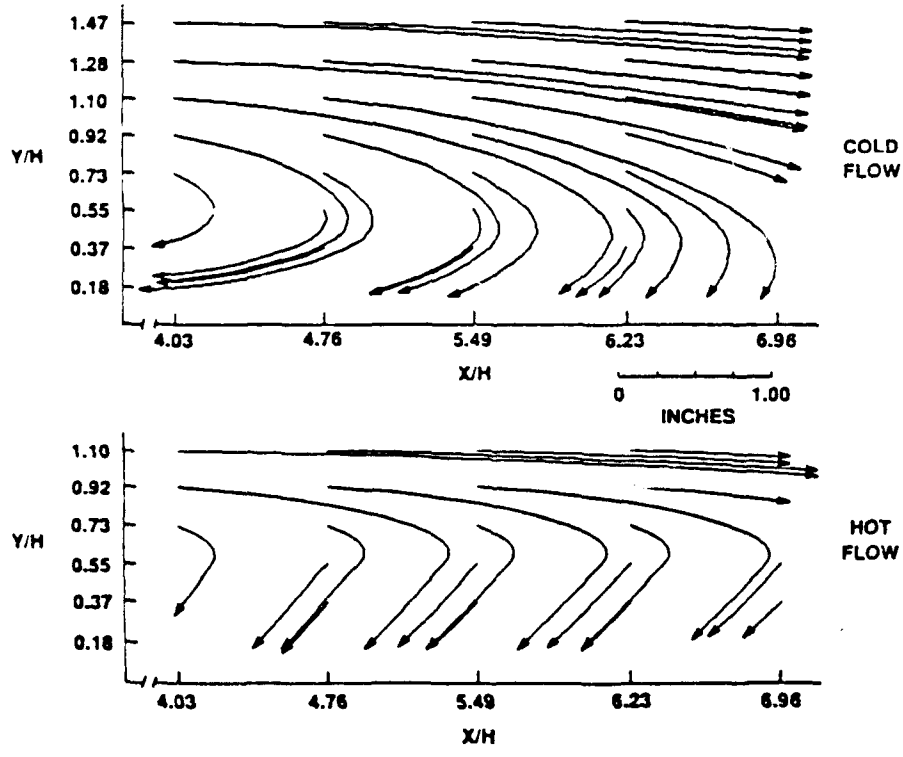

Figure 2. Streamline plots in cold (top) and hot (bottom) flow.

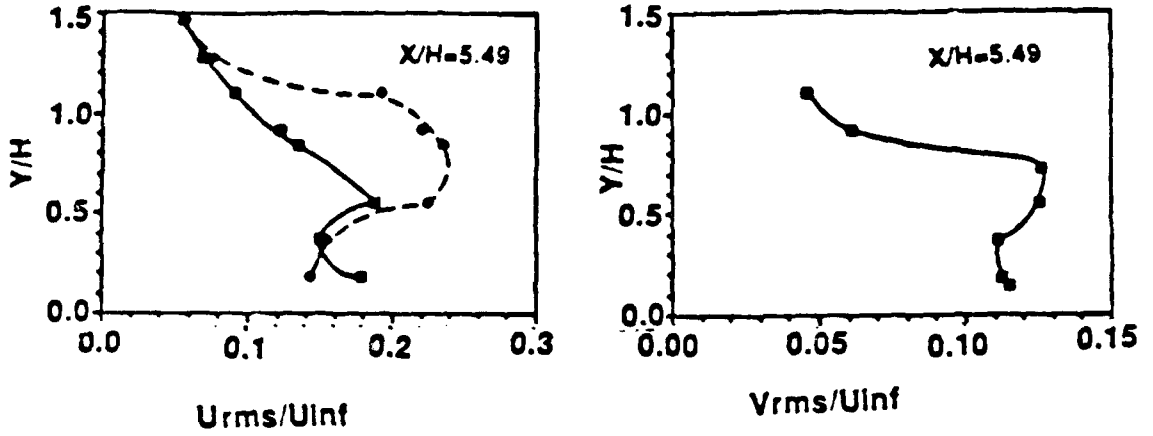

Figure 3. Turbulence intensities for axial (left) and vertical (right) velocities at one representative axial location. Dashed line is the cold flow result.

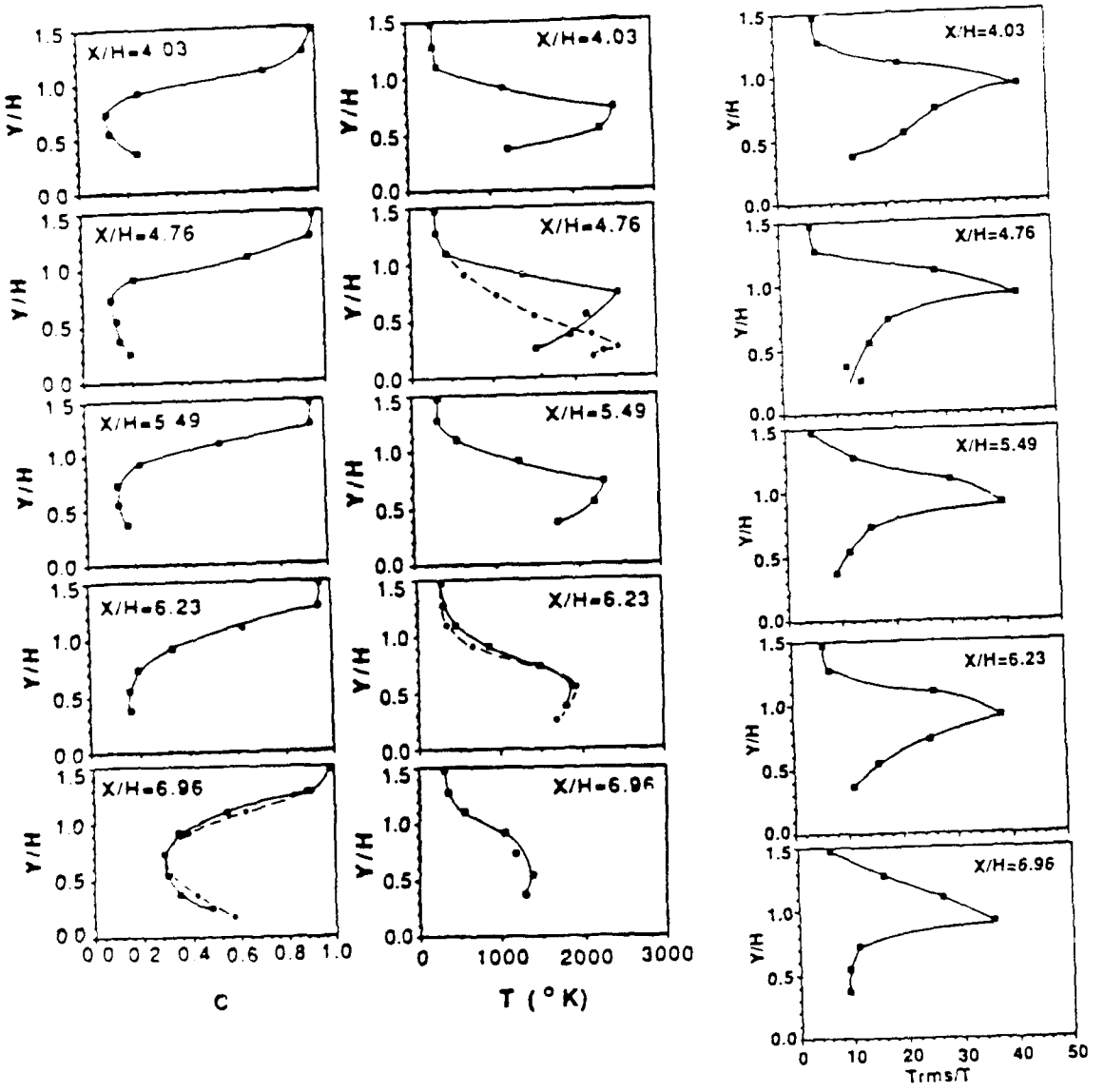

Figure 4. Nitrogen concentration (left), mean temperature (middle) and rms temperature fluctuation (right) for several axial locations.

CHEMICAL KINETIC DATA BASE FOR PROPELLANT COMBUSTION

(AFOSR CONTRACT-issa-90-0033)

Principal Investigator: Wing Tsang

Chemical Kinetics Division
National Institute of Standards and Technology
Gaithersburg, Maryland 20899

Summary:

This work is concerned with the development of an evaluated chemical kinetic data base of single step thermal reactions for use in the computer simulation of propellant combustion in the gas phase. Current efforts are aimed at the gas phase reactions involved in RDX decomposition. All of the possible reactions involving 28 of the most likely compounds that are present in such decomposition systems are considered. The work involves the collection and evaluation of mechanistic and rate information in the literature and the use of various methods for the estimation of rate data where information does not exist. The conditions to be covered range from 500-2500 K and 10^{17}-10^{22} particles/cm^3. The compounds whose reactions have now been covered are H, H_2, H_2O, O, HCHO, HCO, CO, NO, NO_2 HNO, HNO_2, HCN, N_2O, CN, NCO, HNCO. The reactions of the last three compounds involving 36 distinct interactions are the results of the present years activities.

Technical Discussion:

The goal of this work is to develop an evaluated chemical kinetic data base of gas phase reactions pertinent to propellent combustion. Such a data base can have important impacts on the formulation of such mixtures, the optimization of current systems and the design of new combustors. In order to give a complete description of the combustion process, the data base must contain scores of rate expressions of elementary reactions. For many years, the necessary experimental tools and theoretical understanding were not available for the development of such a chemical kinetic information base. The alternative procedure is a to identify key reactions and develop simple mechanisms. This is not an easy task. With these two major impediments, it is not surprising that as far as the chemistry is concerned much work in this area has been empirical. This implies the necessity of a great deal of physical testing. The expense of such efforts is a severe limitation on innovative efforts in this area.

In recent years a number of exciting scientific advances have made it worthwhile to consider the more fundamental approach described here. These include: a) Rapid progress in computational capabilities, so that the simulation of increasingly realistic physico-chemical systems are well or will be within our capabilities. Thus the information in a chemical kinetic data base can be immediately used. b) Development of experimental and theoretical capabilties in chemical kinetics, so that the needed rate constants can be measured or estimated. c) Extensive applications of powerful modern diagnostic techniques to laboratory systems, so that we are developing much better pictures of the micro-structure in both a physical

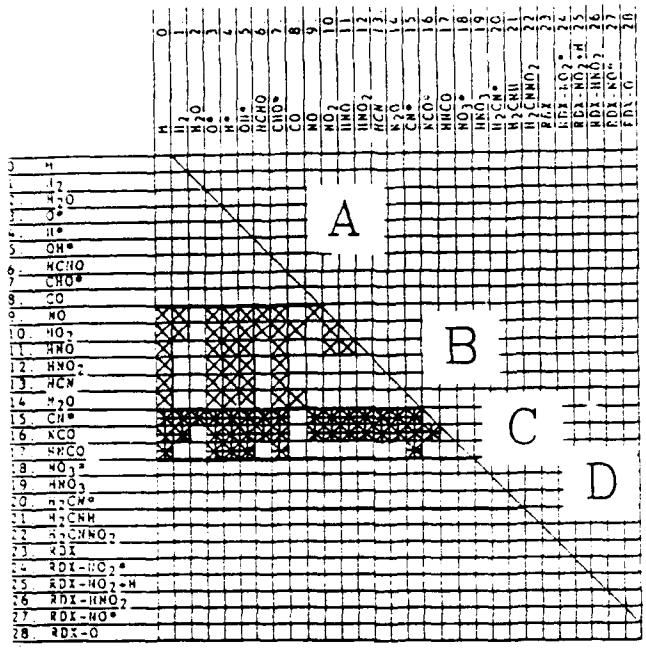

Fig. 1
Reaction grid
(A) from hydrocarbon decomp.
(B) previous year's work
(C) last year's work
(D) this year's work
(×, ✱) reactions covered

and chemical sense of combustion systems. The interpretation and the projection of such results to real system is however crucially dependent on the existence of a correct detailed model. One can always "fit" a particular experimental observation. Only the model with the correct inputs can be expected to project results to real systems.

The approach is based on considering all likely gas phase reactions that are applicable to RDX decomposition. The scope of the work is summarized in the form of the "reaction grid" in Figure 1. The axes contain all the likely species and the intersection of the reactants represents the reaction to be considered. Although there can be no questions regarding the inclusion of atoms and small molecules in the data base, mechanistic considerations enter into the selection of the larger species. We postulate that detrimerization occurs at a very early stage in the decomposition and that all linear species larger than the monomeric methylene nitramine are so unstable that they need not be considered. No claim is made that we have the correct mechanism. We regard this program as merely a first cut. As new data are accumulated species can be added or removed.

In the following we review briefly how we proceed with our evaluations. Having decided on the species to be included in the data base we begin by determining the thermodynamic properties. For many of the stable species the existing JANAF data base is accepted. The properties of the unstable species, many of them radicals, are subject to many uncertainties. For many of these cases we have carried out our own analysis. These are usually based on the existing kinetic data, since it is our experience that for unstable species the most reliable results are obtained from rate data in both directions, thus leading to an equilibrium constant. Since the entropies of many molecules can be estimated with a high degree of confidence, the heats of formation can then be deduced with high accuracy. There is at present no standard method for carrying out data evaluation in

chemical kinetics. Our experience in these matters has led to the following procedure. First preference is given to experimental determinations where the mechanism is clear-cut. Frequently, this is from direct determinations of the rate of disappearance or appearance of reactants or intermediates in real time. We have also found that in a complex (or apparently complex) situation where care and complete final (stable) product analysis are carried out very useful results can be achieved. In many cases these may not be individual rate constants, but very accurate ratios of rate constants. In this manner we are frequently able to generate a very accurate network of reactions. In the absence of kinetic data, thermodynamic considerations in the form of detailed balance are used. In other cases, rate constants are assigned on the basis of analogy or thermokinetic information. In all cases we assign an uncertainty value to our recommendations. It should be realized that this is a subjective number. It is based on the intercomparison of data sets, considerations imposed by related reaction mechanisms and the constraints imposed by thermodynamics and theory. It means that the user of the data should feel free to adjust the rate constant in his models within these limits.

Unimolecular reactions in the broadest sense, including not only decompositions and isomerizations but also combination and chemical activation processes, are rendered more complex than metathesis reactions by their dependence not only on temperature but also on the nature of the bath gas. There is at present a fully developed calculational method, the RRKM procedure, which provides a framework for projecting data over all relevant pressure and temperature ranges. We have applied this technique for a large number of reactions. The results have proven to be very satisfactory in correlating in a wide variety of data. The consistencies in the collisional efficiencies that we have derived have led us to use the general method for predictive purposes.

The reaction grid in Figure 1 is divided into a number of blocks. Block A consists of the reactions involved with formaldehyde oxidation. We have already prepared data sheets for these reactions in the context of hydrocarbon combustion. Block B contains reactions involving the smaller nitrogenated species. Work on these reactions was completed early last year. With its completion it should be possible to model HCHO-NO_2 combustion systems. A paper has been accepted for publication in the Journal of Physical and Chemical Reference Data. The work on the reactions in Block C has recently been completed. The paper is also being submitted for publication in the Journal of Physical and Chemical Reference Data. Its completion will permit the modeling of the HCN-CN-NO_2 system. It is expected that the overall process will involve continuous iteration between data evaluators, modelers and experimentalists.

We now consider some highlights of the current years efforts. Of particular interest is our analysis of the results for C_2N_2 decomposition at very high temperatures. This was of concern because there are no direct measurements on the combination of CN radicals and the approach was therefore to derive the rate constants on the basis of detailed balance. We found that the decomposition data could not be fitted by application of RRKM theory under weak collision conditions on the basis of the JANAF recommendations for the heat of formation of CN and have used instead a value 19 kJ/mol lower. Results are summarized in Figure 2. Furthermore, it appears that at the

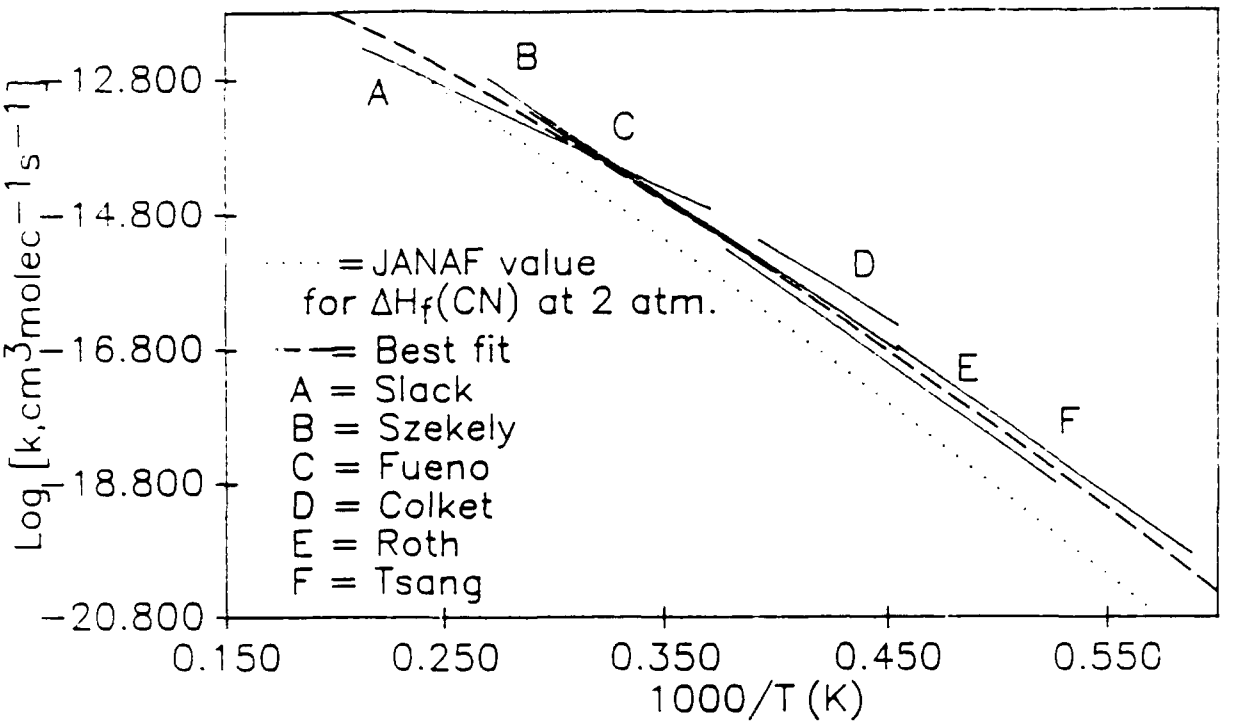

Figure 1. Summary of experimental data and fits on C_2N_2 decomposition

lower temperatures and higher pressures that are more characteristic of propellant applications, CN combination rate constants are between the termolecular and bimolecular limits.

A serious longer term problem is the presence of new species that must be added into our data base. Whenever radicals such as CN or NCO interact with other radicals there is the chance of forming new species. Under high temperature and normal pressure conditions the new species are unstable and will decompose to the reactants or new products. At lower temperatures and very high pressures these new species may have sufficient lifetime so as to undergo other types of reactions. This can have very serious implications with respect to the ignition or preflame chemistry. It will be especially important under very high pressure situation. There is also the potential of changing the subsequent chemistry. In the course of our work we have found that there are virtually no data on these adducts. Thus the prediction of rate constants and expressions are very uncertain. There is need for much more work on the properties of these larger species.

Plans for the next year involve expansion of the data base to cover the reactions of NO_3, HNO_3 and H_2CN radicals (Block D, Figure 1) with the species that have been covered so far and with each other. The importance of these three radicals in the chain of reactions leading to the oxidation of fuel nitrogen means that there is considerable information on their kinetic behavior. H_2CN is particularly interesting since it is the first distinctly "nitramine based" species that we will be treating. Nitric acid and the trioxide are formed in the decomposition of many propellants. It will also extend the scope of our model for the HCN-NO_2 system and open the possibility of modeling the HCN-HNO_3 system.

TWO DIMENSIONAL COHERENT ANTI-STOKES RAMAN SCATTERING WITH APPLICATION TO THE HYDROGEN ARCJET

EDWARD J. BEITING (PRINCIPAL INVESTIGATOR)

The Aerospace Corporation
P. O. Box 92957
Los Angeles, CA 90009

SUMMARY/OVERVIEW

This is an experimental program to extend the utility of coherent anti-Stokes Raman spectroscopy (CARS) as a diagnostic of flows and plasmas. Pump and Stokes radiation focused into a sheet produces a line of anti-Stokes radiation in the cross section of a flow. The anti-Stokes radiation detected with a multichannel array provides one angle of projection data. A cross section of an asymmetrical region is calculated from projection data taken at several angles using tomographic algorithms. Only one projection is required to reconstruct the cross section of a cylindrically symmetric flow. This technique allows the measurement of field maps of internal state distributions (temperatures) and number densities. Currently, CARS is restricted to collecting data sequentially at single points in space. This year the experimental apparatus and the acquisition software were completed, and single pulse, single state projections of a flow of hydrogen gas were acquired.

TECHNICAL DISCUSSION

METHOD

In the CARS process, three fields $E_1(\omega_1)$, $E_2(\omega_2)$, and $E_3(\omega_3)$ impinge on a medium and mix through the third order nonlinear susceptibility χ_{ijkl} to generate a fourth wave $E_4(\omega_4)$ at a frequency ω_4. If we assume the input fields are plane monochromatic waves propagating in the z direction with aligned polarizations, and the medium has no spatial symmetry, then χ_{ijkl} can be written as a scalar and the solution of Maxwell's equations with a nonlinear polarization source term yields

$$\frac{\partial^2 E_4}{\partial z^2} + 2ik_3\frac{\partial E_4}{\partial z} = -4\pi\left(\frac{\omega_4}{c}\right)^2 \chi(\omega_1,\omega_2,\omega_3) E_1 E_2^* E_3 \exp(i\Delta k z) \qquad (1)$$

where $\Delta k = 2k_1 - k_2 - k_3$ and $k \equiv n\omega/c$. Assuming a solution of the form $E_4(z) = E_4^0(z)\exp(ik_4 z)$ and noting $\Delta k << 2k_3$ for phasematched geometries, the spatial variation of E_4^0 is small and the second derivative can be ignored. Accordingly, the spatial variation of the amplitude of the CARS field can be written

$$\frac{dE_4^0}{dz} = K(\omega_4)\chi(\omega_1,\omega_2,\omega_3) E_1 E_2^* E_3 \exp(i\Delta k z) \qquad (2)$$

where $K(\omega_4)$ is a known function of ω_4. This expression can be simplified further using the following assumptions which are valid for most experimental implementations of CARS: $\Delta k = 0$ (phasematched waves); the amplitudes of E_1, E_2, and E_3 are independent of z over the region they coherently interact; $E_1(\omega_1) = E_3(\omega_3)$; and $\omega_1 = \omega_3$. Then Eq. (2) becomes

$$E_4^0(\omega_4) = K(\omega_4)E_1^2E_2^* \int \chi(\omega_4,\omega_2)dz. \tag{3}$$

Noting $I_4(\omega_4) = \frac{n_4 c}{8\pi}|E_4^0(\omega_4)|^2$, the CARS intensity can be written

$$\tilde{I}_4(\omega_4) = A(\omega_4)\left(\left[\int \chi_{nr}(z)dz + \int \sum_j \frac{\delta_j}{\gamma_j}\chi_j'(z)dz\right]^2 + \left[\int \sum_j \chi_j''(z)dz\right]^2\right) \tag{4}$$

where $\chi_j'(z) = a_j(z)\gamma_j/(\delta_j^2+\gamma_j^2)$, $\delta_j = \Omega_j - (\omega_1-\omega_2)$, Ω_j is a Raman resonance frequency, χ_{nr} is the bulk nonresonant susceptibility, γ_j is the halfwidth of the resonance, a_j is the line strength parameter, $A(\omega_4)$ is the amplitude, and the sums are taken over all Raman resonances.

If the lasers are focussed into a thin sheet with a transverse coordinate x and ω_2 is tuned such that δ_j is large for all resonances then the signal that results is due primarily to the interaction of the waves with the nonresonant susceptibility. Then a projection in terms of the molecular density is obtained:

$$P(x) \equiv [\tilde{I}_4(\omega_4)]^{\frac{1}{2}} = \int \chi_{nr}(x,z)dz = \tilde{\chi}_{nr}\int n(x,z)dz \tag{5}$$

where $\tilde{\chi}_{nr}$ is a known constant and $n(z)$ is the number density of the gas. A reconstruction from this projection yields a map of the density directly.

Now if ω_4 is chosen such that $\delta_j = 0$ for a strong resonance that is isolated from neighboring resonances ($\Omega_j - \Omega_{j\pm1} >> \gamma_j$) then $\chi_j'' >> \chi_{nr}$ and only the last term in Eq. (4) contributes:

$$P(x) \equiv [\tilde{I}_4(\omega_4)]^{\frac{1}{2}} = \int \chi_j''(x,z)dz. \tag{6}$$

Noting that $\chi_j'' \propto n(x,z)\Delta_j(x,z)$ one can obtain a spatial map of Δ_j, the population difference between the two states in the Raman resonance j. In thermal equilibrum this defines a temperature. Under nonequilibrium conditions, measuring $\Delta v = 1$ transitions for a line from each vibrational level starting with $v \geq 0$ allows spatial maps of the population of the vibrational energy levels to be constructed.

PROGRESS

Figure 1 shows the experimental setup as currently configured. There a number of major changes in this system from the one shown last year. It became necessary to replace the Spectra Physics Nd:YAG laser for logistical and experimental reasons. This laser was only available on a 30% basis. Furthermore, the beam quality and power from this particular laser were unreliable necessitating frequent realignments and resulting in unpredictable and often unusable projection intensities. The replacement laser, a Continuum NY-82, doubled the energy per pulse available and produced a much improved transverse mode. However, as this laser model was one of the first manufactured, it suffered from beam pointing instabilities for the first few months. Because of space limitations, this laser is hung below the 4' x 8' optics table. This action required that the experimental configuration be completely dismantled and the table returned to the factory for modification. The dye laser oscillator is now pumped by the second harmonic of the residual fundemental. On its return, the new laser was installed and the instrument rebuilt. A dye preamplifier was added to improve the mode stability of the Stokes beam. A beam delay was added to the pump beam to allow better temporal overlap with the Stokes beam. A telescope was required to be inserted before the beam delay to maintain good mode quality. This system now reliably produces CARS projections with acceptable intensity profiles.

The vacuum chamber has been eliminated temporarily. Bowing of the base of the chamber, when it was evacuated, misaligned the optics. While the chamber was being modified, it was learned that good on-resonance projections could be acquired in room air. That is, the nonresonant signal of the ambient nitrogen was insignificantly small compared to the resonant hydrogen signal. Similarly, the spectrograph was been removed temporarily was scattered light could be adequately blocked using interference filters.

A reference arm was added to the system. The feasibility of the technique depends on being able to obtain predictable projections when large shot-to-shot variations of the lasers' mode structure, frequency, and phase take place. The reference channel must exactly duplicate these variations and be used to normalize the signal channel. The beamsplitter and turning mirror used to create this channel are custom precision components designed so as to not introduce any phase distortions and interference effects to either beam.

Experimentally it was found that channel-to-channel, shot-to-shot variations in the signal-to-reference ratios consistently varied between 20% and 50% when single longitudinal mode pump-radiation was used. These large variations occurred even when the CARS images in both reference and signal legs appeared the identical in both spatial dimensions. However, running the Nd:YAG laser in broadband multimode reduced the shot-to-shot variations to approxmately to 1%. Thus, single CARS projections can be taken with this precision even when the intensity of the CARS signal is varying by 500%. The precision of the tomographic reconstruction increases to below this value by a factor equal to the inverse square root of the number of projections used to create the reconstruction.

The reason for the large change in precision of the normalized projections as a function of pump laser mode is under investigation. This behavior is similar to the reduced noise obtained with multiplex CARS when using a multimode pump laser. In the multiplex case, the many modes of both the pump and Stokes radiation create many pairs of the Raman resonant frequencies that average under the linewidth. In this experiment, the dye laser has only three or four longitudinal modes whose relative intensities vary greatly from shot to shot. Accordingly, the spectral content of the radiation will vary as a function of position across the transverse mode structure. This variation may lead to a spatially varying interference effects created by one of the common optical components. For example, a interference pattern is visible across the CARS projection (but not across either the Stokes or pump beams) for certain angles of the dichoric mirror that is used to combine the Stokes and pump beams.

In order to calibrate the projections, two identical rectangular flow channels were built to be used as reference and calibration channels. The calibration channel is placed on a traverse and translated out of the beams as a test flow of up to 8 mm in diameter is inserted in the collinearly phase-matched beams. At this writing, calibrated projections are being taken. Analysis of the projections is imminent. In summary, the instrument has been refined and the acquisition of accurate, calibrated projections has been demonstrated.

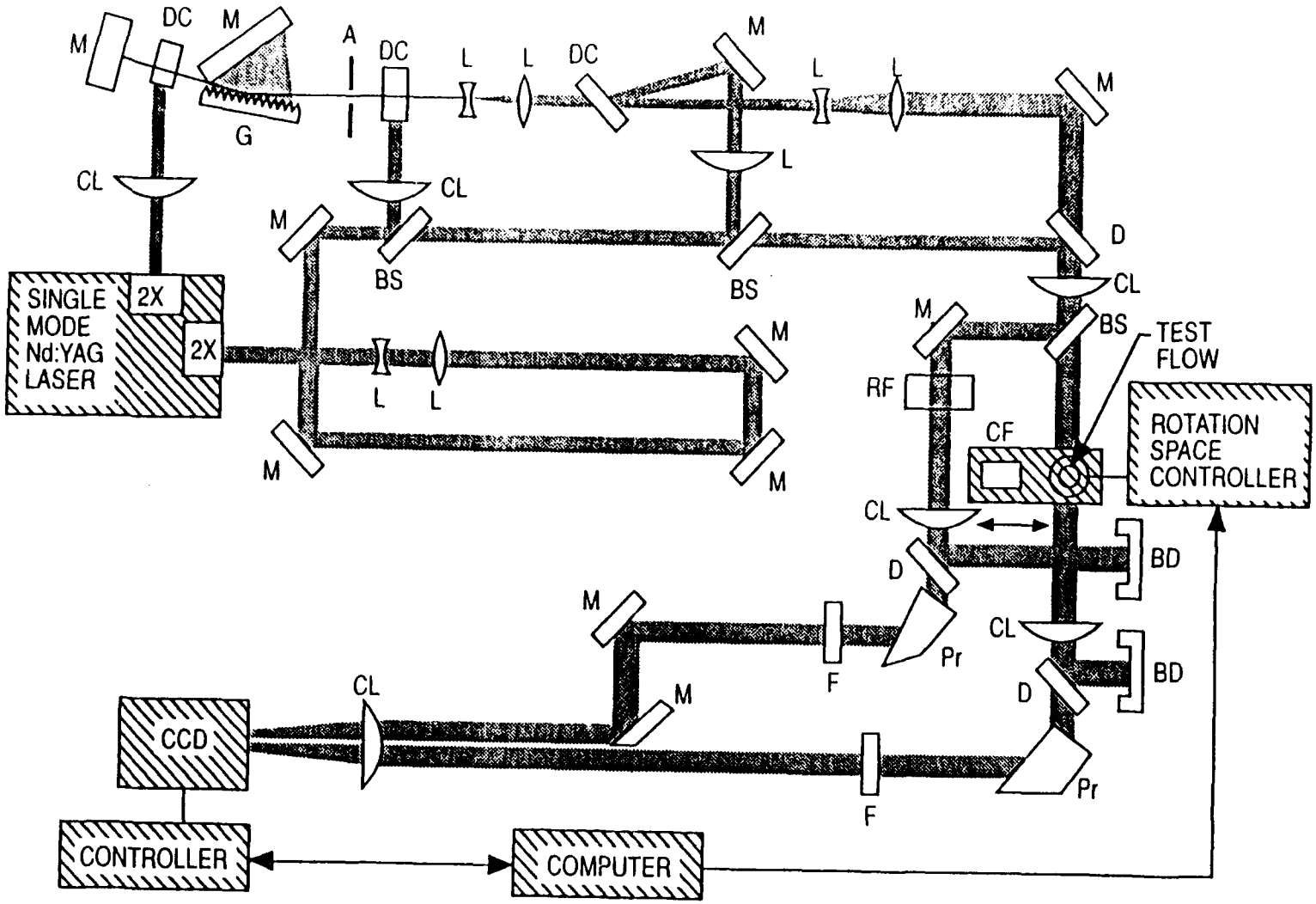

Figure 1. Experimental configuration used to study CATCARS concept. CODE: A, aperture; BD, beam dump; BS, beam splitter; CL, cylindrical lens; D, dichroic mirror; DC, dye cell; F, interference filter; G diffraction grating; L, spherical lens; M, mirror; Pr, prism; 2X, doubler.

NONLINEAR SPECTROSCOPY OF MULTICOMPONENT DROPLETS

(AFOSR Grant No. 91-0150)

Co-Principal Investigator: Richard K. Chang

Yale University
Department of Applied Physics and Center for Laser Diagnostics
New Haven, Connecticut 06520-2157

SUMMARY/OVERVIEW

Noninstrusive in-situ optical diagnostic techniques have the potential of determining the chemical species and physical properties of multicomponent liquid droplets in a spray combustor. Our research is directed toward the understanding of nonlinear optical processes occurring within individual droplets which may or may not retain their spherical shape after irradiation by a high-intensity laser beam or because of intertial effects. The two main research results during the past year are : (1) the realization that the phase velocity of the internally trapped radiation is dependent on the mode number and mode order of the morphology-dependent resonances (MDR's) of a sphere;[1] and (2) the observation that high-resolution interferometric spectra of the stimulated Raman scattering (SRS) from flowing ethanol droplets consist of equally spaced peaks because the droplets are deformed by inertial effects.[2]

TECHNICAL DISCUSSION

The spherical liquid-air interface of a droplet (with radius a much greater than the wavelength) acts as an optical cavity for the internally generated wavelength-shifted radiation, such as fluorescence, spontaneous Raman scattering, and spontaneous Brillouin scattering. Stimulated radiation at specific wavelengths within the spontaneous emission profile will occur when the internally generated waves propagate around the droplet rim with a round-trip gain greater than the round-trip loss. During the input pump pulse, the fluorescence will turn into laser emission, the spontaneous Raman scattering will turn into intense SRS, and the spontaneous Brillouin scattering will turn into SBS. For organic and aqueous liquid droplets without any fluorescent dyes, only SRS and SBS will take place at specific wavelengths corresponding to the droplet MDR's.

The frequency shift of the first-order Stokes SRS from the input pump laser frequency is equal to the molecular vibrational frequency and can, therefore, provide chemical species indentification of the multicomponent liquid droplet. In principle, the relative intensities among the various SRS peaks also contain quantitative information about the relative concentration of the multicomponent species.

Another nonlinear optical diagnostic technique for concentration determination within the droplet is coherent anti-Stokes Raman scattering (CARS). Unlike SRS, which does not have any phase-matching requirement, CARS requires phase matching of the input pump, input Stokes, and output anti-Stokes waves. The phase-matching concepts originally developed for plane-wave propagation in an infinite medium have been extended for guided-wave propagation in optical fibers. To date, the ability to improve the phase-matching velocity of the generating and generated waves circulating within a droplet has not been considered.

The standing wave of a MDR can be decomposed into two counterpropagating traveling waves around the droplet circumference. The phase velocity [$\pm v_{\ell}^{MDR}(\omega)$] of the two counterpropagating waves (forming the standing wave at a MDR with **n**, ℓ) can be calculated. Depending on the ℓ's of the MDR's, $\pm v_{\ell}^{MDR}(\omega)$ varies from c to $c/n(\omega)$, where c is the speed of light in air and $c/n(\omega)$ is the speed of light in liquid. Physical insight about the dependence of $\pm v_{\ell}^{MDR}(\omega)$ on ℓ can be reached by noting the internal field distribution of the MDR's. The low ℓ MDR's are very confined within the droplet and, hence, their phase velocity approaches the phase velocity of a plane wave in liquid [$c/n(\omega)$]. The internal field distribution of the larger ℓ MDR's is more extended outside the droplet and, hence, their phase velocity approaches that of a plane wave in air (c).

Because phase-velocity matching is more difficult to calculate for the CARS process than for the third-order sum-frequency generation (TSFG) process, we have been concentrating our attention on the latter. We have been calculating the phase velocity as a function of the droplet size parameter $\mathbf{x} = 2\pi a/\lambda$ and as a function of the mode order ℓ and mode number **n** of the MDR's at the fundamental and third-harmonic frequencies. We have experimentally investigated the dependence of TSFG as the droplet **a** is changed.

For an axially symmetric perturbed droplet, such as an oblate spheroid, both T-matrix calculations and perturbation theory have shown that each of the $(2\mathbf{n} + 1)$-degenerate MDR of a spherical droplet is frequency shifted and forms $(\mathbf{n} + 1)$ MDR's. Perturbation theory provides an analytical expression for the frequency shifts and mode splitting of each of the $(\mathbf{n} + 1)$ MDR's for an oblate spheroid with a small amplitude of distortion [$e = \frac{r_p - r_e}{a} << 1$, where the polar and equatorial radii are r_p and r_e, respectively]. For a perfect sphere, a $(2\mathbf{n} + 1)$-degenerate MDR is independent of the azimuthal number m, which can assume values $\pm\mathbf{n}$, $\pm(\mathbf{n} - 1)$,..., 0. Figure 1 illustrates[2] the spatial location of the incident radiation and several MDR's (with $m = \mathbf{n}$, $m \approx \frac{\mathbf{n}}{2}$, and $m = 1$) relative to the droplet axisymmetric axis (z), incident beam direction (along x and with $\theta = 90°$), and the collection direction of the SRS (along $\pm y$).

SRS spectral measurements are made downstream where the droplets have reached a velocity of 5 m/s. Assuming that the surrounding air is stationary, this velocity yields a Reynolds number of 15 and a Weber number of 6×10^{-2}. Because the Reynolds number is greater than 1 and the linear stream of droplets entrains the surrounding air, we are unable to estimate the distortion parameter e, other than knowing that the inertial effect causes the droplet to distort into an oblate spheroid (axisymmetric about the z axis). Figure 2 shows[2] that the degeneracy split MDR in the SRS spectrum of flowing ethanol droplets which are deformed into oblate spheroids (with $e \approx 5 \times 10^{-4}$) as a result of hydrodynamic inertial effects.

REFERENCES

1. D.H. Leach, W.P. Acker, and R.K. Chang, "Effect of the Phase Velocity and Spatial Overlap of Spherical Resonances on Sum-Frequency Generation in Droplets," Opt. Lett. 15, 895 (1990).

2. G. Chen, R.K. Chang, S.C. Hill, and P.W. Barber, "Frequency Splitting of Degenerate Spherical Cavity Mode: Stimulated Raman Scattering Spectrum of Deformed Droplets," submitted to Opt. Lett.

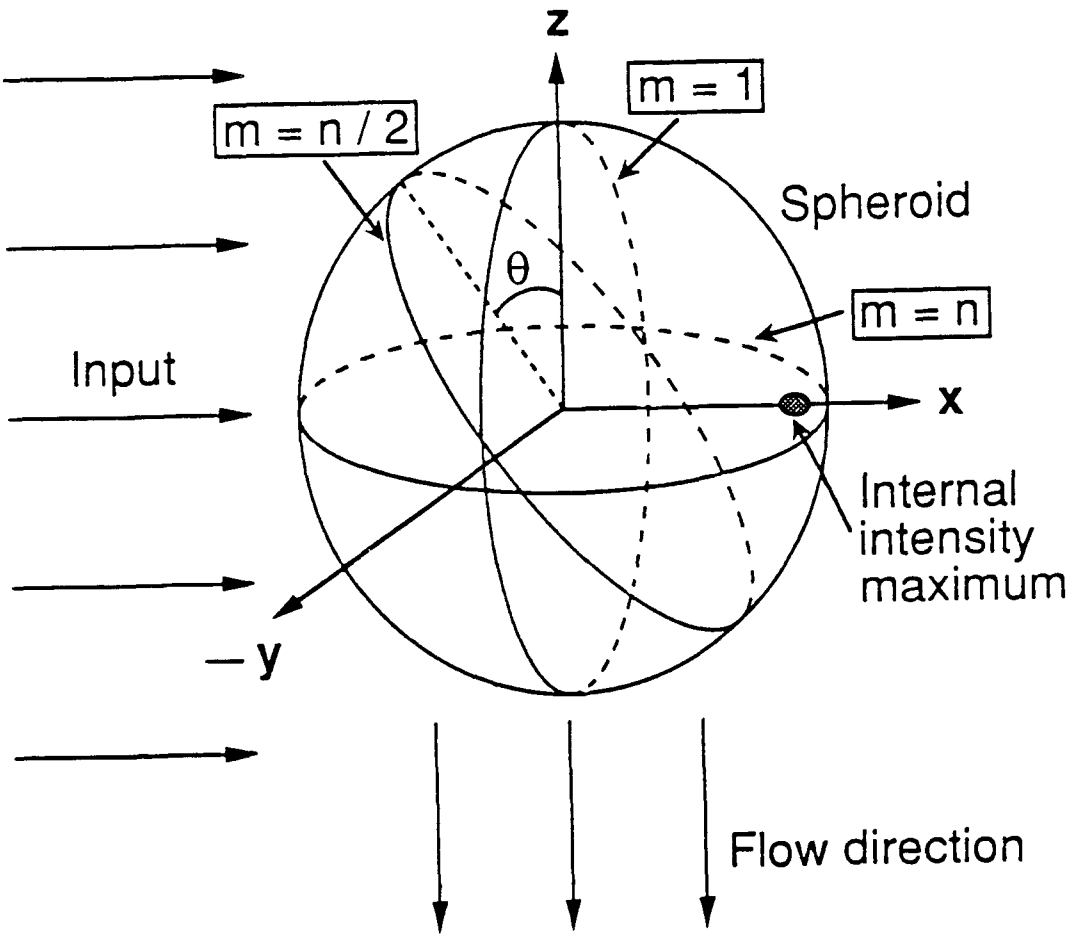

FIGURE 1

The schematic of a spheroid droplet which is axisymmetric along the flow direction (z axis) and irradiated by the input beam along the x axis. SRS is collected along the ±y axes. The maximum of the internal pump intensity distribution is shown as a shaded spot. The MDR's with different azimuthal numbers m are oriented at different q's relative to the z axis.

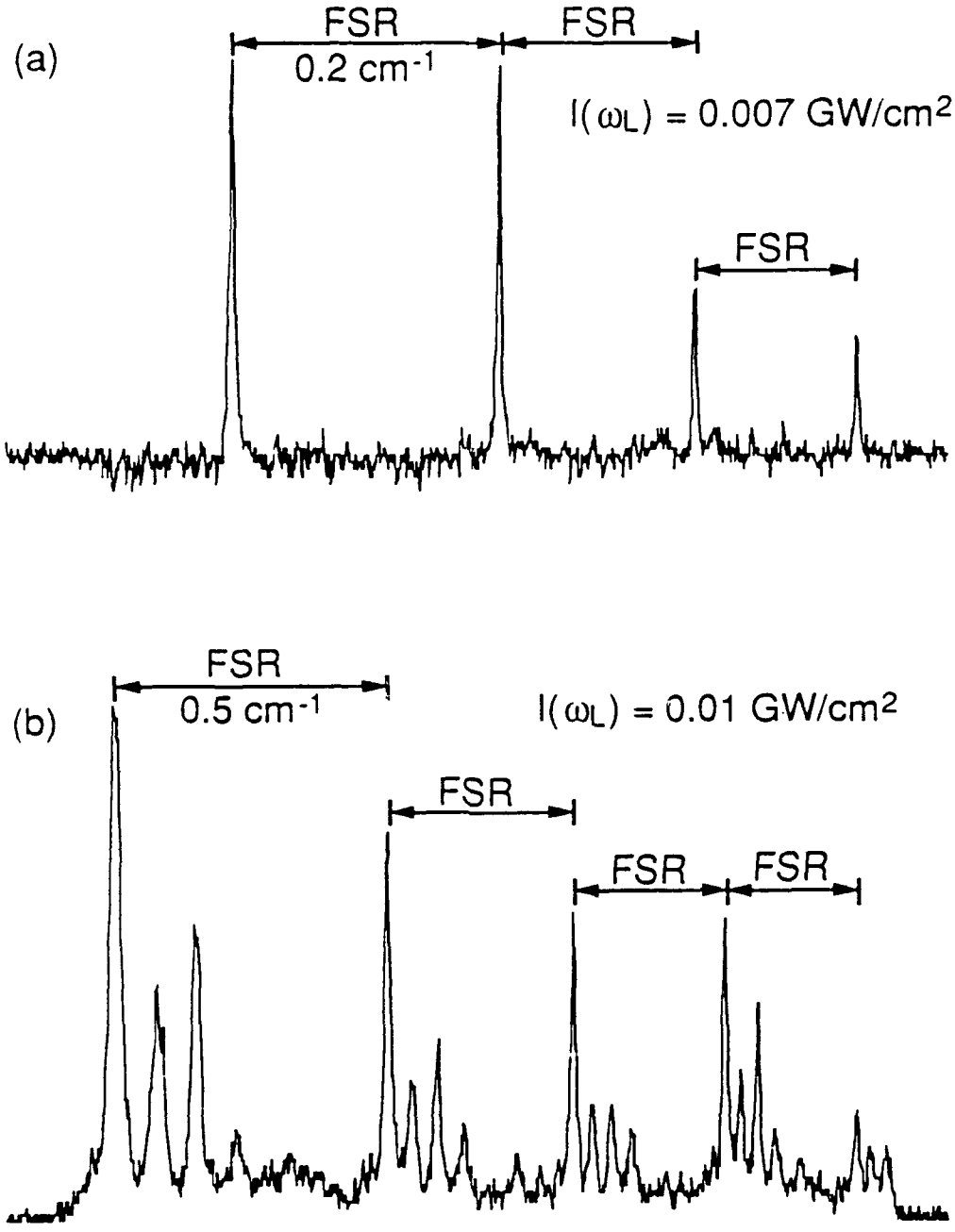

FIGURE 2

(a) High-resolution SRS spectrum measured with an interferometer having a FSR of 0.2 cm^{-1} and at $I(\omega_L) = 0.007$ GW/cm^2, which is just above the SRS threshold (b) SRS spectrum measured with an interferometer having a FSR of 0.5 cm^{-1} and at $I(\omega_L) = 0.007$ GW/cm^2. For both spectra, the SRS is collected from one side of the droplet and the photodiode array simultaneously detects four Fabry-Perot interferometer orders. Note that the frequency spacings between the four SRS peaks are equal ($\approx$0.060 cm^{-1}). We conclude that the newly observed SRS peaks are attributable to the splitting of a $(2n + 1)$-degenerate MDR as a result of small shape deformation associated with inertial effects on flowing droplets.

DETECTING MICROWAVE EMISSION FROM TERRESTRIAL SOURCES: A FEASIBILITY STUDY

AFOSR-88-0257

T. C. Ehlert, T. K. Ishii and Shuming T. Wang

Marquette University, Milwaukee, WI 53233

SUMMARY:

The detection of discrete, spontaneous microwave emission from terrestrial sources has been studied and appears to be feasible. A Dicke receiving system has been designed and built for this purpose. Possible applications include remote detection of processes which produce high temperature gases, e.g. jet engines and explosions, determining the rotational properties of molecules which are difficult to study by absorption spectroscopy, studies of intermolecular energy transfer processes, and studies of the role of rotation in energy transfer to and from surfaces.

TECHNICAL DISCUSSION:

Introduction

The objective of this research is to observe discrete, spontaneous microwave emission from a terrestrial source. We have chosen H_2O vapor's 22 GHz transition because it has been thoroughly studied in absorption and microwave components for this frequency are not exceedingly expensive. As stated in the radiative transfer equation[1] in order to see the emission from the water vapor, the background brightness temperature should be as low as possible. The Dicke receiver, as shown in Fig. 1, includes a waveguide chopper switch, a front end 22 GHz low noise amplifier (LNA), a 30 MHz IF amplifier, and a lock-in amplifier. This receiving system compares two inputs which differ in noise power. One is due to the brightness temperature of the background as the reference, the other one is due to the combination of brightness temperature of the background attenuated by the water vapor and the emission from the water vapor. If the background brightness temperature is low enough, the difference between two inputs is the emission of the water vapor.

Progress

1. Publication and filing: We submitted a paper titled "Digital Video Integration Techniques for Faint Signal Measurements" to the 34^{th} Midwest Symposium on Circuits and Systems and presented in the conference on August 12, 1990. We also submitted a paper, titled " Improving Receiver Sensitivity Using Heterodyned Video Counting Technique for Faint Signal Detection", to Microwave & RF. It will be published in April, 1991.

2. Completion of receiver system and preliminary testing: We designed and built the reference and emission sources: two eight meter long waveguides, filled with dry air and water vapor, respectively. Both waveguides are terminated with low emissivity brass plates as the background. Both waveguides are vacuum tight and leak free down to 20 microns. The preliminary experimental results showing the noise temperature difference between the reference and emission sources are plotted in Fig. 2 with local oscillator(LO) operated at 22.456 GHz and the water vapor at various pressures. This plot shows that the pressure dependence of the detected signal is in agreement with theoretical calculations.

3. Theoretical Investigation: We are attempting to reconcile the two ways of looking at the experiment. One way uses the radiative transfer equation and the other considers the equivalent circuits of microwave sources which are matched and mismatched to the input of a receiver.

4. Improvement of receiving system: The designed receiver can only detect the difference between the reference and the emission source. It is not capable of telling the polarity and compensating for the difference due to the condition of waveguides and terminating brass plates. A new IF amplifier with a pair of internal attenuators and switches has been designed in order to correct for these deficiencies.

References

1. M.L. Meeks, "Methods of Experimental Physics: Volume 12 Astrophysics Part B: Radio Telescopes", Academic Press, NY, 1976.

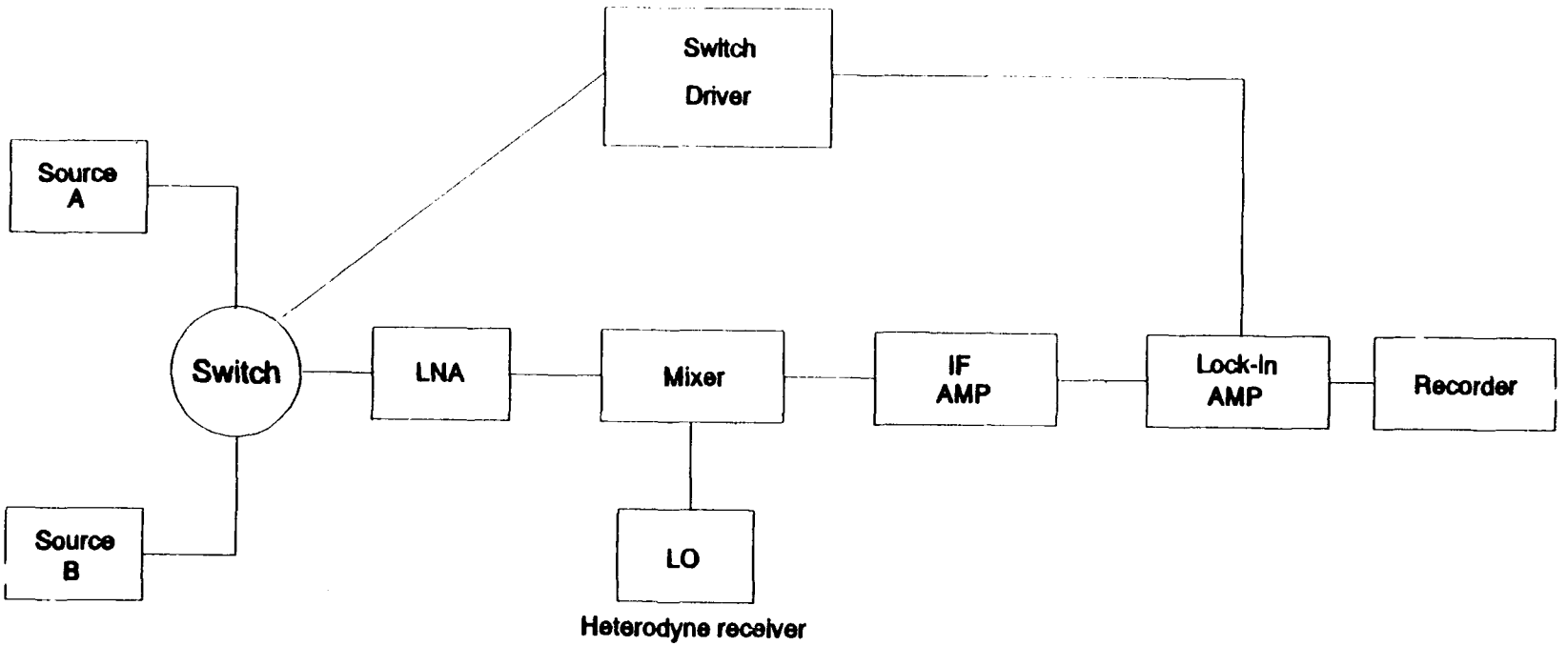

Fig. 1 Block Diagram of Dicke Receiver

Fig. 2 Experimental Result, Detected Output Voltage vs Water Vapor Presssure

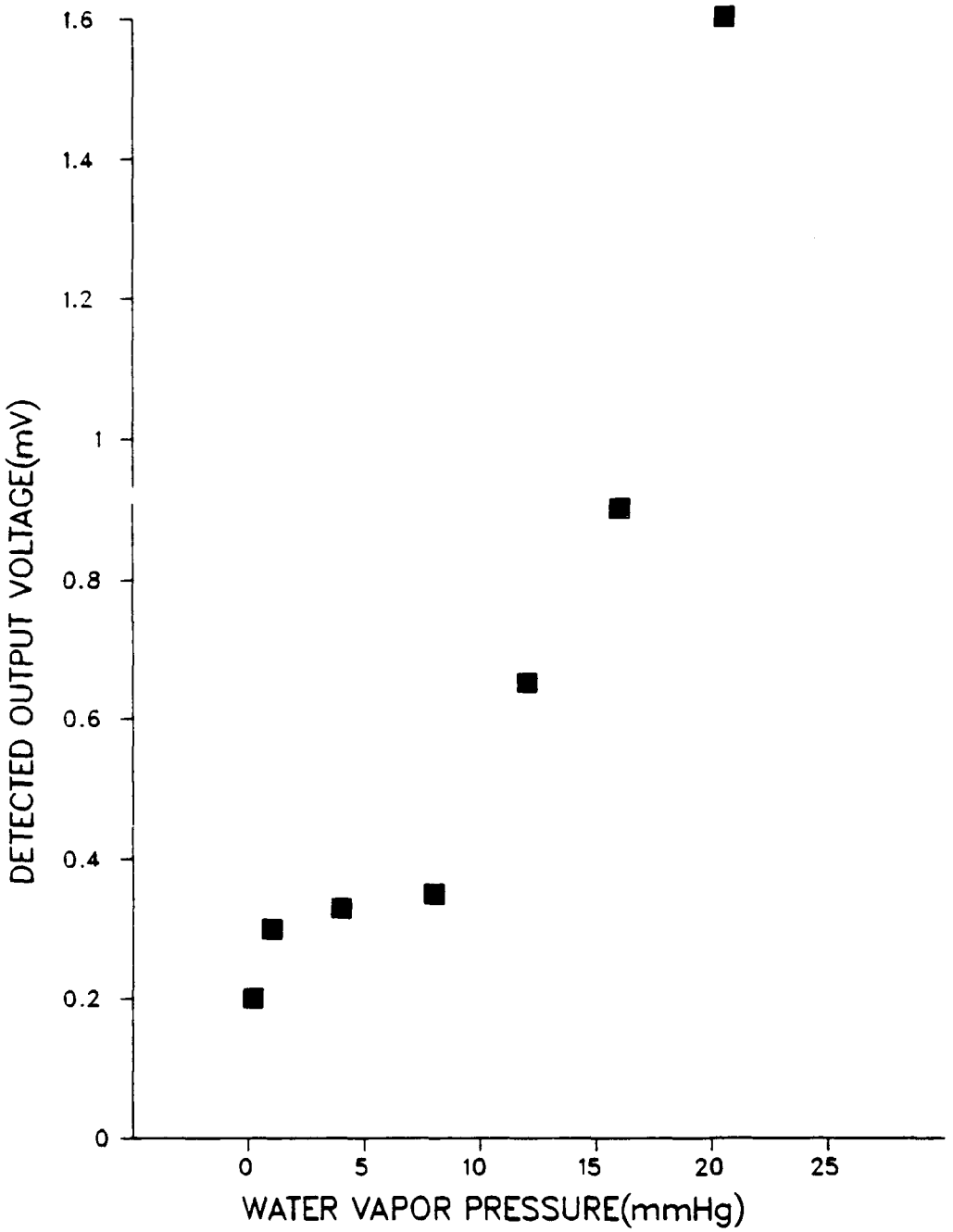

ADVANCED DIAGNOSTICS FOR REACTING FLOWS

AFOSR90-89-0067

Principal Investigator: Ronald K. Hanson

High Temperature Gasdynamics Laboratory
Mechanical Engineering Department
Stanford University, Stanford, CA

SUMMARY/OVERVIEW

This research is directed toward innovation of advanced diagnostic techniques applicable to combustion gases and plasmas, with some emphasis on high speed flows. The primary flowfield parameters of interest are species concentrations, temperature, pressure, mass density, electron density, and velocity, and quantities derivable from these parameters such as mass flow rate and thrust (calculable from mass density and velocity). Techniques under study utilize laser absorption and laser-induced fluorescence, with the latter capable of providing both single-point and multi-point (2-d and 3-d) measurements. Laser sources include tunable cw lasers (ring dye lasers and semiconductor diode lasers) and tunable pulsed lasers (excimer-pumped dye and narrow-linewidth excimer). Wavelength modulation and high-speed frequency modulation (FM) spectroscopy techniques are under study to provide increased data recording rates.

TECHNICAL DISCUSSION

In the following paragraphs we highlight primary activities of the past year.

Plasma Diagnostics

Recent research has involved three activities: (1) a now-completed study of pulsed-laser LIF in a supersonic jet of plasma-heated N_2; (2) a new effort aimed at exploring degenerate four-wave-mixing (DFWM) as a plasma diagnostic; and (3) an ongoing program to apply tunable semiconductor diode lasers for line-of-sight absorption and single-point LIF measurements of plasma properties. The latter study has utilized a home-built RF-powered plasma torch (1 kW) which provides a convenient bench-top plasma source with good optical access. The torch operates at atmospheric pressure on argon, providing temperatures up to 9000 K and electron densities up to 10^{16}/cc, with the capability of adding trace levels of various additives of spectroscopic interest. Present work involves studies of absorption/fluorescence transitions from the 4s state of argon using tunable GaAlAs laser sources. In brief, spectrally resolved lineshapes are recorded, from which it is possible to infer: the kinetic gas temperature (Doppler linewidths), the population temperature of the quantum state being monitored; and the electron density (from the Stark shift or linewidth). A sample data trace is shown in Fig. 1; see Ref. 1 for details.

PLIF Imaging in Shock Tube Flows

Shock tubes and tunnels provide a convenient means of studying nonequilibrium gasdynamic phenomena and of simulating conditions relevant to advanced air-breathing propulsion systems. During the past year we have continued development of our shock tube and tunnel facility, and have made good progress in efforts to establish PLIF imaging techniques for shock-heated flows. Specific results include: PLIF imaging of OH in shock-ignited H_2-O_2-Ar mixtures, using a non-planar shock tube end wall to produce local nonuniformities in temperature and hence ignition times, see Ref. 2; a study of PLIF imaging of NO in vibrationally relaxing shock tube flows, e.g. normal shock waves and shock tube flow over blunt bodies, see Ref. 3; and PLIF imaging of transverse jet mixing and combustion in supersonic, shock-heated flows, see Ref. 4.

Shock Tube Studies of Combustion Kinetics

In addition to providing an attractive test environment for developing laser diagnostics, shock tubes are recognized as the facilities of choice for measurements of reaction rate coefficients at high temperatures. In the past year, we have continued efforts to develop and apply narrow-linewidth laser absorption techniques to the measurement of elementary reactions relevant to combustion and propulsion. Studies of several reactions have been completed, including measurements of: $O + HNCO \rightarrow NH + CO_2$ and $O + HNCO \rightarrow OH + NCO$, Ref. 5; $NO + NO, O_2$ and O, Ref. 6; and $C + H_2 \rightarrow CH + H$ and $C + O_2 \rightarrow CO + O$, Ref. 7. These studies were enabled by our earlier development of sensitive, accurate absorption diagnostics of NH, OH, NCO, CH and C-atoms. The rate coefficients were measured at temperatures in the range 1500-3000 K, and in most cases provide the first direct determinations of these reaction rates at elevated temperatures.

CW Ring Dye Laser Techniques

Tunable monochromatic laser sources provide opportunities for measurement concepts based on spectrally resolved absorption lineshapes. For example, cw ring dye lasers can be rapidly modulated in wavelength to record a pair of absorption lines, using either line-of-sight absorption or single-point LIF, allowing inference of gas temperature through the ratio of the signals for the two lines. The total static pressure can also be inferred, using the width of the recorded lines whenever collision-broadening is significant or the magnitude of the absorption (or fluorescence) signal when chemical composition is fixed. In addition, velocity can be inferred from the shift in spectral line position caused by the Doppler effect; in essence this is molecular velocimetry. Note that by a complete analysis of the spectra for each wavelength scan, one can infer all of these flowfield parameters simultaneously. Finally, with these quantities determined, it is feasible to infer other relevant flowfield parameters, such as mass flux or thrust, by appropriate combinations of the directly measured quantities. See Refs. 8-10 for details.

During the past two years we have demonstrated several of these ideas using detection of OH (306 nm), NO (225nm) and O_2 (220 nm). Important examples include: (1) simultaneous measurements of temperature (T), pressure (P) and velocity (V) at a single point, at a 3 kHz repetition rate, in a supersonic flow of combustion gases using OH detection, Ref. 8; (2) simultaneous measurements of T, P and V along a line-of-sight across a shock tube using OH, NO and O_2 detection, Refs. 9 and 10; and (3) simultaneous measurements of T, P and V at a single point, at a 4 kHz rate, monitoring NO in a supersonic underexpanded jet. Figures 2 and 3 provide a sketch of the arrangement used for the shock tube measurements and representative results. Note, in particular, that the last figure is for the mass flux, a quantity not usually considered in the context of optical measurements. A similar approach could be used to determine "thrust".

Semiconductor Diode Laser Techniques

Tunable diode lasers offer the possibility of an economical, rugged and compact alternative to cw ring dye lasers for spectrally resolved absorption and fluorescence spectroscopy. At present such lasers are available in several wavelength intervals at wavelengths generally in excess of 750 nm, but the trend toward operation at shorter wavelengths is clear. These lasers have significant potential advantages over ring dye lasers, including the possibility of high frequency modulation of laser wavelength through current modulation. At present we are pursuing two projects with these lasers, one aimed at detecting O_2 at 760 nm (the atmospheric band of oxygen) and the other at detecting H_2O near 1.35 microns. The former project is more advanced, and during the past year we have demonstrated the capability of monitoring spectrally resolved absorption lines of O_2 in supersonic flows. The scheme involves combining high-frequency (10 MHz) modulation with a high-speed (10 kHz) current ramp to repetitively tune the laser across one or more O_2 absorption lines. The data yield temperature, O_2 density, velocity and mass flux, all path-averaged over the width of the supersonic stream produced in a shock tube. Agreement with calculated flow properties is excellent, see Ref. 11. It is already clear that these lasers have great potential both for fundamental research and for packaged, user-friendly instruments, e.g. flight instrumentation.

Digital Camera For High-Speed Imaging

Continued progress has been made in the development of a high-speed digital camera for recording instantaneous 3-d images and fast 2-d image "movies." The basic concept involves modifying a commercial image converter camera (Imacon 790) to incorporate CCD detection. In brief, a specially designed tapered fiberoptic bundle is used to transfer the output plane image of the Imacon onto a high-resolution (400x1200 pixels), low-noise CCD array detector. This system is capable of recording a modest number of images at up to 10 million frames per second. Together with a high-energy, long-pulse dye laser source to provide "cw" flowfield illumination, this camera allows rapid recording of multiple PLIF images, constituting either an essentially instantaneous multiple-plane 3-d image data set or a multiple-image movie over a brief time interval (2 microseconds for the current pulsed dye laser); see Ref. 12.

Other Projects

Other projects include: (1) work in progress to develop single-shot temperature imaging strategies based on PLIF; and (2) recently completed work on high-resolution PLIF imaging of turbulent non-reacting jets, see Ref. 13.

REFERENCES

1. D. S. Baer, L. Philippe and R. K. Hanson, "Tunable Diode Laser Diagnostics for Atmospheric Pressure Plasmas," submitted to AIAA 22nd Fluid Dynamics, Plasma Dynamics and Lasers Conference, Honolulu, Hawaii, June 24-26, 1991.
2. B. K. McMillin, M. P. Lee, P. H. Paul and R. K. Hanson, "Planar Laser-Induced Fluorescence Imaging of Shock-Induced Ignition," *Twenty-Third Symposium (International) on Combustion*, The Combustion Institute, in press.
3. B. K. McMillin, P. H. Paul and R. K. Hanson, "Planar Laser-Induced Fluorescence Imaging of Nitric Oxide in Shock Tube Flows with Vibrational Nonequilibrium," AIAA J., in press; also paper AIAA-90-1519 at AIAA 21st Fluid Dynamics, Plasmadynamics and Lasers Conf., Seattle WA, June 1990.
4. M. P. Lee, B. K. McMillin, J. L. Palmer and R. K. Hanson, "Two-Dimensional Imaging of Mixing and Combustion of Transverse Jets in Shock Tube Flows," submitted to J. Prop. and Power, Feb. 1991.
5. J. D. Mertens, A. Y. Chang, R. K. Hanson and C. T. Bowman, "A Shock Tube Study of Reactions of Atomic Oxygen with Isocyanic Acid," submitted to Int. J. Chem. Kinetics, April 1991.
6. J. D. Mertens, A. Y. Chang, D. A. Masten, R. K. Hanson and C. T. Bowman, "A Shock Tube Study of the Reactions of NH with NO, O and O_2," Int. J. of Chemical Kinetics **23**, 173-196 (1991).
7. A. J. Dean, D. F. Davidson and R. K. Hanson, "A Shock Tube Study of Reactions of C-atoms with H_2 and O_2 using Excimer Photolysis of C_3O_2 and C-Atom ARAS," J. Phys. Chemistry **95**, 183-191 (1991).
8. A. Y. Chang, B. E. Battles and R. K. Hanson, "Simultaneous Measurements of Velocity, Temperature and Pressure using Rapid cw Wavelength-Modulation LIF of OH," Optics Letters **15**, 706-708 (1990).
9. D. F. Davidson, A. Y. Chang, M. D. DiRosa and R. K. Hanson, "CW Laser Absorption Techniques for Gasdynamic Measurements in Supersonic Flows," submitted to Applied Optics, July 1990.
10. A. Y. Chang, M. D. DiRosa, D. F. Davidson and R. K. Hanson, "Rapid-Tuning CW Laser Technique for Measurements of Gas Velocity, Temperature, Pressure, Density and Mass Flux Using NO," submitted to Applied Optics, August 1990.
11. L. C. Philippe and R. K. Hanson, "Tunable Diode Laser Absorption Sensor for Temperature and Velocity Measurements of O_2 in Air Flows," paper AIAA-91-0360 at AIAA 29th Aerospace Sciences Meeting, Reno, NV, Jan. 1991.
12. J. M. Seitzman, P. H. Paul, B. Patrie and R. K. Hanson, "Instantaneous 3-D and Temporal Evolution Measurements by Rapid Acquisition of Planar Images," paper AIAA 91-0178 at AIAA 29th Aerospace Sciences Meeting, Reno, NV, Jan. 1991.
13. I. van Cruyningen, A. Lozano and R. K. Hanson, "Concentration Imaging in Turbulent Gaseous Jets," J. F. Mech., in press.

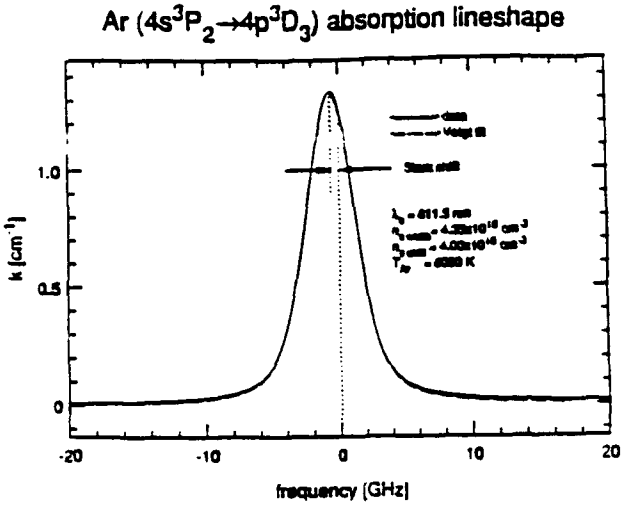

Fig. 1. Absorption lineshape data for argon plasma; inferred temperature and electron density are indicated on figure.

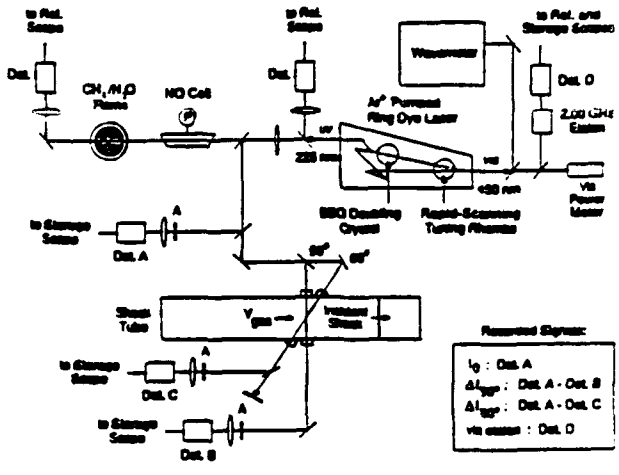

Fig. 2. Experimental schematic for dual-beam shock-tube absorption experiment.

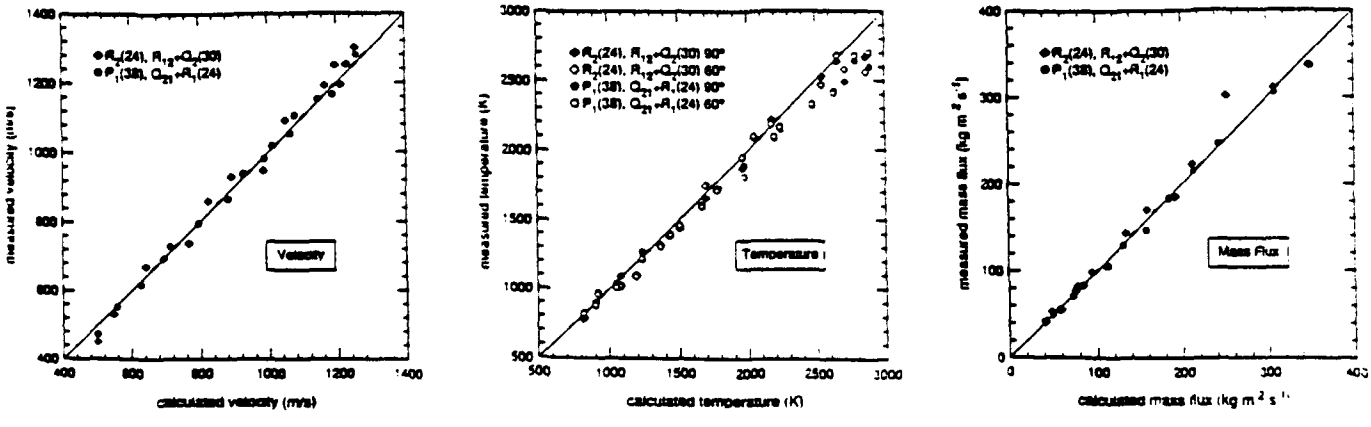

(a) (b) (c)

Fig. 3. Results obtained with NO laser absorption diagnostic in a shock tube.

NOVEL NONLINEAR LASER DIAGNOSTIC TECHNIQUES

(AFOSR Contract No. F-49620-90-C-0044)

Principal Investigators: David L. Huestis, Gregory W. Faris, and Jay B. Jeffries

SRI International
Molecular Physics Laboratory
Menlo Park, CA 94025

SUMMARY/OVERVIEW:

Task 1: UV and VUV Generation and Detection Techniques

We are developing techniques for the extension of laser-based diagnostics into the vuv for detection of atomic ions and other species with important high-lying excited states. We have demonstrated two-photon-resonant four-wave difference frequency mixing of an ArF laser and a frequency-doubled dye laser for the production of high power radiation continuously tunable through vuv range.

Task 2: Laser-Excited Amplified Spontaneous Emission (ASE)

ASE can be used to detect atomic species in reacting gas flows and plasmas; because the ASE signal is collimated along the excitation laser beam, ASE measurements are possible in practical devices with only single port optical access. Quantitative ASE concentration measurements require understanding of the ASE gain, divergence, and collisional loss mechanisms of the excited atoms; temperature and velocity measurements require research on the gain narrowing of the Doppler lineshape. In the first year of this project we have: 1) obtained simultaneous ASE and laser induced fluorescence (LIF) signals from atomic hydrogen in a variety of low-pressure flames, 2) discovered gas collisions can have a significant influence on the amplitude the ASE signals, and 3) demonstrated ASE bandwidth measurements for single laser pulses.

TECHNICAL DISCUSSION

Task 1: UV and VUV Generation and Detection Techniques by Gregory W. Faris and Mark Dyer

We are pursuing the detection of hard-to-detect atoms such as atomic ions which require two-photon excitation with vacuum ultraviolet light. Through generation of higher power radiation in the vacuum ultraviolet, techniques commonly used in the near ultraviolet such as multiphoton ionization, two-photon-excited fluorescence, and amplified spontaneous emission may be applied to other species for better understanding of chemical dynamics, plasma kinetics, and basic spectroscopy.

Under previous support from AFOSR we have used vuv radiation for detection of atomic and molecular fluorine.[1] High power vuv radiation was generated through Raman shifting an ArF laser. Up to 1 mJ at 170 nm was generated in the second anti-Stokes radiation in HD for the excitation of atomic fluorine. While the Raman shifting technique can generate quite high powers, Raman shifting excimer lasers results in a limited tuning range, and Raman shifting frequency-doubled dye lasers gives only moderate energies in the longer vuv wavelengths and suffers from large intensity fluctuations.

The method we are now using for vuv generation is a two-photon-resonant four-wave difference frequency mixing process as is shown in Figure 1. Two fixed frequency photons at ω_1 which are resonant with a two-photon excited state |2> are mixed with a tunable photon at ω_2 to generate a tunable vuv photon at energy $\omega_{vuv} = 2\,\omega_1 - \omega_2$. The ArF excimer laser can excite two-photon resonances in Kr, H_2, and HD. When mixed with the frequency-doubled radiation from a Nd:YAG-pumped dye laser, this allows the generation of tunable vuv radiation through the entire vacuum ultraviolet. This approach takes advantage of the high powers and short wavelength of the ArF laser, allowing access of shorter vuv wavelengths and potentially higher powers than similar schemes using frequency-doubled dye lasers.[2,3] This also takes advantage of modifications we have performed to improve the transverse mode of our ArF laser for previous Raman shifting experiments.[1]

To date, mixing has been performed using the $6p[3/2,2] \leftarrow 4p^6\ ^1S$ resonance in krypton. Attempts using the $E,F\ ^1\Sigma_g^+$ $(v'=6) \leftarrow X\ ^1\Sigma_g^+$ Q(1) transition in H_2 was hampered by the previously observed[4] amplified spontaneous emission in the vuv on the B→X transition. Similar ASE complications are anticipated in HD.

The dependence of vuv radiation generated at 147 nm on the krypton pressure is shown in Figure 2. The energy increases as the square of the krypton density and then drops due to poorer phase matching. The dependence of the vuv power on both the ArF laser power and the frequency-doubled dye laser power show saturation before reaching full power. Extracting high powers from this technique will be greatly enhanced by solving the phase-matching problem, allowing operation at higher gas densities and larger beam waists.

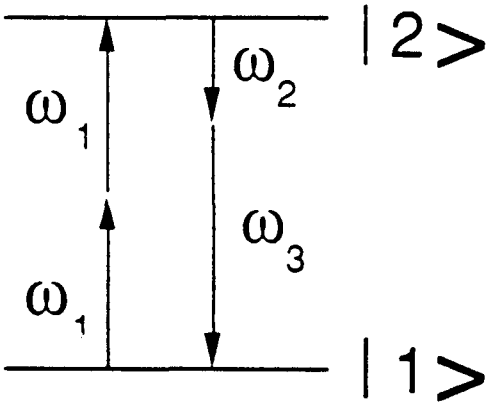

Figure 1. Two-photon-resonant four-wave difference frequency mixing scheme.

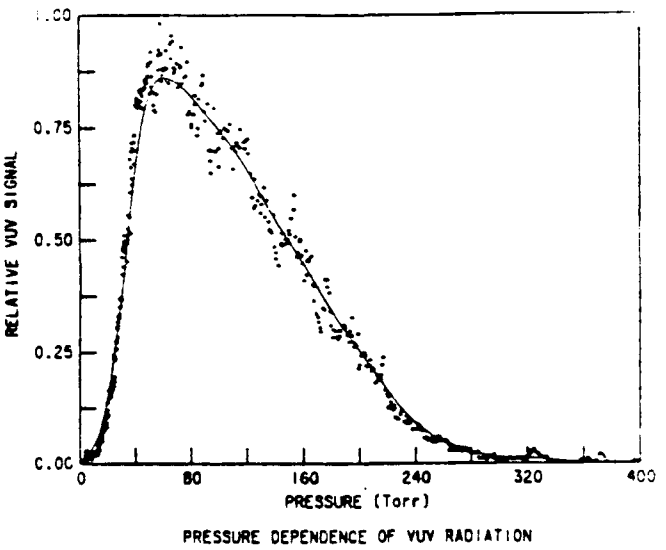

Figure 2. Dependence of the vuv radiation on krypton pressure.

Task 2: Laser Excited Amplified Spontaneous Emission by Jay B. Jeffries and Dwayne E. Heard

Multiphoton laser excitation of atoms followed by fluorescence or ionization detection has been used to detect a variety of atomic species in flames, reacting flows and plasmas. Recently, amplified spontaneous emission (ASE) has been observed from two-photon excited C, O, Cl, and H atoms. ASE has several distinct advantages for atom diagnostic measurements. The ASE signal can be much larger than the laser-induced fluorescence signal, and it can be detected with a small solid angle optical collection. The increased brightness can substantially increase the signal to background ratio in flames, reactive flows, and plasmas, where measurement precision and detectivity is often limited by background optical emission. Because the ASE signal is collimated along the laser beam, the signal collection can share the same optical access port with the excitation laser. This arrangement simplifies optical alignment and significantly reduces the access requirements for measurements on large scale supersonic reacting flows and plasma devices.

During the past year we have studied two photon excited ASE of atomic hydrogen in a variety of low-pressure flames.[5] Two laser photons near 205 nm excite the hydrogen 3S and 3D states from the 1S ground state. These states have allowed Balmer α transitions near 656 nm to the 2P state; the direct single photon transition back to the ground state is not allowed. If the two-photon excitation rate is fast enough, a population inversion is possible and the resulting amplification of the spontaneous emission produces the ASE signal. Since the atoms are excited only along the laser beam, gain over a significant path length only occurs along the laser beam. Thus the ASE signal has a divergence which is derived from the excitation laser and ASE propagates forward and backward along the laser beam.

Low-pressure flames provide an ideal environment to study ASE because they provide stable sources of large concentrations of hydrogen atoms. By choosing flame conditions identical to those used previously in our laboratory to study OH,[6] HCO,[7] and NO[8], estimates of the hydrogen atom concentration and the collision environment are available from our model calculations of the flame chemistry. The premixed flames are supported on a 6 cm porous plug burner; height above the burner in this flat flame can be related to reaction time.

Balmer α ASE signals are observed in all the flames studied. The largest ASE signals were obtained in rich (ϕ=1.42) H_2/O_2 flames. In this flame, we confirmed the forward and backward ASE signal intensities are equal. This test is important to distinguish between ASE and four-wave mixing mechanisms of collimated Balmer α signals; four-wave mixing can only phase match in the forward direction. In Fig. 3 the simultaneous measurement of ASE and LIF as a function of height above the burner surface is shown for fuel rich and lean 7.2 Torr, H_2/O_2 flames. The relative ASE and the LIF signals have the same profile in the rich case, while there is a significant deviation in the burnt gases of the lean flame. Goldsmith[9] has found that the quenching rate in the burnt gas of 20 Torr lean flames to be nearly two times faster than in rich flames. Thus, as the quenching rate increases we see a growing difference between the ASE and LIF signals. This shows that ASE intensities can have a larger sensitivity to quenching collisions than LIF. Measurements of the variation of the ASE signal with laser pulse energy show that these measurements are taken in the threshold region of exponential growth. Additional measurements of beam divergence, polarization, and laser pulse energy dependence have been made to characterize the ASE signals over a wide range of H atom concentration, quenching rates, and gas temperature.

Spectral bandwidth measurements of the ASE signal are shown in Fig. 4. The top panel shows the 2-d image of the Balmer α ASE through a 3.8 cm^{-1} monitor etalon; the interference fringe pattern is evident. In the lower panel a single slice across the image is plotted. The FWHM of the interference fringes is 1.4 cm^{-1} which is about twice the Doppler width in this 1200 K flame. The contributions of Stark broadening, fine structure, and gain narrowing are being evaluated. Bandwidth measurements for single laser shots using less than 200 μJ of 205 nm laser light have

been demonstrated. These measurements show that single laser pulse, single color, temperature measurements are feasible using ASE.

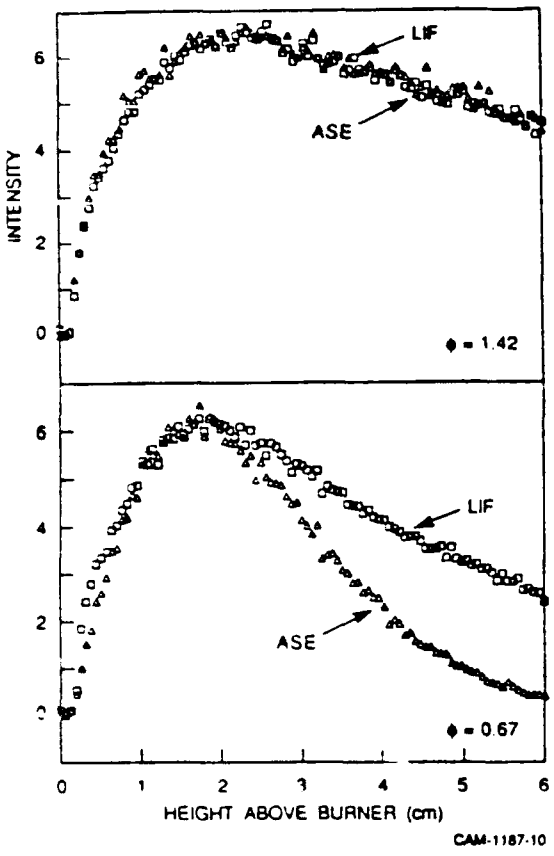

Figure 3. ASE and LIF versus height above burner simultaneously acquired in fuel rich and lean 7.2 Torr H_2/O_2 flames.

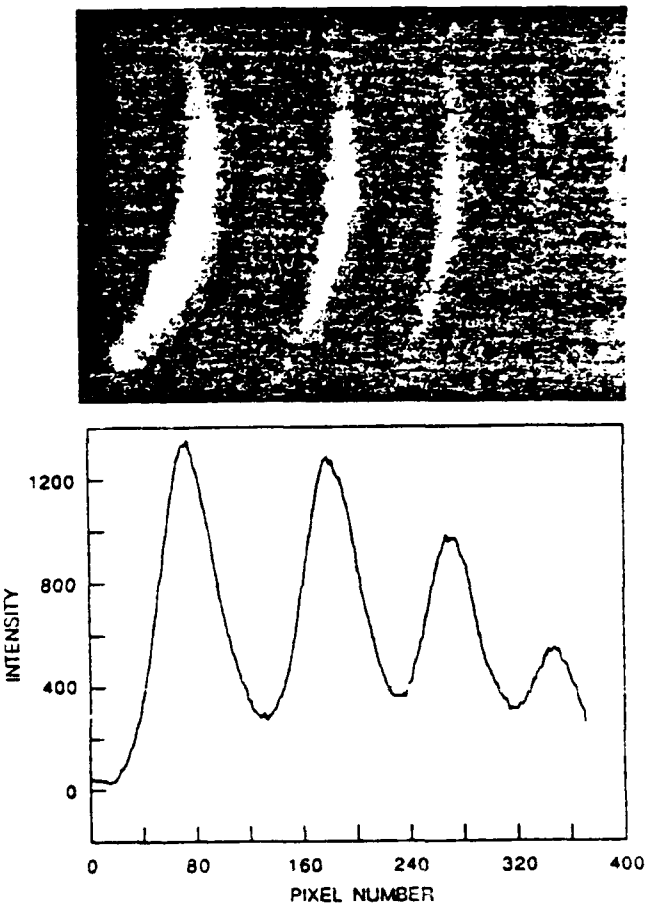

Figure 4. 2-d Image of the ASE signal through a monitor etalon in the rich H_2/O_2 flame; lower panel shows a single slice through the image.

REFERENCES

1. G. W. Faris, M. J. Dyer, W. K. Bischel, and D. L. Huestis, "Multiphoton Detection Techniques for F and F_2," Final Report AFOSR Contract No. F49620-88-K-0003, SRI International, Menlo Park, CA (November 1990).
2. G. Hilber, A. Lago, and R. Wallenstein, J. Opt. Soc. Am. B **4**, 1753 (1978).
3. J. P. Marangos et al., J. Opt. Soc. Am B **7**, 1254 (1990).
4. H. Pummer et al. Phys. Rev. A **28**, 795 (1983).
5. D. E. Heard and J. B. Jeffries, Paper 91-21 Spring Meeting of the Western States Section of the Combustion Institute, Boulder, CO, March 1991.
6. K. Kohse-Höinghaus, J. B. Jeffries, R. A. Copeland, G. P. Smith, and D. R. Crosley, 22nd Symposium (Int) on Combustion, The Combustion Institute, Pittsburgh, PA, 1989, p. 1857.
7. J. B. Jeffries, D. R. Crosley, I. J. Wysong, and G. P. Smith, 23rd Symposium (Int) on Combustion, The Combustion Institute, 1991, in press.
8. D. E. Heard, J. B. Jeffries, G. P. Smith; and D. R. Crosley, Combustion and Flame, submitted.
9. J.E.M. Goldsmith, R.J.M. Anderson, and L. R. Williams, Opt. Lett. **15**, 78 (1990).

AFOSR SPONSORED RESEARCH IN DIAGNOSTICS OF REACTING FLOW

PROGRAM MANAGER: JULIAN M. TISHKOFF

AFOSR/NA
BOLLING AFB DC 20332-6448

SUMMARY/OVERVIEW: The Air Force Office of Scientific Research (AFOSR) program in diagnostics of reacting flow currently is focused on three areas of study: gas-phase measurements, plasmas, and particle/droplet measurements. An assessment of major research needs in each of these areas is presented.

TECHNICAL DISCUSSION

AFOSR is the single manager for Air Force basic research, including efforts based on external proposals and in-house work at Air Force laboratories. The diagnostics of reacting flows task is assigned to the AFOSR Directorate of Aerospace Sciences along with programs in rocket propulsion, airbreathing combustion, and fluid and solid mechanics.

Interests of the AFOSR diagnostics of reacting flow task are given in the SUMMARY section above. This program, now in its tenth year, has produced many "first-ever" laser-based measurements. The instrumentation with which these measurements were made is becoming commonly available for laboratory and bench test utilization. Measurements range from microscopic to macroscopic scales with relevance to: plasma acceleration; combustion aerothermochemistry; the behavior and synthesis of advanced energetic materials; characterization of exhaust plume formation and radiation; and dynamic control of propulsion, weapon and power generation systems.

Decisions on support for research proposals are based on scientific opportunities and technology needs. Current AFOSR perceptions of scientific opportunities appear in Figure 1. As indicated by the orientation of the arrows in Figure 1, the task area with the greatest growth potential is plasmas.

The purpose of this abstract has been to communicate AFOSR perceptions of research trends to the university and industrial research communities. However, communication from those communities back to AFOSR also is desirable and essential for creating new research opportunities. Therefore, all proposals and inquiries for fundamental research are encouraged even if the content does not fall within the areas of emphasis described herein. Comments and criticisms of current AFOSR programs also are welcome.

Air Force Basic Research

Aerospace Sciences

Diagnostics Of Reacting Flow

Research Area	Trend	Decrease	Increase
Gas-Phase Measurements	→		Degenerate Four-Wave Mixing
Plasmas	→		
Particle/Droplet Measurements	→	Sizing	Liquid-Phase Motion & Properties

AIRBREATHING COMBUSTION

Invitees

Dr Griffin Anderson
NASA Langley Research Center
M/S 168
Hampton VA 23665
(804)864-3772

Dr Scott Anderson
Department of Chemistry
State University of New York
Stony Brook NY 11794-3400
(516)632-7915

Dr K Annamalai
Mechanical Engineering Dept
Texas A&M University
College Station TX 77843-3123

Dr Kurt Annen
Aerodyne Research, Inc.
45 Manning Road
Manning Park Research Center
Billerica MA 01821-3976
(508)663-9500

Dr Simon Bauer
Department of Chemistry
Cornell University
Ithaca NY 14853-1301

Dr S L Baughcum
Spectra Technology
2755 Northrup Way
Bellevue WA 98004-1495
(206)828-3517

Dr Howard Baum
National Institute of
Standards and Technology
Center for Fire Research
Gaithersburg MD 20899
(301)975-6668

Dr John Bdzil
Los Alamos National Laboratory
Los Alamos NM 87545

Dr H L Beach
NASA Langley Research Center
MS 168
Hampton VA 23665-5225
(804)864-3772
(804)864-2658

Dr Josette Bellan
Applied Technologies Section
Jet Propulsion Laboratory
4800 Oak Grove Drive
Pasadena CA 91109
(818)354-6959

Dr Paul Bonczyk
United Technologies Research
Center
Silver Lane
East Hartford CT 06108
(203)727-7162

Dr Gary Borman
University of Wisconsin
Engine Research Lab, ME Dept
1500 Johnson Drive, Rm 119 ERB
Madison WI 53706
(608)263-1616
FAX:262-6707

Dr Kevin Bowcutt
Rockwell International
Mail Code NA40
12214 Lakewood Boulevard
Downey CA 90241
(213)420-0317

Dr C T Bowman
Department of Mechanical
Engineering
Stanford University
Stanford CA 94305-3032
(415)723-1745

Dr K N C Bray
University of Cambridge
Department of Engineering
Trumpington Street
Cambridge CB2 1PZ, England UK
0223 332744
0223 337733

Dr Robert Breidenthal
Department of Aeronautics and Astronautics
University of Washington, FS10
Seattle WA 98195
(206)685-1098

Dr Kenneth Brezinsky
Department of Mechanical and Aerospace Engineering
Princeton University
Princeton NJ 08544-5263
(609)258-5225

Dr J E Broadwell
Graduate Aeronautical Labs
California Institute of Technology
Pasadena CA 91125

Dr Garry Brown
Department of Mechanical and Aerospace Engineering
Princeton University
Princeton NJ 08544-5263

Dr R C Brown
Aerodyne Research, Inc.
45 Manning Road
Manning Park Research Center
Billerica MA 01821-3976
(508)663-9500

Lt Col Larry Burggraf
AFOSR/NC
Bolling AFB DC 20332-6448
(202)767-4960
AV297-4960

Dr Dennis Bushnell
NASA Langley Research Center
Mail Stop 168
Hampton VA 23665
(804)864-4546

Dr Ron Butler
WL/POSF
Wright-Patterson AFB OH 45433-6563

Dr T D Butler
Group T-3
Los Alamos National Laboratory
Los Alamos NM 87545
(505)667-4156

Dr H F Calcote
AeroChem Research Laboratories Inc.
P. O. Box 12
Princeton NJ 08542
(609)921-7070

Dr Brian Cantwell
Department of Mechanical Engineering
Stanford University
Stanford CA 94305-3032
(415)723-4825

Dr Tryfon Charalampopoulos
Mechanical Engineering Dept.
Louisiana State University
Baton Rouge LA 70803
(504)388-5792
(504)388-5799

Capt Wayne Chepren
HQ AFESC/RDV
Tyndall AFB FL 32403-6001
(904)283-4234
AV523-4234

Dr Norman Chigier
Department of Mechnanical Engineering
Carnegie-Mellon University
Pittsburgh PA 15213-3890
(412)578-2498

Dr Robert Childs
Nielsen Engineering and Research, Inc.
510 Clyde Avenue
Mountain View CA 94043-2287
(415)968-9457

Dr S Y Cho
Department of Mechanical and Aerospace Engineering
Princeton University
Princeton NJ 08544-5263

Dr M-S Chou
Building R1, Room 1044
TRW Space and Technology Group
One Space Park
Redondo Beach CA 90278
(213)535-4321

Mr R.W. Claus
NASA Lewis Research Center
21000 Brookpark Road
Cleveland OH 44135-3127
(216)433-5869

Mr Steven Clouser
Research and Technology Group
Naval Air Propulsion Center
Trenton NJ 08628
(609)896-5752
AV442-7752

Dr M B Colket
United Technologies Research Center
Silver Lane
East Hartford CT 06108
(203)727-7481

Mr Stephen Corda
Applied Physics Laboratory
Johns Hopkins University
Johns Hopkins Road
Laurel MD 20707-6099
(301)953-5000
Ext 4654

Dr S M Correa
General Electric - Corporate Research and Development
P. O. Box 8
Schenectady NY 12301
(518)387-5853

Dr C Criner
Mach I, Inc
346 East Church Road
King of Prussia PA 19406
(803)292-3345

Dr Clayton Crowe
Department of Mechanical Engineering
Washington State University
Pullman WA 99164-2920
(509)335-3214

Dr E T Curran
WL/CA-P
Wright-Patterson AFB OH 45433-6563
(513)255-2246
AV785-2246

Dr Eli Dabora
Mechanical Engineering Dept
University of Connecticut
Box U-139 ME
Storrs CT 06268
(203)486-2415
(203)486-2189

Dr Werner Dahm
Department of Aerospace Engineering
The University of Michigan
Ann Arbor MI 48109-2140
(313)764-4318

Dr Ron Davis
Chemical Science and Techn Lab
Building 221, Room B312
National Inst of Stds & Tech
Gaithersburg MD 20899

Lt Col Larry Davis
HQ AFSC/XTR
Andrews AFB DC 20334
(301)981-7882

Dr George Deiwert
NASA Ames Research Center
MS 230-2
Moffett Field CA 94035
(415)604-6198

Dr R W Dibble
Department of Mechanical Eng
6159 Etcheverry Hall
University of California
Berkeley CA 94720
(415)642-4901
FAX -6163

Dr Paul Dimotakis
Graduate Aeronautical Labs
California Institute of
Technology
Pasadena CA 91125
(818)356-4456

Mr Lee Dodge
Southwest Research Institute
P O Drawer 28510
San Antonio TX 78284
(512)684-5111
Ext 3251

Dr David Dolling
Department of Aerospace Engrg
and Engineering Mechanics
University of Texas at Austin
Austin TX 78712
(512)471-4470
(512)471-7593

Capt Randy Drabczuk
OL-AQ/SAH
Eglin AFB FL 32542-5434
AV872-0360
(904)882-0360

Dr Michael Drake
Physical Chemistry Department
General Motors Research Labs
Twelve Mile and Mound Roads
Warren MI 48090-9055

Dr Frederick Dryer
Department of Mechanical and
Aerospace Engineering
Princeton University
Princeton NJ 08544-5263
(609)258-5206

Dr C Dutton
Department of Mechanical and
Industrial Engineering
University of Illinois
Urbana IL 61801

Dr Harry Dwyer
Department of Mechanical
Engineering
University of California
Davis CA 95616

Dr Raymond Edelman
WC 70
Rocketdyne
6633 Canoga Avenue
Canoga Park CA 91304
(805)371-7196

Dr J T Edwards
WL/POSF
Wright-Patterson AFB OH 45433-6563
(513)255-2460
FAX:255-1125

Ms Charlotte Eigel
WL/POSF
Wright-Patterson AFB OH 45433-6563
(513)255-5106
AV785-5106

Dr Phillip Emmerman
Harry Diamond Laboratories
Attn. SLCHD-ST-RD
2800 Powder Mill Road
Adelphi MD 20783-1197
(301)394-3000

Dr K C Ernst
Pratt and Whitney Aircraft Group
Government Products Division
West Palm Beach FL 33402

Mr John Facey
Code RP
NASA
400 Maryland Avenue, SW
Washington DC 20546
(202)453-2854

Dr G M Faeth
Department of Aerospace Engineering
University of Michigan
Ann Arbor MI 48109-2140
(313)764-7202

Dr Francis Fendell
TRW Space and Technology Group
Building R1, Room 1022
One Space Park
Redondo Beach CA 90278
(213)812-0327

Dr Michael Frenklach
202 Academic Projects Building
The Pennsylvania State University
University Park PA 16802
(814)865-4392

Mr Jack Fultz
WL/POPR
Wright-Patterson AFB OH 45433-6563
(513)255-2175
AV785-2175

Dr David Fyfe
Laboratory for Computational Physics
Naval Research Laboratory
Washington DC 20375
(202)767-6583
AV297-6583

Dr Alon Gany
Department of Aeronautical Eng
Technion-Israel Institute of Technology
32000 Haifa, ISRAEL
04-292308

Dr Ahmed Ghoniem
Department of Mechanical Engineering
MIT
Cambridge MA 02139
(617)253-2295
FAX:253-5981

Mr R Giffen
General Electric Company
Aircraft Engine Group
Neumann Way
Cincinnati OH 45215

Dr P Givi
Department of Mechanical and Aerospace Engineering
State University of New York
Buffalo NY 14260

Dr Irvin Glassman
Department of Mechanical and Aerospace Engineering
Princeton University
Princeton NJ 08544-5263
(609)258-5199
(813)442-1118

Dr A D Gosman
Department of Mechanical Engrg
Imperial College of Science
and Technology
London WS7 2BX UK

Dr Frederick Gouldin
Department of Mechanical and
Aerospace Engineering
Cornell University
Ithaca NY 14853-1301

Dr F Grinstein
Laboratory for Computational
Physics
Naval Research Laboratory
Washington DC 20375

Dr William Grosshandler
National Science Foundation
Chemical and Process Eng. Div.
1800 G Street, N. W.
Washington DC 20550
(202)357-9606

Dr Ephraim Gutmark
Research Department
Code 3892
Naval Weapons Center
China Lake CA 93555-6001
(619)939-3745
AV437-3745

Dr Howard Hanley
Chem & Sci Tech Lab
National Inst of Stds & Tech
325 Broadway
Boulder CO 80303-3328
(303)497-3320

Dr Robert Hansen
Office of Naval Research
Code 1215
800 North Quincy Street
Arlington VA 22217-5000
(202)696-4715

Lt Col George Haritos
AFOSR/CC
Bolling AFB DC 20332-6448
(202)767-5017
AV297-5017

Dr Stephen Harris
Physical Chemistry Department
General Motors Research Labs
30500 Mound Road
Warren MI 48090-9055
(313)986-1305

Dr James Hermanson
Propulsion Technology
United Technologies Research
Center
East Hartford CT 06108

Mr Norman Hirsch
WL/POPR
Wright-Patterson AFB OH 45433-6563
(513)255-2175
AV785-2175

Mr Robert Holland
United Technologies Chemical
Systems Division
P O Box 49028
San Jose CA 95161-9028
(408)224-7656

Dr M Y Hussain
ICASE, Mail Stop 132C
NASA Langley Research Center
Hampton VA 23665
(804)864-2175

Dr A K M F Hussain
Department of Mechanical
Engineering
University of Houston
Houston TX 77004
(713)749-4444

Dr T A Jackson
WL/POSF
Wright-Patterson AFB OH 45433-6563
(513)255-6462
AV785-6462

Mr Gordon Jensen
United Technologies Chemical
Systems Division
P O Box 49028
San Jose CA 95161-9028
(408)365-5552

Dr Sheridan Johnston
Combustion Sciences
Sandia National Laboratories
Livermore CA 94550
(415)294-2138

Dr W-H Jou
M/S 7K-06
P. O. Box 3707
Seattle WA 98124-2207
(206)865-6102

Dr Ann Karagozian
Mechanical, Aerospace and
Nuclear Engineering Department
University of California, LA
Los Angeles CA 90024
(213)825-5653

Dr Arnold Kelly
Department of Mechanical and
Aerospace Engineering
Princeton University
Princeton NJ 08544-5263
(609)258-5221

Dr John Kelly
Altex Technologies Corporation
650 Nuttman Road
Suite 114
Santa Clara CA 95054
(408)980-8610

Dr Ian Kennedy
Mechanical Engineering Dept
University of California,
Davis
Davis CA 95616
(916)752-2796

Dr James Kezerle
Gas Research Institute
8600 West Bryn Mawr Avenue
Chicago IL 60631
(312)399-8331

Dr Galen King
Department of Mechanical
Engineering
Purdue University
West Lafayette IN 47907
(317)494-2713

Mr R Kirby
Garrett Turbine Engine Company
111 South 34th Street
P. O. Box 5217
Phoenix 85010

Dr Charles Kolb
Aerodyne Research, Inc.
45 Manning Road
Manning Park Research Center
Billerica MA 01821-3976
(508)663-9500

Dr Wolfgange Kollmann
Mechanical Engineering Dept
University of California,
Davis
Davis CA 95616
(916)752-1452

Dr George Kosaly
Department of Mechanical
Engineering
University of Washington
Seattle WA 98195
(206)543-6933
FAX:685-8047

Dr C R Krishna
Department of Nuclear Energy
Brookhaven National Laboratory
Upton NY 11973

Mr David Kruczynski
Attn SLCBR-IBA
Interior Ballistics Division
Ballistic Research Laboratory
Aberdeen Proving Gnd MD 21005-5066
(301)278-6202
AV298-6202

Dr Kenneth Kuo
Department of Mechanical
Engineering
Pennsylvania State University
University Park PA 16802
(814)865-6741
FAX:863-3203

Lt James LaCasse
OL-AQ/SAH
Eglin AFB FL 32542-5434
(904)882-0207
AV872-0207

Dr Marshall Lapp
High Temperature Interfaces
Division
Sandia National Laboratories
Livermore CA 94550
(415)294-2435

Dr John Larue
Department of Mechanical
Engineering
University of California
Irvine CA 92717

Dr A Laufer
Office of Energy Research
U. S. Department of Energy
1000 Independence Avenue, N.W.
Washington DC 20585
(202)353-5820

Dr N M Laurendeau
Department of Mechanical
Engineering
Purdue University
West Lafayette IN 47907
(317)494-2713

Dr Moshe Lavid
ML Energia, Inc.
P. O. Box 1468
Princeton NJ 08540
(609)799-7970

Dr C K Law
Department of Mechanical and
Aerospace Engineering
Princeton University
Princeton NJ 08544-5263
(609)258-5271
FAX:258-6109

Dr Stan Lawton
McDonnell Douglas Research Lab
McDonnell Douglas Corporation
PO Box 516
St Louis MO 63166-0516
(314)233-2547

Dr J Carl Leader
McDonnell Douglas Research Lab
McDonnell Douglas Corporation
PO Box 516
St Louis MO 63166-0516
(314)232-4687

Dr C C Lee
Environmental Protection
Agency
Cincinnati OH 45268
(513)569-7520

Dr Spiro Lekoudis
Office of Naval Research
Mechanics Division, Code 432
800 North Quincy Street
Arlington VA 22217-5000
(202)696-4406

Dr Anthony Leonard
Graduate Aeronautical Labs
California Institute of
Technology
Pasadena CA 91125
(818)356-4465

Dr R S Levine
National Institute of
Standards and Technology
Center for Fire Research
Gaithersburg MD 20899
(301)921-3845

Dr Erwin Lezberg
NASA Lewis Research Center
21000 Brookpark Road
Cleveland OH 44135-3127
(216)433-5884

Dr Paul Libby
Dept. Of. Appl. Mech. and
Engrg. Sci.
University of California
La Jolla CA 92093
(619)534-3168

Dr Wilbert Lick
Department of Mechanical and
Environmental Engineering
University of California
Santa Barbara CA 93106

Dr Hans Liepmann
Graduate Aeronautical Labs
California Institute of
Technology
Pasadena CA 91125
(818)356-4535

Dr F E Lytle
Department of Chemistry
Purdue University
West Lafayette IN 47907
(317)494-5261

Dr Andrej Macek
National Institute of
Standards and Technology
Physics Building, B-312
Gaithersburg MD 20899
(301)975-2610

Dr James Madson
McDonnell Douglas Research Lab
McDonnell Douglas Corporation
PO Box 516
St Louis MO 63166-0516

Dr Edward Mahefkey
WL/POOC-5
Wright-Patterson AFB OH 45433-6563
(513)255-6241
AV785-6241

Dr Oscar Manley
US Department of Energy
Office of Energy Research
1000 Independence Avenue, SW
Washington DC 20585
(202)353-5822

Dr David Mann
U. S. Army Research Office
Engineering Sciences Division
P. O. Box 12211
Research Triangle Pk NC 27709-2211
(919)549-4249
AV832-4249

Dr Nagi Mansour
Computational Fluid Mechanics
Branch, RFT 202A-1
NASA Ames Research Center
Moffett Field CA 94035
(415)604-6420

Dr Frank Marble
Engrg. and Appl. Sci. Dept.
California Institute of
Technology
Pasadena CA 91125
(818)356-4784

Dr John Marek
NASA Lewis Research Center
21000 Brookpark Road
Cleveland OH 44135-3127

Mr C R Martel
WL/PO
Wright-Patterson AFB OH 45433-6563
(513)255-7431
AV785-7431

Dr Bruce Masson
PL/ARDF
Kirtland AFB NM 87117-6008
(505)844-0208
AV244-0208

Dr James McDonald
Code 6110
Naval Research Laboratory
Chemistry Division
Washington DC 20375
(202)767-3340
AV297-3340

Dr D K McLaughlin
233 Hammond Building
Pennsylvania State University
University Park PA 16802
(814)865-2569

Dr James McMichael
AFOSR/NA
Bolling AFB DC 20332-6448
(202)767-4936
AV297-4936

Dr A M Mellor
Mech & Matls Eng Department
Station B, Box 6019
Vanderbilt University
Nashville TN 37235
(615)343-6214

Dr Lynn Melton
Programs in Chemistry
University of Texas, Dallas
P. O. Box 668
Richardson TX 75080
(214)690-2913

Dr R Metcalfe
Department of Mechanical
Engineering
University of Houston
Houston TX 77004
(713)749-2439

Dr D L Mingori
Mechanical, Aerospace and
Nuclear Engineering Dept
University of California
Los Angeles CA 90024
(213)825-1265

Dr Andrzej Miziolek
Ignition and Combustion Branch
Interior Ballistics Division
Ballistic Research Laboratory
Aberdeen Proving Gnd MD 21005-5066
(301)278-6157

Dr Parviz Moin
Center for Turbulence Research
Stanford University
Stanford CA 94305-3032
(415)725-2081

Dr H Mongia
General Motors Corporation
Allison Gas Turbine Operations
P. O. Box 420
Indianapolis IN 46206-0420
(317)242-5945

Dr Peter Monkewitz
Mechanical, Aerospace and
Nuclear Engineering Dept
University of California
Los Angeles CA 90024
(213)825-5217

Dr P J Morris
233-L Hammond Building
Pennsylvania State University
University Park PA 16802
(814)863-0157

Dr Edward Mularz
Aviation Res. and Tech. Activ.
NASA Lewis Res. Ctr., MS 5-11
21000 Brookpark Road
Cleveland OH 44135-3127
(216)433-5850

Dr M G Mungal
Department of Mechanical
Engineering
Stanford University
Stanford CA 94305-3032
(415)725-2019

Dr Arje Nachman
AFOSR/NM
Bolling AFB DC 20332-6448
(202)767-5028
AV297-5028

Dr ABdollah Nejad
WL/POPT
Wright-Patterson AFB OH 45433-6563
(513)255-9991
AV785-9991

Dr Herbert Nelson
Code 6110, Chemistry Division
Naval Research Laboratory
Washington DC 20375
(202)767-3686

Dr David Nixon
Nielsen Engineering and
Research, Inc.
510 Clyde Avenue
Mountain View CA 94043-2287
(415)968-9457

Dr G B Northam
NASA Langley Research Center
MS 168
Hampton VA 23665-5225
(804)864-6248

Dr R C Oldenborg
Chemistry Division
Los Alamos National Laboratory
Los Alamos NM 87545
(505)667-2096
(505)667-3758

Dr A K Oppenheim
Department of Mechanical
Engineering
University of California
Berkeley CA 94720
(415)642-0211

Dr Elaine Oran
Laboratory for Computational
Physics
Naval Research Laboratory
Washington DC 20375
(202)767-2960

Dr Simon Ostrach
Case Western Reserve Univ
Department of Mechanical and
Aerospace Engineering
Cleveland OH 44106

Dr Richard Peterson
Department of Mechanical
Engineering
Oregon State University
Corvallis OR 97331-6001
(503)754-2567

Dr W M Pitts
National Institute of
Standards and Technology
Center for Fire Research
Gaithersburg MD 20899
(301)975-6486

Dr Robert Pitz
Department of Mechanical and Materials Engineering
Vanderbilt University
Nashville TN 37235
(615)322-0209

Dr S B Pope
Department of Mechanical and Aerospace Engineering
Cornell University
Ithaca NY 14853-1301
(607)255-4314

Dr C L Proctor II
Department of Mechanical Engineering
University of Florida
Gainesville FL 32611
(904)392-7555

Dr Herschel Rabitz
Department of Chemistry
Princeton University
Princeton NJ 08544-5263
(609)258-3917

Dr Saad Ragab
Engrg Sci & Mechanics Dept
Virginia Polytechnic Institute and State University
Blacksburg VA 24061
(703)231-5950

Dr S R Ray
National Institute of Standards and Technology
Center for Chemical Engrg
Gaithersburg MD 20899

Dr R G Rehm
National Institute of Standards and Technology
Center for Fire Research
Gaithersburg MD 20899
(301)975-2704

Dr Rolf D Reitz
Mechanical Engineering Dept
University of Wisconsin
1500 Johnson Drive
Madison WI 53706
(608)262-0145
FAX:263-6717

Dr M Renksizbulut
Department of Mechanical Engineering
University of Waterloo
Waterloo, Ontario CN N2L 3G1
(519)885-1211
Ext 3977

Dr David Reuss
Fluid Mechanics Department
General Motors Research Labs
30500 Mound Road
Warren MI 48090-9055
(313)986-0029

Dr William Reynolds
Department of Mechanical Engineering
Stanford University
Stanford CA 94305-3032
(415)723-3840

Dr James J Riley
Department of Mechanical Engineering
University of Washington
Seattle WA 98195

Dr James Riley
Mechanical Engineering Dept
University of Washington
Seattle WA 98195
(206)543-5347

Dr Michael Roco
National Science Foundation
Chemical and Thermal Syst Div
1800 G Street, N W
Washington DC 20550
(202)357-9606

Dr U S Rohatgi
Department of Nuclear Energy
Brookhaven National Laboratory
Upton NY 11973
(516)282-2475

Dr W M Roquemore
WL/POSF
Wright-Patterson AFB OH 45433-6563
(513)255-6813
AV785-6813

Dr Anatol Roshko
Graduate Aeronautical Labs
California Institute of
Technology
Pasadena CA 91125
(818)356-4484

Dr Daniel Rosner
Department of Chemical
Engineering
Yale University
New Haven CT 06520
(203)432-4391

Dr John Ross
Department of Chemistry
Stanford University
Stanford CA 94305-3032
(415)723-9203

Dr Gabriel Roy
Office of Naval Research
Mechanics Division, Code 1132
800 North Quincy Street
Arlington VA 22217-5000
(202)696-4405

Mr Kurt Sacksteder
NASA Lewis Research Center
MS 500-217
21000 Brookpark Road
Cleveland OH 44135
(216)433-2857

Dr Leonidas Sakell
AFOSR/NA
Bolling AFB DC 20332-6448
(202)767-4935
AV297-4935

Dr Mohammad Samimy
Ohio State University
Mechanical Engineering Dept
206 West 18th Street
Columbus OH 43210-1107
(614)422-6988

Dr G S Samuelsen
Department of Mechanical
Engineering
University of California
Irvine CA 92717
(714)856-5468

Mr John Sanborn
Garrett Turbine Engine Company
111 South 34th Street
P. O. Box 5217
Phoenix AZ 85010
(602)231-2588

Dr Billy Sanders
Thermofluids Division, 8363
Combustion Research Facility
Sandia National Laboratories
Livermore CA 94550
(415)294-3113

Dr Joseph Sangiovanni
United Technologies Research
Center
Silver Lane
East Hartford CT 06108
(203)727-7328

Dr Lakshmi Sankar
School of Aerospace Engrg
Georgia Institute of
Technology
Atlanta GA 30332
(404)894-3014

Dr Domenic Santavicca
Department of Mechanical Engineering
Pennsylvania State University
University Park PA 16802
(814)863-1863

Dr R J Santoro
Department of Mechanical Engineering
Pennsylvania State University
University Park PA 16801
(814)863-1285

Mr William Scallion
NASA Langley Research Center
Mail Stop 408
Hampton VA 23665
(804)864-5235

Dr Klaus Schadow
Naval Weapons Center
Code 3892
China Lake CA 93555-6001
(619)939-6532
AV437-6532

Dr John Schaefer
Energy and Environmental Div.
Acurex Corporation
555 Clyde Ave., P. O. Box 7555
Mountain View CA 94039

Dr W H Schofield
Aeronautical Research Labs
506 Lorimer St, Fishermen's Bn
Box 4331, P O
Melbourne, Victoria AUSTRALIA 3001

Dr Thomas A Seder
Rockwell International Sci Ctr
1049 Camino dos Rios
P O Box 1085
Thousand Oaks CA 91360
(805)373-4576

Dr D J Seery
United Technologies Research Center
Silver Lane
East Hartford CT 06108

Dr Hratch Semerjian
National Institute of Standards and Technology
Center for Chemical Engrg
Gaithersburg MD 20899
(301)975-2609

Dr C Senior
PSI Technology Company
Research Park
P O Box 3100
Andover MA 01810
(508)475-9030

Dr K Seshadri
Dept. Of. Appl. Mech. and Engrg. Sci.
University of California
La Jolla CA 92093
(619)534-4876

Dr G S Settles
309 Mechanical Engrg Building
Pennsylvania State University
University Park PA 16802
(814)863-1504

Dr Robert Shaw
Division of Chemical and Biological Sciences
U S Army Research Office
Research Triangle Park NC 27709-221
(919)549-0641

Mr Harold Simmons
Parker Hannifin Corporation
Gas Turbine Fuel Systems Div.
17325 Euclid Avenue
Cleveland OH 44143
(216)531-3000
Ext 2309

Dr William Sirignano
School of Engineering
University of California
Irvine CA 92717
(714)856-6002

Dr Bernard Spielvogel
U S Army Research Office
P O Box 12211
Research Triangle Pk NC 27709-2211

Dr F Dee Stevenson
Office of Basic Energy Science
U. S. Department of Energy
1000 Independence Avenue, N W
Washington DC 20585

Dr David Stewart
Department of Theoretical and
Applied Mechanics
University of Illinois
Urbana IL 61801

Dr Anthony Strawa
NASA Ames Research Center
MS 230-2
Moffett Field CA 94035
(415)604-3437

Dr F D Stull
WL/POPS
Wright-Patterson AFB OH 45433-6563
(513)255-5210
AV785-5210

Dr B Sturtevant
Engrg and Appl Sci Dept
California Institute of
Technology
Pasadena CA 91125

Dr G Sullins
Applied Physics Laboratory
Johns Hopkins University
Johns Hopkins Road
Laurel MD 20707-6099
(301)953-5000

Dr Dexter Sutterfield
National Institute for
Petroleum and Energy Research
Post Office Box 2128
Bartlesville OK 74005
(918)337-4251

Dr Larry Talbot
Department of Mechanical
Engineering
University of California
Berkeley CA 94720
(415)642-6780

Dr Christopher Tam
Department of Mathematics
Florida State University
Tallahasee FL 32306-3027
(904)644-2455

Dr Julian Tishkoff
AFOSR/NA
Bolling AFB DC 20332-6448
(202)767-0465
AV297-0465

Dr T Y Toong
Department of Mechanical
Engineering
MIT
Cambridge MA 02139
(617)253-3358

Dr Michael Trenary
Department of Chemistry
The University of Illinois
Chicago IL 60680

Dr Timothy Troutt
Department of Mechanical Engineering
Washington State University
Pullman WA 99164-2920

Dr Allen Twarowski
Rockwell International Sci Ctr
1049 Camino dos Rios
P O Box 1085
Thousand Oaks CA 91360
(805)373-4576

Dr C J Ultee
United Technologies Research Center
Silver Lane
East Hartford CT 06108

Dr A D Vakili
University of Tennessee
Space Institute
Tullahoma TN 37388

Dr S P Vanka
Department of Mechanical and Industrial Engrg
University of Illinois
Urbana IL 61801

Dr Earl VanLandingham
National Aeronautics & Space Administration, Code RB
400 Maryland Avenue, SW
Washington DC 20546
(202)453-2847

Dr P J Waltrup
Applied Physics Laboratory
Johns Hopkins University
Johns Hopkins Road
Laurel MD 20707-6099
(301)953-5000
Ext. 4186

Dr Charles Westbrook
Lawrence Livermore National Laboratories
P. O. Box 808
Livermore CA 94550

Dr James Whitelaw
Department of Mechanical Engrg
Imperial College of Science and Technology
London SW7 2BX UK

Dr Forman Williams
Department of Applied Mech and Engineering Science
University of California
La Jolla CA 92093
(619)534-5492

Dr Michael Winter
Propulsion Science
United Technologies Research Center
East Hartford CT 06108
(203)727-7805

Dr J M Wu
University of Tennessee
Space Institute
Tullahoma TN 37388

Dr Richard Yetter
Department of Mechanical and Aerospace Engineering
Princeton University
Princeton NJ 08544-5263

Dr Michael Zachariah
National Institute of Standards and Technology
Center for Chemical Engrg
Gaithersburg MD 20899
(301)975-2063

Mr Fred Zarlingo
Code 3246
Naval Weapons Center
China Lake CA 93555-6001
(619)939-7395
AV437-7395

Dr E E Zukoski
Engrg. and Appl. Sci. Dept.
California Institute of
Technology
Pasadena CA 91125
(818)356-4785

ROCKET PROPULSION

Invitees

Mr Robert Acree
OL-AC/VSSC
Edwards AFB CA 93523-5000
(805)275-5598
AV525-5598

Mr Ranney Adams
OL-AC/PA
Edwards AFB CA 93523-5000
(805)275-5465
AV525-5465

Dr George Adams
USA-BRL
AMXBR-I8D
AberdeenProving Gnd MD 21005-5006
(301)278-6168
(301)278-6783

Dr Horst Adolph
Synthesis and Formulations Br
Naval Surface Weapons Center
10901 New Hampshire Avenue
Silver Spring MD 20903-5000

Dr William E Anderson
Department of Mechanical
Engineering
Pennsylvania State University
University Park PA 16802
(814)863-6289

Mr W C Andrepont
P.O. Box 431
858 W. Jackman
Suite 111
Lancaster CA 93534
(805)942-5098

Lt John Andreshak
OL-AC/LKLR
Stop 24
Edwards AFB CA 93523-5000
(805)275-5194
AV525-5194

Mr Chris Andrews
OL-AC/LSVE
Edwards AFB CA 93523-5000
(805)275-5766
AV 525-5766

Dr Ron Atkins
Naval Weapons Center
China Lake CA 93555-6001
(619)939-1630
AV437-1630

Dr William Bailey
AFIT/ENP
Wright-Patterson AFB OH 45433-6583
(513)255-4498
AV785-4498

Dr Joseph Baum
SAIC
1710 Goodridge Drive
P.O. Box 1303,
McLean VA 22102
(703)827-4952

Maj Douglas Beason
Director, Advanced Weapons
and Survivability
Philips Laboratory
Kirtland AFB NM 87117
(505)844-3672
AV244-3672

Dr Roger Becker
KL-462
Research Institute
University of Dayton
Dayton OH 45469
(513)229-3938

Mr Charles Beckman
OL-AC/MKPA
Stop 24
Edwards AFB CA 93523-5000
(805)275-5487
AV525-5487

Dr Merrill Beckstead
Dept of Chemical Engineering
Brigham Young University
Provo UT 84602
(801)378-6239

Dr Robert Beddini
Univ of Illinois
AAE Department
104 South Mathews Avenue
Urbana IL 61801-2997
(217)333-4239

Dr Clifford Bedford
SRI International
Chemistry Laboratory
Menlo Park CA 94025
(415)859-4449

Dr S J Bennett
Adv Technology Projects Div
Morton Thiokol, Inc, Wasatch
Box 524
Brigham City UT 84302
(801)863-2980

Dr Greg Berry
Argonne National Laboratory
9700 South Cass Avenue
Argonne IL 60439
(312)972-6160

Dr Oscar Biblarz
Department of Aeronautics
Naval Post Graduate School
Monterey CA 93943-5100
(408)646-2972
AV878-2972

Mr Robert Biggers
OL-AC/XRX
Stop 24
Edwards AFB CA 93523-5000
(805)275-5241
AV525-5341

Dr S Binkley
Combustion Research Facility
Sandia National Laboratories
Livermore CA 94550

Dr Mitat Birkan
AFOSR/NA
Bolling AFB DC 20332-6448
(202)767-4938
AV297-4938

Dr Fred Blomshield
Code 3892,Propulsion
Research Branch
Naval Weapons Center
China Lake CA 93555
(619)939-3650
AV437-3650

Dr Arthur Bracut
ARDC
LCWSL
Dover NJ 07801
(201)724-3788
AV880-3788

Dr Mel Branch
Mechanical Engineering Dept
University of Colorado
Boulder CO 80309-0427
(303)492-6318
(303)492-7151

Dr John Brandenburg
Mission Research Corporation
8560 Cinderbed Road
Suite 700
Newington VA 22122
(703)339-6500

Dr Thomas Brill
University of Delaware
Department of Chemistry
Newark DE 19716
(302)451-6079

Dr Bruce Broline
PO Box 3999
M/S 82-23
Boeing Aerospace
Seattle WA 98042
(206)773-5846

Dr Robert Brown
United Technologies Corp
Chemical Systems Division
P. O. Box 49028
San Jose CA 95161-9028
(408)778-4680

Dr James Bryant
Naval Weapons Center
China Lake CA 93555-6001
(619)939-7206
AV437-7206

Dr Rodney Burton
Dept. of Aero. And Astro. Engg
University Of Illinois-UC
101 Transportation Building
Urbana IL 61801-2997
(217)333-2651

Mr David Byers
NASA Lewis Research Center
MS 500-219
21000 Brookpark Road
Cleveland OH 44135-3127
(216)433-2447

Dr George Caledonia
Physical Sciences Inc
20 New England Business Center
Andover MA 01810
(617)475-9030

Dr David Campbell
OL-AC/DYC
Stop 24
Edwards AFB CA 93523-5000

Dr Robert Carrol
Pratt & Whitney
P.O. Box 109600
West Palm Beach FL 33410-9600
(407)796-2889

Dr Robert Cassel
Naval Sea Systems Command
Code 62D
Washington DC 20362
(202)692-8635

Dr Robert Cattolica
Sandia National Laboratories
Division 9351
Livermore CA 94550

Dr Leonard Caveny
OSD/SDIO/IST
Pentagon
Washington DC 20301-7100
(202)693-1530

Dr Yunus Ali Cengel
University of Nevada-Reno
Dept of Mechanical Engg
Reno NV 89557-0030

Dr May Chan
Naval Weapons Center
China Lake CA 93555-6001
(619)939-7519
AV437-7519

Dr Franklin Chang-Diaz
Lyndon B Johnson Space Center
Code CB
Houston TX 77058
(713)483-2714

Dr Robert Chapman
OL-AC/LKLR
Stop 24
Edwards AFB CA 93523-5000
(805)275-5416
AV525-5416

Dr Malcolm Chase
Center for Chemical Physics
National Inst of Stds & Tech
Building 222, Room A158
Gaithersburg MD 20899
(301)975-2526

Dr Fan-Bill Cheung
Penn State University
208 Mechanical Engineering
University Park PA 16802
(814)863-4281
FAX 865-3389

Dr Peck Cho
Dept. of Mechanical Engg.
College of Engineering
Michigan Technological Univ.
Houghton MI 49931

Dr Won-Ho Choe
214 Nuclear Engineering Lab
University of Illinois
103 South Goodwin Avenue
Urbana IL 61801
(217)333-2821

Dr Chan K Choi
Purdue University
School of Nuclear Engrg
West Lafayette IN 47907
(317)494-6789

Dr Edgar Choueiri
Department of Mechanical And
Aerospace Engineering
Princeton University
Princeton NJ 08544-5263
(609)452-5221

Dr Karl Christe
Rocketdyne Division
Rockwell International
6633 Canoga Ave
Canoga Park CA 91304
(818)710-3268

Dr T J Chung
University of Alabama
Huntsville AL 35801
(205)895-6394

Dr George Clark
Aerojet Tactical Systems
PO Box 13400
Building 0525
Sacramento CA 95813
(916)988-6919

Dr William Clark
Naval Weapons Center
Code 3895
China Lake CA 93555-6001

Dr Ronald Cohen
The Aerospace Corporation
PO Box 92957
Mail Stop M5-754
Los Angeles CA 90009
(213)336-5946

Dr Norman Cohen
Aerospace Corporation
PO Box 92957
M/S 747
Los Angeles CA 90045
(213)648-7427

Dr Norman Cohen
Professional Services
141 Channing St
Redlands CA 92373
(714)792-8807

Dr Cliff Coon
Lawrence Livermore National Laboratories
Livermore CA 94550
(415)422-6311

Capt Edward Coppola
OL-AC/MKPA
Stop 24
Edwards AFB CA 93523-5000
(805)275-5534
AV525-5534

Mr Robert Corley
OL-AC/DYC
Stop 24
Edwards AFB CA 93523-5000
(805)275-5353
AV525-5353

Dr L Cottle
RARDE, Fort Halstead
Knockholt
Matternrks Kent UK

Dr George Cox
United Technologies
Pratt-Whitney
P.O. Box 109600
West Palm Beach FL 33410-9600
(407)796-2887
FAX 796-5825

Dr F E C Culick
Engrg and Appl Sci Dept
California Institute of Technology
Pasadena CA 91125
(818)356-4470

Dr C L Dailey
TRW Space and Technology Group
Applied Technology Division
One Space Park
Redondo Beach CA 90278
(213)536-1874

Dr John Daily
University of Colorado
Engineering Center ME 1-13
Campus Box 427
Boulder CO 80309-0427
(303)492-7110

Dr B R Daniel
School of Aerospace Rngrg
Georgia Institute of Technology
Atlanta GA 30332

Dr William Deininger
Jet Propulsion Laboratory
California Inst. of Technology
4800 Oak Grove Drive
Pasadena CA 91109
(818)354-7765

Mr S T Demetriades
STD Research Corp
P.O. Box C
Arcadia CA 91006
(818)357-2311

Dr Gregory Dobbs
United Technologies Res. Ctr.
MS 129-90 Silver Lane
East Hartford CT 06108
(203)727-7145
FAX 727-7669

Dr Joel Dubow
Materials Science
Univ of Utah
2008B Mechanical Engrg Bldg
Salt Lake City UT 84112
(801)581-8388

Dr John Eisch
Department of Chemistry
State University of New York
Binghamton NY 13901
(607)798-3994

Dr William Escher
NASA Headquarters
Code RP
Washington DC 20546
(202)453-9111

Dr James Fang
Rockwell/Rocketdyne Division
6633 Canoga Park
Canoga Park CA 91303
(818)718-3728
FAX 718-3600

Mrs Karen Farner
OL-AC/RKLB
Edwards AFB CA 93523-5000
(805)275-5198
AV525-5198

Dr Allan Ferrenberg
Manager, Advanced Comb. Device
Rocketdyne Div, Rockwell Int.
Mail Stop IR06,6633 Canoga Ave
Canoga Park CA 91303
(818)718-3713

Dr John Fischer
Code 3853
Naval Weapons Center
China Lake CA 93555-6001
(619)939-1641
AV437-1641

Dr J E Flanagan
Rocketdyne
6633 Canoga
Canoga Park CA 91304
(818)710-2466

Dr Gary Flandro
School of Aerospace Engg.
Georgia Institute of Tech.
Atlanta GA 30332-0420
(404)853-9160

Dr James Fong
Aerojet Tech Systems
P O Box 13222
Sacramento CA 95813

Dr Arthur Fontijn
Chemical & Environmental
Engineering Department
Rensselaer Polytechnic Inst.
Troy NY 12180-3590
(518)276-6508

Dr Milt Frankel
Rocketdyne
6633 Canoga Avenue
Canoga Park CA 91304
(818)710-4803
(818)710-5088

Dr R A Frederick
Sverdrup Technology, Inc
Mail Stop 900
Arnold AFB TN 37389-9998
(615)454-3130

Dr Sheilah Fultz
Naval Weapons Center
China Lake CA 93555-6001
(619)939-7521
AV437-7521

Mr Robert Geisler
OL-AC/YS
Edwards AFB CA 93523-5000
(805)275-5230
AV525-5230

Dr Eugene Gerber
Univ of Dayton Research
Institute
KL465
Dayton OH 45419
(513)229-3221

Dr Robert Ghirardelli
U.S. Army Research Office
P.O. Box 12211
Research Triangle Pk NC 27709-2211
(919)549-0641
AV935-3331

Lt Col Fred Gilliam
EOARD
Box 14
FPO NY 09510-0200
AV235-4505

Dr David Golden
SRI International
333 Ravenswood Avenue
Menlo Park CA 94025-3696
(415)859-0811

Dr B B Goshgarian
OL-AC/MKPB
Stop 24
Edwards AFB CA 93523-5000
(805)275-5183
AV525-5183

Dr William Graham
Morton Thiokol, Inc
Huntsville Division
Huntsville AL 35807-7501
(205)882-8397

Dr Alten Grandt
Department of Aeronautics
and Astronautics
Purdue University
West Lafayette IN 47907

Dr Ashwani K Gupta
Director, Combustion Lab.
The University of Maryland
Dept. of Mechanical Engrg.
College Park MD 20742
(301)454-8865

Mr Eugene Haberman
OL-AC/MK
Stop 24
Edwards AFB CA 93523-5000
(805)275-5420
AV525-5420

Dr V E Haloulakos
Advanced Propulsion
McDonnell Douglas
5301 Bolsa Avenue
Huntington Beach CA 92647
(714)896-3456

Dr Elmer Hansen
Department of Mechanical
Engineering
University of Florida
Gainesville FL 32611
(904)392-0802

Lt Col George Haritos
AFOSR/NA
Bolling AFB DC 20332-6448
(202)767-4987
FAX:767-0466

Dr Kenneth Harstad
Jet Propulsion Laboratory
4800 Oak Grove Drive
Pasadena CA 91109

Dr David Hastings
Department of Aeronautics
and Astronautics
Massachusetts Inst of Tech
Cambridge MA 02139

Ms Sharon Hasty
John Hopkins Univ/APL
CPIA
John Hopkins Road
Laurel MD 20707
(301)992-7306

Dr Donald Hautman
United Technologies Res. Ctr.
Silver Lane
East Hartford CT 06108
(203)727-7424

Dr Helmut Hellwig
AFOSR/CC
Bolling AFB DC 20332-6448
(202)767-5017
AV297-5017

Dr Alan Hersh
Hersh Acoustical Engineering
9545 Cozycroft Avenue
Chatsworth CA 91311
(818)998-8311
FAX 341-0978

Dr Rich Hollins
Naval Weapons Center
China Lake CA 93555-6001
(619)939-1650
AV437-1650

Dr H R Jacobs
Mechanical Engg Bldg, 208
Penn State University
University Park PA 16802
(814)863-2519
FAX 865-3389

Dr J I Jagoda
Aerospace Engineering Dept
Georgia Institute of
Technology
Atlanta GA 30329
(404)894-3060

Dr Donald Jassowski
Aerojet Technical Systems Co
PO Box 13222
Sacramento CA 95813
(916)355-2849

Dr S M Jeng
University of Tennessee
Space Institute
Tullahoma TN 37388

Dr Robert Jensen
Rockwell/Rocketdyne Division
6633 Canoga Ave
Canoga Park CA 91303
(818)718-3730
FAX 718-3600

Dr M W Johnson
Head of Neutron Inst. Division
Rutherford Appleton Laboratory
Science Department
Chilton, Didcot, Oxon UK OX11 OQX
0235-21900
0235-44-5720F

Dr Abraham Kadish
Earth and Space Sciences Div.
Atmospheric Sciences Group
Mail Stop D466, LANL
Los Alamos NM 87545

Dr Jordin Kare
Building 197, Room 1020
Lawrence Livermore Nat'l Lab
P O Box 808
Livermore CA 94550
(415)423-8300

Dr David Kassoy
Dept of Mechanical Engineering
University of Colorado at
Boulder, Campus Box 427
Boulder CO 80309
(303)492-2991
(303)492-7694

Dr Myron Kaufman
Department of Chemistry
Emory University
Atlanta GA 30322
(404)727-6619

Dr Dennis Keefer
University of Tennessee
Space Institute
Tullahoma TN 37388
(615)455-0631

Dr Arnold A Kelly
Department of Mechanical and
Aerospace Engineering
Princeton University
Princeton NJ 08544-5263
(206)452-5221

Dr Philip Kessel
OL-AC/LSCF
Edwards AFB CA 93523-5000

Dr Sue Kim
California State University
6000 J Street
Sacramento CA 95819
(916)454-6712

Dr David King
Mail Stop 125-224
Jet Propulsion Laboratory
4800 Oak Grove Drive
Pasadena CA 91103
(818)354-3315

Mr Mark Kleim
NASA Lewis Research Center
21000 Brookpark Rd
MS 510-219
Cleveland OH 44135

Dr Kenneth Kolouko
Morton Thiokol
Wasatch Division
P.O. Box 524
Brigham City UT 84302
(801)863-4220

Dr James Komar
Atlantic Research Corp
5390 Cherokee Avenue
Alexandria VA 23312
(703)642-4473

Dr Herman Krier
Dept of Mechanical and
Industrial Engineering
University of Illinois
Urbana IL 61801
(217)333-0529

Prof M Kristiansen
P.W. Horn Professor
Dept of Electrical Engg,MS3102
Texas Tech University
Lubbock TX 79409-4439
(806)792-3007

Dr Warren Krueger
167 Alvana Street, NW16-160
Massachusetts Institute of
Technology
Cambridge MA 02139
(617)253-0236

Dr Al Kudlach
OL-AC/RKLA
Edwards AFB CA 93523-5000
(805)275-5248
AV 525-5248

Dr Kenneth Kuo
Penn State University
208 Mechanical Engineering
University Park PA 16802
(814)863-6741
FAX 863-3203

Dr William Larson
OL-AC/LSVF
Edwards AFB CA 93523-5000
(805)275-5657
AV525-5657

Dr C K Law
Department of Mechanical and
Aerospace Engineering
Princeton University
Princeton NJ 08544-5263
(609)258-5271

Dr Miller Layton
OL-AC/LKLR
Stop 24
Edwards AFB CA 93523-5000

Dr Joel Lebowitz
Rutgers-The State University
Department of Mathematics
Hill Center-Busch Campus
New Brunswick NJ 08903
(201)932-3117

Mr Edward Lee
Special Projects Leader
P.O. Box 808,L-368
LLNL-University of California
Livermore CA 94550
(415)422-1316

Dr Ja H Lee
NASA Langley Research Center
M/S493
Hampton VA 23665
(804)864-4332

Mr Jay Levine
OL-AC/LSCF
Edwards AFB CA 93523-5000
(805)275-5366
AV 525-5366

Dr P Y Liang
Advanced Combustion Devices
Rocketdyne Div, Rockwell Int.
6633 Canoga Avenue
Canoga Park CA 91303

Dr George Lo
Lockheed Palo Alto Research
Laboratory
3251 Hanover St, 8204-93-50
Palo Alto CA 94304
(415)424-2514

Dr Geoffrey Main
School of Mechanical Engrg
Georgia Institute of
Technology
Atlanta GA 30332-0420
(404)894-3242
(404)951-8058

Dr David Mann
Army Research Office
P.O. Box 12211
Research Triangle Pk NC 27709-2211
(919)549-4249
AV832-4249

Prof Alan Marchand
Dept of Chemistry
North Texas State Univ
NTSU Station, Box 13767
Denton TX 76203-5068
(817)565-3823

Dr Stephen Margolis
Combustion Research Facility
Sandia National Laboratories
Livermore CA 94550

Lt Col Charles Martin
Nuclear Weapons Development
The Pentagon
Room 5D543
Washington DC 20330-5040
(202)693-6303
AV244-6303

Dr Manuel Martinez-Sanchez
Aeronautics and Astronautics
Massachusetts Inst of Tech
Building 37-401
Cambridge MA 02139
(617)253-5613

Dr Peter Mattern
Combustion Sciences
Sandia National Laboratories
Livermore CA 94550

Dr Jyotirmoy Mazumder
Department of Mechanical and
Industrial Engineering
University of Illinois
Urbana IL 61801
(217)333-1964

Dr John McKee
McDonnell Douglas Astronautics
5301 Bolsa Avenue
Huntington Beach CA 92647
(714)896-1133

Dr John McVey
Rasor Associates, Inc
253 Humboldt Court
Sunnyvale CA 94086
(408)734-1622

Dr Franklin Mead
OL-AC/LKVE
Edwards AFB CA 93523-5000
(805)275-5540
AV525-5540

Dr Carl Melius
Sandia National Laboratories
Livermore CA 94550
(415)294-2650

Dr Charles Merkle
205 ME
Pennsylvania State University
University Park PA 16802
(814)863-1501
FAX 865-3389

Dr Claude Merrill
OL-AC/MKPL
Stop 24
Edwards AFB CA 93523-5000
(805)275-5169
AV525-5169

Dr Michael Micci
233 Hammond Building
Pennsylvania State University
University Park Pa 16802
(814)863-0043

Dr George Miley
University of Illinois
103 South Goodwin Avenue
214 Nuclear Engineering Lab
Urbana IL 61801
(217)333-3772

Dr Richard Miller
Office of Naval Research
Mechanics Division, Code 432
800 North Quincy Street
Arlington VA 22217-5000
(202)696-4403

Dr Charles Mitchell
Dept. of Mechanical Engineerin
Colorado State University
Fort Collins CO 80523
(303)491-6654

Mr T S Mogstad
McDonnell Douglas Astr.Co-West
Design And Tech. Center
Huntington Beach CA 92647
(714)896-3437

Dr Robert Moriarty
University of Illinois
(Chicago Circle)
Department of Chemistry
Chicago IL 60680
(312)996-2364

Dr Marlow Moser
OL-AC/DYCC
Stop 24
Edwards AFB CA 93523-5000
(805)275-5442
AV525-5442

Dr Kenneth Moses
Fusion Physics and Technology
3547 Voyager Street, Suite 104
Torrance CA 90503-1667
(213)542-3800

Dr Philip Muntz
Dept. of Aerospace Engineering
University of Southern
California
Los Angeles CA 90089

Dr S N B Murthy
Dept of Mechanical Engineering
Purdue University
West Lafayette IN 47907
(317)494-1509
(317)494-5639

Dr Jeffery Muss
Aerojet Techsystems
P.O. Box 13222
Sacramento CA 95813
(916)355-3663

Dr Subhash Narang
Chemistry Laboratory
SRI International
333 Ravenswood Avenue
Menlo Park CA 94025-3696

Dr Vittorio Nardi
Stevens Institute of
Technology
Castile Point Station
Hoboken NJ 07030
(201)420-5938

Dr Thong Nguyen
Aerojet Techsystems
P.O. Box 13222
Sacramento CA 95813
(916)355-3664

Dr Jim Nichols
OL-AC/RKLB
Edwards AFB CA 93523-5000
(805)275-5249
AV 525-5249

Dr Gary Nickerson
Software&Engineering Assoc.
1000 E. William St., Suite 200
Carson City NV 89701
(702)882-1966

Dr Arnold Nielsen
Naval Weapons Center
China Lake CA 93555-6001
(619)939-1614
AV437-1614

Mr Randy Nishiyama
R/E/WPS
US Dept of Commerce
NOAA, 325 Broadway
Boulder CO 80303-3328

Col James Nunn
OL-AC/CC
Edwards AFB CA 93523-5000

Dr Douglas Olson
AeroChem Research Laboratories
Inc.
P. O. Box 12
Princeton NJ 08542
(609)921-7070

Dr Tae-Woo Park
OL-AC/TODP
Stop 24
Edwards AFB CA 93523-5000
(805)275-5196
AV525-5196

Col Arthur Pavel
AFOSR/CD
Bolling AFB DC 20332-6448
(202)767-5018
AV297-5018

Ms Dorothy Pecker
The John Hopkins Univ/APL
John Hopkins Rd
Laurel MD 20707

Dr Don Penn
OL-AC/RKLB
Edwards AFB CA 93523-5000
(805)275-5316
AV525-5316

Dr Jerry Pieper
Aerojet Techsystems
P.O. Box 13222
Sacramento CA 95813
(916)355-3087

Dr Leanne Pitchford
GTE Laboratories
40 Sylvan Road
Waltham MA 02254
(617)466-2704

Dr Robert Poeschel
Plasma Physics Department
Hughes Research Laboratories
3011 Malibu Canyon Road
Malibu CA 90265
(213)317-5443

Dr Dimos Poulikakos
University of Illinois
(Chicago Circle)
Dept. of Mechanical Engg.
Chicago IL 60680
(312)996-5239

Dr Edward Price
School of Aerospace Engrg
Georgia Institute of
Technology
Atlanta GA 30332-0420
(404)894-3063

Dr Richard Priem
Priem Consultants
13533 Mohawk Trail
Cleveland OH 44130
(216)845-1083

Dr Andrej Przekwas
CFD Research Corporation
3313 Bob Wallace Ave,Suite 205
Huntsville AL 35805
(205)536-6576

Dr Lawrence Quinn
OL-AC/DYC
Edwards AFB CA 93523-5000
(805)275-5353
AV 525-5353

Dr Frederick Reardon
Cal State U.-Sacramento
Dept of Mechanical Engineering
6000 J Street
Sacramento CA 95616
(916)278-6727

Dr Russell Reed
Naval Weapons Center
China Lake CA 93555-6001
(619)939-7296
AV437-7296

Dr Robert Rhein
Research Chemist
Code 3244
Naval Weapons Center
China Lake CA 93555-6001
(619)939-7392
AV 437-7310

Dr J W Rich
Department of Mechanical Engineering
The Ohio State University
Columbus OH 43212-1194
(614)292-6309

Dr Frank Roberto
OL-AC/MKP
Stop 24
Edwards AFB CA 93523-5000
(805)275-5430
AV525-5430

Dr Stephen Rodgers
OL-AC/LKLR
Stop 24
Edwards AFB CA 93523-5000
(805)275-5416
AV525-5416

Mr Wayne Roe
OL-AC/XRX
Stop 24
Edwards AFB CA 93523-5000
(805)275-5206
AV525-5206

Dr David Rosen
Physical Sciences Inc.
Dascomb Research Park
Andover MA 01810
(617)475-9030

Dr S D Rosenberg
P O Box 13222
Sacramento CA 95813
(916)355-2609

Dr Thomas Rosfjord
United Technologies Res.Ctr.
Silver Lane
East Hartford CT 06108
(203)727-7418

Dr David Ross
Director,Physical Organic Chem
SRI International
333 Ravenswood Avenue
Menlo Park CA 94025-3696
(415)859-2430

Dr J Reece Roth
Dept of Elec and Comp Engrg
316 Ferris Hall
The University of Tennessee
Knoxville TN 37996-2100
(615)974-4446

Dr Gabriel Roy
ONR Code 1132P
800 North Quincy Street
Arlington VA 22217
(202)696-4405

Dr Kevin Rudolph
Martin Marietta Corporation
Mail Stop S8071
PO Box 179
Denver CO 80201
(303)977-3681

Lt James Rymarcsuk
OL-AC/RKLB
Edwards AFB CA 93523-5000
(805)275-5542
AV 525-5542

Dr Mark Salita
Morton Thiokol/Wasatch Div
MS 280B
PO Box 524
Brigham City UT 84302
(801)863-2163

Dr Michael Salkind
President
Ohio Aerospace Institute
2001 Aerospace Parkway
Brookpark OH 44142
(216)891-2100

Dr Robert Santoro
Penn State University
Mechanical Engineering Dept
208 Mechanical Engineering
University Park PA 16801
(814)863-1285
FAX 865-3389

Dr Robert Schmitt
Chemistry Lab
SRI International
333 Ravenswood Avenue
Menlo Park CA 94025-3696
(415)859-5579

Dr Keith Schofield
Quantum Institute
University of California,
Santa Barbara
Santa Barbara CA 93106

Dr Herbert Schrade
Institut Fur Raumfahrtantriabe
Universitat Stuttgart
Pfaffenwaldring 31
D-7000 Stuttgart GE
7116-852-383
or 375

Dr Gary Sega
Aerospace Corp
P.O. Box 92957
MS/747
Los Angeles CA 90004
(213)648-6501

Maj Scott Shackelford
F J Seiler Research Laboratory
United States Air Force Acad
Colorado Springs CO 80840
(719)472-2655

Dr Pam Sherretz
Naval Weapons Center
China Lake CA 93555-6001
(619)939-7392
AV437-7392

Dr R Shoureshi
School of Mechanical
Engineering
Purdue University
West Lafayette IN 47907
(317)494-5639

Prof Jean'ne Shreeve
Dept of Chemistry
University of Idaho
Moscow ID 83843
(208)885-6552

Dr Isaac F Silvera
Harvard University
Department of Physics
Cambridge MA 02138
(617)495-9075

Dr William Sirignano
College of Engineering
University of California
Irvine CA 92717
(714)856-6002

Ms Elizabeth Slimak
OL-AC/LSCF
Edwards AFB CA 93523-5000

Lt Col LaRell Smith
EOARD/LRC
Box 14
FPO NY 09510-0200
AV235-4505

Dr Ronald Spores
OL-AC/LSVE
Edwards AFB CA 93523-5000
(805)275-5766
AV 525-5766

Dr Warren Strahle
School of Aerospace Engrg
Georgia Institute of Technology
Atlanta GA 30332
(404)894-3032

Dr William C Stwalley
The University of Iowa
Iowa Laser Facility
Chemistry and Physics
Iowa City IA 52242-1294
(319)335-1299

Dr V V Subramaniam
Department of Mechanical Engineering
The Ohio State University
Columbus OH 43212-1194
(614)292-6096

Mr Robert L Talley
Viritay Technologoies, Inc
4845 Millersport Highway
East Amherst NY 14051
(716)689-0177

Dr Mostafa Talukder
OL-AC/LKLR
Edwards AFB CA 93523-5000
(805)275-5416
AV525-5416

Dr James Tien
Case Western Reserve University
Glennan Building, Room 415
Cleveland OH 44106
(216)368-4581

Prof William Trogler
Department of Chemistry
University of California, San Diego
La Jolla CA 92093
(619)452-6175

Dr Wing Tsang
National Institute of Standard and Technology
Chemical Kinetics Division
Gaithersburg MD 20899
(301)975-3507

Dr Peter Turchi
Aero/Astro Engineering
328 CAE Building
Ohio State University
Columbus OH 43210
(614)292-2691

Mr Gary Vogt
OL-AC/DYCR
Stop 24
Edwards AFB CA 93523-5000
(805)275-5258
AV525-5258

Dr Robert Vondra
PO Box 596
Wrightwood CA 92397
(619)249-3451

Dr Nzoo Vu
Naval Weapons Center
China Lake CA 93555-6001
(916)939-7392
AV437-7392

Dr R H Woodrow Waesche
Atlantic Research Corporation
7511 Wellington Road
Gainesville VA 22065

Dr Richard Walker
Aerojet Techsystems
P.O. Box 13222
Sacramento CA 95813
(916)355-2694

Dr Peter Wayner
Dept of Chemical and
Environmental Engineering
Rensselaer Polytechnic Inst
Troy NY 12180-3590
(518)276-6199

Dr David Weaver
OL-AC/DYCR
Edwards AFB CA 93523-5000
(805)275-5657
AV525-5657

Dr Jim Weber
Rocketdyne Division
Rockwell International Corp.
6633 Canoga Ave
Canoga Park CA 91303
(818)710-5558

Dr Richard Weiss
OL-AC/CA
Edwards AFB CA 93523-5000
(805)275-5622
AV525-5622

Dr Rodney Willer
Morton Thiokol Inc
Elkton Division
P.O. Box 241
Elkton MD 21921
(301)398-3000
(301)398-4440

Dr Forman A Williams
Department of Applied Mech
and Engineering Science
University of California
La Jolla CA 92093
(619)534-5492

Dr W S Williamson
Plasma Physics Department
Hughes Research Laboratories
3011 Malibu Canyon Road
Malibu CA 90265
(213)317-5443

Dr D O Woolery
Rocketdyne
6633 Canoga Avenue
Canoga Park CA 91304

Dr Ted Yang
Massachusetts Institute of
Technology
167 Albany Street
Cambridge MA 02139
(617)253-8453

Dr Vigor Yang
Department of Mechanical
Engineering
Pennsylvania State University
University Park PA 16802
(814)863-1502
FAX 865-3389

Dr Thomas York
AERO/ASTRO Engineering
328 CAE Building
Ohio State University
Columbus OH 43210
(614)292-2691

Dr Ben Zinn
School of Aerospace Engrg
Georgia Institute of
Technology
Atlanta GA 30332
(404)894-3033

Capt Joseph Zirrolli
FJSRL/NC
United States Air Force
Academy
Colorado Springs CO 80840
(303)472-2655

Mr Robert Zurawski
Program Manager
Propulsion Technology Programs
NASA HQA, OAST-MAIL CODE RP
Washington DC 20546
(202)453-2261

DIAGNOSTICS IN REACTING MEDIA

Invitees

Mr Leonard Angello
Electric Power Research Institute
3412 Hillview Avenue
Palo Alto CA 94303
(415)855-2873

Dr William Bachalo
Aerometrics, Inc.
894 Ross Drive
Unit 105
Sunnyvale CA 94089
(408)745-0321

Dr Edward Beiting
Aerophysics Lab, Prop & Env Sc
The Aerospace Corporation
P O Box 92957, M5/754
Los Angeles CA 90009-2957
(213)336-7035

Dr William Bischel
Coherent, Inc.
3210 Porter Drive
Palo Alto CA 94304
(415)858-7639

Dr Richard Chang
Electrical Engineering Dept.
P. O. Box 2157, Yale Station
Yale University
New Haven CT 06520
(203)432-4272

Dr Wai K Cheng
Department of Mechanical Engineering
MIT
Cambridge MA 02139
(617)253-4531

Dr David Crosley
Molecular Physics Department
SRI International
333 Ravenswood Avenue
Menlo Park CA 94025-3696
(415)326-6200

Dr Gregory Dobbs
United Technologies Research Center - Mail Stop 90
Silver Lane
East Hartford CT 06108
(203)727-7145

Dr A C Eckbreth
United Technologies Research Center
Silver Lane
East Hartford CT 06108
(203)727-7269

Dr Thomas Ehlert
Department of Chemistry
Marquette University
Milwaukee WI 53233
(414)288-7066

Dr Peter Erbland
AFSC/NAT
Wright-Patterson AFB OH 45433-6503
(513)255-3196
(513)255-9757

Dr Gregory Faris
SRI International
333 Ravenswood Avenue
Menlo Park CA 94025
(415)859-4131

Dr Richard Field
U. S. Army Armament R&D Center
DRSMC-LCA-G(D)
Building 382-S
Dover NJ 07801
(201)724-5844
(201)724-5682

Dr Bish Ganguly
WL/POOC-3
Wright-Patterson AFB OH 45433-6563
(513)255-2923
AV785-2923

Dr Alan Garscadden
WL/POOC-3
Wright-Patterson AFB OH 45433-6563
(513)255-2923
AV785-2923

Dr Larry Goss
Research Applications Division
Systems Research Labs, Inc.
2800 Indian Ripple Road
Dayton OH 45440-3696
(513)252-2706

Dr Ronald Hanson
Department of Mechanical
Engineering
Stanford University
Stanford CA 94305-3032
(415)723-1745

Dr D L Hartley
Combustion Sciences
Sandia National Laboratories
Livermore CA 94550

Dr L Hesselink
Department of Aeronautics and
Astronautics
Stanford University
Stanford CA 94305-3032
(415)723-3466

Dr E D Hirleman
Department of Mechanical and
Aerospace Engineering
Arizona State University
Tempe AZ 85287
(602)965-3895
FAX:965-1384

Dr Donald Holve
Insitec
28 Bobbie Court
Danville CA 94526
(415)837-1330

Dr David Huestis
SRI International
333 Ravenswood Avenue
Menlo Park CA 94025
(415)859-3464

Dr Thomas Ishii
Department of Electrical
Engineering
Marquette University
Milwaukee WI 53233
(414)288-1593

Dr Jay Jeffries
SRI International
333 Ravenswood Avenue
Menlo Park CA 94025
(415)859-6431

Dr Roman Kuc
Department of Electrical
Engineering
Yale University
New Haven CT 06520
(203)432-4891

Dr Marshall Long
Department of Mechanical
Engineering
Yale University
New Haven CT 06520
(203)432-4229

Dr Bruce MacDonald
Research Applications Division
Systems Research Labs, Inc.
2800 Indian Ripple Road
Dayton OH 45440-3696
(513)252-2706

Dr T E Parker
Physical Sciences
20 New England Business Center
Andover MA 01810
(508)689-3232

Dr Timothy Parr
Naval Weapons Center
Code 3893
China Lake CA 93555
(619)939-2521

Dr S S Penner
Dept. Of. Appl. Mech. and
Engrg. Sci.
University of California
La Jolla CA 92093
(619)534-4284

Dr Emil Pfender
Department of Mechanical Engrg
125 Mechanical Engineering
The University of Minnesota
Minneapolis MN 55455

Dr John Renie
Department of Mechanical and
Industrial Engineering
University of Illinois
Urbana IL 61801
(217)333-6199

Dr Won B Roh
Department of Engrg Physics
Air Force Institute of
Teechnology
Wright-Patterson AFB OH 45433-6583

Dr Gregory Smith
Department of Chem Kinetics
SRI International
333 Ravenswood Avenue
Menlo Park CA 94025
(415)859-3496

Dr Alan Stanton
Southwest Sciences, Inc.
1570 Pacheco Street
Suite E-11
Santa Fe NM 87501
(505)984-1322

Dr James Trolinger
MetroLaser
18006 Skypark Circle
Suite 108
Irvine CA 92714-6428
(714)553-0688

Dr John Vanderhoff
Ballistic Research Laboratory
DRSMC-BLI(A)
Aberdeen Proving Ground MD 21005
(301)278-6642

Dr James Verdieck
Rockwell International
Rocketdyne Div, M/S FA26
6633 Canoga Avenue
Canoga Park CA 91303
(818)700-4709

Dr Joda Wormhoudt
Aerodyne Research, Inc.
45 Manning Road
Manning Park Research Center
Billerica MA 01821-3976
(508)663-9500